UNIVERSITÀ
DI PAVIA

UNIVERSITÀ DEGLI STUDI DI PAVIA
DOTTORATO IN SCIENZE CHIMICHE E FARMACEUTICHE
(XXXII Ciclo)

Coordinatore: Chiar.mo Prof. Mauro Freccero

NANOPARTICLES AND NANOFIBERS AS DRUG DELIVERY SYSTEMS OF POORLY SOLUBLE DRUGS

Tutor
Chiar.ma Prof.ssa Maria Cristina Bonferoni

Co-tutor
Chiar.ma Prof.ssa Giuseppina Sandri

Tesi di Dottorato
DALILA MIELE

AA 2018/2019

To my mother and my father,
Thank you!

PREFACE

The systemic route is the most common choice to administrate active molecules and to reach the therapeutic effect. Several limitations, including non-specific drug distribution, uncontrolled side effects and poor therapeutic efficacy, that turn into toxic effects on sites different from the therapeutic target, mostly affect this route. For this reason, locally released administration routes have recently attracted scientific research, and novel systems aimed to carry therapeutic agents directly to specific cells or tissues are nowadays developed. In this context, nanomedicine and tissue engineering are broadly involved. These fields can work together in a synergistic way to design innovative and smart systems for *in situ* drug administration, solving all limitations linked to conventional drug delivery systems. Numerous studies have shown that nanoparticle and nanofibrous systems, obtained from natural and semi-synthetic biopolymers, are particularly effective in conveying poorly soluble or poorly bioavailable active ingredients. When properly functionalized or administered near the target site, both systems favor site-specific drug release, reducing systemic drug exposure, minimizing toxicity and improving its efficacy. The efficiency of these systems is linked either to the biomaterials employed, but especially to the high surface area given by the nanometric dimensions. Biocompatibility, biodegradability and the ability to be easily chemically modified are sought aspects during the formulation of these kind of nanosystems. This doctoral project is specifically aimed in developing novel polymeric nano-systems (nanoparticles, nanofibers and / or hybrid systems) able to improve biostability and bioavailability of poorly soluble drugs and guaranteeing a site-specific release.

La via sistemica rappresenta la scelta più comune per la somministrazione di attivi e per l'ottenimento dell'effetto terapeutico. Ad essa sono associate una serie di limitazioni tra cui la distribuzione aspecifica del farmaco responsabile della scarsa efficacia terapeutica e degli effetti collaterali che si tramutano in effetti tossici su siti differenti dal bersaglio terapeutico. Per questo motivo, vie di somministrazione a rilascio locale hanno di recente attratto la ricerca scientifica nel formulare sistemi in grado di veicolare l'agente terapeutico su cellule o tessuti specifici; tale operazione è nota come drug targeting. In questo contesto, trovano largo interesse la nanomedicina e l'ingegneria tissutale, campi che, in maniera sinergistica, collaborano nell'ideazione di sistemi innovativi volti alla somministrazione del farmaco in situ. La strategia si basa sulla realizzazione di impianti intelligenti, capaci di risolvere limitazioni legate ai convenzionali sistemi di somministrazione. Numerose ricerche hanno messo in evidenza come sistemi nanoparticellari e nanofibrosi, ottenuti tramite l'impiego di biopolimeri naturali e semisintetici, siano particolarmente efficaci nella veicolazione di principi attivi poco solubili o scarsamente biodisponibili. Quando opportunamente funzionalizzati e somministrati in prossimità del sito bersaglio, entrambi i sistemi favoriscono il rilascio sito-specifico del farmaco, riducendo l'esposizione sistemica dell'attivo, minimizzando la tossicità e migliorandone l'efficacia. L'efficienza di tali sistemi è sia legata alla scelta dei biomateriali, ma soprattutto all'elevata area superficiale data dalle dimensioni nanometriche. Biocompatibilità, biodegradabilità e capacità di essere facilmente suscettibili a modifiche chimiche sono aspetti ricercati nella formulazione di sistemi di rilascio di questo tipo. Il presente progetto di dottorato si inserisce in questo ambito ed è, specificatamente volto all'ottenimento di nanosistemi (nanoparticelle, nanofibre e/o sistemi ibridi) in grado di migliorare la biostabilità e la biodisponibilità di farmaci poco solubili e garantire un rilascio sito-specifico.

Contents

CHAPTER I

CHITOSAN COATED POLYMERIC NANOPARTICLES

Article

Chitosan Oleate Salt as an Amphiphilic Polymer for the Surface Modification of Poly-Lactic-Glycolic Acid (PLGA) Nanoparticles. Preliminary Studies of Mucoadhesion and Cell Interaction Properties

Dalila Miele [1], Silvia Rossi [1], Giuseppina Sandri [1], Barbara Vigani [1], Milena Sorrenti [1], Paolo Giunchedi [2,*], Franca Ferrari [1] and Maria Cristina Bonferoni [1,*]

[1] Department of Drug Sciences, University of Pavia, 27100 Pavia, Italy; dalila.miele01@universitadipavia.it (D.M.); silvia.rossi@unipv.it (S.R.); giuseppina.sandri@unipv.it (G.S.); barbara.vigani@unipv.it (B.V.); milena.sorrenti@unipv.it (M.S.); franca.ferrari@unipv.it (F.F.)

[2] Department of Chemistry and Pharmacy, University of Sassari, 07100 Sassari, Italy

***** Correspondence: cbonferoni@unipv.it (M.C.B.); pgiunc@uniss.it (P.G.); Tel.: +39-0382-987-357 (M.C.B.); +39-079-228-754 (P.G.)

Received: 30 September 2018; Accepted: 12 November 2018; Published: date

Miele D. et al. "Chitosan oleate salt as an amphiphilic polymer for the surface modification of poly-lactic-glycolic acid (PLGA) nanoparticles. Preliminary studies of mucoadhesion and cell interaction properties." *Marine drugs* 16, 11, 2018: 447-468.

Abstract: Most of the methods of poly-lactic-glycolic acid (PLGA) nanoparticle preparation involve the passage through the emulsification of a PLGA organic solution in water followed by solvent evaporation or extraction. The choice of the droplet stabilizer during the emulsion step is critical for the dimensions and the surface characteristics of the nanoparticles (NPs). In the present work, a recently described ionic amphiphilic chitosan derivative, chitosan oleate salt (CS-OA), was proposed for the first time to prepare PLGA NPs. A full factorial design was used to understand the effect of some formulation and preparation parameters on the NP dimensions and on encapsulation efficiency (EE%) of Nile red, used as a tracer. On the basis of the DoE study, curcumin loaded NPs were prepared, having 329 ± 42 nm dimensions and 68.75% EE%. The presence of a chitosan coating at the surface was confirmed by positive zeta potential and resulted in mucoadhesion behavior. The expected improvement of the interaction of the chitosan surface modified nanoparticles with cell membrane surface was confirmed in Caco-2 cell culture by the internalization of the loaded curcumin.

1. Introduction

Poly-lactic-glycolic acid (PLGA) is one of the most widely used biodegradable polymers in nanoparticle (NP) formulations, thanks to possible modulation of biodegradation rate by means of the choice of suitable PLGA grades and thanks to good regulatory position, as they are well accepted by FDA and EMA [1,2].

Most of the methods of PLGA NPs preparation involve the passage through the emulsification of a PLGA organic solution in water followed by solvent evaporation or extraction. The choice of the droplet stabilizer during the emulsion step is critical for the dimensions and the surface characteristics of the NPs. The most used stabilizer in the literature is PVA[3]. Few other polymers were demonstrated to be useful to stabilize nanoemulsions, such as carbomer and poloxamer, while other macromolecules, such as cellulose derivatives and gelatin, resulted in NPs with acceptable dimensions only when used in association with PVA[4]. In most cases the zeta potential resulted negative, with the only exception of the association between PVA and the cationic gelatin A[4].

A growing interest can be seen in recent years in the literature for PLGA NPs coating to modify the surface to cationic charge. Positively charged NPs can in fact more efficiently interact with negatively charged cellular membranes triggering cell uptake[5–8]. From this perspective, the coating with chitosan is in many cases a first choice for its low cost, good

biocompatibility, and interesting biological properties such as mucoadhesion[9], that in turn can support the efficiency of nanosystems for mucosal vaccination[10,11]. Moreover, chitosan coated PLGA NPs are described as useful tools to improve transfection in nucleic acids delivery [12,13]. An early systematic study was performed to assess the possible employment of chitosan as stabilizing agent in the preparation of NPs, with and without PVA. While chitosan alone resulted not suitable to stabilize the particles, PVA-chitosan blends led to NPs of low dimensions and positive surface charge[14]. A further approach involves the preparation of PVA-stabilized NPs coated in a second step by chitosan electrostatic adsorption[6,15,16].

Polymeric surfactants present peculiar efficiency in the stabilization of nanoemulsions, due to the multiple contact points of the hydrophobic moieties with the o/w interface and steric effect of hydrated hydrophilic chains[17]. If a derivative of a bioactive polymer is used, some of the polymer properties can be maintained by the nanoemulsion. Recently, some evidence was given of the ability of a new amphiphilic chitosan salt, chitosan oleate CS-OA[18], obtained by ionic interaction between chitosan and oleic acid, to stabilize an essential oil nanoemulsion[19]. It was observed that a low energy method could be combined with the self-assembling behavior of chitosan after electrostatic interaction with the hydrophobic moieties of oleic acid. Nanoemulsions of dimensions in the nanometric range were obtained, depending on chitosan concentration and resulted physically stable for at least three months. The zeta potential of the nanoemulsion confirmed that the chitosan derivative was adsorbed at the droplet interface thanks to affinity of oleic chains for hydrophobic phase, while chitosan backbone resulted arranged towards the aqueous medium[19]. Chitosan oleate maintained in this case an antimicrobial effect, in accordance with literature findings [20,21]. Nanoemulsions based on alpha tocopherol and stabilized by means of chitosan oleate salt were studied on fibroblast and keratinocyte cell lines, on ex vivo human biopsies, and in vivo on a rat burn model, showing the biological effects of both chitosan and oleic acid on the wound healing promotion[22,23].

In the present work, the physical stabilization of nanoemulsions by chitosan oleate was for the first time exploited in the preparation of chitosan coated PLGA NPs. The peculiar arrangement of the hydrophobically modified polymer at the oil to water interface around the droplets should in fact result in the exposure of polysaccharide chains towards the aqueous environment so that solvent removal would lead to the occurrence of PLGA NPs coated with a chitosan shell. In the perspective of a Quality by Design-based pharmaceutical development, the DoE approach is more and more encouraged. In this frame, screening factorial designs are a useful instrument to study the relevance of formulation, preparation and assessment variables on product properties[24,25]. A screening full factorial design was here used to understand the effect of the ratio between chitosan and oleic acid, of chitosan concentration and of stirring rate on the NP dimensions and on encapsulation efficiency of Nile red used as a tracer. To confirm the interaction with the biological substrates, curcumin loaded NPs were prepared and tested for mucoadhesion properties and internalization in Caco-2 substrates. Curcumin was chosen as a hydrophobic model molecule for its largely studied behavior, and the possibility to compare the results obtained with the proposed new CS-OA based systems with those obtained with NPs previously described in the literature[26–28].

2. Results and Discussion

Figure 1 shows the results of the preliminary study performed to assess the relationship between the amount of CS-OA used during the preparation of the nanoparticles and their final dimensions. The CS-OA was obtained in situ by electrostatic interaction between the polysaccharide and the oleic acid, at a 1:1 stoichiometric ratio. Increasing polymer dispersion volumes were added during the emulsification step to stabilize the dispersion of PLGA ethyl acetate solution in water. Final CS concentrations resulted in a range between 725 and 840 µg/mL, while the amount of ethyl acetate PLGA solution and polymer concentration were maintained constant. The three samples prepared with the lowest volumes of CS-OA dispersion corresponded to the highest mean particle size values, of 7.99 (± 1.87) µm, 3.11 (± 0.82) µm, and 1.54 (± 0.23) µm. These samples were characterized by laser diffraction apparatus and showed a clear decrease of the percentage of dispersion exceeding the nanometer dimensions with the increase in chitosan derivative volume. By further increasing the CS-OA amount, the resulting particulate dimensions decreased below 1000 nm. The comparison between the two series of data can of course be considered just indicative, as the measurements of the dimensions are obtained with two different apparatus, but nevertheless suggested the use of CS-OA concentrations in a higher range. To better assess the relevance of CS-OA amount, CS to OA ratio, and of a preparative parameter such as ULTRA-TURRAX speed, a DoE-based evaluation was performed on Nile red loaded NPs.

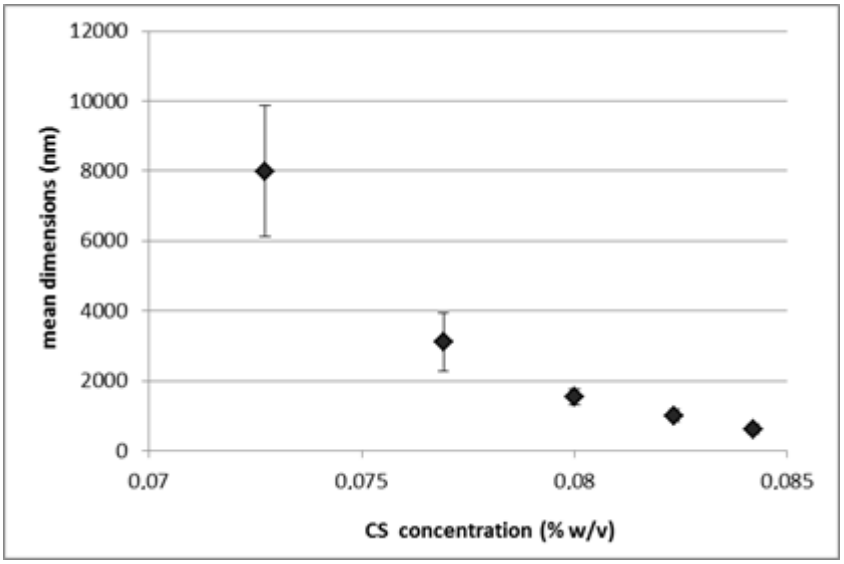

Figure 1. Dimensions of the dispersion (mean ± SD; *n* = 3) for different chitosan (CS) final concentrations.

2.1. Relevance of Formulation and Preparation Parameters on Nile Red Loaded NPs through DoE Study

In this phase of the development study, the volume of CS-OA dispersion was maintained constant (at 10 mL) and Nile red-loaded NPs were prepared by checking the possible further reduction of the dimensions by increasing the stirring rate and the initial chitosan concentration. The relevance of hydrophobic modification level was evaluated by comparing CS-OA at 1:0.2 and at 1:1 chitosan:oleic acid molar ratio, in a range between a low substitution and the maximum stoichiometric ratio.

Stirring rate range was from 13,500 rpm, slightly higher than the stirring rate used in Phase 1, to 20,500 rpm, the highest rate for the used apparatus.

Chitosan concentration was studied in the range 0.1% (*w*/*v*) slightly higher than the maximum one considered in Phase 1, and 0.2% (*w*/*v*), that in a previous work allowed the authors to obtain nanoemulsions of a few hundred nanometers in size[19].

Nile red was encapsulated in the NPs as a fluorescent tracer, for its hydrophobic character, compatible with loading in PLGA core of the NPs. A full factorial was designed and both the dimensions of the PLGA NPs and the encapsulation efficiency of Nile red were evaluated as a response.

Table 1 reports the data obtained for the eight samples and for the three central points of the Full Factorial 2^3 experimental design.

All the data come from analysis replicates (whose variability is described by the standard deviation values) while the replicates necessary for the variability evaluation of the model were performed on the central point. Each set of data was evaluated for standardized skewness and standardized kurtosis and the values resulted within the range expected for data from a normal distribution.

Apart from the two samples with the lowest concentration of chitosan and the lowest ratio between chitosan and oleic acid, whose dimensions were as high as 1830 nm and 1186 nm for 13,500 and 20,500 rpm stirring rate, respectively, in all other cases the average size is maintained in the range of NP systems. All the samples analyzed have an encapsulation efficiency higher than 65%, and as high as 89.58% in the case of the sample prepared with chitosan concentration 0.2% (*w*/*v*), CS-OA ratio 1:1 and stirring rate 13,500 rpm.

Table 1. Dimensions and encapsulation efficiency (EE%) (mean ± SD; n = 4) of the samples prepared according to the 23 full factorial experimental design taking into account, as factors, the chitosan (CS) concentration 0.1–0.2% (w/v), the stoichiometric ratio chitosan: oleic acid (CS-OA) (1:0.2–1:1), and the ULTRA-TURRAX stirring speed (13,500–24,000 rpm).

Independent Variables (Factors)			**Dependent Variables (Responses)**	
CS conc (% w/v)	**CS-OA Ratio**	**Stirring Rate (rpm)**	**Dimensions nm (±sd)**	**EE% (±sd)**
−1	−1	−1	1829 (±303)	70.83 (±1.31)
1	−1	−1	610 (±47)	80.92 (±0.06)
−1	1	−1	627 (±16)	85.42 (±1.72)
1	1	−1	591 (±26)	89.58 (±0.09)
−1	−1	1	1186 (±197)	68.35 (±7.37)
1	−1	1	832 (±93)	79.39 (±2.54)
−1	1	1	634 (±19)	72.19 (±5.60)
1	1	1	620 (±24)	86.51 (±1.33)
0	0	0	760 (±23)	71.28 (±0.80)
0	0	0	759 (±17)	72.68 (±2.04)
0	0	0	733 (±32)	76.62 (±1.36)

The model used to fit the data of NP dimensions is as follows.

dimensions = 834,636 − 202,875*A − 248,125*B − 48,125*C + 190,375*A*B + 110,875*A*C + 57,125*B*C

The Pareto chart for NP dimensions (**Figure 2**) and the ANOVA table (Table 2), show that both chitosan concentration and stoichiometric ratio between chitosan (CS) and hydrophobic agent (OA) significantly influence the response. Both these effects have a negative sign, so that the higher concentration (0.2% w/v) and the higher CS:OA ratio (1:1) contribute to decrease the average size of the particles. The effect of concentration factor confirms the trend observed in the preliminary part of the study (**Figure 1**). The effect of hydrophobic modification seems to confirm its importance for the anchoring of CS-OA at oil to water interface. This is in line with literature data that found poor stabilization of the emulsion with chitosan alone[14]. It is conceivable however that the theoretical stoichiometry between chitosan and oleic acid does not correspond to the final composition of the modified polymer, as it is likely that not all the amino groups of the polymer are involved in the interaction with the fatty acid.

The graph of interaction between concentration and polymer ratio and hydrophobic agent shows a very clear interdependence, confirmed by the statistics that see this significant interaction (**Figure 3**). However, each of the factors assumes a marked importance in decreasing the particle size when the other factor is at the lowest level, and the stability of the dispersion is probably more critical.

The Pareto chart shows that the mechanical agitation during preparation is not significant, contrary to what could be expected.

Table 2. ANOVA table obtained from the statistical analysis of the 2^3 full factorial design for the effects of the three factors considered and of their binary interactions on NP dimensions.

Source	*Sum of Squares*	*Df*	*Mean Square*	*F-Ratio*	*p-Value*
A: CS concentration	329,266	1	329,266	11.13	**0.0290**
B: CS:OA ratio	492,528	1	492,528	16.64	**0.0151**
C: rpm	18528.1	1	185,28.1	0.63	0.4731
AB	289,941	1	289,941	9.80	**0.0352**
AC	98,346.1	1	98,346.1	3.32	0.1424
BC	26,106.1	1	26,106.1	0.88	0.4008
Total error	118,385	4	29,596.2		
Total (corr.)	1.3731×10^6	10			

R-squared = 91.3752 percent; R-squared (adjusted for d.f.) = 78.4381 percent.

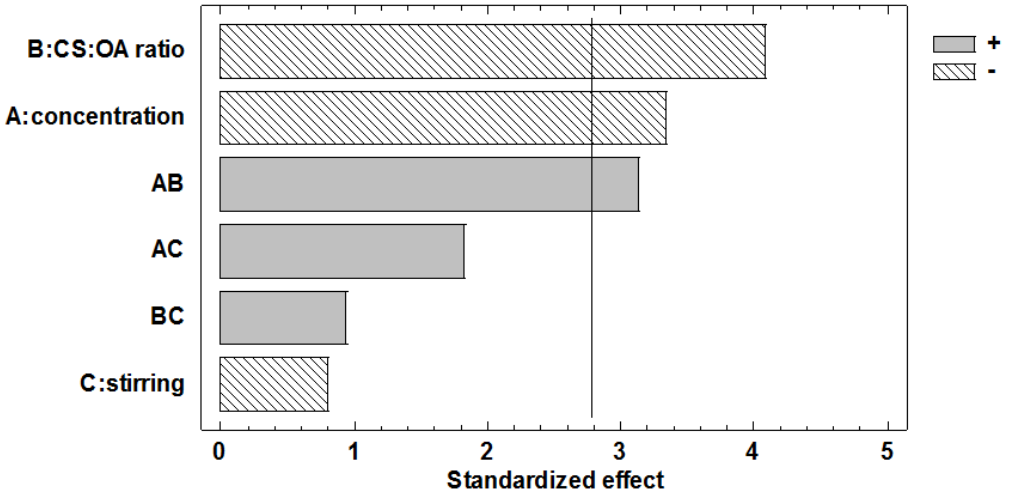

Figure 2. Pareto chart obtained from the statistical analysis of the 2^3 full factorial design and illustrating the effects of the three factors considered and of their interactions on poly-lactic-glycolic acid (PLGA) nanoparticle (NP) dimensions.

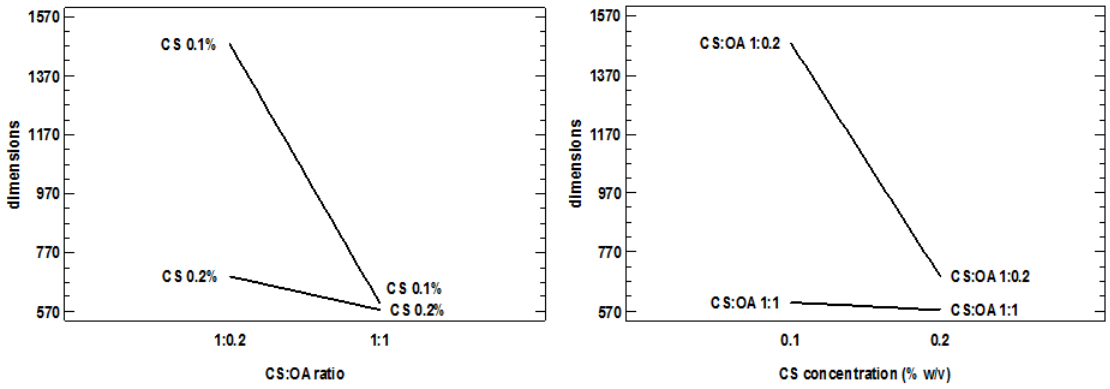

Figure 3. Interaction plots obtained from the statistical analysis of the 2^3 full factorial design and illustrating the interactions between the factors concentration (CS % *w*/*v*) and chitosan:oleic acid (CS:OA) ratio.

The model used in the case of EE% as response is as follows.

$$EE\% = 77.6151 + 4.94963*A + 4.27651*B - 2{,}54119*C - 0.332076*A*B + 1.38938*A*C - 1.53579*B*C$$

In this case a reduced model obtained by exclusion of the not significant interaction with the lowest coefficient was chosen.

Regarding the effect of the factors on the efficiency of encapsulation, the Pareto graph (Figure 4) and the corresponding ANOVA (**Table 3**), suggest that also in the case of EE% response, the chitosan concentration and the molar ratio between the polymer and the hydrophobic agent have a significant and positive effect. This is in line with their relevance on

nanoemulsion stabilization during nanoparticle preparation as it seemed conceivable that quick and efficient coating of the droplets should help the retention of the marker inside the NPs.

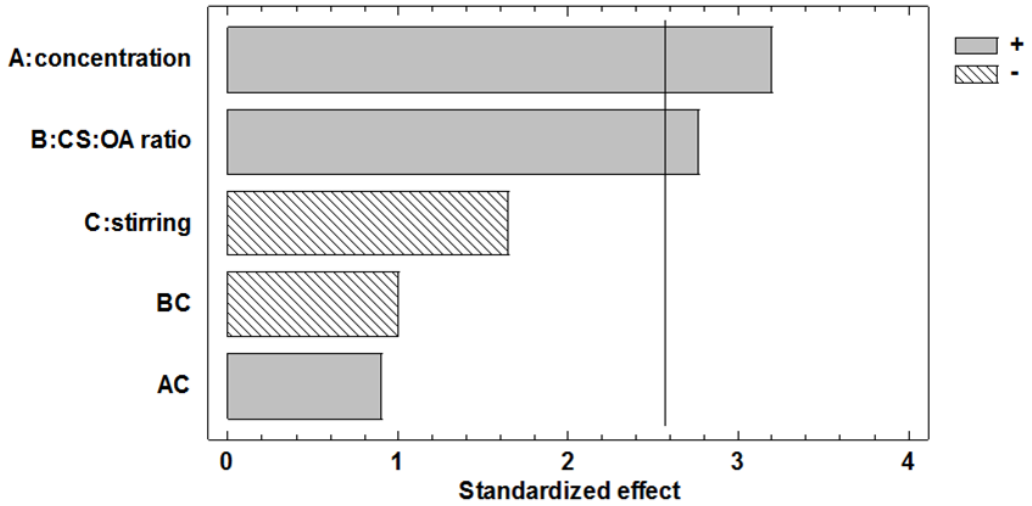

Figure 4. Pareto chart obtained from the statistical analysis of the 23 full factorial design illustrating the effects of the three factors considered and their interactions on Nile red encapsulation efficiency (EE%) in PLGA NP.

Table 3. ANOVA table obtained from the statistical analysis of the 23 full factorial design for the effects of the three factors considered and their binary interactions on encapsulation efficiency (EE%).

Source	*Sum of Squares*	*Df*	*Mean Square*	*F-Ratio*	*P-Value*
A: CS concentration	195.991	1	195.991	10.24	**0.0240**
B: CS-OA ratio	146.308	1	146.308	7.64	**0.0396**
C: stirring	51.6612	1	51.6612	2.70	0.1614
AC	15.4429	1	15.4429	0.81	0.4103
BC	18.8691	1	18.8691	0.99	0.3664
Total error	95.7231	5	19.1446		
Total (corr.)	523.996	10			

R-squared = 81.7321 percent; R-squared (adjusted for d.f.) = 63.4641 percent.

2.2. Curcumin Loaded NPs

Considering the results of the DoE study on critical parameters, the following conditions were chosen to prepare chitosan coated PLGA NPs: chitosan concentration 0.2% (*w*/*v*), chitosan:oleic acid ratio 1:1, and 24,000 rpm ULTRA-TURRAX stirring rate. As reported in Table 1, however, the dimensions of the NPs were even in this case higher than 500 nm. To further reduce the dimensions, acetone 5% *v*/*v* was added together with the hydrophobic phase. It is reported in the literature that acetone, as water miscible solvent, during addition to aqueous environment is subject to quick diffusion. This effect lowers the interfacial tension and makes the dispersion of the droplets finer, resulting in turn in small NP dimensions[29].

According to this mechanism, the dimensions of the CS-OA stabilized NPs were reduced, making possible a direct comparison of CS-OA-stabilized NPs with samples obtained by using PVA to stabilize the nanoemulsion, according to the procedure described in the literature[3]. The comparison of the two nanosystems, prepared with CS-OA and with PVA, both unloaded and loaded with curcumin, was performed by considering dimensions, polydispersion index, and zeta potential (**Table 4**). EE% values are also given in **Table 4** in the case of curcumin loaded systems.

Considering the dimensions, the NPs obtained by using CS-OA as stabilizer, both unloaded (CS-OA PLGA) and curcumin loaded (Cur-CS-OA PLGA), were in a range of few hundred nanometers, comparable to the results obtained by using PVA. As the dimensions, at the same process conditions, are influenced mainly by surfactant effect of the polymers during

emulsification, these results confirm the efficiency of CS-OA as amphiphilic polymer in emulsion stabilization. EE% was slightly higher for PVA NPs (~82%) with respect to CS-OA NPs (~70%). EE% differences can be here explained by a different arrangement of curcumin at the NP surface. This could represent also a possible explanation for the different zeta potential values observed for unloaded and curcumin loaded NPs. Zeta potential is clearly positive for both the unloaded and curcumin loaded CS-OA NPs, confirming the presence of a chitosan shell at the NP surface.

In both the systems the NPs showed EE% values quite high, in line with the hydrophobic nature of curcumin and its good affinity for the PLGA core. On the basis of EE% values, the curcumin colloidal concentration was calculated, ranging between approximately 82 μg/mL in the case of Cur-CS-OA PLGA and almost 100 μg/mL in the case of Cur- PVA PLGA. In both cases a clear improvement of concentration was observed with respect to curcumin solubility, that literature reports as low as 11 ng/mL[30].

Table 4. Characterization of CS-OA-stabilized NPs prepared with acetone and comparison with PVA stabilized NPs, unloaded and loaded with curcumin (mean ± SD, *n* = 3).

	Dimensions (nm)	***Poly Dispersion Index***	***Zeta Potential (mV)***	***EE (%)***	***Curcumin Concentration (μg/mL)***
CS-OA PLGA	*346 ± 88*	*0.32 ± 0.10*	*59.0 ± 2.34*	-	-
PVA PLGA	*310 ± 74*	*0.68 ± 0.15*	*−26.33 ± 1.52*	-	-
Cur-CS-OA PLGA	*329 ± 42*	*0.501 ± 0.016*	*35.45 ± 3.35*	*68.75 ± 0.83*	*82.5 ± 0.99*
Cur-PVA PLGA	*274 ± 9*	*0.648 ± 0.083*	*−0.09 ± 2.4*	*81.99 ± 1.58*	*98.1 ± 1.47*

Figure 5 reports some representative TEM images of CS-OA PLGA NPs. The NPs observed in TEM analysis, like those reported in **Figure 5**, showed dimensions of few hundred nanometers, in accordance with the results of PCS analysis shown in **Table 4**, although the two methods differ by physical principle, sampling, and information obtained. From the morphological point of view, TEM images show nonaggregated, spherical NPs. In particular, for those CS-OA PLGA NPs in which the chitosan coating was partially interrupted, like in the images selected for **Figure 5**, it was possible to appreciate a less dense homogeneous core corresponding to the PLGA inner matrix, and the presence of a more dense surface outer layer conceivably represented by the chitosan coating.

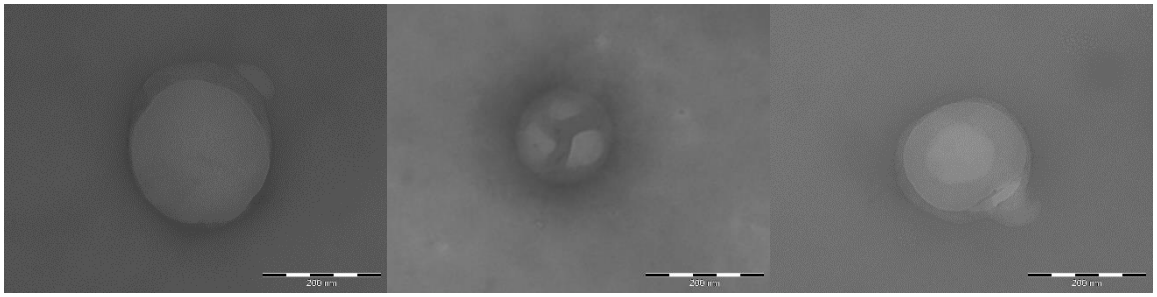

Figure 5. Representative TEM images of CS-OA PLGA nanoparticles. Bars = 200 nm.

2.2.1. Curcumin Loaded NPs Mucoadhesion Behavior

The mucoadhesion behavior of the NPs is illustrated in **Figure 6**. In particular, **Figure 6** shows the results of the test performed in vitro based on the interaction between the NPs and a commercial mucin dispersion. The difference in absorption (ΔA) between the measured absorbance A and the theoretical one (Atheor), indicated as interaction parameter, was proposed in the literature[31] and gives a measure of the interaction between the mucin and the NPs. When no interaction takes place, $\Delta A = 0$ while values of $\Delta A >> 0$ indicate a strong interaction between the mucin and the micelles. This approach was previously validated for NP systems[32] by correlation of the positive values of interaction parameter with positive interaction between NP surface and mucin assessed with different other in vitro and ex vivo tests. A positive mucoadhesive interaction clearly occurs here with Cur-CS-OA PLGA chitosan-coated NPs

while it is not visible for uncoated ones, as it could be expected for the chitosan presence on the NP surface thanks to its well-known mucoadhesive behavior.

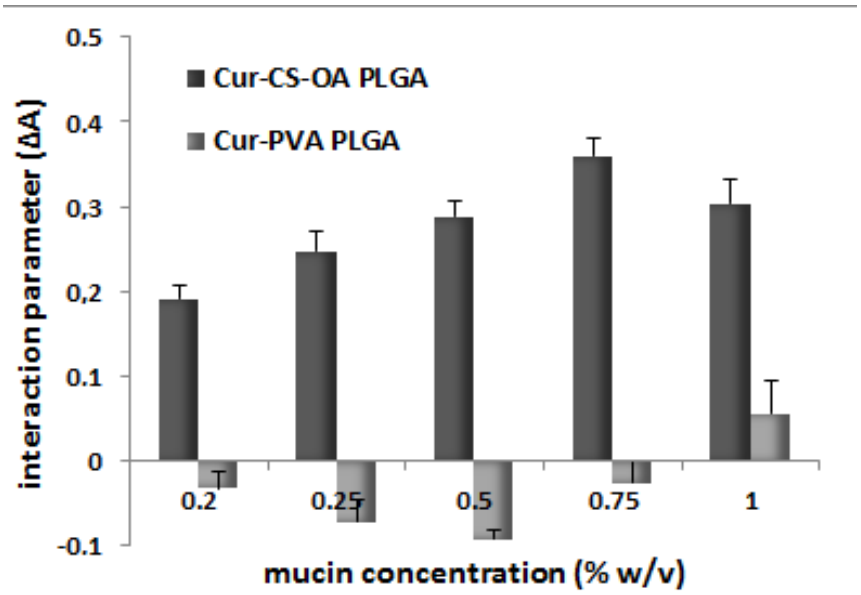

Figure 6. Interaction parameter (mean ± SD, $n = 4$) as a function of mucin concentration for Cur-CS-OA and Cur-PVA NPs. The differences between the two samples were statistically significant at all the mucin concentrations (Mann–Whitney, $p < 0.05$).

2.2.2. Curcumin Loaded NPs. Interaction with Caco-2 Cell Lines

Figure 7 confirms the good biocompatibility of the curcumin loaded samples in a range of curcumin concentrations up to 25 µg/mL. In all cases cell viability was around 80% of the controls, without differences between the free curcumin in DMSO and the two NP samples. This result is in line with what was observed by Beloqui et al.[27] that on the basis of cytotoxicity studies, treated Caco-2 cells with NPs combining poly(lactide-co-glycolide) acid (PLGA) and a polymethacrylate polymer with curcumin concentration of 75 µg/mL. Therefore, Caco-2 cells seem less sensitive to curcumin effect than other cell lines such as A2780 CP or MDA-MB-231 studied by Yallapu et al.[33] or some tumoral cells studied by other authors [26,34] that found 25 µM curcumin both free and loaded in NPs strongly cytotoxic, close in many cases to DL_{50} values.

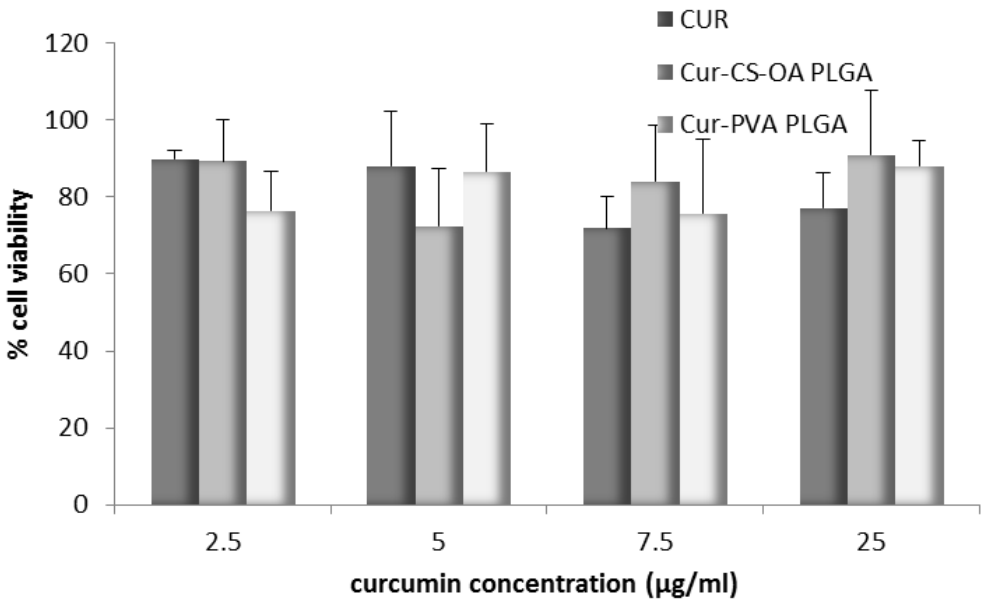

Figure 7. Biocompatibility with Caco-2 cell lines for the samples Cur-CS-OA PLGA, Cur-PVA PLGA, and free curcumin at different curcumin concentrations, as % of cell vitality with respect to the controls after 24 h (mean ± SD, *n* = 8).

The association of curcumin with Caco-2 cells grown 48 h on microscope slides is illustrated in **Figure 8a,b**. The pictures in **Figure 8a** are representative images of clusters of cells whose nuclei are stained in red by propidium iodide, while the blue staining indicates the curcumin presence in cytoplasm. In **Figure 8b**, the curcumin quantified in the cells by image analysis elaboration of the Confocal Laser Scanning Microscopy (CLSM) fluorescence signal, is illustrated for each sample. Cur-CS-OA PLGA sample shows strong positive association to the cells. The good internalization of free curcumin inside the cells is probably determined by its hydrophobic character, that allows easy passage of the cell membranes of the molecule once it is in solution.

Figure 9a,b refers to cells grown on transwell membranes. In this experimental set the Caco-2 cells reach full polarization and are able to express tight junctions. Also in this case, curcumin can be seen inside the cells, as indicated by the blue staining around the nuclei and along the Z axis. **Figure 9b** shows the results of fluorescence quantification. CS-OA coated NPs seem to be responsible of good internalization in cells, slightly lower than that of free curcumin, but higher than that of PVA NPs.

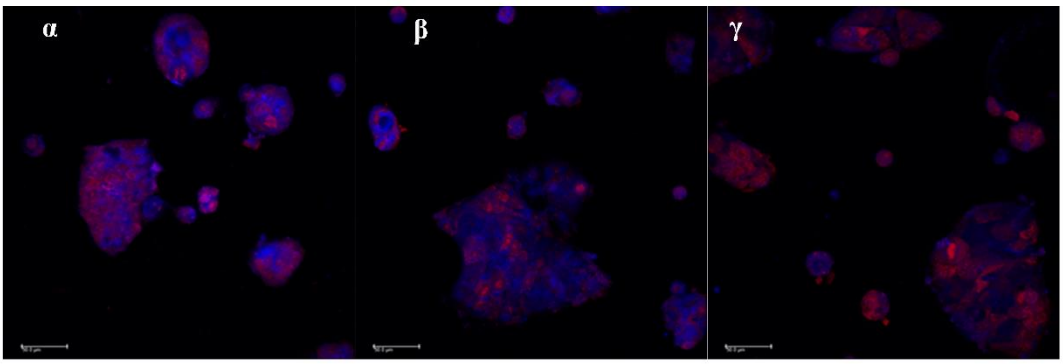

(**a**)

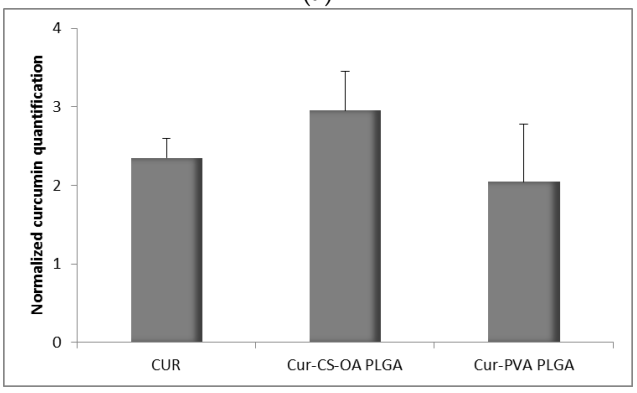

(**b**)

Figure 8. (**a**) Representative CLSM photomicrographs of Caco-2 cell substrates grown after 48 h on microscope slides and treated 24 h with the samples. (α) Free curcumin; (β) Cur-CS-OA PLGA; (γ) Cur-PVA-PLGA. Bar: 50 μm; (**b**) CLSM fluorescence quantification, obtained by image analysis, of the amount of curcumin associated to the cells grown on microscope slides (mean ±sd; *n* = 3).

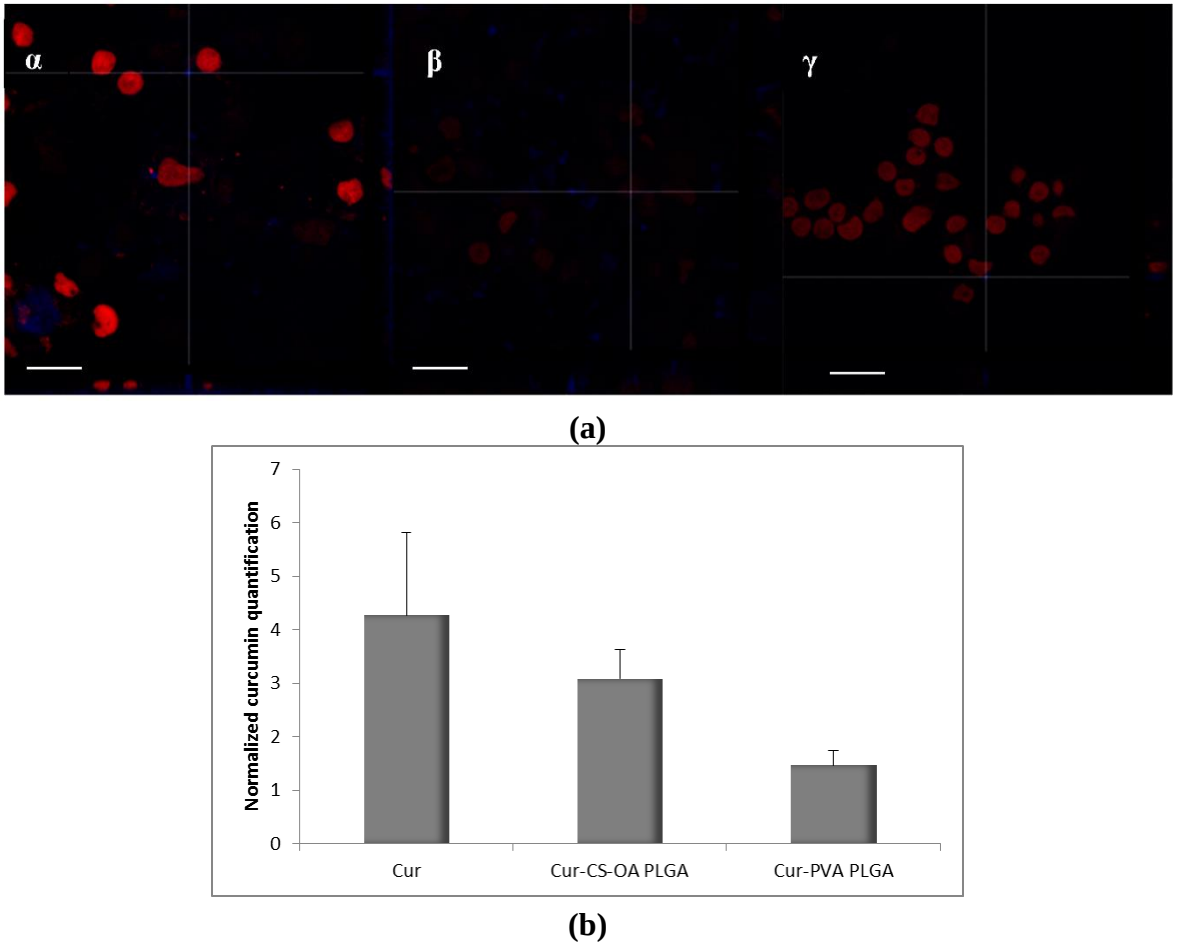

Figure 9. (**a**) Representative CLSM photomicrographs with z planes of Caco-2 cell substrates grown on transwell membranes, and treated for 3 h with the samples. (α) Free curcumin; (β) Cur-CS-OA PLGA; (γ) Cur-PVA PLGA. Bar: 20 μm; (**b**) CLSM fluorescence quantification, obtained by image analysis, of the amount of curcumin associated to the Caco-2 cells grown on transwell membrane (mean ± SD; *n* = 3).

In no case curcumin could be quantified in the acceptor compartment, in line also in this case with other author results, that did not find quantifiable Papp values for curcumin through Caco-2 cells[27]. However, it was possible to measure the curcumin concentration by fluorescence analysis in the apical compartment at the end of the 3 h test. On the basis of these results the amount of curcumin associated with Caco-2 substrate treated with the samples was calculated by difference. The results are illustrated in **Figure 10** and support what previously observed by CLSM pictures. In the case of Cur-CS-OA PLGA sample about 40% of the curcumin put in contact with the cell substrates seems associated with the cell layers. Statistically significant differences can be seen between Cur-CS-OA PLGA and both curcumin and Cur-PVA PLGA (one-way ANOVA, post-hoc Fisher's test).

The transepithelial electrical resistance (TEER) profiles during the three hours of contact of the samples with the substrates (**Figure 11**) show that no decrease occurred, even with the CS-OA-coated sample, indicating that the presence of the chitosan layer around the NPs does not influence in this case the tight junction structure. This result was not expected, as there are many example in the literature reporting that chitosan-based NPs open tight junctions. The result obtained in this case could be due to a concentration effect, as previously observed with chitosan coated PLGA nanoparticles on Calu3[35], or to tight association of chitosan with the NPs in line with previous studies on chitosan palmitate polymeric micelles in which it was put in evidence that among different substitution grades, only the less substituted and more hydrophilic derivative was able to maintain the capability to decrease TEER values[36].

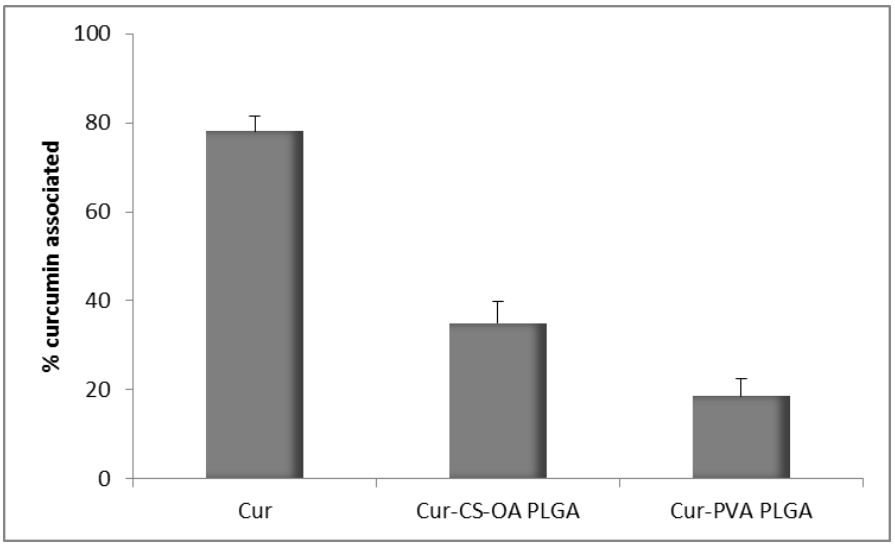

Figure 10. Percentage of curcumin associated to the Caco-2 cell substrates (mean ± SD; n = 8) detected by fluorescence analysis. Statistically significant differences (one-way ANOVA , post-hoc Fisher's test, $p < 0.05$): Cur vs. Cur-CS-OA PLGA, Cur vs. Cur-PVA PLGA, Cur-CS-OA PLGA, and vs. Cur-PVA PLGA.

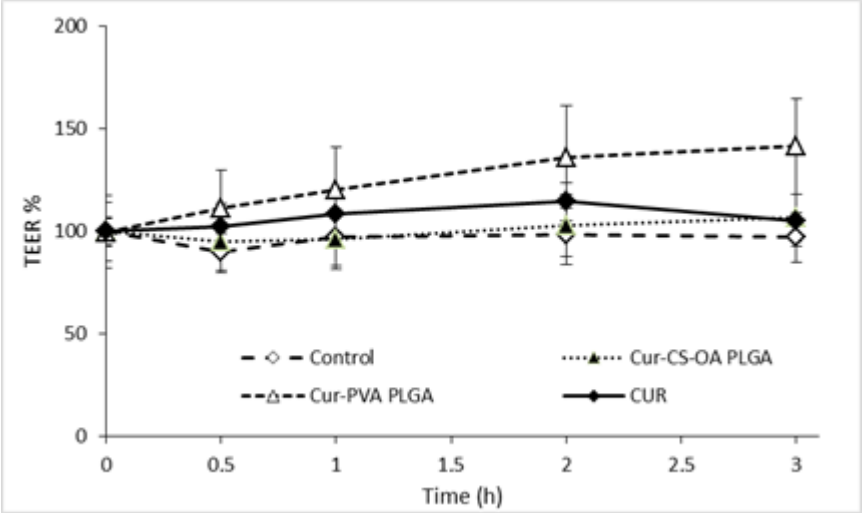

Figure 11. Transepithelial/endothelial electrical resistance (TEER) % profiles of Caco-2 substrates on transwell membranes after contact with Cur-CS-OA PLGA, with Cur-PVA PLGA, and with free curcumin (mean ± SD;n =4).

3. Materials and Methods

- *Materials*

The following materials were used, chitosan (CS) was obtained as HCl salt from low molecular weight (LMW, chitosan base, deacetylation degree 80% (Sigma-Aldrich, Milan, I), by addition of HCl 0.5 N to chitosan until complete dissolution, dialysis in bidistilled water for 24 h and freeze-drying (HetoDrywinner, Analitica de Mori, Milan, I). Oleic acid was from Fluka (Milan, I). PLGA Resomer RG 503H, Low MW grade poly-vinyl-alcohol (PVA), Nile red and curcumin were all from Sigma-Aldrich (Milan, I). Acetone, acetic acid, sodium acetate, and sodium chloride were acquired from Carlo Erba (Milan, I).

- *Methods*

3.1. Preparation of the Chitosan Coated NPs

Chitosan oleate (CS-OA) was obtained in situ, as previously described[19,22], by self-assembling during the preparation of the samples. Briefly, oleic acid dissolved in acetone was added to chitosan HCl solution at either 0.1 or 0.2 % *w*/*v* and acetone was removed under stirring for about 20 min. The ratio between chitosan and oleic acid was calculated as molar ratio taking into account the molecular weight of glucosamine unit and the theoretical free amino groups of chitosan. Considering the 80% deacetylation degree in accordance with the used chitosan grade, a 1:1 ratio corresponded to 1.4 mg of oleic acid per each mg of chitosan.

In a first step a 0.1% (*w*/*v*) of chitosan concentration and 1:1 stoichiometric ratio with oleic acid were used. 2.5 mL of ethyl acetate solution containing 12 mg PLGA were added to 3 mL distilled water. Emulsification started at 9500 rpm by means of ULTRA-TURRAX T25 (Janke&Kunkel, IKA® Labortechnik, Germany) equipped with 10 mm probe (S25 N-10 G) and after 5 min different volumes of CS-OA dispersion, between 8 and 16 mL, were added. After 10 min, ethyl acetate was removed under stirring at 40 °C for about 45 min. The weight lost during evaporation was assessed and the initial volume reconstituted with distilled water.

3.2. Dimensional and Zeta Potential Characterization of Dispersed Phase

The particle size of the dispersed phase was measured by laser diffraction, Microtrac (Microtrac® SRA 150 ASVR, Honeywell, Phoenix, AZ, USA) for samples exceeding the nanometer range. For the samples in the nanometric range the dimensions and the Polydispersity Index (PI) were measured by Photon Correlation Spectroscopy (PCS) (N5 Submicron Particle Size Analyzer Beckman Coulter, IL, Milan, Italy). PCS analysis were performed at 90° detection angle after dilution in 0.22 µm filtered bidistilled water. PI indicates the width of the size distribution ranging between 0 (monodispersity) and 1. At least three replicates were performed. Zeta potential measurements were performed by means of a Zetasizer® Nanoseries (Malvern Instruments Ltd., Worcestershire, United Kingdom). Three measurements were performed for each sample. For TEM analysis the samples have been layered on 300 mesh cupper grids. The images have been obtained with a JEOL JEM1200EX II apparatus.

3.3. Nile Red Loaded NPs

For Nile red-loaded NPs, a full factorial 2^3 design was used to study the following formulation and preparation factors (independent variables) each of them set at two levels as hereafter indicated, chitosan concentration 0.1% *w*/*v* (−1) and 0.2% *w*/*v* (+1), chitosan to oleic acid ratio 1:0.2 (−1) and 1:1 (+1), and ULTRA-TURRAX speed at 13,500 rpm (−1) and 20,500 rpm (+1). In this study, 100 µL of 1 mg/mL Nile red in ethyl acetate were added together with 2.5 mL of 4.8 mg/mL ethyl acetate PLGA solution to 10 mL of chitosan oleate aqueous dispersion prepared as previously described. Two response (dependent) variables, that is nanoparticle dimensions and Nile red encapsulation efficiency, were considered. According

with the 2^3 full factorial design, eight experiments were performed. Moreover, one central point was added and replicated three times. All the experiments were performed in a randomized sequence.

Nile Red Encapsulation Efficiency (EE%) Evaluation

Nile red was quantified by UV–Vis detection (Perkin Elmer Instrument Lambda 25 UV–Vis Spectrometer, Monza, Italia) in CH_3CN and acetate buffer 0.1M pH 4.0, 80:20 mixture, where it was previously verified that all the NP components could be solubilized. Absorbance was read at 552 nm, where the maximum of absorbance was found in the solvent used. The encapsulation efficiency (EE%) was calculated as the percentage ratio between the amount of the tracer quantified in the NPs and the amount added to the formulation. To determine the EE% the samples, after centrifugation 10 min at 6000 rpm to remove by precipitation the amount not encapsulated, the supernatant was diluted in CH_3CN and acetate buffer mixture and spectrophotometrically read.

3.4. Preparation of Curcumin Loaded NPs

Curcumin loaded NPs were obtained with the same solvent evaporation procedure (Figure 12) described above for Nile red loaded NPs. 1.2 mg of curcumin dissolved in 500 µL of acetone were added together with 2.5 mL of 4.8 mg/mL ethyl acetate PLGA solution to 10 mL of chitosan oleate aqueous dispersion prepared as previously described, to obtain a final concentration of 120 µg/mL. In this case, to stabilize the nanoemulsion, the CS-OA dispersion obtained as previously described from 0.2% *w/v* chitosan and 1:1 chitosan and oleic acid ratio was used. For comparison purposes, NPs stabilized with 2% *w/v* PVA solution according to the literature[37] were prepared. In both cases, ULTRA-TURRAX homogenization was performed at 20,500 rpm.

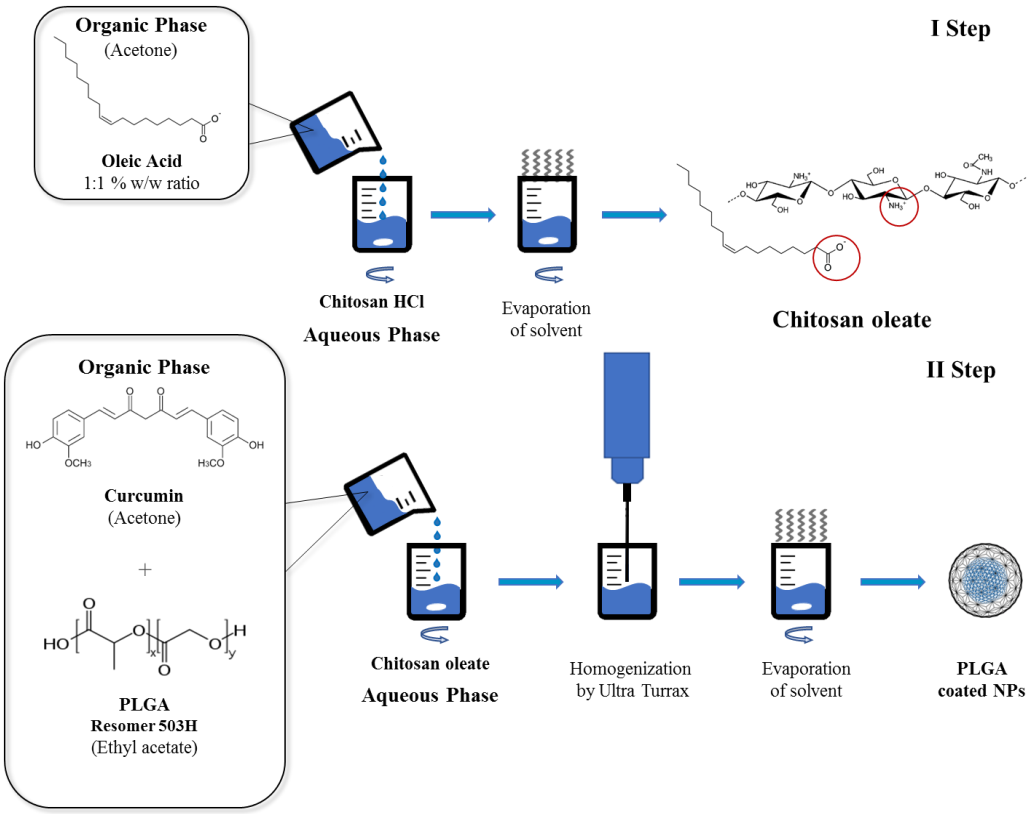

Figure 12. Schematic representation of the preparation method of chitosan-coated NPs.

3.5. Curcumin Quantification and EE% Evaluation

Curcumin was quantified by UV–Vis detection in CH_3CN and acetate buffer 0.1M pH 4.0, 80:20 mixture. Absorbance was read at 431 nm wavelength. To determine the EE% of the samples (after centrifugation at 10 min at 6000 rpm to remove by precipitation the amount not encapsulated) the supernatant was diluted in CH_3CN and acetate buffer mixture and spectrophotometrically read.

3.6. Mucoadhesion Evaluation

For the in vitro test, different concentrations, ranging between 0.1% and 1.0% *w*/*v* of mucin type I (Sigma-Aldrich, Milan, I), were prepared and put in contact with 200 µL of NP sample for 2 min. Turbidimetric measurements were carried out using a spectrophotometer (UV–Vis Lamba 25, Perkin Elmer, Milan, Italy) at $\lambda = 500$ nm. The mixtures of samples and mucin at increasing concentrations, were compared with the dispersions containing the same concentration of mucin as in the mixture[32]. The turbidimetry values were also elaborated according to the method described in the literature[31]: the effective absorbance (A) was that of the mixture of mucin and NPs. The theoretical absorbance (Atheor) was calculated by adding the absorbance of NPs and that of mucin dispersion at the same concentration. The interaction parameter was the difference in absorption (ΔA) between the measured absorbance and the theoretical one.

3.7. Caco-2 Biocompatibility Test

Caco-2 cell culture was grown in a polystyrene flask in complete culture medium consisting of DMEM added with 1% *v*/*v* of a penicillin–streptomycin–amphotericin 100× solution (pen/strep/amph; Euroclone, Milan, I), 10% *v*/*v* of inactivated fetal FBS bovine serum (Fetal Bovine Serum; Euroclone, Milan, I) and 1% *v*/*v* of nonessential amino acids 100× (Mem Nonessential Amino Acid Solution 100×; Sigma-Aldrich, Milan, I). The cells were grown in an incubator (CO_2 Incubator, PBI International, Milan, I) at 37 ° C, in a humidified atmosphere, containing 5% of CO_2.

For the cytotoxicity test, Caco-2 cells were seeded ($0.35 \cdot 10^5$ cells per well) in 96-well plates (Cellstar 96 Well Culture Plate, Greiner Bio-One, G) with an area of 0.36 cm^2. After seeding, the plates were placed in the incubator for 24 h, then the cells were washed with 100 µL of PBS, and the samples were added.

NPs loaded with curcumin were tested on cell lines to assess biocompatibility at final curcumin concentration ranging from 2.5 to 25 µg/mL concentration. After 24 h of contact with the samples, an MTT test was performed. The MTT test is based on conversion of tetrazolium salt (3- (4,5-dimetiltiazol-2-)-2,5-diphenyltetrazolium bromide) to formazan by mitochondrial dehydrogenases of vital cells[38]. Briefly, 50 µL of 2.5 mg/mL MTT solution (Sigma-Aldrich, Milan, I) in HBSS (Hank's Buffered Salt Solution) pH 7.4 was put in contact with each cell substrate for 3 h. After removing the reagent, the substrates were washed with 200 µL of PBS. Then 100 µL of DMSO was put in each well. The absorbance was read at 570 nm by means of an ELISA plate reader (Imark Absorbance Reader, Biorad, Milan, I). Cell viability was calculated as percentage ratio between the absorbance of each sample and the absorbance of controls (cell substrates in growth medium).

3.8. Cell Uptake Studies

Cell uptake was evaluated by means of confocal laser scanning microscopy (CLSM). This was performed both on cells grown 48 h on slides and on cells grown on transwell membranes. In the first case the cells were seeded in 24-well plates. At the bottom of each well was a 13 mm diameter slide (Coverglass Borosilicate, VWR International, Milan, I) on which the cells were made to adhere and grow for 24 h. The samples were added and left in contact with the cells another 24 h, after which the cell substrates were washed with 500 µL of PBS and fixed with a

3% *v*/*v* glutaraldehyde solution in PBS for one hour at 4 ° C. The glutaraldehyde was removed and the wells were washed twice with 500 µL of PBS.

Cells were also seeded on transwell membranes (0.4 µm pores, 1.13 cm^2 surface, Cellstar® permeable support tissue culture plate, Greiner bio one ®, Milano, Italia) and grown 20 ±1 days until complete confluence. Monolayer integrity was verified by checking TEER values. The basolateral compartment was filled with 1.5 mL of DMEM without Phenol red to avoid fluorescence interferences. Five-hundred microliters of each sample was diluted in DMEM at a final curcumin concentration of 24 µg/mL and placed in donor chamber. After 3 h curcumin was quantified by fluorescence analysis in the apical and basolateral compartment by means of a microplate reader (Plate reader, Synergy HT, 14,041,014) at 485 nm excitation and 528 nm emission. The cell substrates were washed with PBS, treated 10 min with paraformaldehyde and washed twice with PBS.

Nuclei were stained just before the microscope analysis with 150 µL of propidium iodide (PI) 20 µg/mL in PBS for 5 min in the dark. The PI was then removed, and the cells washed with 200 µL of PBS. The slides were examined using a laser scanning confocal microscope (CLSM, Leica TCS SP5II, Leica Microsystems CMS GmbH), which allows visualization of fluorescence of propidium iodide (λ_{ex} = 520 nm and λ_{em} = 630 nm) and of curcumin (λ_{ex} = 440 nm and λ_{em} = 520 nm). The fluorescence was quantified on all the microphotographs collected (at least 3 for each sample) by means of an Image analysis program (ImageJ 1.46r, NIH)). The blue intensity of curcumin was normalized per each image by the red fluorescence of nuclei.

3.9. Statistical Analysis

Statistical evaluations were performed by means of Statgraphics 5.0, Statistical Graphics Corporation, MD, USA. Differences were determined according to one-way ANOVA and were considered significant at $p < 0.05$. The same statistical package was used to analyze the results of the full factorial design.

4. Conclusions

The results obtained in this study appear promising for the application of an ionic chitosan derivative, such as the chitosan oleate salt, in the easy preparation of nanoparticles with hydrophobic cores that are surface modified with a hydrophilic polysaccharide corona. The high zeta potential values confirm the presence of chitosan at the nanoparticle surface. Chitosan coating can be advantageous for its well-known biological properties and for increased possibilities of further derivatization. Efficiency of the chitosan derivative in PLGA NP preparation resulted comparable to that of PVA. Clear improvement of mucoadhesion behavior has been obtained for CS-OA-based NPs. Further work will be necessary to better understand the mechanism of association between chitosan and oleic acid and its final stoichiometry. Also, the interaction of the nanoparticles with biological substrates and the possible improvement of absorption enhancement properties would deserve better investigation, although the preliminary results here obtained confirm a positive cell internalization of the surface modified nanoparticles, likely due to the interaction of cationic chitosan with the anionic cell membrane. Considering the good potentiality of the PLGA core in the loading of hydrophobic drugs and the mucoadhesion and penetration enhancement properties of the chitosan shell, applications in the delivery of poorly soluble and poorly absorbable drugs can be envisaged.

In a more general perspective, the use of amphiphilic derivatives of bioactive polymers, like chitosan, as nanoemulsion stabilizers in solvent evaporation methods can be proposed as a useful approach for surface modification of nanoparticles with bioactive polymeric shells.

Author Contributions: Conceptualization, M.C.B.; Methodology, M.C.B., S.R., G.S., F.F.; Formal Analysis, M.S.; Investigation, D.M., B.V.; Data Curation, D.M., S.R., G.S., B.V.; Writing-Original Draft Preparation, M.C.B., P.G.; Writing-Review & Editing, M.C.B., P.G.; Supervision, M.C.B., P.G.;

Funding: This research received no external funding

Conflicts of Interest: The authors declare no conflict of interest

References

1. Danhier, F.; Ansorena, E.; Silva, J.M.; Coco, R.; Le Breton, A.; Preat, V. PLGA-based nanoparticles: an overview of biomedical applications. J Control Release 2012, 161, 505-522, 10.1016/j.jconrel.2012.01.043
2. Mir, M.; Ahmed, N.; Rehman, AU. Recent applications of PLGA based nanostructures in drug delivery. Colloids Surf B Biointerfaces 2017, 159, 217–231, 10.1016/j.colsurfb.2017.07.038
3. Astete, C.E.; Sabliov, C.M. Synthesis and characterization of PLGA nanoparticles. J Biomater Sci Polym Ed, 2006, 17, 247–289
4. Vandervoort, J.; Ludwig, A. Biocompatible stabilizers in the preparation of PLGA nanoparticles: a factorial design study. Int J Pharm 2002, 238, 77–92.
5. Tahara, K.; Sakai, T.; Yamamoto, H.; Takeuchi, H.; Hirashima, N.; Kawashima, Y. Improved cellular uptake of chitosan-modified PLGA nanospheres by A549 cells. Int J Pharm 2009, 382, 198–204, 10.1016/j.ijpharm.2009.07.023
6. Alqahtani, S.; Simon, L.; Astete, C.E.; Alayoubi, A.; Sylvester, P.W.; Nazzal, S.; Shen, Y.; Xu, Z.; Kaddoumi, A.; Sabliov, C.M. Cellular uptake, antioxidant and antiproliferative activity of entrapped a-tocopherol and c-tocotrienol in poly (lactic-co-glycolic) acid (PLGA) and chitosan covered PLGA nanoparticles (PLGA-Chi), J Colloid Interface Sci 2015, 445, 243–251, 10.1016/j.jcis.2014.12.083
7. He C, Hua Y, Yin L, Tang C, Yin C. Effects of particle size and surface charge on cellular uptake and biodistribution of polymeric nanoparticles. Biomaterials 2010, 31, 3657–3666, 10.1016/j.biomaterials.2010.01.065
8. Yameen B, Choi WI, Vilos C, Swami A, Shi J, Farokhzad OC. Insight into nanoparticle cellular uptake and intracellular targeting. J Control Release 2014, 190, 485–499, 10.1016/j.jconrel.2014.06.038
9. Martínez-Pérez, B.; Quintanar-Guerrero, D.; Tapia-Tapia, M.; Cisneros-Tamayo, R.; Zambrano-Zaragoza, M.L.; Alcalá-Alcalá, S.; Mendoza-Muñoz, N.; Piñón-Segundo, E. Controlled-release biodegradable nanoparticles: From preparation to vaginal applications. Eur J Pharm Sci. 2018, 115, 185-195, 10.1016/j.ejps.2017.11.029
10. Pawar, D.; Mangal, S.; Goswami, R.; Jaganathan, K.S. Development and characterization of surface modified PLGA nanoparticles for nasal vaccine delivery: Effect of mucoadhesive coating on antigen uptake and immune adjuvant activity. Eur J Pharm Biopharm. 2013, 85, 550–559, 10.1016/j.ejpb.2013.06.017.
11. Rose, F.; Wern, J.E.; Gavins, F.; Andersen, P.; Follmann, F.; Foged, C. A strong adjuvant based on glycol-chitosan-coated lipid-polymer hybrid nanoparticles potentiates mucosal immune responses against the recombinant Chlamydia trachomatis fusion antigen CTH522. J Control Release 2018, 271, 88–97, 10.1016/j.jconrel.2017.12.003.
12. Nafee, N.; Taetz, S.; Schneider, M.; Schaefer, U.F.; Lehr, C.; Chitosan-coated PLGA nanoparticles for DNA/RNA delivery: effect of the formulation parameters on complexation and transfection of antisense oligonucleotides. Nanomedicine 2007, 3, 173-183.
13. Jagani, H.V.; Josyula, V.R.; Palanimuthu, V.R.; Hariharapura, R.C.; Gang, S.S.; Improvement of therapeutic efficacy of PLGA nanoformulation of siRNA targeting anti-apoptotic Bcl-2 through chitosan coating. Eur J Pharm Sci. 2013, 48, 611-8, 10.1016/j.ejps.2012.12.017.
14. Kumar, R.M.N.V.; Bakowsky, U.; Lehr, C.M.; Preparation and characterization of cationic PLGA as DNA carriers. Biomaterials 2004, 25, 1771-1777, 10.1016/j.biomaterials.2003.08.069
15. Badran, M.M.; Mady, M.M; Ghannam, M.M.; Shakeel F. Preparation and characterization of polymeric nanoparticles surface modified with chitosan for target treatment of colorectal cancer. Int J Biol Macromol. 2017, 95, 643–649, 10.1016/j.ijbiomac.2016.11.098
16. Kang, B.S.; Choi, J.S.; Lee, S.E.; Lee, J.K.; Kim, T.H.; Jang, W.S.; Tunsirikongkon, A.; Kim, J.K.; Park, J.S. Enhancing the *in vitro* anticancer activity of albendazole incorporated into chitosan-coated PLGA nanoparticles. Carbohydr Polym. 2017, 159, 39-47, 10.1016/j.carbpol.2016.12.009
17. Tadros, T. Polymeric surfactants in disperse systems. Adv Colloid Interface Sci. 2009, 147–148, 281–299, 10.1016/j.cis.2008.10.005
18. Bonferoni M.C.; Sandri G.; Dellera E.; Rossi S.; Ferrari F.; Mori M.; Caramella C. Ionic polymeric micelles based on chitosan and fatty acids and intended for wound healing. Comparison of linoleic and oleic acid. Eur J Pharm Biopharm. 2014 May;87(1):101-6. doi: 10.1016/j.ejpb.2013.12.018.
19. Bonferoni, M.C.; Sandri, G.; Rossi, S.; Usai, D.; Liakos, I.; Garzoni, A.; Fiamma, M.; Zanetti, S.; Athanassiou, A.; Caramella, C.; Ferrari, F. A novel ionic amphiphilic chitosan derivative as a stabilizer of nanoemulsions: Improvement of antimicrobial activity of Cymbopogon citratus essential oil. Colloids Surf B Biointerfaces 2017, 152, 385–392, 10.1016/j.colsurfb.2017.01.043
20. Liu, X.F.; Guan, Y.L.; Yang, D.Z.; Li, Z., Yao, K.D. Antibacterial action of chitosan and carboxymethylated chitosan. J Appl Polym Sci. 2001, 79, 1324–1335.
21. Zheng, C.J.; Yoo, J.S.; Lee, T.G.; Cho, H.Y.; Kim, Y.H.; Kim, W.G. Fatty acid synthesis a target for antibacterial activity of unsaturated fatty acids, FEBS Lett. 2005, 579, 5157–5162.

22. Bonferoni, M.C.; Riva, F.; Invernizzi, A.; Dellera, E.; Sandri, G.; Rossi, S.; Marrubini, G.; Bruni, G.; Vigani, B.; Caramella, C.; Ferrari F. Alpha tocopherol loaded chitosan oleate nanoemulsions for wound healing. Evaluation on cell lines and *ex vivo* human biopsies, and stabilization in spray dried Trojan microparticles. Eur. J. Pharm. Biopharm. 2018, 123, 31–41, 10.1016/j.ejpb.2017.11.008
23. Bonferoni M.C.; Sandri G., Rossi S., Dellera E., Invernizzi A., Boselli C., Icaro Cornaglia A., Del Fante C., Perotti C., Vigani B., Riva F., Caramella C., Ferrari F. Association of Alpha Tocopherol and Ag Sulfadiazine Chitosan Oleate Nanocarriers in Bioactive Dressings Supporting Platelet Lysate Application to Skin Wounds. Mar Drugs 2018, 16, 56, doi:10.3390/md16020056
24. Pramod K, Tahir MA, Charoo NA, Ansari SH, Ali J. Pharmaceutical product development: A quality by design approach. Int J Pharma Investig 2016;6:129-38. doi: 10.4103/2230-973X.187350
25. Bonferoni, M.C., Rossi, S., Ferrari, F., Stavik, E., Pena-Romero, A., Caramella, C. Factorial analysis of the influence of dissolution medium on drug release from carrageenan-diltiazem complexes (2000) AAPS PharmSciTech, 1 (2), art. n. 15
26. Anand, P.; Nair, H.B.; Sung, B.; Kunnumakkara, A.B.; Yadav, V.R.; Tekmal, R.R.; Aggarwal, B.B. Design of curcumin-loaded PLGA nanoparticles formulation with enhanced cellular uptake, and increased bioactivity *in vitro* and superior bioavailability *in vivo*. Biochem Pharmacol 2010, 79, 330–338, 10.1016/j.bcp.2009.09.003
27. Beloqui, A.; Coco, R.; Memvanga, P.B.; Ucakar, B.; des Rieux A.; Preat, V. pH-sensitive nanoparticles for colonic delivery of curcumin in inflammatory bowel disease. Int J Pharm 2014, 473, 203–212, 10.1016/j.ijpharm.2014.07.009.
28. Chuah, L.H.; Roberts, C.J.; Billa, N.; Abdullah, S.; Rosli, R. Cellular uptake and anticancer effects of mucoadhesive curcumin-containing chitosan nanoparticles. Colloids Surf B Biointerfaces 2014, 116, 228–236, 10.1016/j.colsurfb.2014.01.007
29. Bouchemal, K.; Briancon, S.; Perrier, E.; Fessi, H. Nanoemulsion formulation using spontaneous emulsification: solvent, oil and surfactant optimization. Int J Pharm 2004, 280, 241–251.
30. Kaminaga, Y.; Nagatsu, A.; Akiyama, T.; Sugimoto, N.; Yamazaki, T.; Maitani, T.; Mizukami, H. Production of unnatural glucosides of curcumin with drastically enhanced water solubility by cell suspension cultures of Catharanthus roseus. FEBS Lett. 2003, 555, 311–316
31. He, P.; Davis, S.S.; Illum, L. *In vitro* evaluation of the mucoadhesive properties of chitosan microspheres. Int J Pharm 1998, 166, 75-68.
32. Bonferoni, M.C.; Sandri, G.; Ferrari, F.; Rossi, S.; Larghi, V.; Zambito, Y.; Caramella, C. Comparison of different *in vitro* and *ex vivo* methods to evaluate mucoadhesion of glycol-palmitoyl chitosan micelles. J Drug Deliv Sci Technol 2010, 20, 419-424.
33. Yallapu, M.M.; Gupta, B.K.; Jaggi, M.; Chauhan, S.C. Fabrication of curcumin encapsulated PLGA nanoparticles for improved therapeutic effects in metastatic cancer cells. J Colloid Interface Sci. 2010, 351, 19–29, 10.1016/j.jcis.2010.05.022
34. Mohanty, C.; Sahoo, S.K. The *in vitro* stability and *in vivo* pharmacokinetics of curcumin prepared as an aqueous nanoparticulate formulation. Biomaterials 2010, 31, 6597-611, 10.1016/j.biomaterials.2010.04.062.
35. Nafee, N.; Schneider, M.; Schaefer, U.F.; Lehr, C.M. Relevance of the colloidal stability of chitosan/PLGA nanoparticles on their cytotoxicity profile. Int J Pharm 2009, 381, 130–139.
36. Bonferoni, M.C.; Sandri, G.; Dellera, E.; Rossi, S.; Ferrari, F.; Zambito, Y.; Caramella, C. Palmitoyl Glycol Chitosan Micelles for Corneal Delivery of Cyclosporine. J Biomed Nanotechnol. 2016, 12, 231-40.
37. Mukerjee, A.; Vishwanatha, J.K. Formulation, characterization and evaluation of curcumin-loaded PLGA nanospheres for cancer therapy. Anticancer Res. 2009, 29, 3867-75
38. Stockert, J.C.; Horobin, R.W.; Colombo, L.L.; Blazquez-Castro, A. Tetrazolium salts and formazan products in Cell Biology: Viability assessment, fluorescence imaging, and labeling perspectives. Acta Histochem. 2018, 120, 159-167. Doi:10.1016/j.acthis.2018.02.005

CHAPTER II

POLYMERIC NANOPARTICLES vs MICELLES: A COMPARATIVE STUDY

Article

Chitosan Oleate Coated Poly Lactic-Glycolic Acid (PLGA) Nanoparticles versus Chitosan Oleate Self-Assembled Polymeric Micelles, Loaded with Resveratrol

Dalila Miele[1], Laura Catenacci[1], Milena Sorrenti[1], Silvia Rossi[1], Giuseppina Sandri[1], Lorenzo Malavasi[2], Giacomo Dacarro[2], Franca Ferrari[1] and Maria Cristina Bonferoni[1]*.

[1] Department of Drug Sciences, University of Pavia, Viale Taramelli 12, 27100 Pavia, Italy
[2] Department of Chemistry, University of Pavia, Viale Taramelli 14, 27100 Pavia, Italy

* Correspondence: cbonferoni@unipv.it; Tel.: +39-0382-987375

Received: 30 July 2019; Accepted: 28 August 2019; Published: 1 September 2019

Miele D. et al. "Chitosan Oleate Coated Poly Lactic-Glycolic Acid (PLGA) Nanoparticles versus Chitosan Oleate Self-Assembled Polymeric Micelles, Loaded with Resveratrol." *Marine drugs* 17, 9, 2019: 515-535.

ABSTRACT

Chitosan oleate (CS-OA), a chitosan salt with amphiphilic properties, has demonstrated the ability to self-assemble in aqueous environment to give polymeric micelles useful to load poorly soluble drugs. More recently, CS-OA was proposed to stabilize nanoemulsions during the preparation by emulsification and solvent evaporation of poly lactic-glycolic acid (PLGA) nanoparticles (NPs) loaded with curcumin. Positive mucoadhesive behavior and internalization properties were demonstrated for these NPs attributable to the presence of positive charge at the NP surface. In the present paper, two CS-OA-based nanosystems, micelles and PLGA NPs, were compared with the aim of elucidating their physico-chemical characteristics, and especially their interaction with cell substrates. The two systems were loaded with resveratrol (RSV), a hydrophobic polyphenol endowed with anti-cancerogenic, anti-inflammatory, and heart/brain protective effects, but with low bioavailability mainly due to poor aqueous solubility. Calorimetric analysis and X-ray spectra demonstrated amorphization of RSV, confirming its affinity for hydrophobic domains of polymeric micelles and PLGA core of NPs. TGA decomposition patterns suggest higher stability of PLGA-NPs compared with polymeric micelles, that anyway resulted more stable than expected, considering the RSV release profiles, and the cell line interaction results.

1. Introduction

Many reports have been focused on the preparation and on the possible exploitation of amphiphilic derivatives of chitosan[1]. Chitosan (CS) and chitosan derivatives have been hydrophobically modified by interaction with different hydrophobic pendant groups, usually by covalent derivatization[2–6]. Less common in the literature is the design and characterization of amphiphilic derivatives based on ionic interaction between the polymer and the hydrophobic moieties[7,8]. Amphiphilic polymers are known for their ability to self-assemble into nanoparticles with a hydrophobic core or inner hydrophobic domains and outer shell layers made by the chains of the polymer hydrophilic portions. This mechanism, common to polymeric micelles, was also previously shown for chitosan oleate (CS-OA), a chitosan salt with amphiphilic properties and whose self-assembling in aqueous environment resulted suitable to efficiently load hydrophobic poorly soluble molecules[7,9]. In the case of chitosan amphiphilic derivatives, this behavior results in nanocarriers that maintain the favorable biological properties of the polysaccharide, among which are mucoadhesion, penetration enhancement, or antibacterial effect [1,6,10,11]. More recently, CS-OA was proposed to stabilize nanoemulsions during the preparation by emulsification and solvent evaporation of poly lactic-glycolic acid (PLGA) nanoparticles (NPs). It was demonstrated that the resulting NPs were suitably loaded with curcumin in the PLGA hydrophobic core and maintained a chitosan shell on the surface. They were characterized by a positive charge promoting cell internalization and mucoadhesive behavior[12].These results were in line with the relevance of surface modification of polymeric nanoparticles that has been evidenced in recent literature pointing out the positive effect of surface cationic charge on the interaction with biological substrates[13,14]. Some more work to elucidate the physico-chemical characteristics of these CS-OA-based nanosystems, and especially their interaction with cell substrates seems, however, still to be necessary. This goal was afforded in the present paper by comparing CS-OA micelles and CS-OA PLGA NPs. Although both of the nanosystems compared are based on CS-OA, they present quite different structural characteristics. In the case of polymeric micelles, CS-OA represents the only component of the carrier, and the hydrophobic domains are represented by the self-assembled chains of oleic acid[7]. In the case of PLGA NPs, CS-OA is layered around the NPs, whose core is made by a matrix of the biodegradable polymer[12]. Therefore, different behavior could be envisaged for the two systems, concerning not only drug loading or release, but also interaction with cell substrates. A close comparison could guide in the future choice of the most suitable carrier according to the therapeutic objective. The two carriers were loaded with resveratrol (RSV), a hydrophobic polyphenol from the stilbene family with interesting biological properties, strongly studied for its benefits in human health, such as anti-cancerogenic, anti-inflammatory, and heart/brain protective effects[15–17], but with low bioavailability due to poor aqueous solubility[18,19]. Most RSV benefits are, like for other polyphenols, strictly concentration dependent, so that at low concentrations, the antioxidant effect prevails, and RSV has a cancer preventive and anti-inflammatory protective effect, while at high concentrations pro-oxidant effect occurs, and ROS produced by RSV contribute to cancer cell growth arrest[20]. The concentration-dependent interaction of the RSV and RSV loaded NPs with cell substrates therefore seems especially useful to elucidate. In the present paper, the viability of

two cell lines, Caco-2 cells, and Hela cells was studied following exposure to different concentrations of RSV in CS-OA-based micelles or NPs.

2. Results and discussion

2.1. Particle Size and Zeta Potential

The effect of CS concentration and of CS:oleic acid (OA) ratio on dimensions of CS-OA-based micelles was previously studied, indicating that higher concentration corresponded to larger dimensions, while no differences could be seen when 1:1 or 1:0.5 CS:OA molar ratio were compared [9]. For this reason, CS 0.05% (w/v) and a CS:OA molar ratio of 1:0.5 were used here. The relevance of CS-OA concentration on particle size was investigated for PLGA-NPs. The final concentration of CS-OA was varied among 4.8, 2.4, and 1.2 mg/mL, corresponding to a PLGA:CS-OA ratio in the final systems of 1.5:1, 3:1 and 6:1, respectively. **Figure 1** shows the occurrence of a relevant and statistically significant decrease in particle size with a decrease in CS concentration from 4.8 to 1.2 mg/mL (one-way ANOVA, post-hoc Fisher's test). This result does not seem to be in line with what had previously been observed[12], where a decrease in dimensions was seen when CS concentration was increased, an effect that was probably attributable to the distribution of CS-OA at the oil/water interface. It must be pointed out that in the present case, the range of CS concentration was higher than in the previous study. In the case of 4.8 and 2.4 mg/mL, the result can therefore be explained by the presence of excess CS-OA with respect to the amount necessary to saturate the droplet surface. As the amphiphilic character of the modified polymer determines its layering around the hydrophobic surface of the nanoemulsion droplets during NPs preparation, we can imagine that the exceeding CS-OA amount is not dispersed as well as the CS-OA that layers at the droplets' surface, and a possible aggregation can occur.

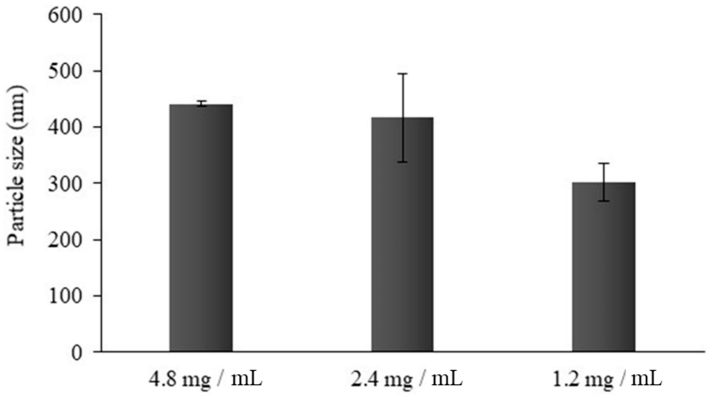

Figure 1. Average particle size (nm) of PLGA-NPs prepared with different CS-OA concentrations, corresponding to 1.5:1, 3:1 and 6:1 PLGA:CS-OA ratios (mean ± s.d.; n = 10).

On the basis of these data, a batch of PLGA-NPs was used in the present study, prepared with a CS-OA concentration of 1.2 mg/mL. The dimensions, the polydispersity index (PI), and the zeta potential of these NPs are reported in **Table 1** for comparison with polymeric CS-OA micelles. The dimensional characterization of the RSV-loaded nanosystems is reported too. Both polymeric micelles and PLGA-NPs are characterized by a particle size in the nanometric range (250–300 nm), and a PI between 0.2 and 0.5, in line with results

reported in previous work about similar systems[7,12], confirming the suitability of the preparation methods to obtain colloidal nanosystems with acceptable dispersion. The values of zeta potential are confirmed to be strongly positive for the unloaded nanosystems, in accordance with previous results[12], and RSV loading did not change these values.

Table 1. Comparison between the dimensions of the two nanosystems, both unloaded and loaded with RSV (mean ± s.d.; n = 3).

		Mean Diameter (nm) ± sd	**PI ± sd**	**Zeta Potential (mV) ± sd**
unloaded	Micelles	266 ± 1	0.51 ± 0.08	54.1 ± 1.2
	PLGA-NPs	300 ± 4	0.53 ± 0.03	53.6 ± 0.8
RSV loaded	Micelles	289 ± 13	0.33 ± 0.06	57.9 ± 1.1
	PLGA-NPs	273 ± 3	0.24 ± 0.02	54.6 ± 1.2

2.2. Encapsulation Efficiency and Drug Loading

Figure 2 shows the encapsulation efficiency (EE%), drug loading (DL%) values and final RSV concentration for both nanosystems. In NPs, RSV is entrapped in the inner lipophilic PLGA core during emulsification with CS-OA, while in polymeric micelles, it is positioned among the fatty acid chains during the occurrence of self-assembling micelle hydrophobic domains. As illustrated, RSV is efficiently loaded in polymeric NPs with an EE% value two-fold higher than in micelles (**Figure 2a**). The DL% values (**Figure 2b**) are in line with those of EE and support the different distribution of RSV into the two types of nanosystems. **Figure 2c** illustrates the final concentrations of RSV in colloidal dispersions of micelles and PLGA-NPs compared to RSV saturated solution. The increase in concentration is about three times in the case of polymeric micelles, and about ten times in the case of NPs, suggesting the potential positive effect of both nanosystems in overcoming the bioavailability problems of RSV due to its low solubility. The results obtained evidence the higher efficiency of NPs as a carrier with respect to polymeric micelles, probably due to the presence of the PLGA core, in which more RSV molecules can be loaded with respect to the hydrophobic domains occurring by self-assembling of oleic acid chains inside the CS-OA polymeric micelles.

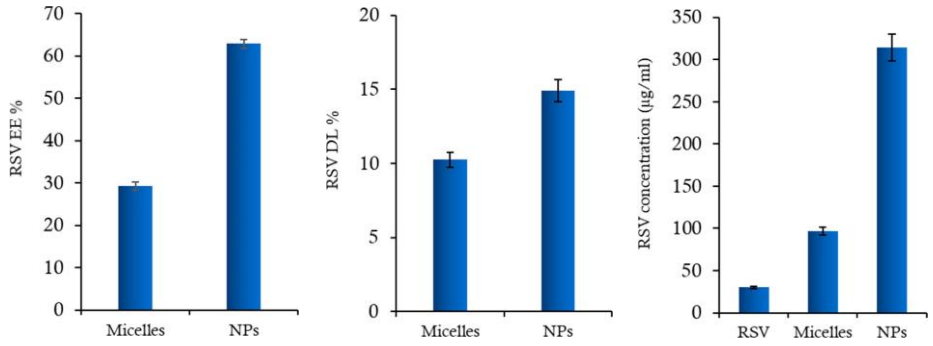

a **b** **c**

Figure 2. (**a**) Encapsulation efficiency (EE%), (**b**) drug loading (DL%) and (**c**) final RSV concentration, compared with RSV saturated solution (RSV), for polymeric micelles and PLGA NPs (mean values ± s.d.; n = 3).

2.3. Physico-Chemical Characterization

2.3.1. Thermal Analysis Characterization

The results of DSC analysis performed on both the nanosystems, unloaded and RSV loaded, are given in **Figures 3** and **4** for micelles and PLGA-NPs, respectively.

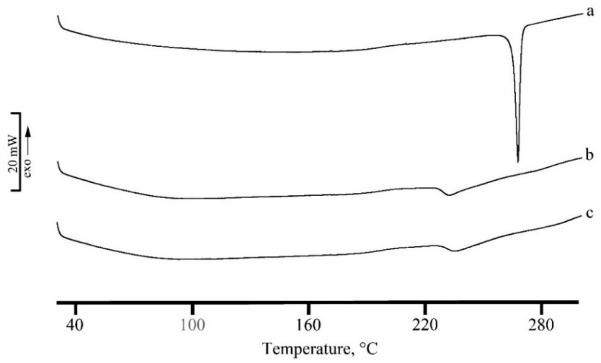

Figure 3. DSC profiles of RSV (**a**), unloaded micelles (**b**), and RSV loaded micelles (**c**). The y bar scale corresponds to 20 mW.

RSV is a commercial microcrystalline white powder with a thermal profile typical of an anhydrous drug (**Figure 3a)** with a melting endothermic effect at $T_{peak,m}$ = 265.1 °C ($T_{onset,m}$ = 263.1 °C; ΔH_m = 281 J g^{-1}). This peak disappeared in the DSC profile of RSV loaded micelles where only an exo-endothermic effect due to CS-OA decomposition is recorded (Figure3curve c). This thermal profile suggests the encapsulation of RSV in the micellar structure. A similar thermal behavior is recorded for PLGA-NPs, where the entrapment of RSV in NPs and its homogeneous dispersion in the polymeric matrix is confirmed by the disappearance of its melting effect in DSC curve of RSV loaded NPs (**Figure 4b**). In **Figures 5** and **6**, the TGA curves of the unloaded (curves a) and loaded (curves b) nanosystems are reported for micelles and NPs, respectively. The first mass loss (about 7%) is due to the dehydration of the lyophilized samples and the second one to decomposition. The presence of RSV does not influence the thermal stability for NP systems that show exactly the same temperatures of onset ($T_{onset, dec}$ = 189.2 ± 0.3 °C) and very close temperatures of peak (maximum rate of weight loss), as obtained from the calculation of the first derivative (about 279 °C for both the systems). In the case of the micelles, the same temperature of peak was observed for unloaded and loaded samples ($T_{onset, dec}$ =165.8 ± 0.2 °C). A small difference in decomposition peak temperatures can be evidenced in this case between 237 ± 2 °C for the unloaded sample and 243 ± 3 °C for the RSV loaded one, suggesting quite a small stabilization effect due to the presence of the drug. As the self-assembling of the NPs is driven by the hydrophobic interactions between fatty acid moieties, it seems conceivable that the presence of the hydrophobic molecule of RSV plays a stabilization effect. This mechanism could be even more relevant in the case of PLGA-NPs, in which the fatty acid chains interact during the preparation, with the hydrophobic PLGA core of the NPs. These in fact appear to be more stable than micelles, with higher values of thermal stability (189 °C versus 166 °C for $T_{onset,dec}$ and 279 °C versus about 237–243 °C for $T_{peak,dec}$).

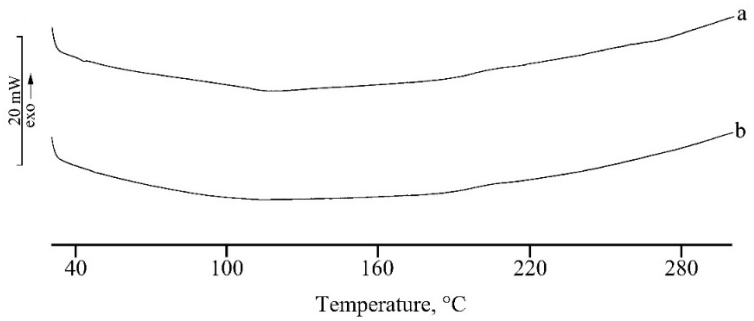

Figure 4. DSC profiles of unloaded PLGA-NPs (a), and RSV loaded PLGA-NPs (b). The y bar scale corresponds to 20 mW.

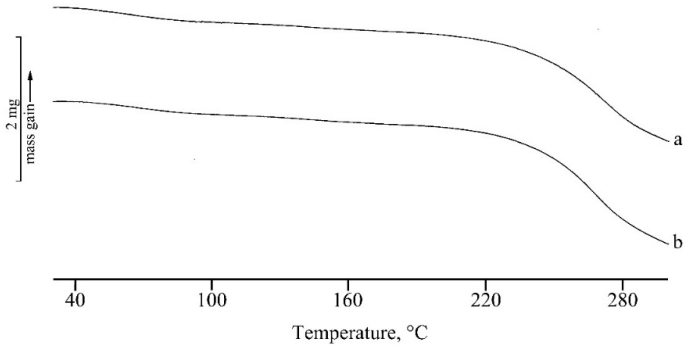

Figure 5. TGA curves of unloaded (**a**) and RSV-loaded (**b**) micelles. The y bar scale corresponds to 2 mg of weight variation.

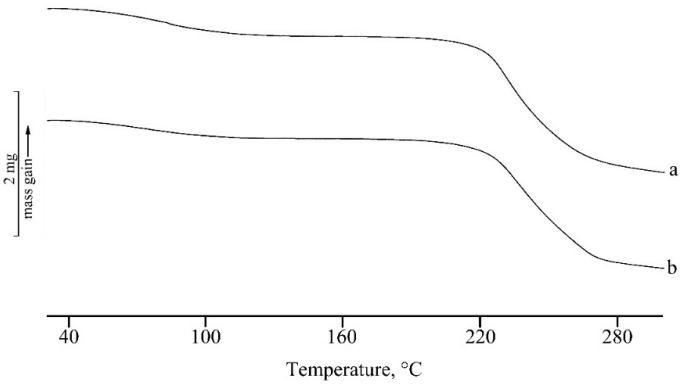

Figure 6. TGA curves of unloaded (**a**) and RSV-loaded (**b**) PLGA-NPs. The y bar scale corresponds to 2 mg of weight variation

2.3.2. ATR Fourier-Transform Infrared (FT-IR) Spectroscopy

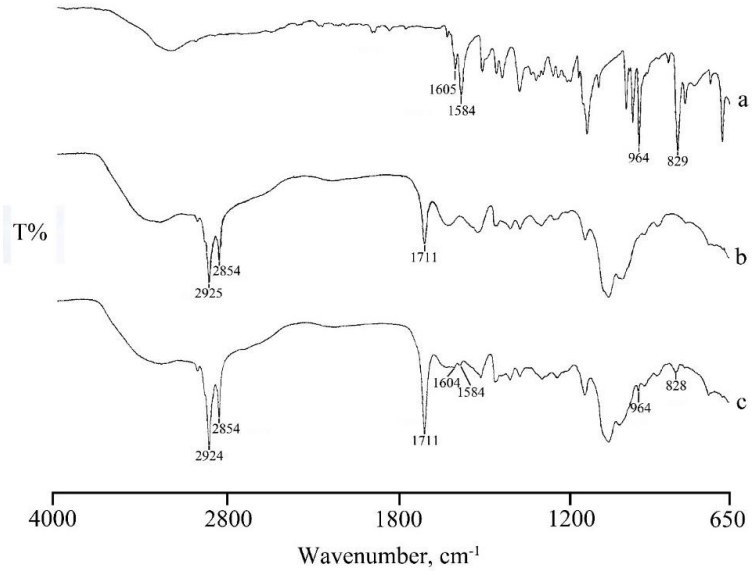

Figure 7. FTIR spectra of RSV (a), and unloaded (b) and RSV-loaded (c) micelles.

The FT-IR spectrum of RSV (**Figure 7a**) presents a broad band at around 3200 cm^{-1} due to the O-H stretching vibration, a set of typical bands at 1605, 1584 cm^{-1} corresponding to C-C aromatic double bond stretching and C-C olefinic stretching, respectively, a band at 964 cm^{-1} attributable to trans olefinic bond, and a band at 829 cm^{-1} due to the bending vibration band of C-H in aromatic rings[21]. In the FT-IR spectrum of RSV loaded micelles (**Figure 7c**) in addition to the characteristic band of CS-OA C=O stretching at 1711 cm^{-1}, the presence of the typical RSV bands suggest that RSV was encapsulated in the core of the micelles through hydrophobic interactions, supporting the thermal data. Also, in NP systems the loading of RSV is confirmed by the FT-IR spectra (**Figure 8**). The spectrum of NPs (**Figure 8** spectrum a) shows bands at 1750 cm^{-1} and 1711 cm^{-1} due to stretching vibration of C=O in PLGA and in CS-OA, respectively, and a band at 1636 cm^{-1} due to C-O-O stretching vibration of PLGA. The same bands appear also in the RSV-NPs sample (**Figure 8b**) where the characteristic bands of RSV loaded in the polymeric material are also evident.

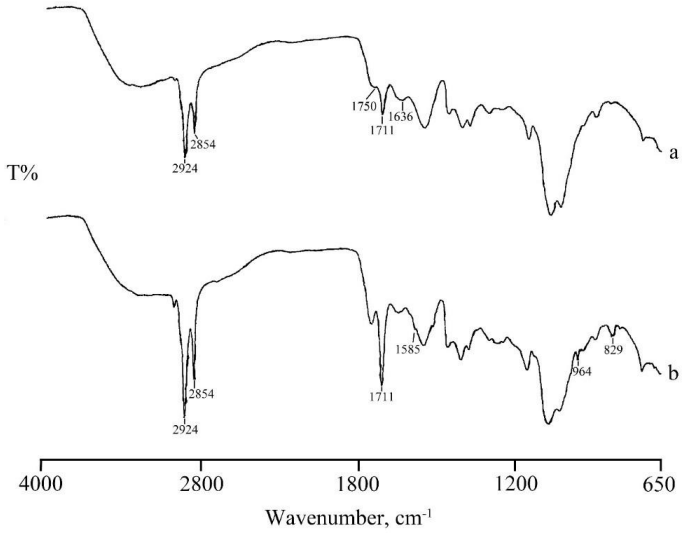

Figure 8. FTIR spectra of PLGA-NPs: unloaded (**a**) and RSV-loaded (**b**).

2.3.3. X-ray Diffraction Characterization

The XRD patterns of micelles and PLGA-NPs are reported in **Figure 9a, b**, respectively. In both Figures, the black curve refers to unloaded nanosystems, the red one to nanosystems loaded with RSV, whose diffraction pattern is reported in the inset.

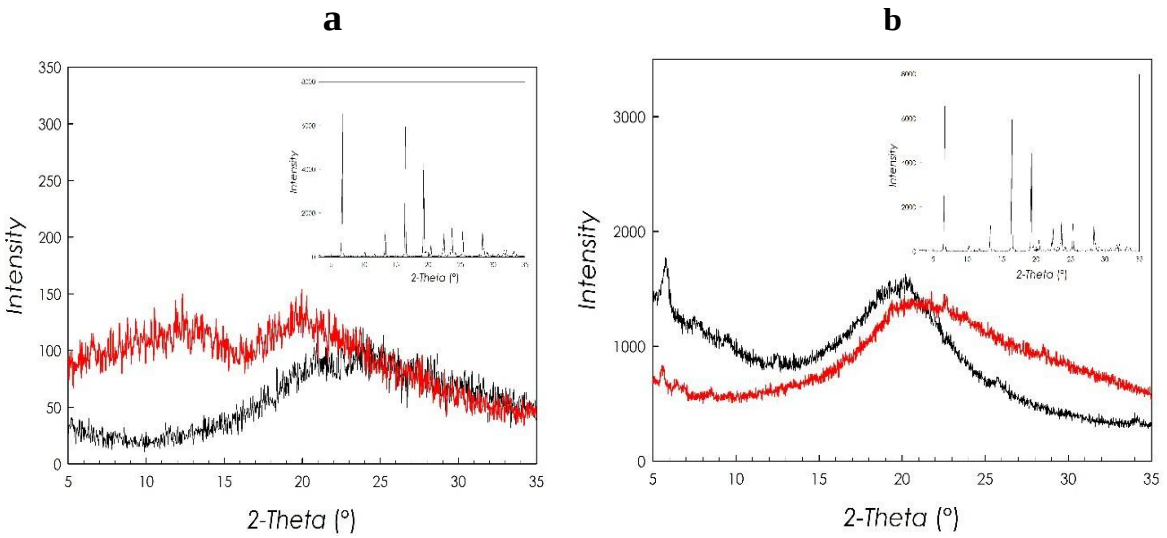

Figure 9. (**a**) XRD pattern of unloaded micelles (black curve) and RSV-loaded micelles (red curve); (**b**) XRD pattern of unloaded NPs (black curve) and RSV-loaded NPs (red curve); in both Figures the XRD pattern of RSV is reported in the inset.

It is possible to see that both unloaded systems present a typical diffraction pattern, pertaining to an amorphous system. This characteristic is also found in the samples loaded with RSV. On the other hand, the diffraction pattern of the RSV shows the typical features of a good crystalline material with well-defined and narrow diffraction peaks. The absence of any diffraction in the patterns of RSV loaded micelles and NPs allows to conclude that RSV becomes amorphous during the preparation of both nanosytems, confirming the results of the DSC analysis. This result suggests that RSV is dispersed at the molecular level both inside the hydrophobic domains of the polymeric micelles and inside the PLGA polymeric matrix, which represents the core of CS-OA-coated PLGA NPs. It can be argued that this is due to the good affinity of the drug for the fatty acid and for the PLGA chains inside the two nanocarriers.

2.4. Drug Release Profiles

In **Figure 10,** the release profiles of RSV from the two types of nanosystems are reported. In both cases, a fast-initial release was followed by a slower phase. This seemed conceivable for PLGA NPs, that require polymer degradation to complete the RSV release from the inner core[22]. The degradation depends on several factors, encompassing polymer characteristics, but also the presence of the drug and of other components, the particle dimensions and the environmental conditions, and it is likely to require some days to be completed[23]. For the micelle system, a slightly higher release profile was observed, as at each time point, a greater % of RSV was released from micelles than from PLGA-NPs. However, the difference did never exceed 12%, indicating that the structure of micelles was more tough than it could be expected considering that it is based on weak electrostatic and hydrophobic interactions. It can be argued that the high number of interactions involved along a single chitosan chain can anyway stabilize the NPs, despite their weak nature, and of the potential sensitivity to the presence of salts in the release medium.

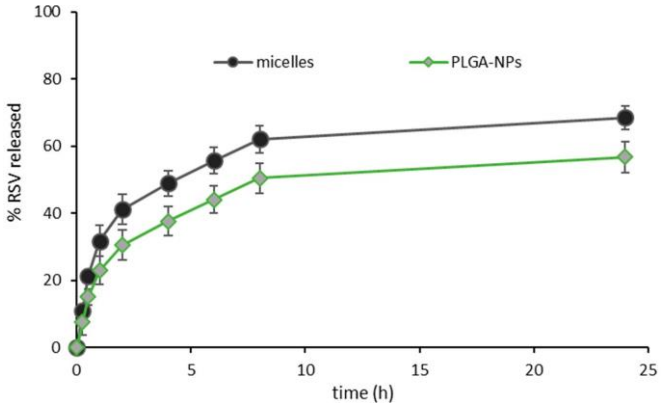

Figure 10. RSV release profiles from micelles and PLGA-NPs (mean values ± s.d.; n = 3).

2.5. Biocompatibility

The results of the MTT test carried out on the two cell lines, Caco-2 and HeLa, are shown in **Figures 11** and **12**, respectively. The percentage of viability after treatment with the two loaded nanosystems (**Figures 11b** and **12b**) is compared with the values measured after contact with free RSV, tested at same concentrations. Unloaded systems were assessed at concentrations comparable to those used for RSV loaded ones (**Figures 11a** and **12a**).

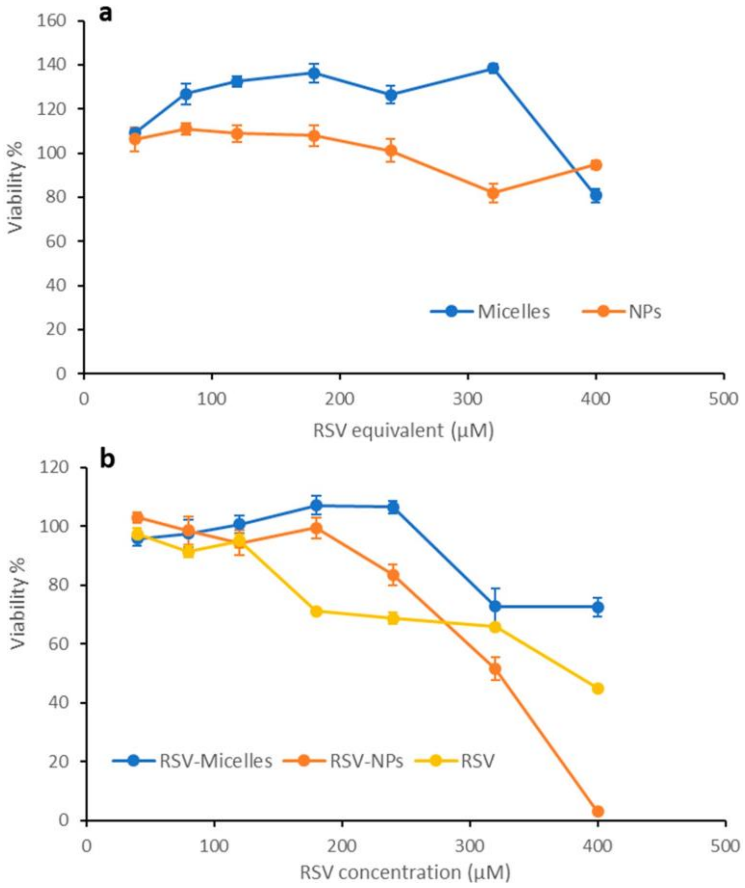

Figure 11. Viability of CaCo-2 cells treated with free RSV or nanosystems based on CS-OA, as a function of RSV concentration. Unloaded nanosystems were tested at the same concentrations of the loaded ones (indicated as RSV equivalent concentration). (**a**) Unloaded nanosystems; (**b**) free RSV and RSV-loaded nanosystems (mean values ± s.d.; n = 8).

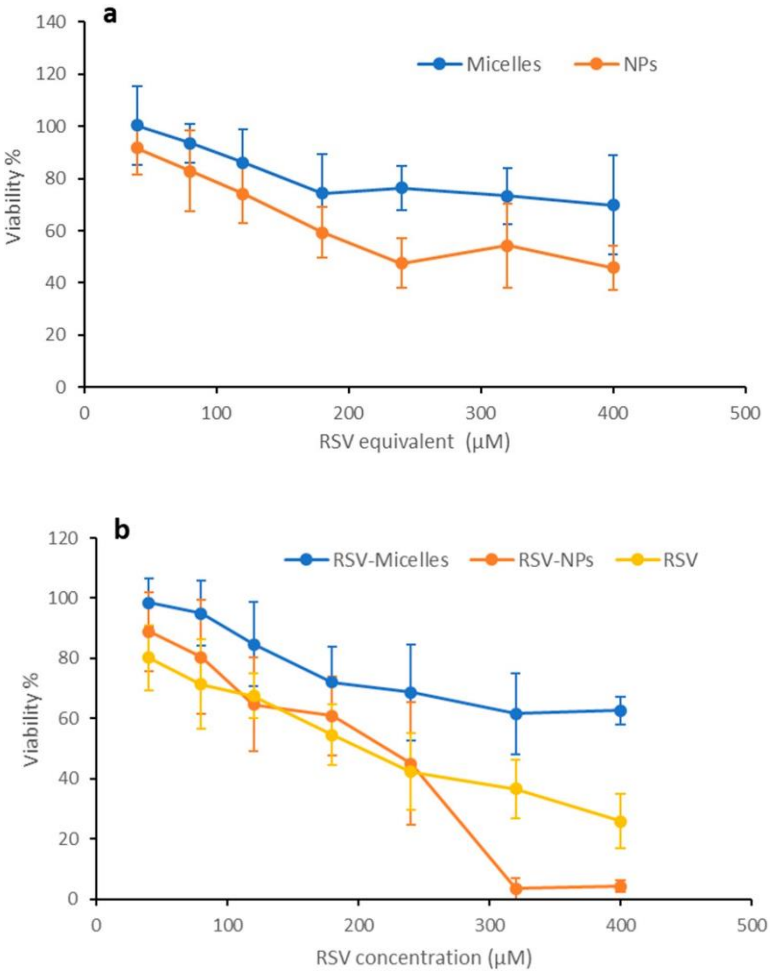

Figure 12. Viability of HeLa cells treated with free RSV or nanosystems based on CS-OA as a function of RSV concentration. Unloaded nanosystems were tested at the same concentrations of the loaded ones (indicated as RSV equivalent concentration). (**a**) Unloaded nanosystems; (**b**) free RSV and RSV-loaded nanosystems (mean values ± s.d.; n = 8).

Looking at the unloaded systems, no considerable cytotoxic effects took place when Caco-2 cells were treated with both nanosystems, that resulted compatible with good cell vitality (more than 80%) until the highest concentration (**Figure 11a**). HeLa cells (**Figure 12a**) resulted more sensitive to the exposure to unloaded micelles, with a viability of about 70% at the highest concentration, and especially to the exposure to PLGA-NPs, that induced a residual viability of about 45% at the highest concentration tested. These same differences between the two cell lines can be seen in the case of free RSV and of RSV loaded nanosystems (**Figures 11b** and **12b**). Concerning free RSV, the results here obtained are in line with those reported in the literature [24,25]. In contrast, when the Caco-2 cell line was exposed to RSV-loaded nanosystems, a more evident dose-dependent cytotoxic effect is revealed; in particular, in the case of PLGA-NPs, a higher and significant reduction in viability in comparison with free RSV and polymeric micelles occurs (**Figure 11b**). While viability for micelles remains above that of free RSV, in the case of PLGA-NPs at the highest concentrations (300 and 400 μM) the viability is lower than for free RSV. These results are in line with similar data obtained with other colon cancer cell lines such as HT29 and LS147T [25]. HeLa cells appear more sensitive than Caco-2 cells to the treatment with unloaded nanosystems, with viability levels lower than in the case of Caco-2 cell line. In the case of RSV loaded nanosystems, however, a quite similar trend can be observed for the two cell lines. For PLGA-NPs, viability decreases more quickly with concentration increase than in the case of free RSV and of RSV loaded micelles. As shown in **Figure 12b**, for polymeric micelles cell viability remained higher than for RSV at all concentrations. With a trend quite similar to that observed in Caco-2 cells, PLGA-NPs at concentrations higher than 250 μM seems to determine higher cytotoxicity with respect to free RSV. This difference suggests that the different structure of nanosystems can markedly affect their interaction with the cell substrate, conceivably due to different amount of drug internalization. In this process, a role is conceivably played by CS-OA, which thanks to its hydrophilic/hydrophobic balance and to the presence of positive surface charges, makes the colloidal systems suitable for stronger interaction with the cell membranes, and more efficiently subject to endocytosis[26].

2.6. Cell Internalization Properties

In **Figure 13**, Laser Scanning Confocal Microscopy (CLSM) photographs of Caco-2 and HeLa cell lines treated with polymeric micelles and PLGA-NPs loaded with Nile red are reported. Confocal images confirm the presence of Nile red fluorescence signal inside the cells in all the samples; in particular, the red dye appears not only around, but also close to the blue-stained nuclei, as it is possible to appreciate by looking at the Z-axis projections (arrows). The localization of red staining in well-defined spots suggests the internalization of the nanosystems instead of the Nile red released from them. However, to better investigate this aspect, both micelles and PLGA-NPs were prepared using as stabilizer rhodamine labeled CS-OA[27]. In this case, the red staining indicates the presence of the labeled polymer. CLSM images of Caco-2 cells treated with these nanosystems (**Figure 14**) show the internalization of rhodamine, with a localization in the cytosol and close to the nuclei, similarly to what was previously observed for Nile red-loaded nanosystems. This result suggests that both nanocarriers are effectively included in the cells. It is conceivable that the nanometric particle

size of both nanosystems and the ability of interaction of positively charged chitosan shell with cell membranes played a role in triggering an endocytic mechanism.

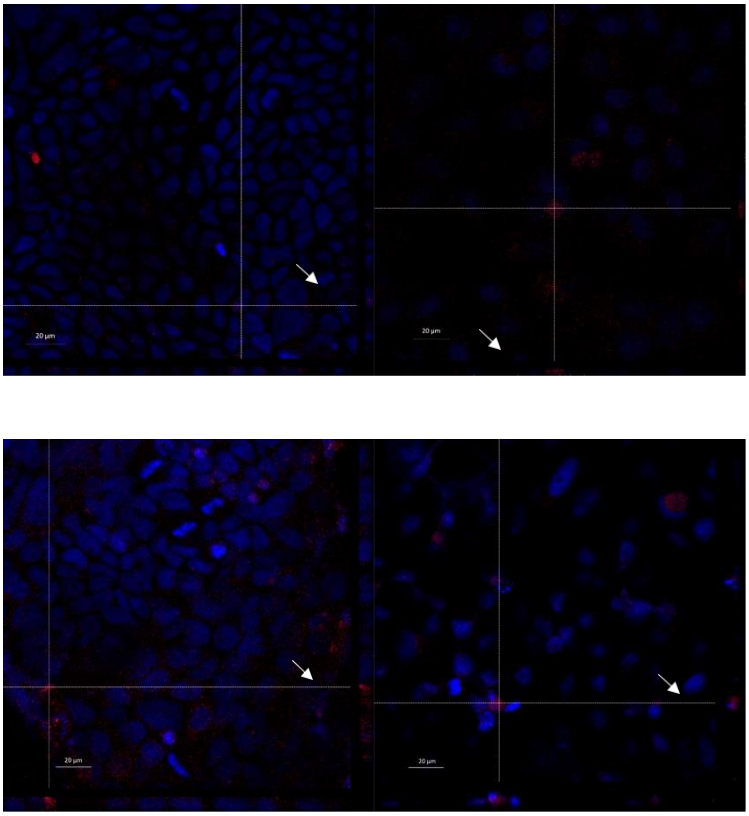

Figure 13. CLSM of Caco-2 and HeLa cells treated with the two nanosystems loaded with Nile red. (**a**) Micelles on Caco-2 cells, (**b**) micelles on Hela cells, (**c**) PLGA-NPs on Caco-2 cells, (**d**) PLGA-NPs on HeLa cells.

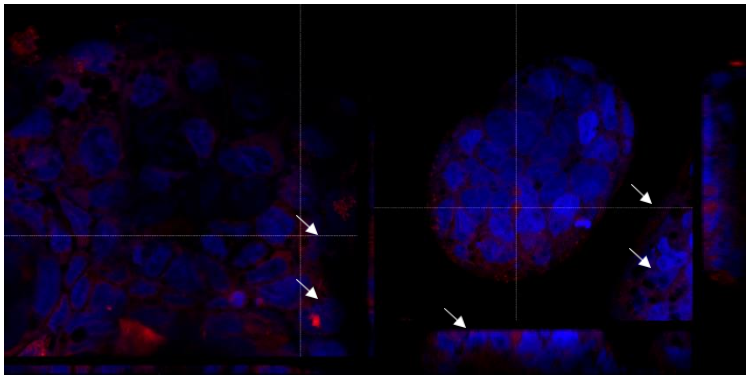

Figure 14. CLSM of Caco-2 cells treated with nanosystems prepared with CS-OA rhodamine labeled. (**a**) Micelles, (**b**) PLGA-NPs.

CLSM visualization does not allow a clear differentiation between the samples treated with PLGA-NPs and micelles, in line with the structure of micelles more tough than expected, as evidenced by the RSV release test. However, the biocompatibility test suggests a different behavior for the two nanosystems, which can be explained by the hypothesis that the micelles have a less compact structure and lower stability with respect to PLGA-NPs, which is suggested also by thermal analysis.

3. Materials and Methods

- *Materials*

Chitosan LMW (CS) (80% Deacetylation Degree, DD), Poly lactic-glycolic acid (PLGA) (Resomer RG 503H), Nile red were purchased from Sigma-Aldrich (Milan, Italy). Oleic acid (OA) was purchased from Fluka (Milan, Italy) and 99% Pure Trans-Resveratrol (RSV) from Mega Resveratrol (Candlewood Stars Inc., Danbury, CT, U.S.A.). Acetone, ethyl acetate, acetic acid, sodium acetate, and methanol were acquired from Carlo Erba (Milan, Italy).

- *Methods*

3.1. Preparation of the Nanosystems

As reported in previous works[7,9], polymeric micelles were obtained starting from a 0.5 mg/mL chitosan HCl solution. HCl salt was in turn obtained from low molecular weight (LMW) chitosan base, deacetylation degree (DD) 80% (Sigma-Aldrich, Milan, Italy), by addition of HCl 0.5 N to chitosan until complete dissolution, dialysis in bidistilled water for 24 h and freeze-drying (HetoDrywinner, Analitica de Mori, Milan, Italy). Considering the 80% DD, the 1:0.5 CS:OA molar ratio corresponded to 0.7 mg of oleic acid per each mg of chitosan. OA was dissolved in acetone and dropwise added to the aqueous solution of CS under stirring. After solvent evaporation under stirring overnight, a micelle dispersion was obtained, that was sonicated (Elmasonic S 80 H, Elma Hans Schmidbauer GmbH & Co, Singen, Germany) in an ice bath for 15 min. To obtain loaded micelles, RSV was dissolved in acetone together with OA, at a final concentration of 0.33 mg/mL. To remove RSV not encapsulated the samples were centrifuged (ALC 4218 centrifuge) for 10 min at 3000 rpm. RSV loaded micelles were prepared in amber glass vials.

To prepare PLGA-NPs, CS was added to 100 mL of bidistilled water under magnetic stirring (300 rpm) containing 250 µL of glacial acetic acid to obtain a 1% w/w polymer concentration. To functionalize the 50% of CS binding sites with OA, a stoichiometric amount of fatty acid was solubilized in acetone and added dropwise to the CS solution, to obtain chitosan oleate (CS-OA). After acetone evaporation, CS-OA was freeze dried.

Freeze-dried CS-OA was employed to obtain PLGA-NPs by partially modifying the solvent evaporation method previously described[12]. CS-OA was dispersed in 3 mL of distilled water and 0.25 mL of ethyl acetate solution containing 24 mg/mL of PLGA were added during the emulsification step. This step was carried out at 20,500 rpm by means of Ultra-Turrax T25 (Janke & Kunkel, IKA® Labortechnik, Germany) equipped with 8 mm probe (S25 N-8 G). After 5 min, 7 mL of distilled water was added, and emulsification was carried out for further 5 min. Then, ethyl acetate was removed under stirring overnight. The weight lost due to evaporation was determined and the initial volume (10 mL) was reconstituted with distilled water. Finally, NPs were sonicated for 15 min in an ice bath and centrifuged for 10 min at 3000 rpm. Different CS-OA concentrations were employed (4.8, 2.4 and 1.2 mg/mL). To obtain RSV-loaded PLGA-NPs, RSV was added to the organic phase together with PLGA, in a final concentration of 0.5 mg/mL. RSV-loaded NPs were prepared in amber glass vials.

Rhodamine-labeled CS was obtained according to the literature[27]. Briefly, 200 mg of CS was dissolved in 20 mL of acetic acid overnight. 20 mL of anhydrous methanol was added to the solution under magnetic stirring for 3 h, and nitrogen was flushed for 15 min to remove the oxygen present. 13.8 mg of rhodamine B isothiocyanate (RITC) (Sigma Aldrich, Milan, Italy) was solubilized in anhydrous methanol at a concentration of 2 mg/mL and added dropwise to the CS solution under constant stirring. The reaction was kept at room temperature and in the dark for 18 h. CS-RITC was precipitated using 10 N NaOH. Dialysis cycles in distilled water, in HCl 0.5 N, and in distilled water again were performed before freeze drying.

3.2. Particle Size and Zeta Potential

The mean particle size and the polydispersity index (PI) of the samples were assessed by means of Photon Correlation Spectroscopy (PCS; N5 submicron particle size analyzer, Beckman Coulter, Milan, Italy). Analyses were carried out at a 90° detection angle, at room temperature, by diluting 50 µL of the sample in 3 mL of distilled and filtered (0.22 µm) water. PI is a measure of particle size distribution usually ranging between 0.05 for highly monodisperse samples and 0.7 for broadly dispersed ones. Zeta potential was evaluated by a Zetasizer® nano series (Malvern Instruments Ltd., Worcestershire, United Kingdom) in aqueous suspension, with conductivity ranging between 0.263 and 0.479 mS/cm, by setting a dielectric constant of 78.5 and a refractive index of 1.33.

3.3. Encapsulation Efficiency and Drug Loading

The % RSV amount encapsulated in the nanosystems was calculated by difference according to Equation (1). The nanosystems were centrifuged at 3000 rpm for 10 min. The free drug precipitated was solubilized in mobile phase and analyzed by HPLC (Perkin-Elmer Series 200 HPLC) equipped with a C18 column (125 Angstrom, Waters, 150-mm length, 4.6-mm inner diameter, packing size 10 µm) and using as mobile phase methanol:water:acetic acid 52:48:0.05 (*v*/*v*). The analysis was performed at 25 °C in isocratic conditions (flow rate 1 mL/min), using UV detection at 303 nm wavelength. Injection volume was 20 µL.

% encapsulation efficiency was measured according to the following Equation (1):

$$\%EE = \frac{Wi - Wf}{Wi} \times 100 \quad (1)$$

where Wi = total drug amount; Wf = free drug amount.

Based on the results of EE%, the percentage drug loading (%DL) was calculated using the following

Equation (2):

$$\%DL = \frac{We}{We + Wexcipients} \times 100 \quad (2)$$

where We = encapsulated drug amount, derived from EE%; Wexcipients = excipients amount in the nanosystems.

RSV concentration in final colloidal solution was calculated by difference between the initial RSV concentration and the RSV amount not encapsulated and removed by centrifugation.

3.4. Physico-Chemical Characterization

3.4.1. Differential Scanning Calorimetry (DSC)

DSC analyses were performed with a Mettler STAR^e system (Mettler Toledo, Novate Milanese, MI, Italy) equipped with a DSC821^e Module and an Intracooler device for sub-ambient temperature analysis (Julabo FT 900) on 2–3 mg (Mettler M3 Microbalance) samples in sealed aluminum pans with pierced lid (heating rate $\beta = 10$ K min^{-1}, nitrogen air atmosphere (flux 50 mL min^{-1}), 30–300 °C temperature range). The instrument was previously calibrated with Indium as standard reference. Measurements were carried out at least in triplicate.

3.4.2. Simultaneous Thermogravimetric Analysis (TGA/DSC)

Mass losses were recorded with a Mettler STAR^e system (Mettler Toledo, Novate Milanese, MI, Italy) TGA with simultaneous DSC (TGA/DSC1) on 3–4 mg samples in alumina crucibles with lid (heating rate $\beta = 10$ K min^{-1}, nitrogen air atmosphere (flux 50 mL min^{-1}), 30–300 °C temperature range). The instrument was previously calibrated with Indium as standard reference and measurements were carried out at least in triplicate.

3.4.3. ATR Fourier-Transform Infrared (FT-IR) Spectroscopy

IR spectra were recorded using a Fourier transform infrared spectrophotometer (Perkin Elmer SpectrumOne, Monza, Italy) with a single reflection ATR accessory (PIKE MIRacle™). Approximately 10mg of each sample were placed on ATR crystal of ZnSe and pressed down to the crystal. The spectra were collected with a resolution of 4 cm^{-1} within the spectral range of 650–4000cm^{-1}.

3.4.4. X-ray Analysis

X-ray diffraction data were collected on micelles and PLGA-NPs, both unloaded and loaded with RSV, by means of a D8 Bruker Advance diffractometer equipped with a Cu source. Samples have been measured in a zero-background sample holder in the 5–35° range, step/size 0.04°, counting time 10 s/step.

3.5. Release Test

A dialysis bag method was employed to assess drug release from the nanosystems. Briefly, the dialysis bag (cellulose acetate, cutoff 12–14,000 Da) was filled with 5 mL of the NP suspension (diluted to obtain a RSV amount compatible with the release in sink conditions) and was placed in 45 mL of Phosphate Buffered Saline (PBS)/EtOH (90:10 *v*/*v*) as receiving phase. Samples (45 mL) of receiving phase were withdrawn at fixed times, ranging from 15 min to 24 h. The sink conditions were ensured by replacing the volume withdrawn at each sampling time with fresh receiving phase. The drug amount was quantified by the HPLC method previously described.

3.6. Cytotoxicity Assay

The cytotoxicity of micelles and PLGA-NPs (unloaded and loaded with RSV) and free RSV suspended in PSB/EtOH (90:10 *v*/*v*) was assessed against two different human cancer cell lines: colonic adenocarcinoma (Caco-2) and human cervical cancer (HeLa) cell lines. Cells were sub-cultured in Dulbecco's Modified Eagle Medium (DMEM) supplemented with 1% *v*/*v* antibiotic/antimycotic solution and 10% *v*/*v* inactivated fetal calf bovine serum; 1% *v*/*v* of non-essential amino acid was added to Caco-2 medium. Both cell types were seeded in 96-well plates (2.5×10^4 cells in 200 µL medium/well) and incubated (37 °C and 5% CO_2 atmosphere) for 24 h to reach semi-confluence. All samples were diluted with medium to obtain different RSV concentrations (40, 80, 120, 180, 240, 360, 400 µM) calculated on the basis of EE% results. The same dilutions were performed for the unloaded carriers to obtain concentrations comparable to those of the loaded ones. Cells were treated with 200 µL of each sample solution for 24 h and medium was used as reference. After 24 h contact, an MTT assay was performed. Cells were washed with 100 µl of PBS (pH 7.4) and then incubated for 3 h (37°C and 5% CO_2) with 50 µL of an MTT 7.5 µM solution in 100 µL of DMEM, without phenol red. Finally, 100 µL of dimethylsulfoxide (DMSO) was added to each well, to allow the complete dissolution of formazan crystals, obtained from MTT dye reduction by mitochondrial dehydrogenases of cells alive. The solution absorbance was determined, after 60 s shaking, at 570 nm, with a 690 nm reference wavelength, by means of an IMark1 Microplate reader (Bio-Rad Laboratories S.r.l., Segrate, Milan, Italy). Results were expressed as % viability calculated by normalizing the absorbance measured after contact with samples with the absorbance of the positive control (cells alive in medium). Eight replicates were performed for each sample.

Laser Scanning Confocal Microscopy (CLSM)

CLSM analyses were performed on samples labeled with two different fluorescent tracers. Micelles and PLGA-NPs were loaded with Nile red to track the drug fate. At the same time, cell internalization of micelles and NPs was assessed by preparing nanosystems with a modified rhodamine labeled CS-OA [27]. The CLSM analyses were conducted as described below: a microscope slide (Ø= 13 mm) was inserted into each well in a 24-well plate, and 10×10^5 cells were seeded in 500 µL medium. After 24 h culture, samples, diluted with medium to reach a 20 µM drug concentration, were loaded onto the cells and left in contact for further 24 h. Afterwards, cells were washed twice with 500 µL of PBS and fixed for 15 min at 4 °C with a 4% (*v*/*v*) paraformaldehyde solution diluted in PBS. Then, substrates were flushed with 500 µL of PBS and, before confocal microscopic analysis, were treated in the dark with 100 µL of Hoechst 33258 (diluted 1:10000 in PBS) for 15 min. Finally, Hoechst was removed, and cells were washed with PBS. The slides with fixed cells were removed from the wells and were examined with confocal laser scanning microscopy (CLSM, Leica TCS SP5II, GmbH) by setting the fluorescence of labeled nuclei (Hoechst 33258, λ_{ex} = 346 nm and λ_{em} = 460 nm), Nile red (Nile red, λ_{ex}= 440 nm and λ_{em} = 520 nm) and rhodamine CS-OA (λ_{ex} = 553 nm; λ_{em} = 627 nm).

3.7. Statistical Analysis

Statistical evaluations were performed by means of Statgraphics 5.0, Statistical Graphics Corporation, MD, USA. Differences were determined according to one-way ANOVA, post-hoc Fisher's test and were considered significant at $p < 0.05$.

4. Conclusions

The results presented in this paper confirm that CS-OA, for its ability to self-assemble and to stabilize emulsions, is suitable for preparing both micelles and PLGA-NPs containing RSV as lipophilic model drug. The two types of nanocarriers were characterized by particle size lower than 300 nm and drug loading capacity between 10 and 15%, confirming the affinity of the RSV molecule for the hydrophobic core of the nanosystems. The effectiveness of CS coating was verified by positive values of zeta potential. Even though physical properties of polymeric micelles and PLGA core NPs looked similar, the interaction of the two systems loaded with RSV onto Caco-2 and Hela cells was different. Only PLGA core-loaded NPs determined a strong decrease in cell viability at high concentrations, in comparison with loaded micelles and free RSV, with a Lethal Dose 50% (LD50) value measured at 240 µM. This result can be attributed to the different hydrophobicity of the two types of nanocarriers and to the more compact nanostructure of PLGA core. The CS-OA micelle structure appeared more stable than expected, but probably less stable than that of PLGA-NPs. CLSM microphotographs confirmed the good internalization of the entire nanocarriers into the cytosolic portion of the cells. Thanks to their lipophilicity, both polymeric carriers based on CS-OA are promising candidates to enable molecular dispersion of the loaded drug, characterized by suitable drug loading, size and cell internalization properties. So far, their use for topical drug delivery systems is envisaged: in particular, depending on the dose of RSV, two different goals can be targeted. At low RSV concentration, nanocarriers could be useful for skin wound treatment, thanks to the peculiar antioxidant and anti-inflammatory properties of the drug that can accelerate the wound healing process. At high RSV concentrations, a cytotoxic effect is expected from PLGA-NPs, which could be profitably exploited for the topical treatment of skin tumors.

Author Contributions: Conceptualization, M.C.B.; Investigation, D.M., L.C., M.S., L.M. and G.D.; Project administration, M.C.B.; Resources, F.F.; Supervision, M.S., S.R., G.S., L.M. and M.C.B.; Visualization, L.C.; Writing—original draft, M.C.B.

Funding: This research received no external funding.

Acknowledgments: The authors wish to thank P. Vaghi, Centro Grandi Strumenti, University of Pavia, for the assistance with Confocal Laser Scanning Microscopy analysis.

Conflicts of Interest: The authors declare no conflict of interest.

References

1. Aranaz, I.; Harris, R.; Heras, A. Chitosan amphiphilic derivatives. Chemistry and applications. *Curr. Org. Chem.* **2010**, *14*, 308–330. [CrossRef]
2. Gang-Biao, J.; Daping, Q.; Kairong, L.; Haihua, W. Novel Polymer Micelles Prepared from Chitosan Grafted Hydrophobic Palmitoyl Groups for Drug Delivery. *Mol. Pharm.* **2006**, *3*, 152–160. [CrossRef]
3. Le Tien, C.; Lacroix, M.; Ispas-Szabo, P.; Mateescu, M.-A. *N*-acylated chitosan: Hydrophobic matrices for controlled drug release. *J. Control. Release* **2003**, *93*, 1–13. [CrossRef]
4. Mahmoudzadeh, M.; Fassihi, A.; Emami, J.; Davies, N.M.; Dorkoosh, F. Physicochemical, pharmaceutical and biological approaches toward designing optimized and efficient hydrophobically modified chitosan-based polymeric micelles as a nanocarrier system for targeted delivery of anticancer drugs. *J. Drug Target.* **2013**, *21*, 693–709. [CrossRef] [PubMed]
5. Bonferoni, M.C.; Sandri, G.; Dellera, E.; Rossi, S.; Ferrari, F.; Zambito, Y.; Caramella, C. Palmitoyl Glycol Chitosan Micelles for Corneal Delivery of Cyclosporine. *J. Biomed. Nanotechnol.* **2016**, *12*, 231–240. [CrossRef] [PubMed]
6. Motiei, M.; Kashanian, S.; Khazaei, M.; Lucia, L.A. Intrinsic parameters for the synthesis and tuned properties of amphiphilic chitosan drug delivery nanocarriers. *J. Control. Release* **2017**, *260*, 213–225. [CrossRef] [PubMed]
7. Bonferoni, M.C.; Sandri, G.; Dellera, E.; Rossi, S.; Ferrari, F.; Mori, M.; Caramella, C. Ionic polymeric micelles based on chitosan and fatty acids and intended for wound healing. Comparison of linoleic and oleic acid. *Eur. J. Pharm. Biopharm.* **2014**, *87*, 101–106. [CrossRef]
8. Motiei, M.; Kashanian, S. Novel amphiphilic chitosan nanocarriers for sustained oral delivery of hydrophobic drugs. *Eur. J. Pharm. Sci.* **2017**, *99*, 285–291. [CrossRef]
9. Dellera, E.; Bonferoni, M.C.; Sandri, G.; Rossi, S.; Ferrari, F.; Del Fante, C.; Perotti, C.; Grisoli, P.; Caramella, C. Development of chitosan oleate ionic micelles loaded with silver sulfadiazine to be associated with platelet lysate for application in wound healing. *Eur. J. Pharm. Biopharm.* **2014**, *88*, 643–650. [CrossRef]
10. Bonferoni, M.C.; Sandri, G.; Rossi, S.; Usai, D.; Liakos, I.; Garzoni, A.; Fiamma, M.; Zanetti, S.; Athanassiou, A.; Caramella, C.; et al. A novel ionic amphiphilic chitosan derivative as a stabilizer of nanoemulsions: Improvement of antimicrobial activity of Cymbopogon citratus essential oil. *Colloids Surf. B Biointerfaces* **2017**, *152*, 385–392. [CrossRef]
11. Xing, K.; Chen, X.G.; Kong, M.; Liu, C.S.; Cha, D.S.; Park, H.J. Effect of oleoyl-chitosan nanoparticles as a novel antibacterial dispersion system on viability, membrane permeability and cell morphology of Escherichia coli and Staphylococcus aureus. *Carbohydr. Polym.* **2009**, *76*, 17–22. [CrossRef]
12. Miele, D.; Rossi, S.; Sandri, G.; Vigani, B.; Sorrenti, M.; Giunchedi, P.; Ferrari, F.; Bonferoni, M.C. Chitosan Oleate Salt as an Amphiphilic Polymer for the Surface Modification of Poly-Lactic-Glycolic Acid (PLGA) Nanoparticles. Preliminary Studies of Mucoadhesion and Cell Interaction Properties. *Mar. Drugs* **2018**, *16*, 447. [CrossRef] [PubMed]
13. Hühn, D.; Kantner, K.; Geidel, C.; Brandholt, S.; De Cock, I.; Soenen, S.J.H.; Rivera_Gil, P.; Montenegro, J.-M.; Braeckmans, K.; Müllen, K.; et al. Polymer-Coated Nanoparticles Interacting with Proteins and Cells: Focusing on the Sign of the Net Charge. *ACS Nano* **2013**, *7*, 3253–3263. [CrossRef] [PubMed]
14. Rose, F.; Wern, J.E.; Gavins, F.; Andersen, P.; Follmann, F.; Foged, C. A strong adjuvant based on glycol-chitosan-coated lipid-polymer hybrid nanoparticles potentiates mucosal immune responses against the recombinant Chlamydia trachomatis fusion antigen CTH522. *J. Control. Release* **2018**, *271*, 88–97. [CrossRef] [PubMed]
15. Andrade, S.; Ramalho, M.J.; Pereira, M.D.C.; Loureiro, J.A. Resveratrol Brain Delivery for Neurological Disorders Prevention and Treatment. *Front. Pharmacol.* **2018**, *9*, 9. [CrossRef] [PubMed]
16. Shi, Y.; Zhou, J.; Jiang, B.; Miao, M. Resveratrol and inflammatory bowel disease. *Ann. N. Y. Acad. Sci.* **2017**, *1403*, 38–47. [CrossRef] [PubMed]
17. Bonferoni, M.C.; Rossi, S.; Sandri, G.; Ferrari, F. Nanoparticle formulations to enhance tumor targeting of poorly soluble polyphenols with potential anticancer properties. *Semin. Cancer Boil.* **2017**, *46*, 205–214. [CrossRef] [PubMed]
18. Santos, A.C.; Pereira, I.; Pereira-Silva, M.; Ferreira, L.; Caldas, M.; Collado-González, M.; Magalhães, M.; Figueiras, A.; Ribeiro, A.J.; Veiga, F. Nanotechnology-based formulations for resveratrol delivery: Effects on resveratrol in vivo bioavailability and bioactivity. *Colloids Surf. B Biointerfaces* **2019**, *180*, 127–140. [CrossRef] [PubMed]
19. Monika; Garg, R.; Sardana, S. Research Problems Associated with Resveratrol (trans-3, 5, 4′-trihydroxystilbene; RSV) and Various Strategies to Overcome those Problems. *Curr. Drug Deliv.* **2017**, *14*, 364–376. [CrossRef]
20. Mileo, A.M.; Miccadei, S. Polyphenols as Modulator of Oxidative Stress in Cancer Disease: New Therapeutic Strategies. *Oxid. Med. Cell. Longev.* **2016**. [CrossRef]

21. Glaser, T.K.; Plohl, O.; Vesel, A.; Ajdnik, U.; Ulrih, N.P.; Hrnčič, M.K.; Bren, U.; Fras Zemljič, L. Functionalization of Polyethylene (PE) and Polypropylene (PP) Material Using Chitosan Nanoparticles with Incorporated Resveratrol as Potential Active Packaging. *Materials* **2019**, *12*, 2118. [CrossRef] [PubMed]
22. Conti, B.; Bucolo, C.; Giannavola, C.; Puglisi, G.; Giunchedi, P.; Conte, U. Biodegradable microspheres for the intravitreal administration of acyclovir: In vitro/in vivo evaluation. *Eur. J. Pharm. Sci.* **1997**, *5*, 287–293. [CrossRef]
23. Anderson, J.M.; Shive, M.S. Biodegradation and biocompatibility of PLA and PLGA microspheres. *Adv. Drug Deliv. Rev.* **2012**, *64*, 72–82. [CrossRef]
24. Nutakul, W.; Sobers, H.S.; Qiu, P.; Dong, P.; Decker, E.A.; McClements, D.J.; Xiao, H. Inhibitory effects of resveratrol and pterostilbene on human colon cancer cells: A side by side comparison. *J. Agric. Food Chem.* **2011**, *59*, 10964–10970. [CrossRef] [PubMed]
25. Summerlin, N.; Qu, Z.; Pujara, N.; Sheng, Y.; Jambhrunkar, S.; McGuckin, M.; Popat, A. Colloidal mesoporous silica nanoparticles enhance the biological activity of resveratrol. *Colloids Surf. B Biointerfaces* **2016**, *144*, 1–7. [CrossRef] [PubMed]
26. He, C.; Hu, Y.; Yin, L.; Tang, C.; Yin, C. Effects of particle size and surface charge on cellular uptake and biodistribution of polymeric nanoparticles. *Biomaterials* **2010**, *31*, 3657–3666. [CrossRef] [PubMed]
27. Ma, O.; Lavertu, M.; Sun, J.; Nguyen, S.; Buschmann, M.D.; Winnik, F.M.; Hoemann, C.D. Precise derivatization of structurally distinct chitosans with rhodamine B isothiocyanate. *Carbohydr. Polym.* **2008**, *72*, 616–624. [CrossRef]

CHAPTER III

COLLAGEN/PCL NANOFIBERS ELECTROSPUN IN GREEN SOLVENT

ABSTRACT

Collagen is the main fibrous protein of human body and it represents an important component of ECMs that provides both structure and flexibility to cells. This protein is one of the most used biomaterials due to its excellent biocompatibility, biodegradability and weak antigenicity[6]. In tissue engineering collagen is employed in skin replacement, bone substitutes, and artificial blood vessels and valves[7]. The mechanical stability and the solubility of collagen can be controlled by adding poly- ε-caprolactone (PCL), a synthetic and biodegradable aliphatic polyester. In recent years, PCL attracted considerable attention in the biomedical fields of controlled-release drug delivery systems, absorbable surgical sutures and three-dimensional (3-D) scaffolds. In most cases PCL/collagen combination has been electrospun by using significantly toxic solvents such as hexafluoroisopropanol (HFIP) or trifluoroethanol (TFE). In a few researches PCL/collagen nanofibers has been electrospun in acidic aqueous solutions showing however a poor morphology and bead formation[15]. In this work PCL, collagen and PCL/collagen random nanofibers were prepared in acetic acid solution. The rheological behaviors of polymer solutions, the electrospinning parameters and fibers size and morphology were compared to find the best conditions to obtain continuous nanofibers without beads. PCL, collagen and PCL/collagen nanofibers solubility were investigated and a biocompatibility test on PCL and collagen fibers was performed.

1. Introduction

The reparative medicine, specifically in tissue engineering field, is based on the availability of non-toxic, safe and effective artificial substrates or scaffolds capable to support cell growth and therefore restore, maintain or recover damaged tissues.

As is well known, the development of suitable scaffolds requires keen understanding of the mechanisms of neogeneration of tissues and of the role played by the extracellular matrix (ECM) as both a structural framework and a regulation of cell-response behavior[1,2]. Precisely, scaffolds are designed to promote the formation of an appropriate environment for tissue regeneration and guarantee an optimal structural stability to enhance cell proliferation and migration. Biocompatible and anti-immunogenic materials are required. Natural polymers commonly found in extracellular matrix as proteins (collagen, elastin, fibronectin) or glycosaminoglycans (chondroitin sulfate, hyaluronic acid) are mostly employed to best mimic the physiological environment. At the same time, the biomimetic approach suggests the use of the electrospinning, though not a new idea itself, as an optimal technique, as it is suitable to obtain scaffolds with a remarkable structural similarity to the network of the ECM[3,4]. Collagen is the main fibrous protein of human body and it represent an important component of ECMs that provides both structure and flexibility to cells. As the main constituent of the extracellular matrix of the connective tissue, collagen is responsible for the integrity of individual cells, migration, adhesion, cell differentiation, as well as angiogenesis[5]. Collagen represents one of the most used natural biomaterials due to its excellent biocompatibility, biodegradability and weak antigenicity[6]. In tissue engineering it is employed in skin replacement, bone substitutes, and artificial blood vessels and valves[7]. Thanks to all these excellent properties, it can be processed by cross-linking, freeze drying or electrospinning in order to obtain hydrogels, membranes, matrices and fibers[8]. Gelatin is usually employed as an alternative of collagen in

developing dressings or scaffolds. Basically, gelatin derives from collagen thermal denaturation and hydrolysis, mediated by acidic or base condition leading to respectively gelatin A and gelatin B. According to the process used, the physiochemical properties of gelatin can vary. Gelatin preparations consist of a distribution of polypeptide fragments of different sizes, different isoelectric points (pI), and different gelling properties, and often exhibit batch to batch variability[9]. Even if this biomaterial is not naturally occurring, its extensive use in biomedical field is related to its low-cost and easy achievement. The amino acid compositions of collagen and gelatin are almost identical; however, other characteristics such as secondary structure, isoelectric point, and molecular weight distribution are different, affecting the physical properties of the 3D-tissue substitutes. The mechanical and morphological stability of collagen or gelatin scaffolds can be improved by combining the protein to poly-ε-caprolactone (PCL) in the electrospun solution. PCL is an FDA-approved synthetic, hydrophobic and biodegradable aliphatic polyester obtained by the ring opening polymerization of the cyclic monomer ε-caprolactone. Furthermore, the only degradation product of PCL is caproic acid, a non-toxic metabolite which is either metabolized via citric acid cycle or eliminated via urinary secretion[10]. In recent years, this polymer has attracted considerable attention in the biomedical fields for controlled-release drug delivery systems, absorbable surgical sutures and three-dimensional (3-D) scaffolds. However, due to a lack of cell-recognition sites and poor hydrophilic character, PCL has shown reduced cell adhesion, proliferation and migration when utilized for a support of cell growth. This limit can be properly overcome by an addition of highly hydrophilic substance such as collagen or gelatin. Therefore, a synergistic effect is achieved, and this combination not only allows to decrease significantly PCL hydrophobicity, but also has a favorable influence on cellular response of the scaffold[11]. In most cases collagen/PCL combination has been electrospun by using organic, extremely toxic and expensive solvents such as 1,1,1,3,3,3-hexafluoro-2-propanol (HFIP) or 2,2,2-trifluoroethanol (TFE)[12,13,14]. In a few researches, nanofibers based on collagen/PCL have been electrospun in benign acidic aqueous solutions, however showing a poor morphology, rich in imperfections (beads) [15,16]. In this work PCL, collagen and collagen/PCL randomly collected nanofibers were prepared in acetic acid aqueous solution. During the first phase, rheological analyses were performed to investigate the effect of the concentration of each polymer in the formulations on fiber occurrence and by determining the characteristic entanglement concentration (CEC). At the same time, all solutions were characterized by conductivity and surface tension; then solutions were electrospun and thanks to a DoE approach, the effect of electrospinning process parameters, on the obtainment of homogeneous and continuous nanofiber structures from protein/PCL mixture, was studied. Morphology and physical properties of PCL, collagen and collagen/PCL nanofibrous membranes were assessed by SEM analyses, solubility and wettability tests and tensile strength. The integrity of the collagen triple helix was investigated by X-ray analyses. A cytotoxicity test was performed to evaluate nanofiber biocompatibility on normal human dermal fibroblasts and cell proliferation and adhesion were visualized by scanning electron and laser confocal microscopies. Finally, collagen/PCL and gelatin/PCL nanofibrous membranes were compared in term of mechanical properties and biocompatibility in order to identify differences between the two scaffolds.

2. Results and discussion

2.1.Rheological Studies

Rheological studies were performed at 25 ° C on PCL, collagen and collagen/PCL 1:1 weight ratio mixture prepared at different concentrations in acetic acid 90 % v/v.

Figure 1a and **1b** show viscosity (Pa.s) versus shear rate (s^{-1}) profiles respectively measured for PCL and collagen solutions. In both cases at the highest polymer and protein concentration an increase in viscosity trend occurred although only in the case of the 50% PCL solutions the pseudoplastic behaviour was evident due to in the occurrence of polymer chain entanglement. The same characterization was performed on collagen/PCL 1:1 weight ratio mixture (**Figure 1c**). The viscosity curve of the 20% 1:1 mixture shows values quite higher than the curves of both PCL and collagen alone 20% solutions. This could be explained with the occurrence of an interaction between the two components of the mixture, in line with literature findings. Some authors in fact demonstrated by FTIR analysis the occurrence of hydrogen bonds between the carboxyl groups of PCL and the amide groups of collagen[15].

On the basis of the rheological characterization, the critic entanglement concentrations (CEC) for both PCL and collagen/PCL 1:1 w/w ratio were also evaluated. The CEC represents the lowest concentration at which the entanglement of the polymeric chains occurs; it depends on polymer molecular weight, chain morphology, and affinity of the solvent used[17,18]. For each PCL and protein/PCL concentration analysed, a shear stress (τ) versus shear rate (s^{-1}) profile was built to calculate the zero-shear viscosity (η_0) and infinite shear viscosity (η_∞) values. $\eta 0$ describes the polymeric rheological behaviour when the sample is in no stress condition; instead, $\eta\infty$ represents the viscosity value of the polymer solution when the polymer chains are completely untightened. The average values of η_0 and η_∞ graphically extrapolated (mPa ·s) are illustrated vs PCL or protein/PCL concentration (% w / w) in **Figure 2** and **3**.

The log–log profiles of the viscosity parameters (η_0 and η_∞) vs PCL or collagen/PCL concentration allow the identification of CEC, which corresponds to the intersection point between the two straight lines that best represent, on a statistical basis, the experimental data[19]. The same study was not performed on collagen solutions, because not even at the highest concentration a clear pseudoplastic behaviour occurred and the CEC cannot be assessed. For PCL solutions, the polymer entanglement concentration in acetic acid 90 % v/v corresponded to 22 % w/w on the other side, when polymer is mixed with the protein, the entanglement concentration decreased to 7 % w/w. This quite relevant lowering of the PCL CEC after the addition of the protein in collagen/PCL mixtures, can represent a further evidence of a possible interaction between the two components, in accordance with the previously observed increase of viscosity.

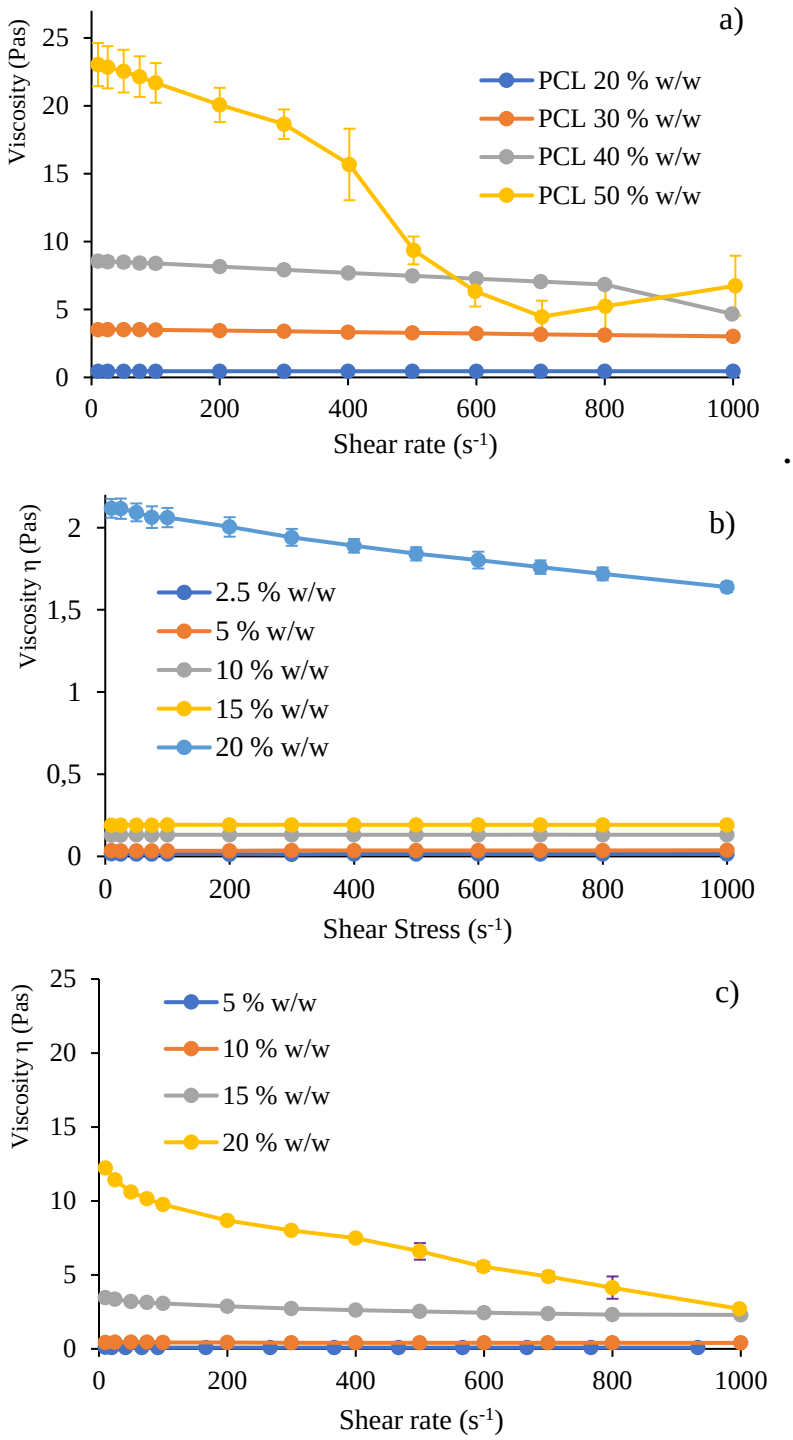

Figure 1 Viscosity (Pa) vs shear rate (s -1) profiles of polymeric solutions prepared at different concentrations (% w/w) in acetic acid at 90% v / v at a temperature of 25 ° C: a) PCL, b) collagen, c) collagen/PCL mixtures. (mean values ± s.d.; n = 3).

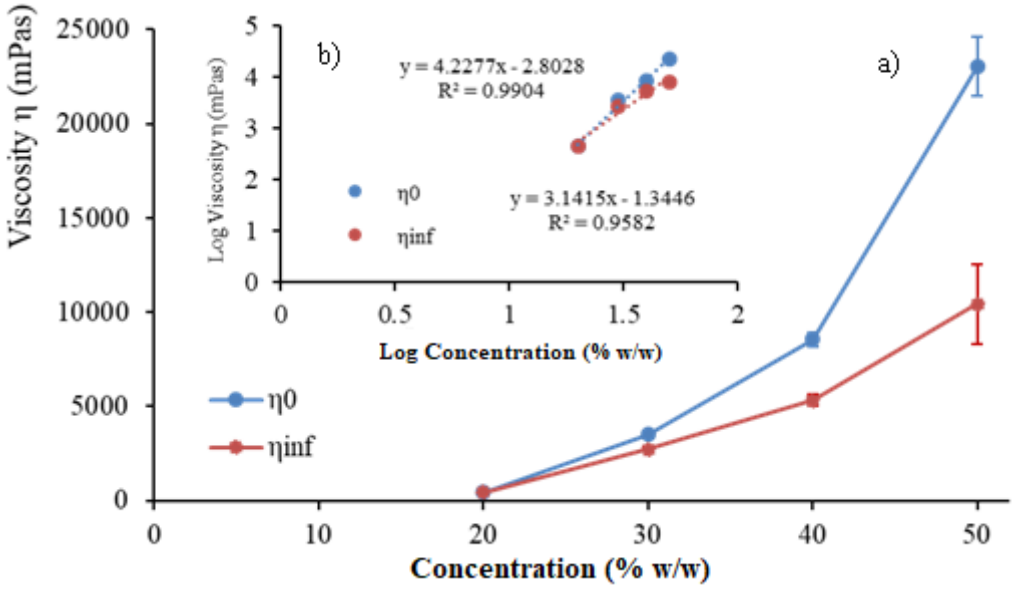

Figure 2 Average values of η0 and η∞ of polycaprolactone (PCL) against concentration (a) and bi-logarithmic transformation of the same profiles (b) evaluated for the polymer solutions prepared acetic acid at 90% v / v at a temperature of 25 ° C (mean values ± s.d.; n = 3)

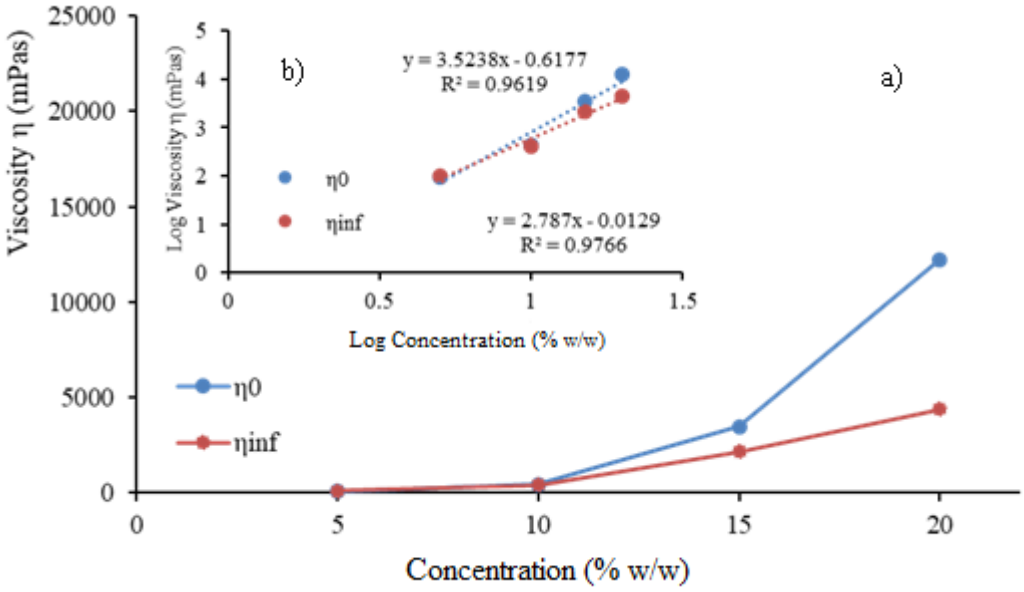

Figure 3 η_0 and η_∞ average values of PCL / collagen against concentration (a) and bi-logarithmic transformation of the same profiles (b) evaluated for the polymer/protein mixtures prepared acetic acid at 90% v / v at a temperature of 25 ° C (mean values ± s.d.; n = 3).

2.2.Physical properties of collagen, PCL and collagen/PCL solutions

As known, surface tension and conductivity solution parameters modulate the efficiency of the electrospinning technique by influencing the nanofiber's homogeneity[20,21]. Surface tension and

conductivity were assessed to investigate if any differences in physical properties occurred when collagen and PCL were prepared individually (20 % w/w in acetic acid 90 % v/v) or blended at two different weight ratios (1:1 and 1:2). The results are illustrated in **Figures 4** and **5**. Even if the solvent is the same in all cases, the conductivity values (µS / cm) highlighted the presence of statistically significant differences between collagen and PCL solutions (**Figure 4**). Clearly, the amount of surface charges in acidic condition differed widely from the material employed. The protonated aminoacidic moieties of collagen, in fact, impacted significantly maintaining a high conductance while, as PLC is a non-ionic polymer, the polymer did not contribute positively to conductivity. A balance between the charged protein amino groups and uncharged polymer function was evident for the mixtures at two weight ratios, where intermediate conductivity values were recorded. Surface tension, on the contrary, was not influenced by the material employed, as shown in **Figure 5**. all values were higher than the acetic acid 90 % v/v solution (≈ 27 mN/m at 25 °C), however statistical differences from collagen and PCL or the blends did not occur. Therefore, this factor could not affect in the present case the efficiency of the electrospinning process and the morphology of the solid nanofibrous membranes.

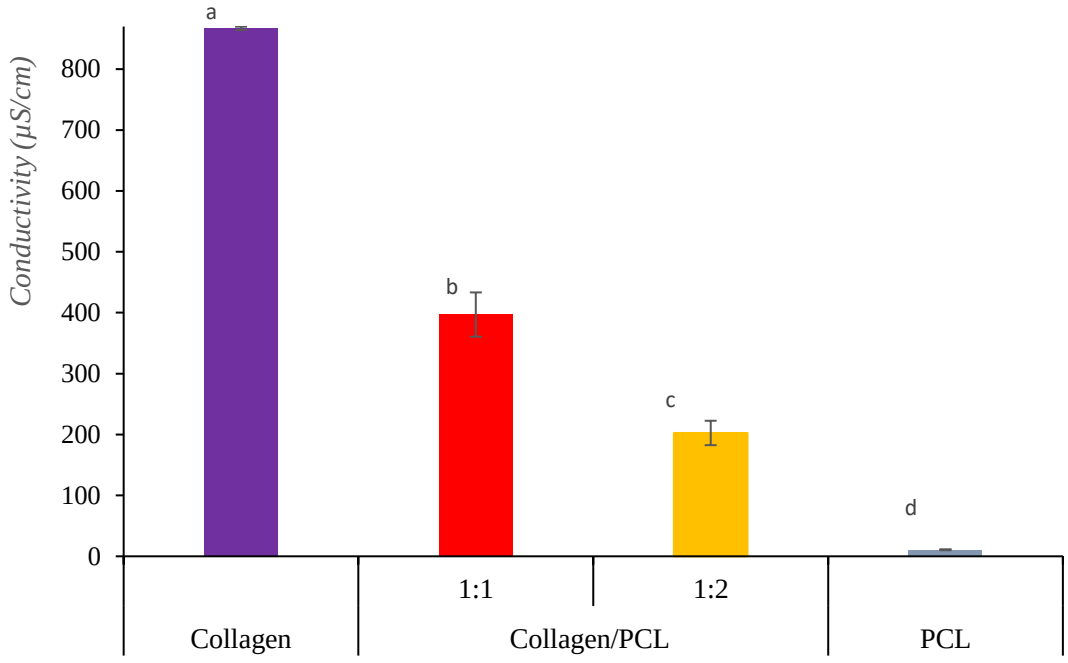

Figure 4 Conductivity (µS/cm) values of collagen (20 % w/w), collagen/PCL at two weight ratios and ε-policaprolacton (PCL) and PCL (20 % w/w)solutions prepared in acetic acid 90 % v/v. ANOVA 1 VIA – MRT ($p < 0,05$) (mean values ± s.d.; n=5): a vs b, a vs c, a vs d, b vs c, b vs d, c vs d.

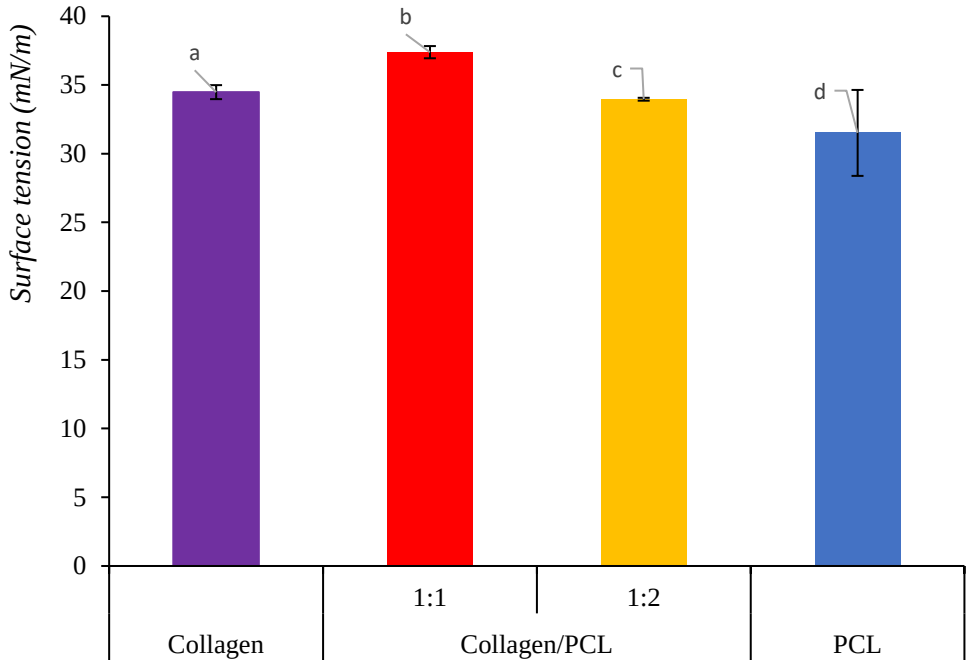

Figure 5 Surface Tension values of collagen (20% w/w), collagen/PCL at two weight ratios and ε-policaprolacton (PCL) and PCL (20% w/w) solutions prepared in acetic acid 90 % v/v. ANOVA 1 VIA – MRT ($p < 0,05$) (mean values ± s.d.; n=5).

2.3.Electrospun nanofibers

2.3.1. Preliminary studies

Different PCL, collagen and collagen/PCL (1:1 and 1:2) formulations were prepared in 90 % v / v acetic acid and electrospun using the process parameters indicated in **Table 1**. The photomicrographs obtained in SEM analyses are given in Figure 7. Beads constitute the more common imperfections highlighted by SEM analyses on electrospun membranes. Sign "+" and "-" in **Table 5** respectively represent fiber-like or not fiber-like structures. The results obtained in the rheology studies are in this case confirmed. As evident in SEM photomicrographs, in fact, below the critic entanglement concentration (CEC) the electrospinning process led to non-continuous jet and collected fibers resulted rich in beads and with structural imperfections (fibers P1, C1, C2, C4). These defects were not evident in nanofibers obtained by electrospinning of solutions above the CEC and continuous nanofibers from 20 % w/w PCL (P3) and collagen/PCL 1:1 (CP1) and 1:2 (CP3) solutions were obtained. The increase of the polymer concentration to 30 % w / w for PCL solution (P4) and 15 % w/w for collagen/PCL 1:2 (CP2) solution reported a non-homogeneous ribbon-like morphology and higher dimensions which reach the micrometric range for CP2.

In the case of collagen, the electrospinnability of solutions at different acetic acid concentrations was also evaluated to reduce the exposition of the protein to acidic environment, with possible negative effect on the collagen native structure. As shown in **Figure 6**, no fibers were obtained by using collagen solubilized in 25 % v/v and 45 % v/v of acetic acid, but when the protein was electrospun in acetic acid 90 % v/v at all concentrations evaluated, nanofibrous structure was achieved. The result obtained highlight how the balance between the applied

electric field, the solution's surface tension and its conductivity drastically affected the process while maintaining the same collagen concentration. Furthermore, strong differences were observed in nanofibers obtained with 15% and 20 % w/w protein solutions, and nanofibers with large diameters were collected at the highest concentration.

Table 1 Morphological results and mean fibers dimensions of PCL, collagen and collagen/PCL electrospun formulations ("beads" represent the structural imperfections on nanofibrous membranes, "+" a fiber morphology occurred and "–" fiber did not occur).

Formulation	PCL (% w/w)	CH3COOH (% v/v)	Process parameters (kV, cm, ml./h)	Fibers	Fiber Dimension (nm)
P1	10	90	20 kV –15 cm– 0.793 ml/h	beads	110.93±29.40
P2	15			beads	197.08±58.55
P3	20			+	211.60±59.51
P4	30			+	494.80±93.30

Formulation	Collagen (% w/w)	CH3COOH (% v/v)	Process parameters (kV, cm, ml./h)	Fibers	Fiber Dimension (nm)
C1	10	25	25 kV – 15 cm – 0.397 ml/h	-	-
C2		45		-	-
C3		90		+	175.55±59.21
C4	15	45		-	-
C5		90		+	159.63±53.01
C6	20	90		+	668.24±152.42

Formulation	Collagen/PCL (% w/w)	Collagen (% w/w)	PCL (% w/w)	Process parameters (kV, cm, ml./h)	Fibers	Fiber Dimension (nm)
CP1	1:1	10	10	25 kV – 20cm– 0.397 ml/h	+	517.71±144.42
CP2	1:2	7.5	15	25 kV –15cm – 0.397 ml/h	+	2584.02±753.70
CP3		5	10	20 kV – 15cm – 0.397 ml/h	+	167.11±41.81

Figure 6 Photomicrographs SEM of electrospun nanofibers prepared from different concentration of PCL solutions in acetic acid 90 % v/v: 10 % w / w (P1); 15 % w / w (P2); 20 % w / w (P3); 30 % w / w (P4); collagen 10% w / w solutions prepared in acetic acid 25% v / v (C1), 45% v / v (C2), 90% v / v (C3); collagen 15 % w/w solutions in acetic acid 45 % v/v (C4) and 90 % v / v (C5); collagen 20% w / w solutions prepared in acetic acid 90 % v / v (C6); collagen/PCL solutions at two different weight ratio 1:1 and - 2:1 and different concentrations: 10 % w / w collagen +10 % w / w PCL (CP1), 7,5 % w / w collagen + 15 % w / w PCL (CP2) and 5 % w / w collagen + 10 % w / w PCL (CP3).

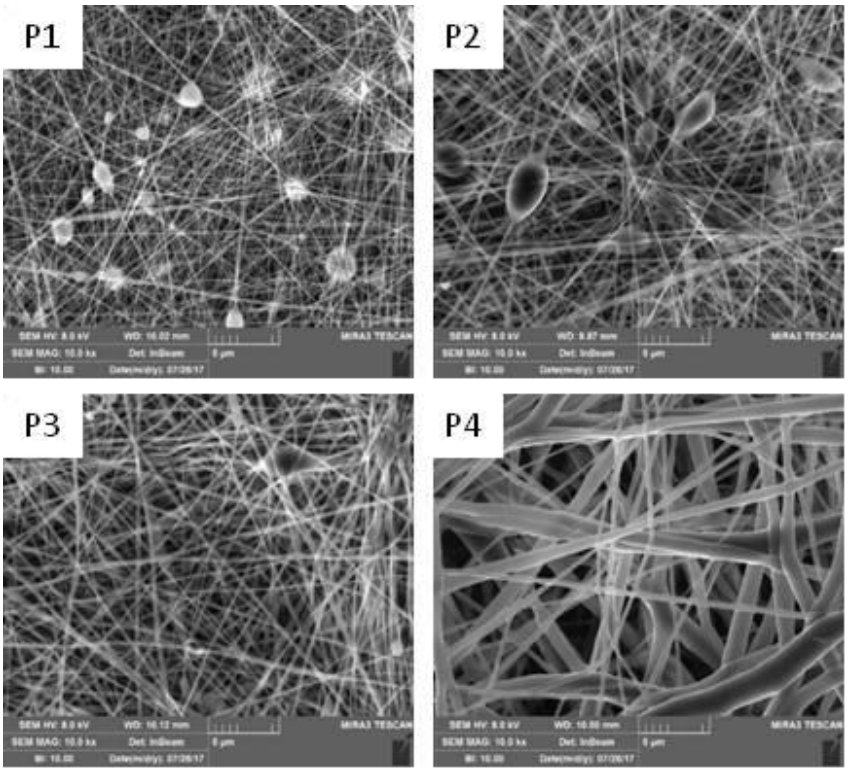

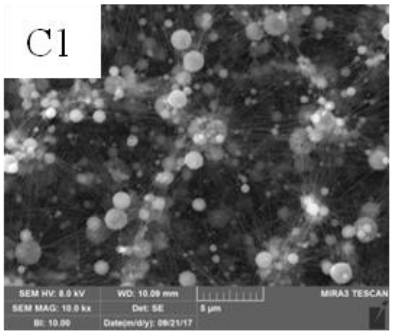
C1
SEM HV: 8.0 kV
WD: 10.09 mm
MIRA3 TESCAN
SEM MAG: 10.0 kx
Det: SE
5 µm
BI: 10.00
Date(m/d/y): 09/21/17

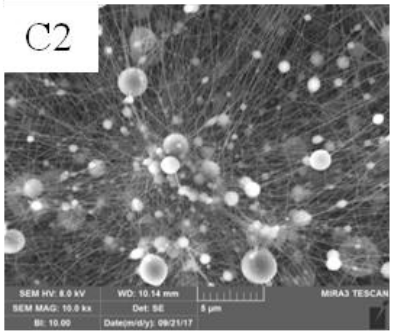
C2
SEM HV: 8.0 kV
WD: 10.14 mm
MIRA3 TESCAN
SEM MAG: 10.0 kx
Det: SE
5 µm
BI: 10.00
Date(m/d/y): 09/21/17

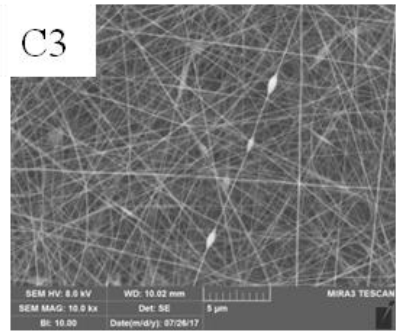
C3
SEM HV: 8.0 kV
WD: 10.02 mm
MIRA3 TESCAN
SEM MAG: 10.0 kx
Det: SE
5 µm
BI: 10.00
Date(m/d/y): 07/26/17

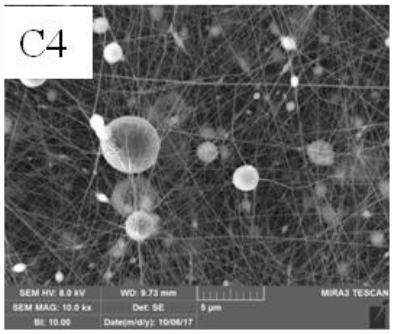
C4
SEM HV: 8.0 kV
WD: 9.73 mm
MIRA3 TESCAN
SEM MAG: 10.0 kx
Det: SE
5 µm
BI: 10.00
Date(m/d/y): 10/06/17

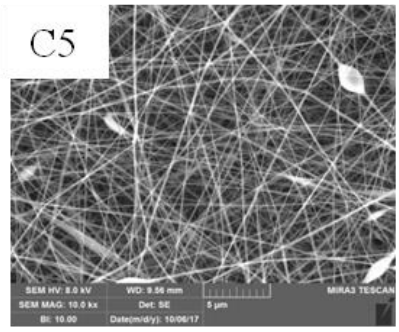
C5
SEM HV: 8.0 kV
WD: 9.56 mm
MIRA3 TESCAN
SEM MAG: 10.0 kx
Det: SE
5 µm
BI: 10.00
Date(m/d/y): 10/06/17

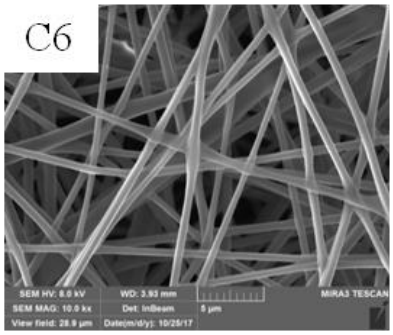
C6
SEM HV: 8.0 kV
WD: 3.93 mm
MIRA3 TESCAN
SEM MAG: 10.0 kx
Det: InBeam
5 µm
View field: 28.9 µm
Date(m/d/y): 10/25/17

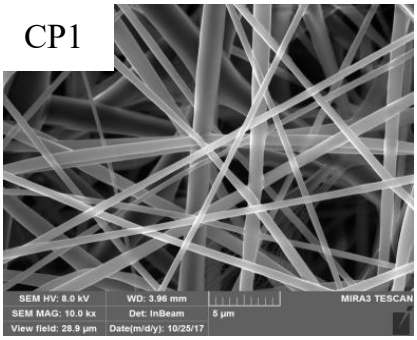
CP1
SEM HV: 8.0 kV
WD: 3.96 mm
MIRA3 TESCAN
SEM MAG: 10.0 kx
Det: InBeam
5 µm
View field: 28.9 µm
Date(m/d/y): 10/25/17

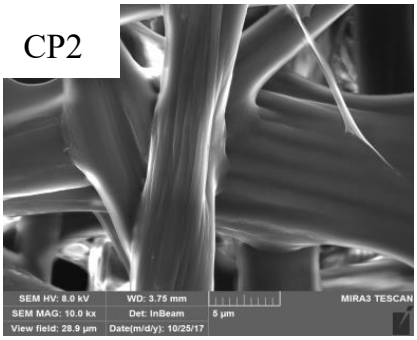
CP2
SEM HV: 8.0 kV
WD: 3.75 mm
MIRA3 TESCAN
SEM MAG: 10.0 kx
Det: InBeam
5 µm
View field: 28.9 µm
Date(m/d/y): 10/25/17

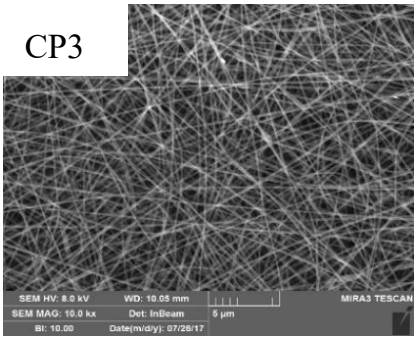
CP3
SEM HV: 8.0 kV
WD: 10.05 mm
MIRA3 TESCAN
SEM MAG: 10.0 kx
Det: InBeam
5 µm
BI: 10.00
Date(m/d/y): 07/26/17

2.4.Design of Experiment (DOE): effect of the process parameters

The process parameters (flow, voltage and distance) play an important role in the electrospinning technique, influencing the structure and morphology of the resulting nanofibers. The influence of these parameters was investigated on a statistical basis by an experimental design (DoE), specifically using a full factorial design. In the experimental design, flow (ml / h), distance needle-collector (cm) and voltage (kV) were considered as factors and both protein/polymer mixtures at 1:2 and 1:1 weight ratio were evaluated. For each factor, two levels (low and high) were identified according to the **Table 3** (in method section). Nanofibers dimensions, number of beads into a fixed, standardized area and the coefficient of variation (CV%) of dimensions were set as response variables. This last parameter was chosen to describe the dimensional uniformity of the resulting fibers. The statistical analysis indicated the relevance of the effects of each parameter and their interactions on the response variables. The results obtained from the experimental design for the formulations based on collagen/PCL in a 1: 1 weight ratio (CP1), showed a poor correlation, not statistically significant between the factors and the responses dimensions or the coefficient of variation (CV%). None process parameters considered had a significant influence in obtaining small nanofibers and with a dimensionally homogeneous structure (**Figure 7**). Considering the response represented by the number of beads, the effect of the distance needle-collector highlighted a positive and statistically significant effect on beads formation during the electrospinning process (**Figure 8**). An increase in the distance was associated to an excessive stretching of the polymer solution jet. Due to the sudden solvent evaporation, the jet thus became discontinuous and the electrospinning process was displaced by the electrospray one. For this reason, fibers appeared not continuous and beads occurred. On the other side, flow factor showed a negative and statistically significant effect on the development of irregular fibers rich in beads (**Figure 9**). An increase in flow led to a greater amount of solution on the tip of the needle decreasing the risk of a discontinuous and interrupted jet. The voltage did not show any statistically significant effect on the number of beads, however the interaction between distance and flow (indicated in Pareto Chart as AC) influences in negative and statistically significant way the response. Therefore, to make continuous and dimensionally homogeneous fibers, it would be necessary to keep both factors at high level (25 cm and 0.793 ml / h). Furthermore, the interaction between distance and voltage (shown in Pareto Chart as AB) affected positively and significantly the number of beads, demonstrating how the increase of voltage, associated with increased distance, can compromise the efficiency of the process.

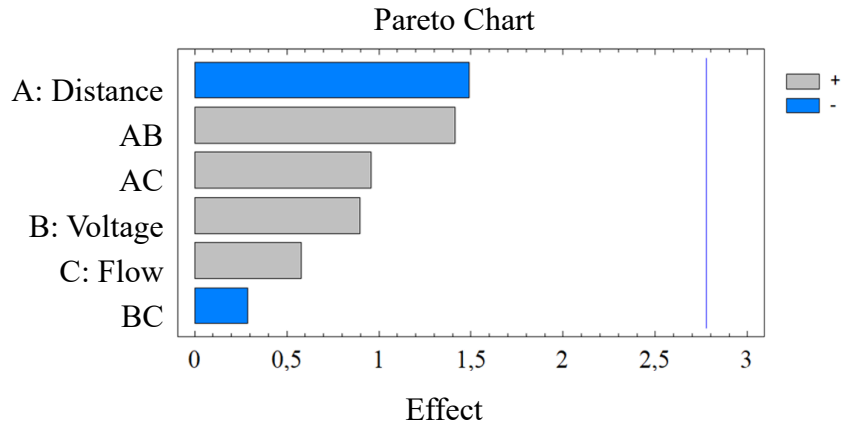

Figure 7 Pareto Chart of "Dimension" response parameter for CP1 (collagen 10% w / w and PCL 10% w / w).

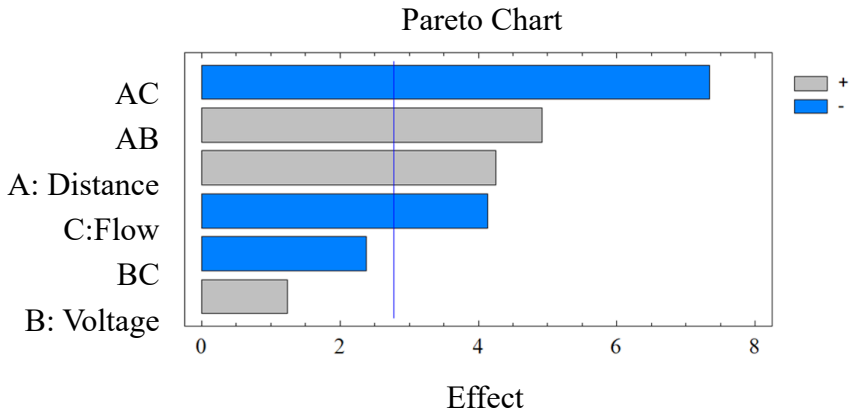

Figure 8 Pareto Chart of "Number of beads" response parameter for CP1 (collagen 10% w / w and PCL 10% w / w).

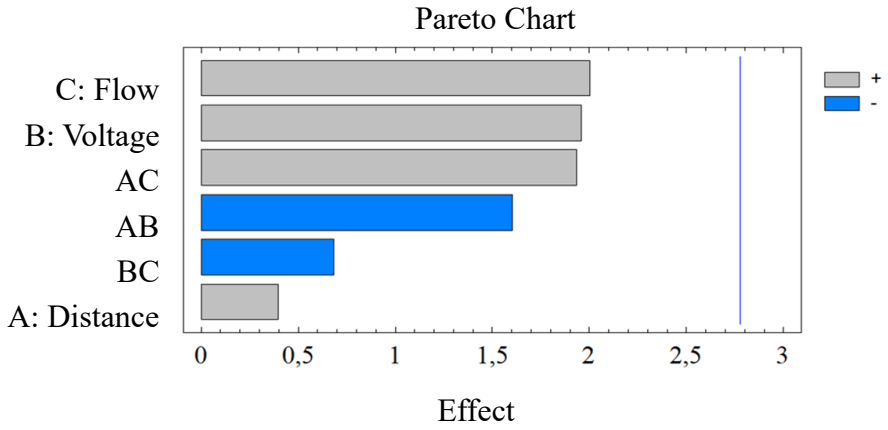

Figure 9 Pareto Chart of "Coefficient of variation (CV%)" response parameter for CP1 (collagen 10% w / w and PCL 10% w / w).

Dimensions and number of beads responses for the formulations based on collagen/PCL 1:2 weight ratio (formulation CP3), showed a poor correlation, not statistically significant with all

the factors. Hence, these process parameters did not have a significant influence in obtaining small and continuous nanofibers (**Figures 10** and **11**).
When coefficient of variation (CV%) was considered as response (**Figure 12**), a negative and statistically significant effect of the flow on the dimensional homogeneity of the nanofibers was evident, while the distance needle-collector and the voltage applied did not cause a statistically significant effect. Given this evidence, the flow factor should be kept at a higher level to obtain fibers dimensionally homogeneous. The interaction between voltage and flow (indicated in Pareto Chart as BC) influenced in a negative and statistically significant way the coefficient of variation of the nanofibers and, at the same time, the interaction between distance and voltage (indicated in Pareto Chart as AB) influenced positively the response. When voltage and distance are kept at high levels, a jet instability occurs, no continuous fibers can be collected, and the electrospinning process is stopped. Finally, the interaction between distance and flow (indicated in Pareto Chart as AC) influenced positively and significantly the response, demonstrating how the increase in both flow and distance, can compromise the efficiency of the process.

.

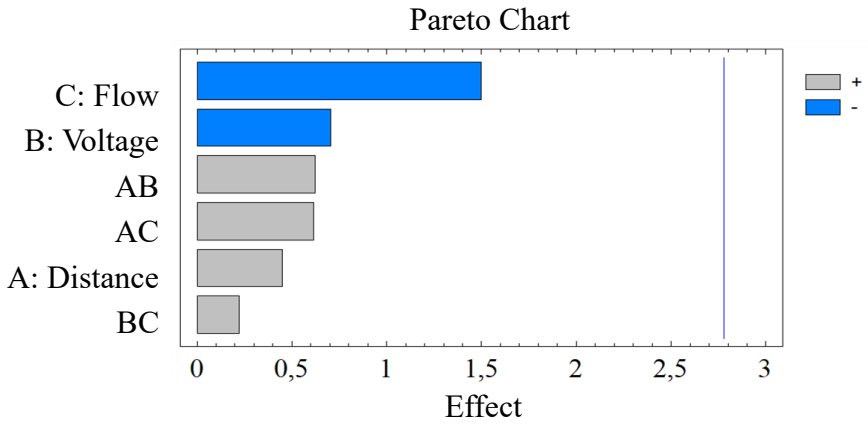

Figure 10 Pareto Chart of "Dimension" responce parameter for CP2 (collagen 5% w / w and PCL 10% w / w).

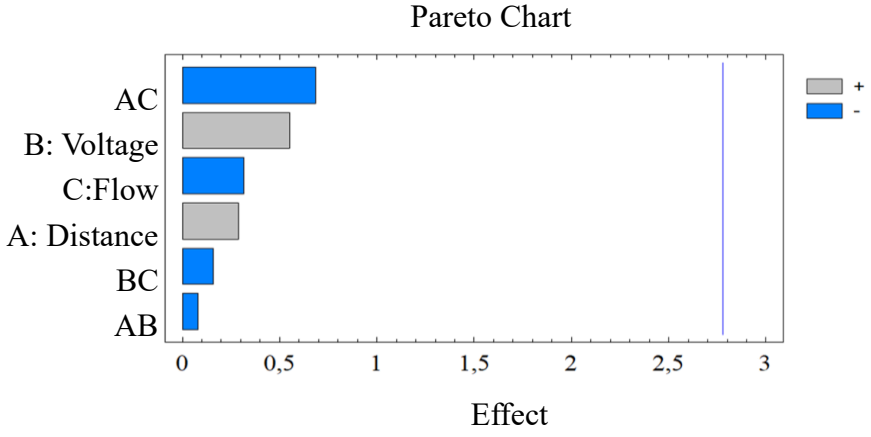

Figure 11 Pareto Chart of "Number of beads" responce parameter for CP2 (collagen 5% w / w and PCL 10% w / w).

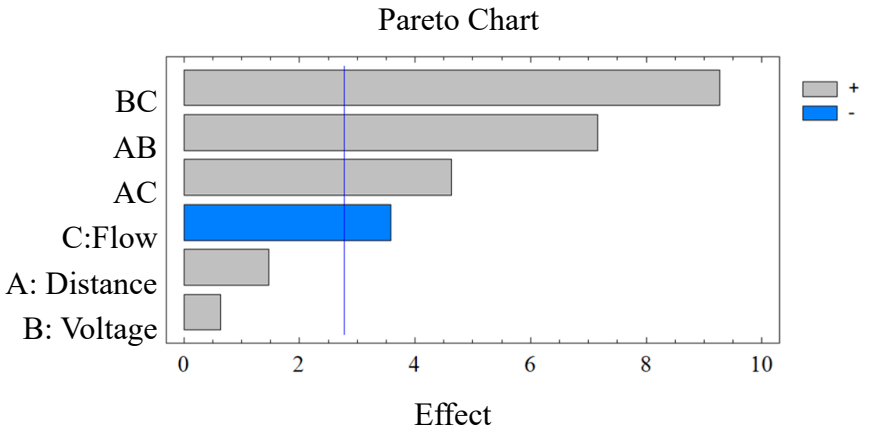

Figure 12 Pareto Chart of "Coefficient of variation (CV%)" responce parameter for CP2 (collagen 5% w / w and PCL 10% w / w).

2.5.Optimized nanofibrous membranes

The solutions based on collagen, PCL and collagen/PCL at two different weight ratios (1:1 and 1:2) were electrospun by setting the process parameters according to the results of the DOE based development phase. For collagen/PCL 1:1 weight ratio (formulation CP1) 25 cm, 20 kV and 0.8 ml/h were employed as electrospinning parameters, while 20 cm, 20 kV and 0.8 ml/h for collagen/PCL 1:2 ratio (formulation CP3). Homogeneous and reproducible nanofibrous membranes were collected and characterized by stability in the hydrate state, wettability, mechanical properties, in vitro biocompatibility and cell adhesion. In **Figure 13** SEM photomicrographs and size diameters of the four best nanofibrous membranes are proposed. Nanofibers in all cases resulted in a continuous structure with no evident beads or imperfections.

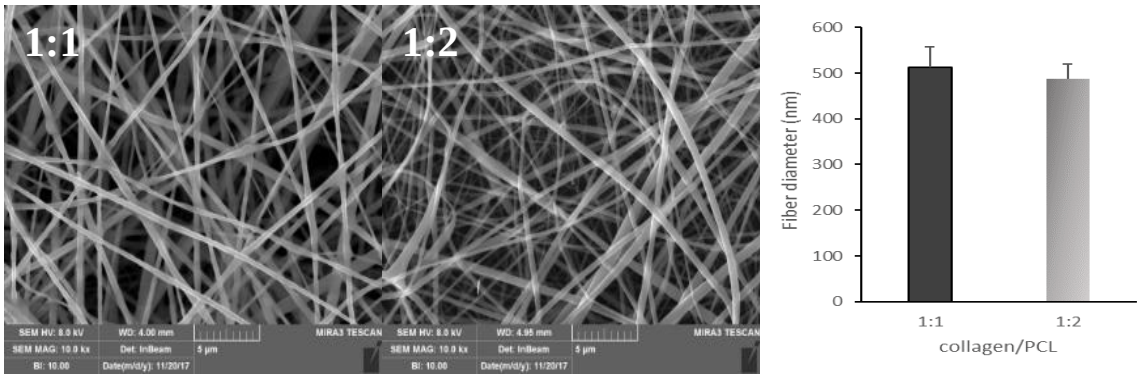

Figure 13: Morphological and dimensional characterization of the nanofibers based on collagen/PCL mixtures 1:1 and 1:2 obtained with optimized process parameters.

2.6.WAXS analyses

The possible denaturation of collagen during the electrospinning process was evidenced by some authors in the literature [22]. However, in all cases the protein was solubilized either in perfluorated solvents or in acetic acid/formic acid mixtures. In the present work, only acetic acid was used to solubilize collagen, so the effect of the solvent and of the process on the protein conformation seemed worthwhile to be checked. The integrity of collagen triple helix structure on solutions and electrospun nanofibrous membranes based on collagen and collagen / PCL in blended mixtures with two different weight ratios, was characterized by X-ray analyses. **Figure 14** shows the 1D profile of native collagen 1 % v/v from bovine origin. The structure of the intact triple helix is clearly visible; a strong meridional reflection and an equatorial reflection were evident: the first one confirmed the typical collagen triple-helix structure (0.8 Å <d <4.8 Å), while the other highlighted the amount of fibrillar packing (9 Å <D <13 Å).

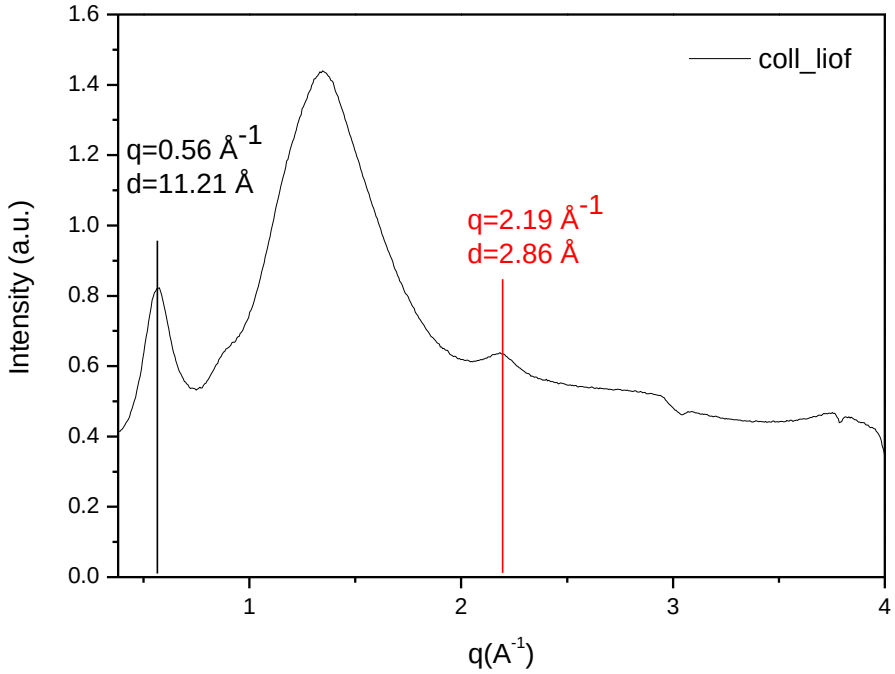

Figure 14 WAXS Spectrum of native collagen.

Collagen freeze-dried

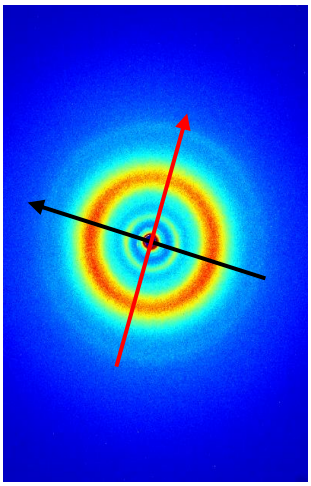

Collagen freeze-dried after acidic treatment

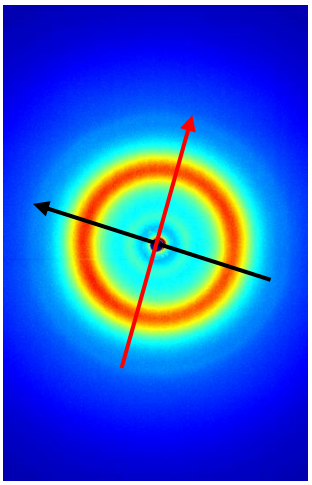

Table 2 Equatorial, meridional and diffuse reflections of native soluble collagen (Kelisema, CO, IT).

	q (Å-1)	***D(Å)***
Equatorial Refl	0.56 ± 0.02	11± 0.02
Meridional Refl	2.19 ± 0.02	2.8± 2
Diffuse Scatter	0.8<q<2.09	7.8<d<3

Figure 15a shows the WAXS profiles of the native collagen (pattern in black) and of collagen after treatment with acetic acid 90% v / v (pattern in red). After the acidic treatment of collagen 20 % w/w in acetic acid 90 % v/v, the meridional reflection (marker of the triple helix) was barely visible and an increase in the width at half height (FWHM) of the equatorial reflection (marker of fibrillar packing) was also found. Therefore, collagen treated in acetic acid showed a lower triple-helix organization and conformation, a decreased fibrillar packing with a loss of the preferential molecule orientation towards a specific direction.

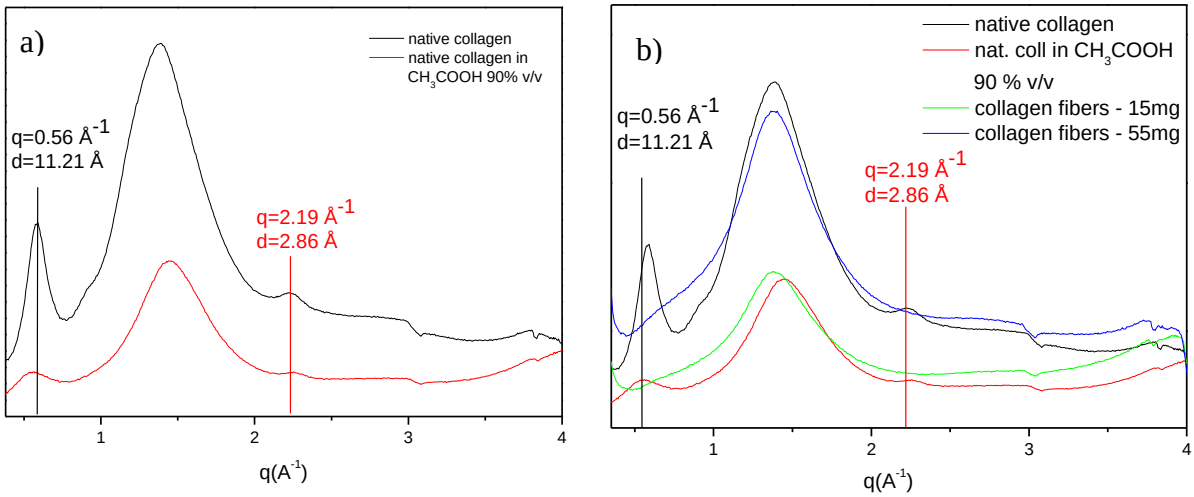

Figure 15 a) Comparison WAXS spectra of native collagen and native collagen treated in acid condition (acetic acid 90 % v/v); b) WAXS spectra comparison of native collagen, collagen in acidic condition and collagen electrospun nanofibers (protein concentration in all samples: 20 % w/w).

An evaluation of the effect of the electrospinning process on the protein structure stability was performed on the collagen treated in 90% v / v acetic acid, where triple helix is lost. **Figure 11b** shows the diffraction profiles of native collagen 20 % w/w in 90% v / v acetic acid before and after they were subjected to the electrospinning process. Collagen based electrospun membranes with different weights were characterized **(Figure 15b**, 15 mg green pattern, 55 mg blue pattern). In both backgrounds, the meridional and the equatorial reflections almost disappeared. These data demonstrated that after electrospinning process, the triple helix structure is no longer visible and a further decrease in fibrillar packing occurs. Moreover, compared to acidic treatment only, the preferential molecule orientation towards a specific direction is not evident. The integrity of the triple helix structure of collagen is lost when collagen is blended with polycaprolactone in 90% v / v acetic acid at two different weight ratios (1:1 and 1:2). In **Figure 16** the diffraction profiles of native collagen are compared with collagen treated in acetic acid 90% v / v and mixtures of collagen/PCL prepared for two different weight ratios (1:1 and 1:2). In both mixtures, the meridional and equatorial reflection disappeared in the background, confirming the substantial denaturation of the protein.

Figure 17 compares the diffraction profiles of native collagen and collagen prepared in 90 % v / v acetic acid with nanofibrous membranes obtained with the solutions of collagen/PCL prepared with two different protein/polymer ratios (1: 1 and 1:2) in acetic acid 90% v / v. After electrospinning process, in both membranes, the meridional and the equatorial reflections were absent. The additional peaks shown in the nanofibrous membranes, near the meridional reflection region, were typical of the PCL.

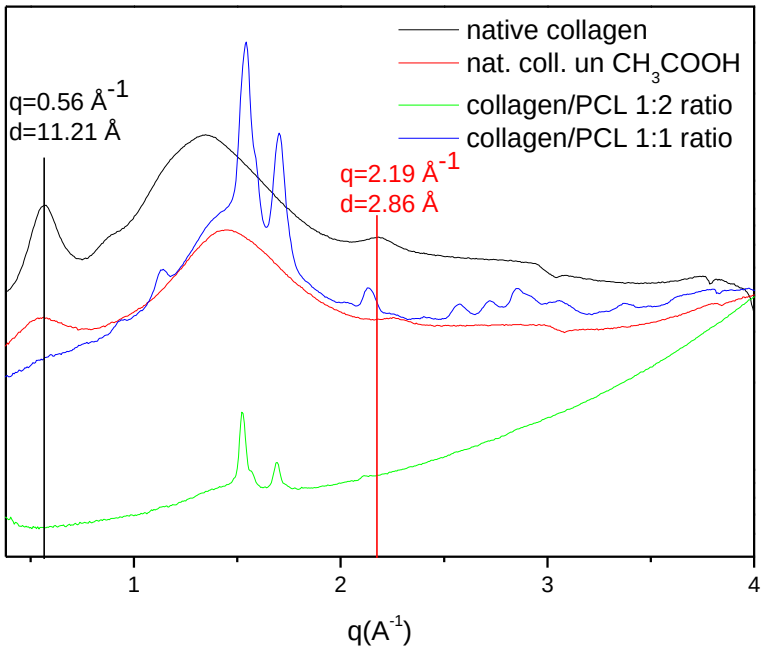

Figure 16 Comparison of WAXS spectra of native collagen, collagen in acetic acid 90 % v/v and collagen/PCL not electrospun mixtures (1:2 and 1:1 weight ratio).

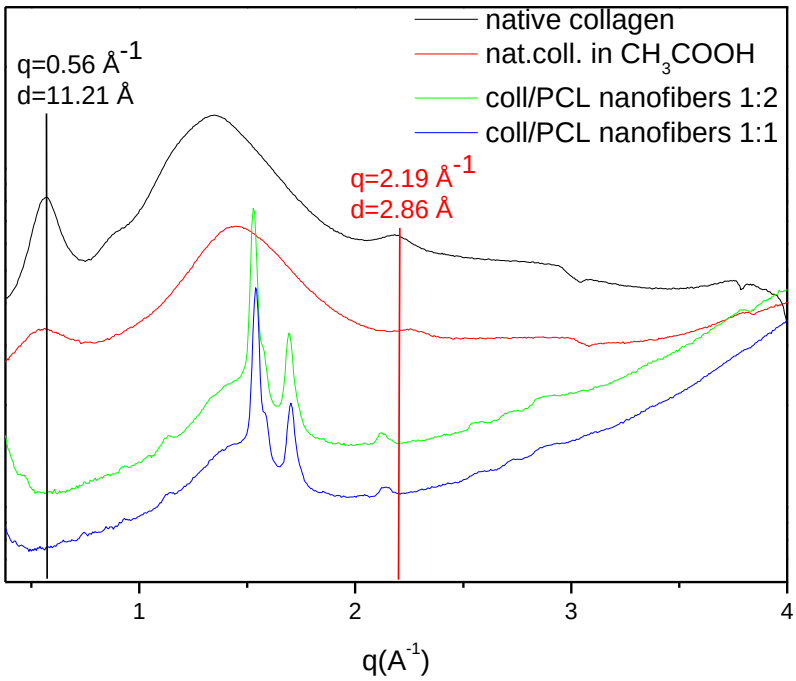

Figure 17 Comparison of WAXS spectra of native collagen, collagen in acetic acid 90 % v/v and collagen/PCL electrospun nanofibers (1:2 and 1:1 weight ratio).

2.7.Stability of nanofiber structure in the hydrated state

For the collagen/PCL nanofibers the morphology stability in the hydrated state was evaluated. From 24 h up to 1 week of immersion in deionized water, the architectural structure of nanofibers was preserved, and an increase of fiber diameters occurred. **Figure 18** and **19** show representative images and the measured dimensions for the samples with the highest content of the soluble protein (CP1 1:1 weight ratio). Similar results were recorded for collagen/PCL nanofibers obtained with less soluble protein into the formulation (CP3 1:2 weight ratio, data not shown).

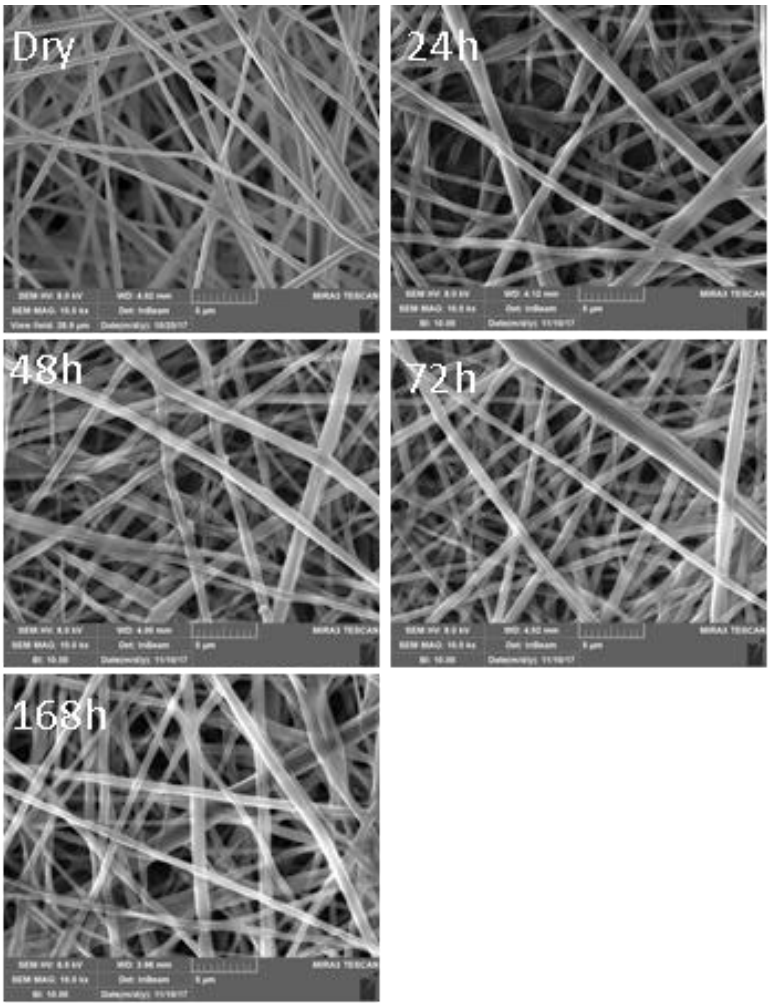

Figure 18 Photomicrographs SEM of 1:1 weight ratio collagen/PCL nanofibers in dry and hydrate states from 24h up to 1 week (168 h), room temperature.

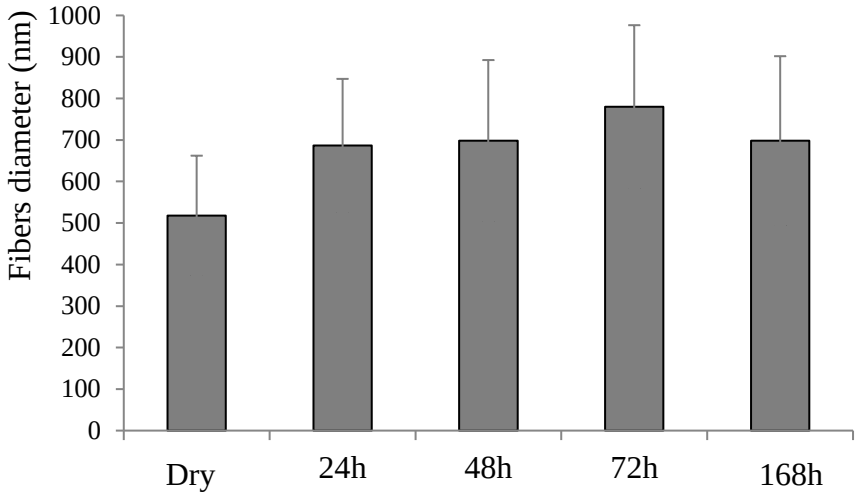

Figure 19 Size diameters comparison of PCL/collagen 1:1 % w/w (PC1) nanofibers at different hydration times in water, (room temperature) (mean values ± s.d., n=60).

2.8.Wettability

Figure 20 shows the results of wettability analyses for PCL and collagen/PCL at two weight ratios (1:1 and 1:2) electrospun nanofibers. As expected, the addition of collagen in the solution, and therefore in the composition of the nanofibers, involved a substantial reduction of the contact angle values compared to the nanofibrous membranes obtained with PCL only. The wettability increased thanks to the presence of the hydrophilic protein which reduced the interfacial tension between the liquid (water) and the solid surface of the nanofibers. The hydrophobic behavior of the polymer was evident in PCL nanofibers, but it was overcome by the hydrophilicity of collagen in collagen/PCL nanofibers, both 1:1 and 1:2 composition.

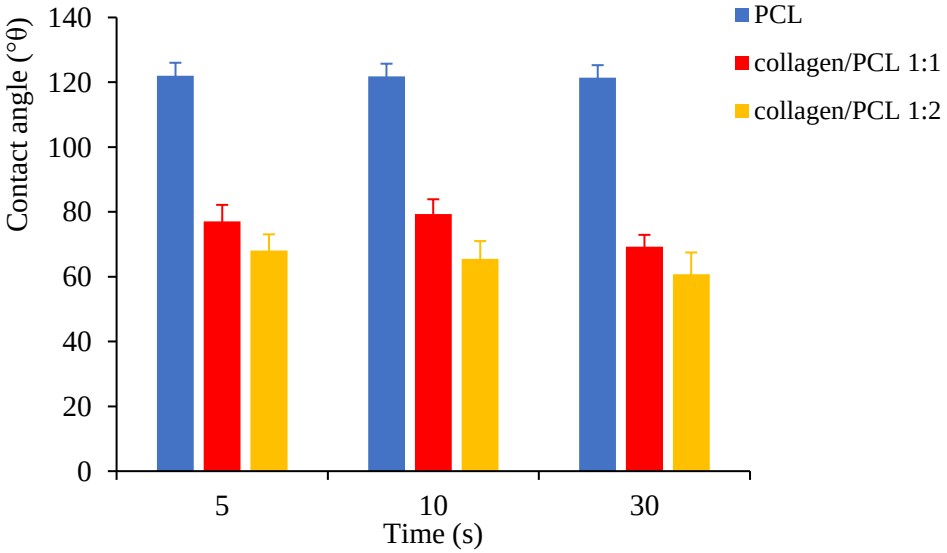

Figure 20 Comparison of contact angle values for PCL and collagen / PCL nanofibers at two weight ratios (1: 1 and 1:2, mean values ± s.d. n=3).

2.9.Mechanical properties

Figures 21 and 22 show the maximum strength values normalized with the section area exposed during the mechanical test (Stress in Pa) against the % elongation of collagen, PCL and collagen/PCL nanofibers at two weight ratios (1:1 and 1:2). The tensile distance was fixed between 20 and 30 mm. All nanofibrous membranes analyzed in the dry state (**Figure 21**) showed different behaviors depending on the collagen concentration. The nanofibers obtained with 100% collagen (formulation C6) show high elasticity, high maximum strength at the break point (≈ 4500 Pa) and low elongation %. This evidence indicated a rigid material with low deformation. When PCL is added to obtain a weight ratio 1: 1% w / w, the tensile strength drastically decreased and a brittle material, with very poor elasticity was obtained. The further decrease of collagen concentration in the protein:polymer 1:1 weight ratio of nanofibrous membranes led to a better plastic behavior with a decrease of the maximum breaking force together with a considerable increase of the % elongation. Fibers containing PCL only, compared to other nanofibrous membranes, were characterized by high plasticity with lower tensile strength and higher deformation. The tensile strength was assessed in the hydrated state, to evaluate the mechanical behavior of the nanofibrous membranes when exposed to aqueous fluids as a simulate use condition in a biological environment. Collagen-based fibers were not analyzed in hydrated conditions as these fibers undergo to a complete solubilization in the aqueous medium. The results (**Figure 22**) highlight a significant variation in mechanical properties for all nanofibrous membranes compared to the same fibers tested in the dry state. In the hydrated state, the plasticity of PCL plays a role in all cases. In particular, for collagen/PCL membranes 1:1 weight ratio, the combination between the highest content of water-soluble collagen and the plasticity of PCL led to a high elasticity nanofiber with a better elongation and deformation of the material. As commonly reported, lot of factors could affect the mechanical behavior of nano-scaffolds as electrospun nanofibrous membranes. For instance, to a high crystallinity of the material is associated a higher elastic modulus[23]. Another important factor which might influence this physical property is the average diameter, so the thickness of the mats. Some reports considered that thinner fibers have higher elasticity modulus than thicker ones[24,25].

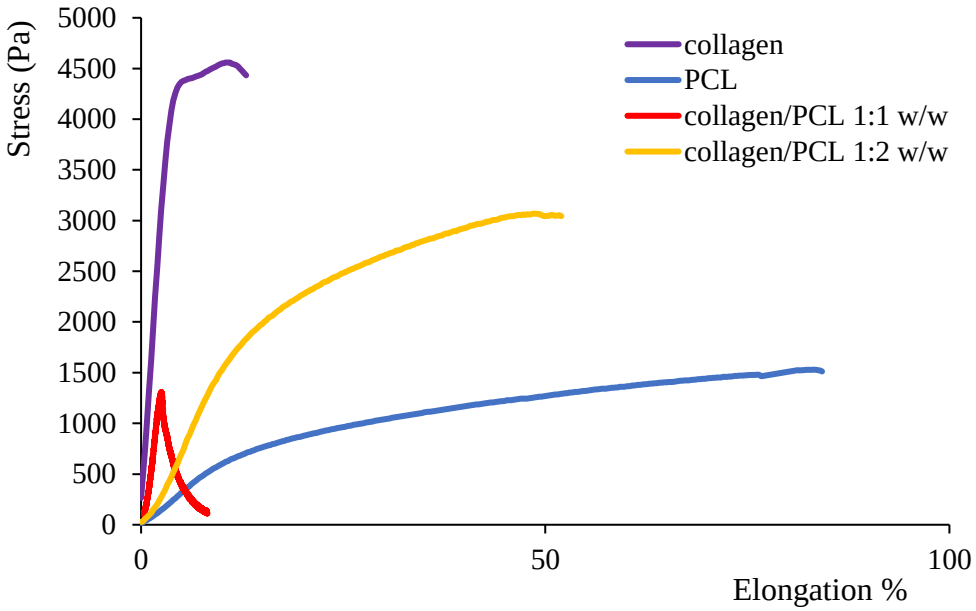

Figure 21 Stress (Pa) vs Elongation % profiles of dry nanofibrous membranes (mean values ± s.d., n=6).

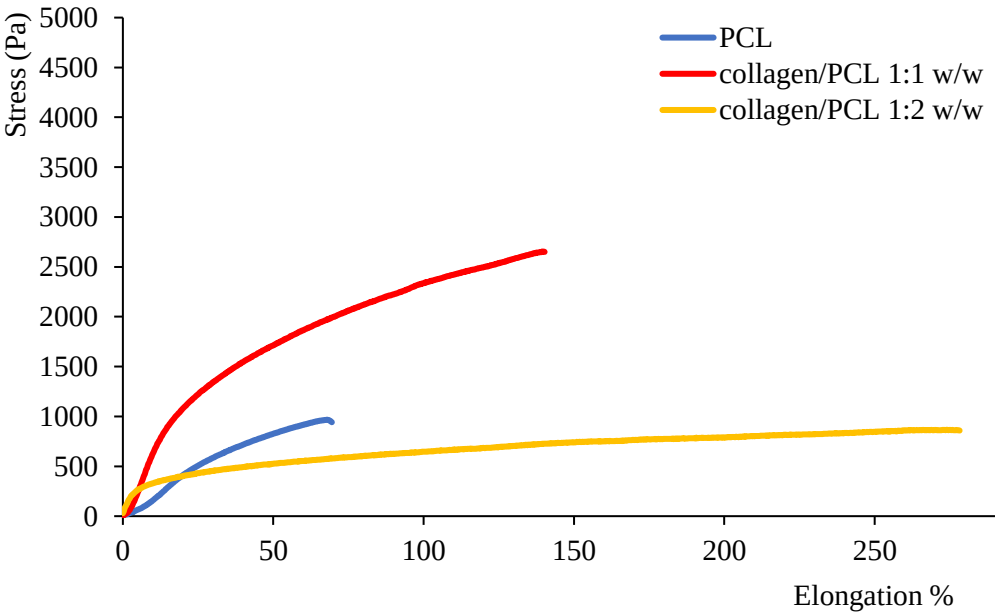

Figure 22 Stress (Pa) vs Elongation % profiles of wet nanofibrous membranes (mean values ± s.d., n=6).

2.10. Biocompatibility

A beneficial effect of collagen addition on the growth of cells onto the fibrous membranes is related to the presence of RGD sequence in polypeptide molecules – an Arg-Gly-Asp tripeptide that plays an important role in mediating cell adhesion interactions. This sequence, found in many extracellular matrix proteins, is recognized by integrins and acts as cell binding site[26]. The biocompatibility was assessed by seeding normal human dermal fibroblasts from neonatal tissue (NHDF) onto collagen, PCL and collagen/PCL nanofibrous membranes and culture the cells for 3 and 7 days. Samples were compared to a control where the cells were seeded at the bottom of the well and grown for the same time (standard growth conditions). After 3 days of culture all nanofibrous membranes showed viability values comparable to the control, only

slightly lower for collagen/PCL nanofibers 1:2 weight ratio. However, a substantial increase in cell growth after 7 days of treatment occurred for collagen/PCL mixtures. In particular, collagen/PCL nanofibers with the highest amount of protein (1:1 w/w ratio) showed a statistical increase in proliferation of NHDF, compared to the nanofibers with the lowest content of protein. (**Figure 23**). The combination between the stable architecture of nanofiber given by the insoluble polymer (PCL) and the highest amount of water-soluble protein which exposes more RGD region to the cells, ensure a better adhesion and proliferation activities. This result confirms not only the value of collagen in stimulation of cell adhesion and growth, but also the importance of the reticular solid structure which ensures an architectural support for migration and proliferation of fibroblasts. As reported in literature, these membranes represent a good biocompatible substrate for regenerative medicine with a synergistic effect given by the safety materials employed and their 3D stable, biocompatible and biodegradable structure[27,28].

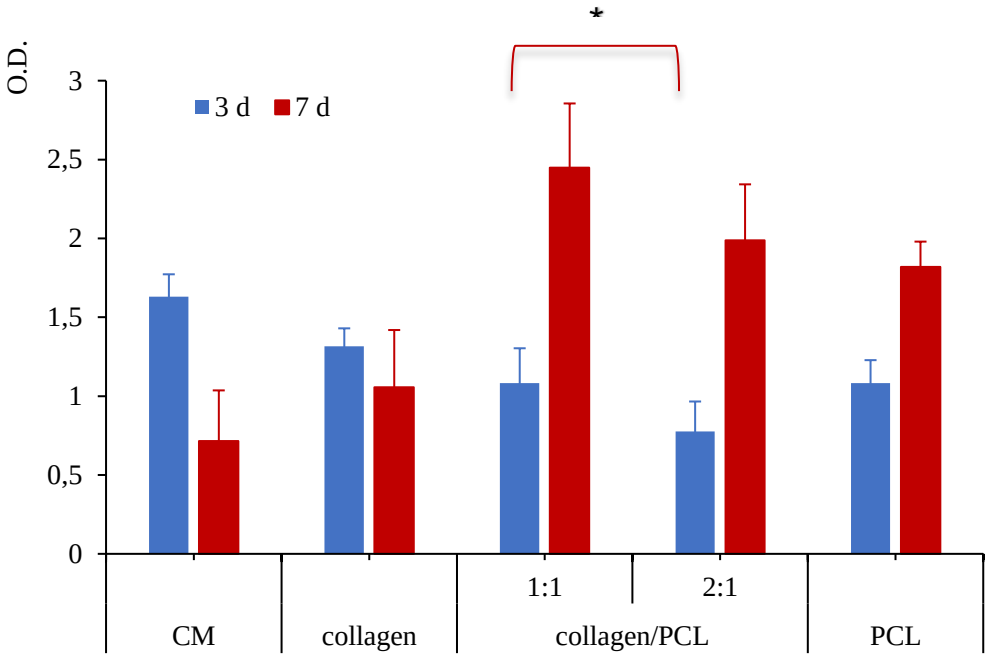

Figure 23 Optical density (O.D.) values of cell viability after seeding of normal human dermal fibroblasts (NHDF) on nanofibrous membranes. Culture for 3 and 7 days (ANOVA 1 via – MRT ($p<0,05$) (mean values ± s.d., n=8).

2.11. Cell Adhesion

SEM photomicrographs (magnification 10 kx) of cellular substrates grown on nanofibrous membranes for 3 days and 7 days are shown in **Figure 24**. SEM analysis confirms viability data. An extended cell adhesion was evident for each formulation. In all cases fibroblast were well attached onto the scaffold nanofibers and spread all over the surface reaching the confluence. The typical cell morphology was preserved, and cells appeared deeply incorporated

into the membrane, in particular, in the case of collagen/PCL nanofibers 1: 1 weight ratio. CLSM photomicrographs of cellular substrates grown for 3 and 7 days (labeled nuclei in blue with Hoerchst 33582 and cytoskeletons marked in red with phalloidin TRITC) on PCL, collagen/PCL 1: 1 and 1:2 weight ratios confirmed the quantitative data of viability obtained

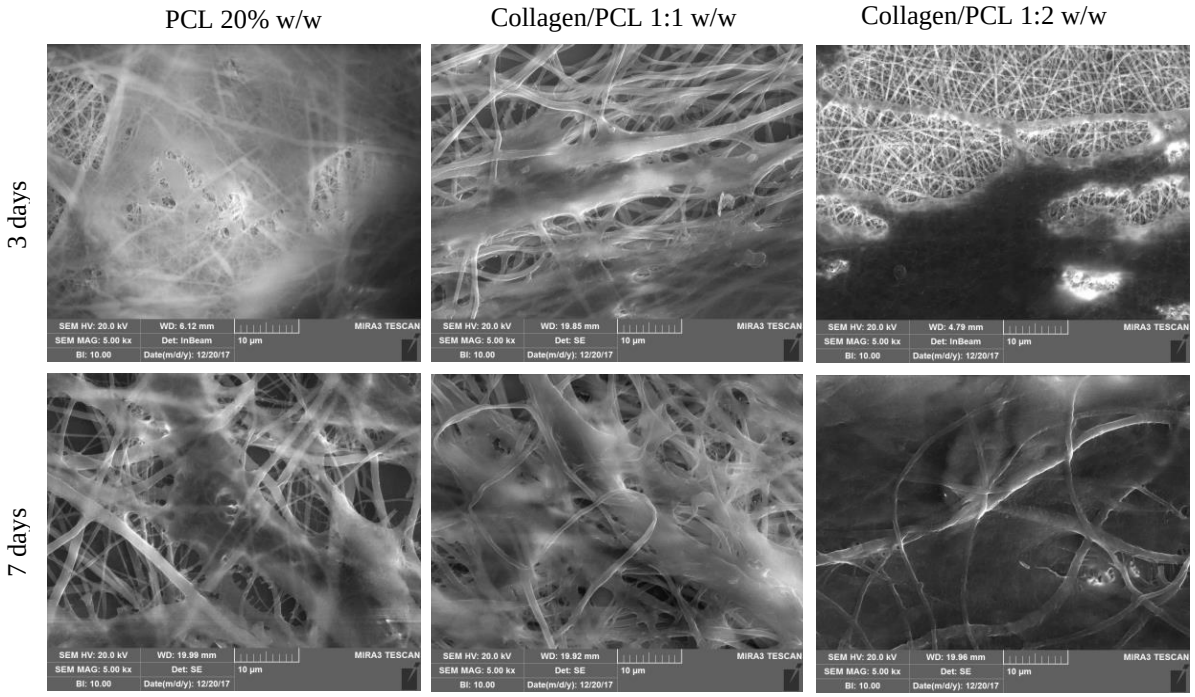

Figure 24 Photomicrographs SEM images of cell substrates grown upon nanofibrous membranes in 3- and 7-days culture – Normal Human Dermal Fibroblasts from neonatal tissue (NHDF).

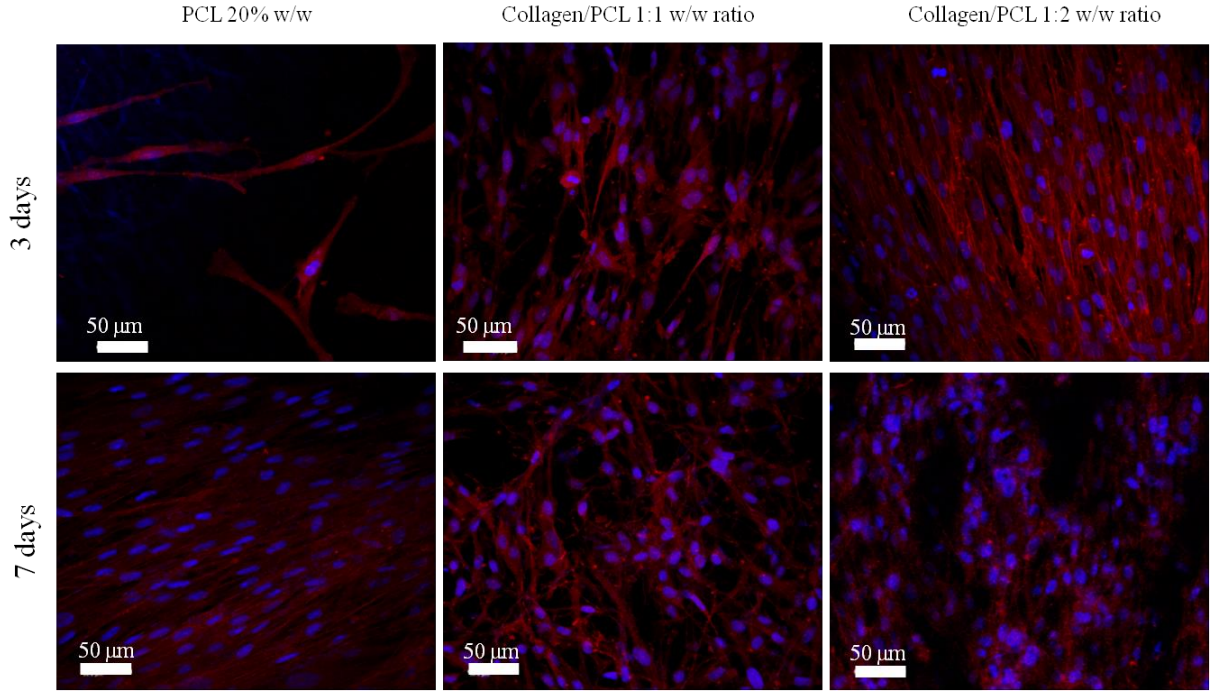

Figure 25 CLSM images of cell substrates (nucleus blue marked with Hoechst 33582) grown upon nanofibrous membranes in 3- and 7-days culture – Normal Human Dermal Fibroblasts from neonatal tissue (NHDF).

by the MTT test and the cell morphology presented in SEM photomicrographs (**Figure 25**). In all cases the cells were numerous, adhered to the membranes and with a healthy morphology.

2.12. Collagen vs Gelatin based fibers characterization

Previous studies reported in the literature demonstrated the denaturation of collagen in electrospun nanofibrous membranes, leading to the occurrence of gelatin-based scaffolds[29,30]. This occurrence was observed when electrospinning was performed in fluorurated solvents, or with acetic-formic acid mixtures. Analogous results were obtained in the present study with the solubilization of collagen in 90% v/v acetic acid, as demonstrated by the progressive loss of collagen native triple helix structure after acid solubilization and electrospinning process. The consequences of the denaturation on collagen wound-dressing were studied by a comparison of the mechanical and biological characteristics of collagen and gelatin nanofibers with and without PCL. As known, gelatin is the product of thermal denaturation or disintegration of insoluble collagen, obtained by controlled hydrolysis. In pharmaceutical and medical fields, gelatin has long been used in the preparation of carriers for drug delivery and of dressings for wound healing thanks to its relative low cost and easy commercial availability[27]. In our study nanofibrous membranes based on collagen and gelatin were compared in terms of fibers morphology, mechanical properties and fibroblast biocompatibility**.**

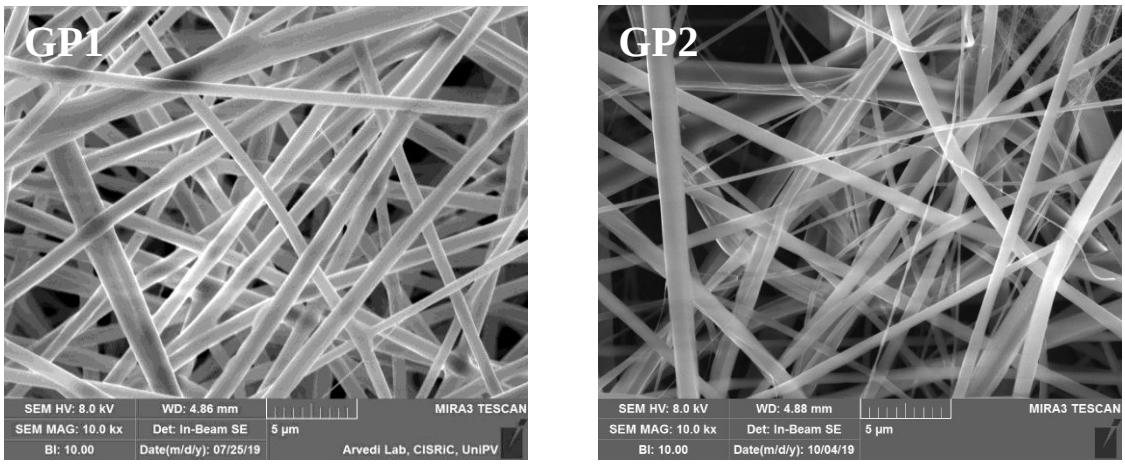

Figure 26 Photomicrographs SEM images of the gelatin/PCL nanofibrous membranes at two weight ratios GP1 (1:1) and GP2 (1:2) prepared in acetic acid 90 % v/v and electrospun using the same process parameters employed for collagen/PCL formulations.

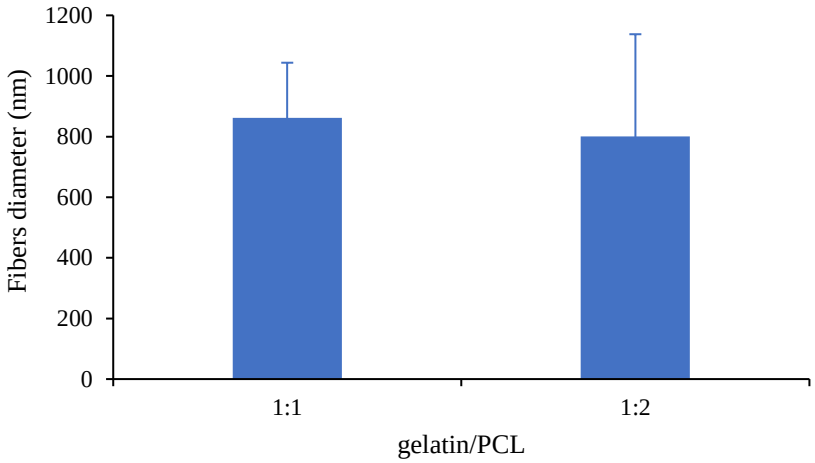

Figure 27 Size diameters (nm) comparison of gelatin/PCL nanofibers at two different ratios (mean values ± s.d., n=30). (ANOVA 1 via – MRT ($p<0,05$) mean values ± s.d., n=30)

Figure 26 shows the photomicrographs SEM images of electrospun gelatin/PCL nanofibers obtained from solutions prepared in acetic acid 90 % v/v at two different gelatin/PCL weight ratios (GP1 1:1 and GP2 1:2). Solutions were electrospun with the same process parameters employed for collagen/PCL nanofibers after DOE experiment. In both cases, even if nanofibers based on gelatin/PCL 1:2 showed a consistent variability in fiber diameters, dimensions between the two formulations were comparable and not statistical differences were denoted (**Figure 27**).

Figure 28 shows the profiles of the maximum breaking force normalized to the section area (stress) versus the % elongation values measured for the dry nanofibrous membranes based on gelatin/PCL (GP1 1: 1 weight ratio). Collagen/PCL (CP1 1:1 weight ratio) profiles are repeated for comparison purposes. The nanofibrous membranes based on gelatin/PCL show a behavior similar to that observed in the case of collagen/PCL fibers, with slightly higher elasticity. In **Figure 29** the stress versus elongation profiles of nanofibrous membranes evaluated in the hydrated state, are illustrated, to simulate the in vivo mechanical behavior of the dressings exposed to the wound exudates. In the hydrate state, stronger differences are evident with respect to the results obtained in the dry state. Under these conditions, collagen/PCL fibers, in fact, showed a higher tensile strength and a better deformability compared to nanofibers based on gelatin. In collagen/PCL nanofibers an improved synergistic effect between the plastic deformation of the synthetic polymer and the high elastic module of the protein makes these membranes an appropriate support able to follow the body movements and enhance wound healing even in case of application on joints and articulations. These data are in accordance with the evidence reported in literature, where scaffolds based on collagen/PCL seemed preferable for in vivo implantation, appearing smooth and glossy with good elasticity, while the gelatin/PCL electrospun scaffolds were relatively soft and easily collapsible[14].

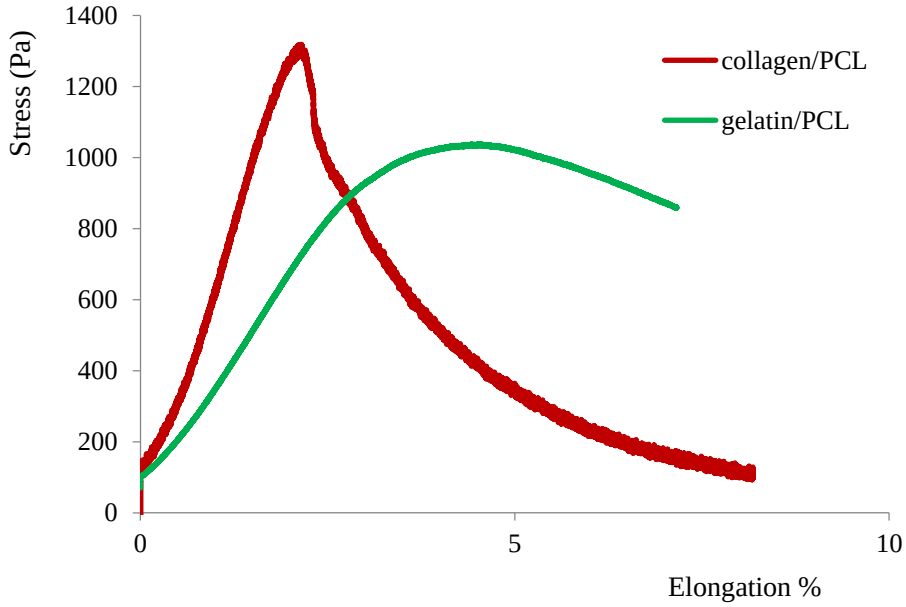

Figure 28 Stress (Pa) vs Elongation % of dry nanofibrous membranes (mean values ± s.d., n=6).

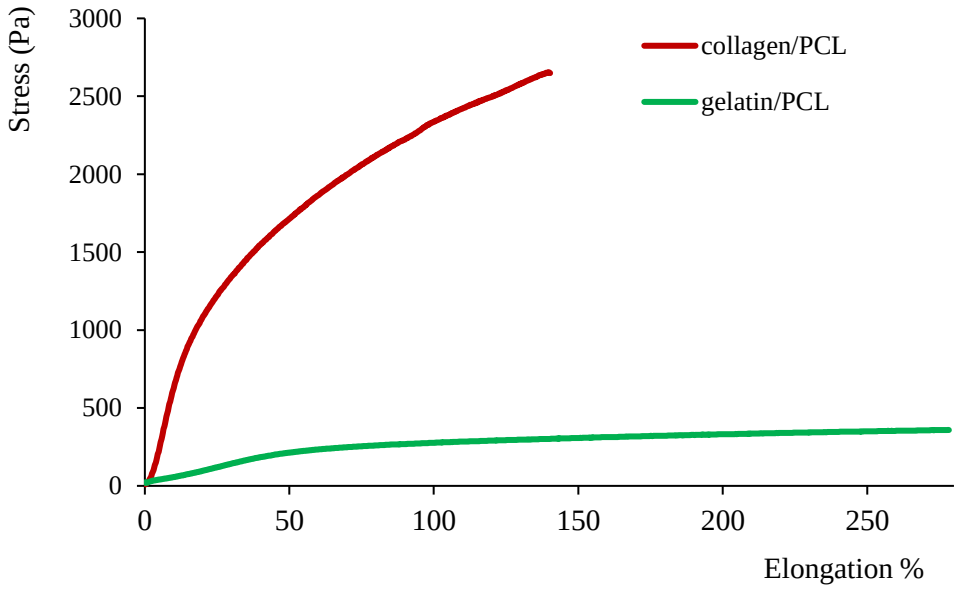

Figure 29 Stress (Pa) vs Elongation % of wet nanofibrous membranes (mean values ± s.d., n=6).

A biocompatibility test was performed to compare the efficacy of nanofibrous membranes in stimulating migration and proliferation of fibroblasts and predicting in vitro their efficacy to promote cells growing. Nanofibrous membranes based on collagen, gelatin, collagen/PCL and gelatin/PCL at two different weight ratios (1:1 and 1:2) were assessed. The results are illustrated in **Figure 30**. In all cases, it was evident that addition of both polypeptides increased statistically cell viability, by enhancing cells adhesion to the scaffolds. After 7 days in cultures, a significantly better performance in fibroblasts growth was evident for all nanofibrous membranes containing the insoluble polymer (PCL) compared to the control and the soluble membranes based on collagen and gelatin. Moreover, collagen/PCL scaffolds were able to support cell proliferation more than the gelatin-based samples, demonstrating the great

combined effort of collagen and the insoluble fiber architecture given by PCL in cell migration and spreading. These data are supported by results collected in literature on similar scaffolds, where cell proliferation increased with the addition of both collagen and gelatin, with some more efficient behavior in presence of collagen[26].

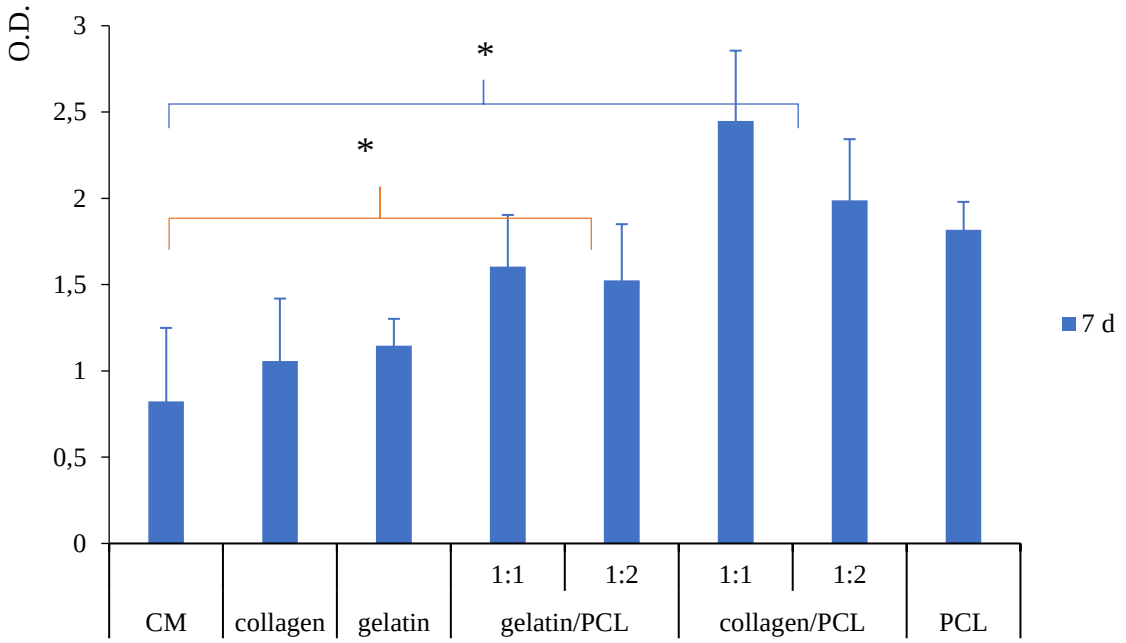

Figure 30 Optical density (O.D.) values of cell viability after seeding of normal human dermal fibroblasts (NHDF) on nanofibrous membranes based on collagen, gelatin, gelatin/PCL, collagen/PCL and PCL (ANOVA 1 via – MRT ($p<0,05$) mean values ± s.d., n=8).

3. Materials and Methods

- *Materials*

Polycaprolactone (PCL - Mw 80 000) and gelatin type B were purchased from Sigma Aldrich (Milan, Italy). Soluble native collagen 1% (w/v) from Kelisema S.R.L. (Como, Italy) and glacial acetic acid from Carlo Erba (Milan, Italy) was employed as solvent.

- *Methods*

3.1.Protein and Polymer Solutions

Native soluble collagen was dialyzed for 24 h in a dialysis bag (cut-off 12-14 kDa dialysis tubes, Emanuele Mires Ø = 36/32" – 28,6 mm) to remove the preservative agents; then the protein solution was freeze-dried for 48 h. The solid residue was dissolved at different concentrations (Table 1) in acetic acid solutions obtained by diluting glacial acetic acid with distilled water (25, 45 or 90 % v / v). Poly-caprolactone (PCL) was solubilized at various concentrations (**Table 3**) in 90 % (v / v) acetic acid solution, in a water bath at 37 ºC and under magnetic stirring (400 rpm) for 4 h; subsequently the polymer solution was sonicated for 30 min at the same temperature. Finally, collagen / PCL mixtures were obtained in 90% (v / v) acetic acid by adding under magnetic stirring the freeze-dried collagen to the PCL solution in two different weight ratios,1:1 and 1:2 (**Table 3**).

Table 3: % w / w composition of collagen, PCL and collagen / PCL solutions prepared in acetic acid at different concentrations.

Formulation	**% w /w concentration**	**% v / v CH_3COOH**
Collagen		
C1	10	25
C2		45
C3		90
C4	15	45
C5		90
C6	20	90
PCL		
P1	10	90
P2	15	90
P3	20	90
P4	30	90

collagen / PCL			
	collagen	*PCL*	*weight ratio*
CP1	10 7.5	10	1:1
CP2	5	15	1:2
CP3		10	

3.2.Electrospinning of polymer, collagen and collagen/polymer solutions

All the solutions reported in **Table 2** were subjected to electrospinning. Nanofibers were obtained by using the STKIT-40 (Linari Engineering equipment Pisa, Italy, **Figure 31**). A 10 ml glass syringe with a stainless-steel needle (OD = 0.8 mm, L = 15 mm) was filled with the proper solution and a volumetric pump (Razel R99-E) was employed for conveying. A high voltage generator (5 - 40 kV) charged the solution by applying a potential difference between the metal needle and a static collector covered with an aluminum foil. The operating spinning conditions, such as flow rate, voltage applied, and needle-collector distance were modulated according to the characteristics of the polymer solutions and to obtain continuous fibers without beads. The process was carried out at atmospheric pressure, maintaining temperature and relative humidity (RH) within an optimal set interval (24-30 °C, 22-30 % RH) to allow the solvent evaporation and avoid beads formation.

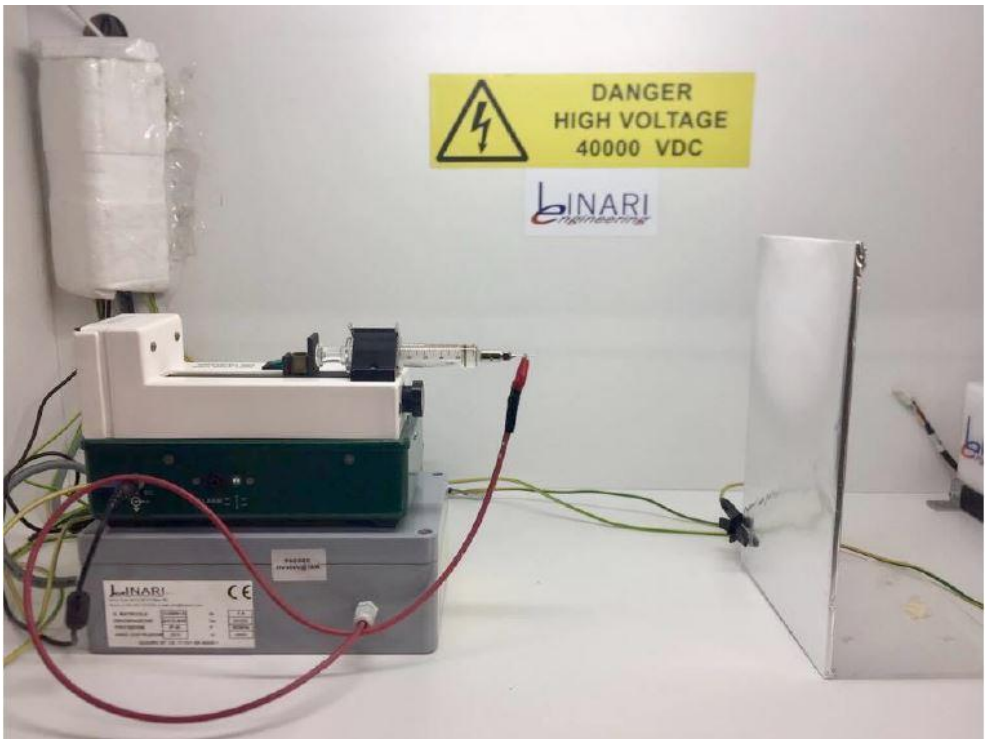

Figure 31 Electrospinning set-up, STKIT-40 Linari Engineering, I.

3.3.Characterization of polymeric and protein solutions

After the preliminary step carried out to identify the formulations suitable to obtain nanofibers from PCL, collagen and collagen/PCL mixtures, a physical characterization on solutions prepared in acetic acid 90 % (v/v) was performed.

3.3.1. Rheological analysis – critical entanglement concentration (CEC)

Solutions at different concentrations of PCL and collagen/PCL in a 1:1 weight ratio were prepared in acetic acid 90 % (v/v) with the aim of identifying the critical entanglement concentration (CEC).
At this concentration PCL, alone or in mixture with collagen, shows a non-Newtonian behavior as a consequence of the polymeric chain rearrangement. Critic entanglement concentration represents the minimum concentration needed to obtain nanofibers. PCL and collagen /PCL solutions prepared for rheological analysis are listed in **Table 4**.

Table 4: % w / w composition of PCL and collagen / PCL solutions in acetic acid 90 % v / v.

% w/w				
PCL	20	30	40	50
collagen/PCL 1:1	5	10	15	20

Rheological analyses were carried out using a rotational rheometer (Rheostress 600, Haake, Enco, Spinea, Italy). Solution viscosity (η) was measured at 25°C and at increasing shear rates in the range 10–1,000 s^{-1}. Three replicates were performed for each solution.
According to Rossi et. al 2001[31], for each concentration analyzed a shear stress (τ) versus shear rate (s−1) plot was processed to extrapolate zero shear viscosity (η0) and infinite shear viscosity (ηinf) values. These values were plotted against % w/w polymer concentration; after log-log transformation of the values on the axes, the critical polymer entanglement concentration (CEC) was determined as the intersection point of the two straight lines.

3.3.2. Physical properties – Conductivity (µS / cm) and Surface Tension mN/m

Physical analyses were performed on PCL (formulation P3), collagen (formulation C6) and collagen/PCL mixtures at two different weight ratios (formulations CP1 and CP3). Conductivity analyses were performed using FiveGoTM - Mettler Toledo conductimetry. Before the analyses, the instrument was calibrated at room temperature (≈25°C) with a standard of 1413 µs/cm. Three replicates were effected for each solution. Dynamic surface tension measurements were carried out by means of an automatic tensiometer (DyneMaster DY-300; Kyowa Interface Science Co. Ltd., Saitama, Japan) at 25°C. The analyses were performed by recording a surface tension value every 3 seconds up to 300 seconds in a measurement range from 0 to 100 mN/m (ds±0,2mN/m). Three replicates were considered for each solution.

3.4.Experimental design

3.4.1. Full factorial design

A Design of Experiment (DoE) approach was used to assess the influence of the electrospinning parameters on nanofiber dimensions and morphology for both collagen/PCL electrospun mixtures (2:1 and 1:1 weight ratio). A full factorial design 23, where 2 is the number of levels of each factor and 3 is the number of factors was considered. Namely the factors were the distance between the tip and the collector (cm), the voltage applied (kV) and the pump flow of the syringe (ml/h). Two levels (upper and lower) were considered for each factor. The levels considered for each of the three factors were: 15 and 25 cm for distance, 15 and 30 kV for voltage, 0.4 and 0.8 ml/h for flow. Eight experiments were therefore carried out to complete the 23 full factorial design (Figure 32). Three additional experiments were performed at central points (20 cm, 25 kV and 0.6 ml/h) of the space design.
All the process parameters considered are reported in Table 5: for each of them the upper level is indicated as +1, the lower level as -1 and the central point (C.P.) as 0. The response variables considered were: fiber dimensions (nm), number of beads and coefficient of variation (% CV) indicating the fiber morphology divergence. These response variables were acquired from nanofiber SEM images. The statistical analysis of the data was carried out with a statistical software package (Statgraphics5.0 Statistical Graphics Co., Rock villle, MD, USA).

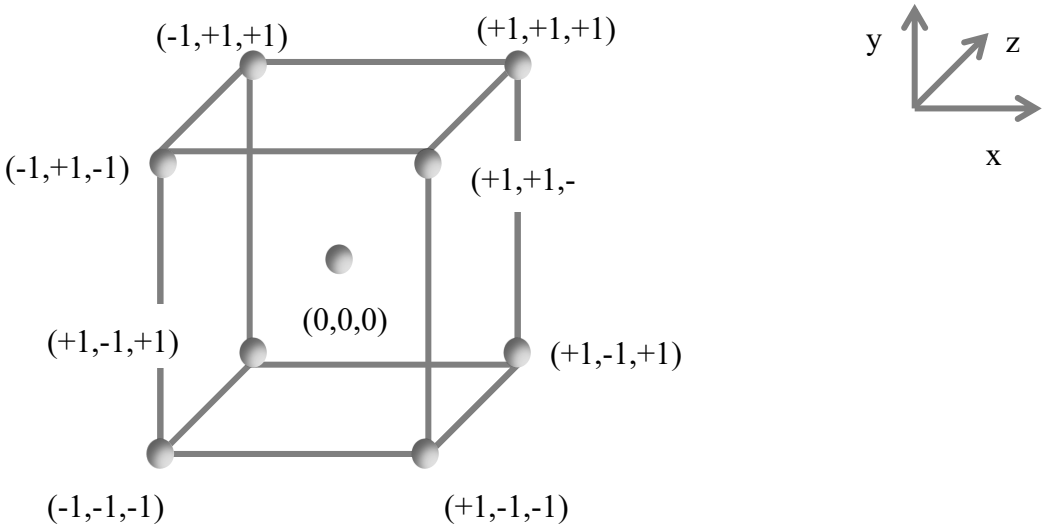

Figure 32: Factor space and experimental points of a “full factorial design”.

Table 5: Experimental points of the "full factorial design"

	Distance (nm)	**Voltage (kV)**	**Flow (ml /h)**
C.P.	0	0	0
1	-1	-1	-1
2	+1	-1	-1
3	-1	+1	-1
4	+1	+1	-1
C.P.	0	0	0
5	-1	-1	+1
6	+1	-1	+1
7	-1	+1	+1
8	+1	+1	+1
C.P.	0	0	0

3.5.Characterization of electrospun nanofibers

Scanning electron microscopy (SEM) images were acquired at room temperature by using a high-resolution FE-SEM scanning electron microscope (Tescan Mira3 XMU series); a high voltage (20 kV) and a high vacuum ($6 \cdot 10^2$ Pa) were applied. Different magnifications of 10.0kx; was considered for the morphological evaluation. Fiber diameters were analyzed and processed by SEM photomicrographs using *imageJ*. Software (https://imagej.net/ImageJ). Measures were effected on at least 60 fibers of each type.

3.6.Solubility test

Collagen / PCL nanofibrous membranes (at the two different weight protein/polymer ratios, formulation CP1 and CP2) were cut in small pieces (2 cm^2) and kept at room temperature in 5 ml of deionized water from 24 h up to 7 days. After the fixed times, membranes were dried overnight and morphology and stability of nanofibers, were evaluated by SEM analysis.

3.7.WAXS analyses

The wide-angle X-ray scattering experiments were performed at the X-ray Micro Imaging laboratory (XMI-LAB, Institute of Crystallography (IC), National Research Council, Bari, Italy) equipped with a Fr-E + SuperBright rotating copper anode micro-source ($\lambda = 0.154$ nm, 2475 W) which is coupled by a multilayer focus optics (Confocal Max-Flux CMF 15-105) to a SAXS/WAXS three pinhole camera. WAXS analysis data were collected using an image

detector (IP) (250 × 160 mm2, with 100 μm effective pixels) and an offline RAXIA reader. Samples were directly placed on a sample holder, the detector was located 10 cm away from them, giving a range of scattering vector moduli ($q = 4\pi\sin\theta / \lambda$) from 0.3 to about 3.5 Å-1, which correspond to a 1.8-25 Å d-spacing range. Furthermore, collagen structure was evaluated at the atomic level by recording two distinct signals: i) the meridional reflection, the distance between adjacent amino acid residues along the central axis of the triple helix of collagen (periodicity index of the triple helix); ii) the equatorial reflection, the distance between the triple collagen helices within the fibril (index of lateral packing). The analyses were carried out in duplicates, on collagen, PCL and collagen/PCL samples prepared as non-electrospun films, by evaporating the solvent of 2 ml solution overnight and on the same electrospun samples (formulations C6, P3, CP1).

3.8.Wettability

Wettability test on nanofibrous membranes was carried out by the aid of a Cam tool 200 Contact Angle and Surface Tension Meter, KSV Instrument. The instrument was equipped with a telecentric camera and 55 cm focal length, monochromatic LED source, which allowed the measurement of the contact angle of a drop (volume 5μl) left lay on the scaffold and dispensed by the needle of a syringe pump. The instrument is equipped with a camera captured an image every second for 30 seconds. Before proceeding with the measurement, PCL and collagen / PCL nanofibers (square 2 cm^2) were hydrate in water for 30s and properly adhered on a coverslip. For each sample three replicates were done.

3.9.Mechanical properties of nanofibrous membranes

The mechanical properties of the nanofibrous membranes prepared from collagen (C6), PCL (P3) and collagen/ PCL (1:1 and 1:2 weight ratio, CP1 and CP3) solutions were measured with a TA.XT plus Texture Analyzer (Stable MicroSystems, Godalming, UK), equipped with a 5 kg load cell. Before testing, fiber thickness was measured by a Sicutool 3955 G-50 (Sicutool, Milan, I) apparatus. The nanofibrous membranes were cut (1x3 cm) and inserted between two clamps (A/TG grips probe) to expose a surface area of 1 cm^2. The upper grip was raised at a trigger force of 1 mN under a controlled speed of 1 mm/s either 30 mm or until to the break point. Mechanical properties were evaluated in the dry and hydrated state (after 450 μL distilled water addition for 2 min). For each sample the stress / % elongation profile was recorded. Five replicates were effected for each sample.

3.10. In vitro cell culture experiments

3.10.1. Biocompatibility

Normal human dermal fibroblasts (NHDFs) NHDFs (Promocell GmbH, Heidelberg, G) from 5^{th} to 10^{th} passage were used. Cells were sub-cultured in complete medium (CM) consisting of DMEM supplemented with 1% v/v antibiotic/antimycotic solution and 10% v/v inactivated fetal calf bovine serum. Collagen (C6), PCL (P3) and collagen/PCL nanofibers at the two

different weight ratios (1:1 and 1:2 – CP1 and CP3 respectively), were cut in round pieces with a punch (Ø = 4 mm) and UV irradiated for 24 h. The pieces were placed into a 96-well plate and conditioned with 10 µl of CM. NHDFs (35.000 x well in 200 µl of CM) were seeded onto the nanofibrous membrane for 3 and 7 days. Subsequently, the eventual cytotoxic effect of nanofibrous membranes was assessed by an MTT test. First the medium was withdrawn and 50 µl per well of 7.5 µM MTT reagent in DMEM without red phenol was added in each well; subsequently the plates were placed in incubator at 37 ° C for 3h. Finally, the MTT reagent was removed and 100 µL of DMSO were added to each well to lyses the cellular membranes and to allow the complete dissolution of formazan crystals, derived from mitochondrial dehydrogenases reduction of the MTT dye. Results were expressed as % absorbance measured after contact with each sample with that measured for CM. This solution absorbance was measured by means of an iMark® Microplate reader (Bio-Rad Laboratories Inc., Hercules, CA, USA) at a wavelength of 570 and 690 nm (reference wavelength) after 60 s of mild shaking. Eight replicates were performed for each sample.

3.10.2. Cell adhesion and morphology

Fibroblast adhesion and morphological shape after treatment with PCL and collagen/PCL nanofibers at the two different weight ratios (1:1 and 1:2) was assessed by means of scanning electron microscopy (SEM) and confocal laser scanning microscopy (CLSM). Briefly, nanofibers were cut in round pieces to get a surface area of 1.9 cm^2 and UV irradiated for 24 h. The pieces were laid down into a 24-well plate and conditioned with 50 µl of CM. 100,000 NHDF in 450 µl of CM were seeded in each well onto the nanofibers. After 3 and 7 days of culture, media was withdrawn, samples were washed with PBS and cells were fixed for 1 h at room temperature with 3 % v/v of a glutaraldehyde solution. Subsequently, the samples were rinsed twice with 200 µl of PBS. For SEM analysis, samples were dehydrated with increasing concentration of ethanol (25%, 50%, 75% and 100% v/v) and air dried at room temperature overnight. For CLSM analysis, samples were at first treated with Tryton 0.1 % v/v for 5 min to permeabilize cell membranes in order to enable cytoskeleton staining with 100 µl of Phalloidin-TRITC (concentration 50 µg/ml, Sigma, I) for 40 min, at room temperature and protected from light. Afterwards, substrates were washed twice with PBS and treated for 10 min, at room temperature and protected from light with 100 µl of Hoechst 33258 (Sigma, I) diluted in PBS 1: 10000, in order to stain the nuclei. Stained samples were then examined by CLSM and the fluorescence of Phalloidin TRITC and Hoechst 33258 (λex = 346 nm and λemm = 460 nm) were metered. The acquired images were processed using a "LAS X Life Science" software (Leika Microsystem, I).

3.11. Comparison of collagen and gelatin-based nanofibers

Since collagen was denatured after acidic treatment and electrospinning process, nanofibrous membrane based on collagen/PCL at two weight ratios (formulation CP1 and CP3) were compared with gelatin, a hydrolytic derivative of collagen. Gelatin/PCL nanofibers were obtained from the formulations listed in **Table 6** in acetic acid 90 % v/v using the same process

parameters fixed for collagen/PCL mixtures. SEM analyses, fiber dimensions, mechanical properties and a biocompatibility test were performed, using the methods previously described, to better highlight differences between the two polypeptides discriminating vantages and disadvantages of employing collagen instead of gelatin in nanofiber preparation.

Table 6 % w / w composition of gelatin / PCL solutions prepared in acetic acid 90 % v/v.

Gelatin / PCL			
Formulation	% w /w concentration		
	gelatin	PCL	weight ratio
GP1	10	10	1:1
GP2	5	10	1:2

3.12. Statistical Analysis

Statistical evaluations were performed by means of Statgraphics 5.0, Statistical Graphics Corporation, MD, USA. Differences were determined according to one-way ANOVA and were considered significant at $p < 0.05$. The same statistical package was used to analyze the results of the full factorial design.

4. Conclusion

Nanofibrous membranes based on collagen and PCL alone or combined were successfully obtained by electrospinning in 90% (v/v) acetic acid as solvent. The preliminary development phase indicated that all the tested solutions had very similar surface tension, that could not be considered a key parameter for their spinnability. Conductivity was on the other hand strongly variable, ranging from the very low values of the non-ionic PCL solution, to the high values observed with the increase of collagen concentration in the mixtures. No influence of conductivity on solution spinnability was therefore evidenced in the present study. A DOE approach resulted useful to evaluate the relevance of process parameters used to electrospin collagen/PCL mixtures, improving the process standardization. Both mixtures at 1:1 and 1:2 collagen/PCL ratios showed improved mechanical properties in the hydrate state with respect to both collagen and PCL alone. For both collagen/PCL formulations an excellent biocompatibility was highlighted, associated with an increase in proliferation and with a marked cell adhesion. Significantly higher proliferation was obtained in the case of the highest content of collagen, demonstrating that the protein positively influenced the behavior of the scaffolds. WAXS analyses on collagen and collagen/PCL fibers confirmed the loss of the triple helix structure due both to the strongly acidic solvent and to the high shear of electrospinning process. However, the comparison between collagen/PCL and gelatin/PCL electrospun nanofibers in term of mechanical behavior and biocompatibility showed better results for collagen-based nanofibers, characterized by higher mechanical strength and enhancement in fibroblast proliferation, especially for the 1:1 ratio. Therefore, collagen/PCL nanofibrous membranes with the highest amount of protein seem to be promising supports for growth and cell migration and proliferation.

Collaborations

This work was conducted in collaboration with XMI-LAB, Institute of Crystallography (IC), National Research Council, Bari, Italy, where wide-angle X-ray scattering experiments were performed.

References

[1] Bonassar L. J. et al., «Tissue Engineering: The First Decade and Beyond», *Journal of Cellular Biochemistry. Supplement* 30–31, 1998: 297–303.

[2] O'Brien F. J., «Biomaterials & scaffolds for tissue engineering», *Materials Today* 14, 2011, 3: 88–95.

[3] Dulnik J. et al., «Biodegradation of Bicomponent PCL/Gelatin and PCL/Collagen Nanofibers Electrospun from Alternative Solvent System», *Polymer Degradation and Stability* 130, 2016: 10–21.

[4] Sandri G. et al., «Chitosan/glycosaminoglycan scaffolds for skin reparation», *Carbohydrate Polymers* 220, 2019: 219–27.

[5] Neve A. et al., «Extracellular Matrix Modulates Angiogenesis in Physiological and Pathological Conditions», *BioMed Research International*, 2014: 1-10.

[6] Lee Chi H. et al., «Biomedical Applications of Collagen», *International Journal of Pharmaceutics* 221, 2001: 1–22.

[7] Georgiana M. et al., «Collagen-Based Drug Delivery Systems for Tissue Engineering», in *Biomaterials Applications for Nanomedicine*, 17, 2011: 333-348.

[8] Yogeshwar Chakrapani V. et al., «Electrospinning of Type I Collagen and PCL Nanofibers Using Acetic Acid», *Journal of Applied Polymer Science* 125, 4, 2012: 3221–27.

[9] Olsen D. et al., «Recombinant Collagen and Gelatin for Drug Delivery», *Advanced Drug Delivery Reviews* 55, 12, 2003: 1547–67.

[10] Anjum F. et al., «Biocomposite Nanofiber Matrices to Support ECM remodelling by Human Dermal Progenitors and Enhanced Wound Closure», *Scientific Reports* 7, 1, 2017: 10291-10308.

[11] Dulnik J. et al., «Biodegradation of bicomponent PCL/gelatin and PCL/collagen nanofibers electrospun from alternative solvent system», *Polymer Degradation and Stability*, 130, 2016: 10-21.

[12] Aguirre-Chagala Y.E. et al., «Physicochemical Properties of Polycaprolactone/Collagen/Elastin Nanofibers Fabricated by Electrospinning», *Materials Science and Engineering: C* 76, 2017: 897–907.

[13] Bertram U. et al., «Vascular Tissue Engineering: Effects of Integrating Collagen into a PCL Based Nanofiber Material», *BioMed Research International* 2017: 1–11.

[14] Fu W. et al., «Electrospun Gelatin/PCL and Collagen/PLCL Scaffolds for Vascular Tissue Engineering», *International Journal of Nanomedicine*, 2014,9,1, 2335-44.

[15] Dippold D. et al., «Novel Approach towards Aligned PCL-Collagen Nanofibrous Constructs from a Benign Solvent System», *Materials Science and Engineering: C* 72, 2017: 278–83.

[16] Dippold D. et al., «Investigation of the Batch-to-Batch Inconsistencies of Collagen in PCL-Collagen Nanofibers», *Materials Science and Engineering: C* 95 2019: 217–25.

[17] Bonferoni, M.C. et al. «Rheological behaviour of hydrophilic polymers and drug release from erodible matrices», *Journal of Controlled Release*, 18 (3), 1992: 205-212.

[18] Rossi S. et al., «Characterization of Chitosan Hydrochloride--Mucin Rheological Interaction: Influence of Polymer Concentration and Polymer: Mucin Weight Ratio», *European Journal of Pharmaceutical Sciences: Official Journal of the European Federation for Pharmaceutical Sciences* 12, 4, 2001: 479–85.

[19] Vigani B. et al., «Coated electrospun alginate-containing fibers as novel delivery systems for regenerative purposes», *International Journal of Nanomedicine* 13, 2018: 6531–50.

[20] Vlachou M. et al., «Electrospinning and Drug Delivery», *Electrospinning and Electrospraying - Techniques and Applications*, 2019, 1-22.

[21] Leidy R: et al., «Use of electrospinning technique to produce nanofibres for food industries: A perspective from regulations to characterisations», *Trends in Food Science & Technology* 85, 2019: 92–106.

[22] Zeugolis D.I. et al., «Electro-Spinning of Pure Collagen Nano-Fibres - Just an Expensive Way to Make Gelatin?», *Biomaterials* 29,15, 2008: 2293–2305.

[23] Aguirre-Chagala Y.E. et al., «Physicochemical Properties of Polycaprolactone/Collagen/Elastin Nanofibers Fabricated by Electrospinning», *Materials Science & Engineering. C, Materials for Biological Applications* 76, 2017: 897–907.

[24] Janković B. et al., «The Design Trend in Tissue-Engineering Scaffolds Based on Nanomechanical Properties of Individual Electrospun Nanofibers», *International Journal of Pharmaceutics* 455, 1–2,2013: 338–47.

[25] Baker S.T. et al., «Determining the Mechanical Properties of Electrospun Poly-ε-Caprolactone (PCL) Nanofibers Using AFM and a Novel Fiber Anchoring Technique», *Materials Science and Engineering: C* 59, 2016: 203–12.

[26] Judyta Dulnik et al., «The Effect of a Solvent on Cellular Response to PCL/Gelatin and PCL/Collagen Electrospun Nanofibres», *European Polymer Journal* 104, 2018: 147–56.

[27] Zhang Y. Z. et al., «Characterization of the Surface Biocompatibility of the Electrospun PCL-Collagen Nanofibers Using Fibroblasts», *Biomacromolecules* 6, 5, 2005: 2583–89.

[28] Zhang Q. et al., «Characterization of Polycaprolactone/Collagen Fibrous Scaffolds by Electrospinning and Their Bioactivity», *International Journal of Biological Macromolecules* 76, 2015: 94–101.

[29] Zeugolis D.I. et al., «Electro-spinning of pure collagen nano-fibres – Just an expensive way to make gelatin? », *Biomaterials* 29, 15, 2008: 2293–2305.

[30] Ismail A.F. et al., «Nanofiber Membranes for Medical, Environmental, and Energy Applications», CRC Press, 1st edition, 2019, 1-300.

[31] Rossi S. et al., «Characterization of chitosan hydrochloride–mucin rheological interaction: influence of polymer concentration and polymer: mucin weight ratio», *European Journal of Pharmaceutical Sciences* 12, 4, 2001: 479–85.

CHAPTER IV

COLLAGEN/PCL NANOFIBERS AS DRUG DELIVERY SYSTEM OF POORLY SOLUBLE POLYPHENOLS

ABSTRACT

A bioactive dressing is a tool designed to interact with the wound surface providing an optimal micro-environment and releasing bioactive molecules to accelerate the healing process. To get an effective action, it must consider some essential characteristics such as: the type of wound, the wound healing rate and the physical - chemical properties of the materials employed. Electrospun nanofibers can be employed as excellent wound dressing devices; in fact, through the combination between natural and synthetic materials it is possible to obtain systems characterized by a porous nature particularly suitable to drain the exudates released by the lesion, to allow an adequate gas exchange and to prevent microbial attack, which could lead to a delayed healing. The aim of this work is focused on the design of electrospun nanofibers as substitutes of biological tissues that mimic the natural structure of tissues by interacting selectively with cells through specific biomolecular recognition. The electrospun nanofibers are obtained from a native soluble collagen, an abundant structural protein and a synthetic and biocompatible polymer (polycaprolactone - PCL) blended together. As bioactive molecules in the tissue regeneration process, two polyphenols were loaded separately into these systems: curcumin and resveratrol. These molecules have important anti-inflammatory and antioxidant properties and therefore useful to accelerate and to promote the repair of damaged tissue.

1. Introduction

Alterations in the integrity of tegumentary apparatus, caused by injuries, burn wound or ulcers, usually induce repair processes that involve a series of coordinated events including bleeding, coagulation, inflammatory response, migration and division of connective tissue and parenchyma cells, angiogenesis, formation of extracellular matrix (ECM) and, finally, the remodeling phase for the maturity of proliferative epithelium with the formation of scar tissue[1,2] However, there is an incredible diversity in how this process occurs and studying wound repair, helps to identify molecules or pathways that can be targeted to restore the lost regenerative capacity[2]. Generally, therapeutic wound care relies on preventing or eradicating existing infections and accelerating the healing process of the injured tissue. To do this, the wounded area is treated with anti-infectives and physically covered with wound dressings. Recently, classical dressings are substitute with bioactive systems capable to promote faster wound healing through angiogenesis acceleration and improving cellular communication, at the same time preventing invasion of bacteria and allowing gas exchange[3]. Even if native or artificial wound grafts are a well-established treatment, to address chronic wounds, the failure rates of skin grafts in the setting of ischemic wounds is still particularly high[4]. The first reason is the occurrence of an imbalance between the metabolic or nutritional demands of the grafted skin tissue causing molecular events that include the generation of free radicals due to peroxidation of lipids present in the cell membranes, and the delay in neovascularization and the degradation of extracellular matrix (ECM) due to proteases secreted by inflammatory cells[5,6]. To avoid all these issues, active molecules with proven anti-inflammatory and antimicrobial activities can be loaded into scaffolds. Medicinal plants can be considered as a source of potent and promising therapeutics for improvement of wound healing. Flavonoids, essential oils, alkaloids, phenolic compounds, terpenoids, are widely studied for their possible therapeutic applications[7]. Based on these premises, our goal

was to develop a bioactive dressing loaded with well-known natural therapeutic molecules curcumin (CUR) and resveratrol (RSV), with the aim to improve their anti-inflammatory and antioxidant activities by enhancing their poor solubility in biological fluids and promote cellular migration and proliferation to the wound area. As well described in literature, CUR and RSV are polyphenols, exploiting anti-oxidant, anti-inflammatory and anti-microbial effect; for all these activities they can be employed in wound repair to protect tissues from microbial contamination and to treat wound area, promoting the healing and tissue repairing. CUR and RSV show *in vivo* low bioavailability and rapid metabolism and, to overcome these limits, a promising solution relies on using nano-formulations, like nanofibers, that prevent their degradation and ensure higher concentrations at the treated area. Several studies reported the therapeutic effect of CUR and RSV; specifically, wound healing studies have shown curcumin improves dermal wound healing by reducing reactive oxygen species (ROS) and lipid peroxidation LPx, compound associated to the initiation of oxidative stress[8,9,10,11]. The potent antioxidant activity of curcumin is the result of its ability to shift electrons or easily give H-atoms from two methoxy phenol groups. Further, the activation of cytoprotective signaling components from, for example, the nuclear factor erythroid 2-related factor (Nrf2) pathway is associated to molecular mechanisms responsible for antioxidant activity of curcumin[12]. On the other hand, *in vivo* studies, underline the effect of resveratrol in accelerate wound healing, through an effective vascularization, by activating AMPK signaling pathway when it is locally applied (50 μM) in the dorsal skin wound bed[13]. Furthermore, the topical administration of resveratrol, studied thought gene array technology show enhanced gene expression of anti-aging protein Sirtuin 1 (SIRT1), major extracellular matrix proteins (collagen and elastin) and antioxidants (catalase, superoxide dismutase, lysyl-oxidase) followed by down-regulation of inflammatory marker proteins (IL-1∝, IL-6)[14,15]. A novel generation of bioactive wound dressings relies on electrospun fibers, with diameter ranging from tens of nanometers up to few micrometers. The great surface area and the extremely thin structure give optimum topographical and mechanical properties, suitable for the drainage of exudates released by the lesion, allowing an adequate permeation of atmospheric oxygen. Additionally, they simulate closely the structure of the native ECM improving cell migration and proliferation[16]. One of the methods more commonly employed to develop micro-or nanofibrous dressings is the electrospinning process. In the last few decades the interest for this method increased drastically thanks to its peculiar versatility. Several materials, especially natural, biocompatible compounds can be employed. In our research, to develop a polyphenol nanofibrous drug delivery system we choose a binary combination of natural and synthetic biomaterials. In a previous study, different formulations at different concentrations collagen/PCL blended at two weight ratios were prepared and electrospun. In all cases nanofibers were successfully obtained, however scaffold based on final concentration of collagen/PCL 1:1 weight ratio showed the best performance in terms of mechanical properties and an optimal biocompatibility promoting migration and proliferation of normal human dermal fibroblasts (Chapter III). Collagen was chosen, as the natural fraction of the scaffold, for its high biocompatibility and important physiological properties. As well known, collagen synthesis increases after an injury in cells located under the dermis due to inflammatory responses and its production triggers the tissue re-epithelialization by improving cells communications[17,18,19]. Poly-caprolactone (PCL)

represents the insoluble synthetic portion, required to both co-adjuvate the electrospinning technique, to improve mechanical properties of the scaffold and to support cells migration during healing processes. Poorly soluble polyphenols (CUR and RSV) were therefore loaded in the previously developed collagen/PCL nanofibers and characterization was performed by physical-chemical analysis, release studies, biocompatibility and cell adhesion. A second step of the work relied on coating the same polyphenols scaffold with solutions of native water-soluble collagen. The aim was to ensure better cellular adhesion and spreading, either of fibroblast and keratinocytes. Native collagen, can, in fact, enhance scaffold hydrophilicity improving scaffold biological affinity and, at the same time, exposes RGD regions that actively interact with various integrin on cell surface promoting cell adhesion and migration.

2. Results and discussion

2.1.Rheological Analyses

A rheological study onto all solutions electrospun was performed. The plots show the comparison of the rheological properties from collagen/PCL mixtures without and with polyphenols. The addition of curcumin into the solution did not affect in a statistical way the rheological behavior if compared to the solution without polyphenol. On the other hand, mixture loaded with resveratrol induced a slight increase of viscosity, may due to a different rearrangement of the moiety into protein/polymer complex (**Figure 1**).

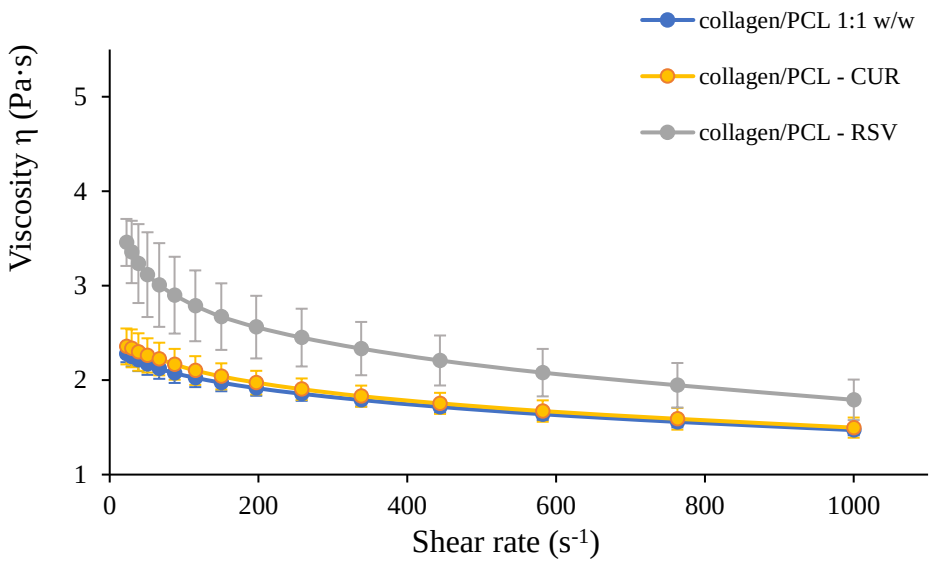

Figure 1 Viscosity (Pa) vs shear rate (s -1) profiles of collagen/PCL solutions 1:1 w/w ratio prepared in acetic acid at 90% v / v at a temperature of 25 ° C .with and without polyphenols: CUR (curcumin) and RSV (resveratrol). (mean values ± s.d.; n = 3).

2.2.Conductivity and Surface Tension

The results of surface and the conductivity for collagen/PCL mixtures unloaded and loaded with curcumin or resveratrol are respectively shown in **Figure 2a and 2b**. Surface tension values were comparable for all solutions analyzed, demonstrating how the addition of the active ingredients did not affect this physical parameter and, therefore, played no significant part in collecting nanofiber with good morphological aspect during the electrospinning process. On the other hand, even if the solvent is the same for all solutions analyzed, the conductivity values were strongly influenced by the composition of the solution. Collagen/PCL blend showed a trend in between collagen and PCL solutions alone (as shown in **Figure 4** and **5** Chapter III), while the addition of polyphenols did not affect the parameter.

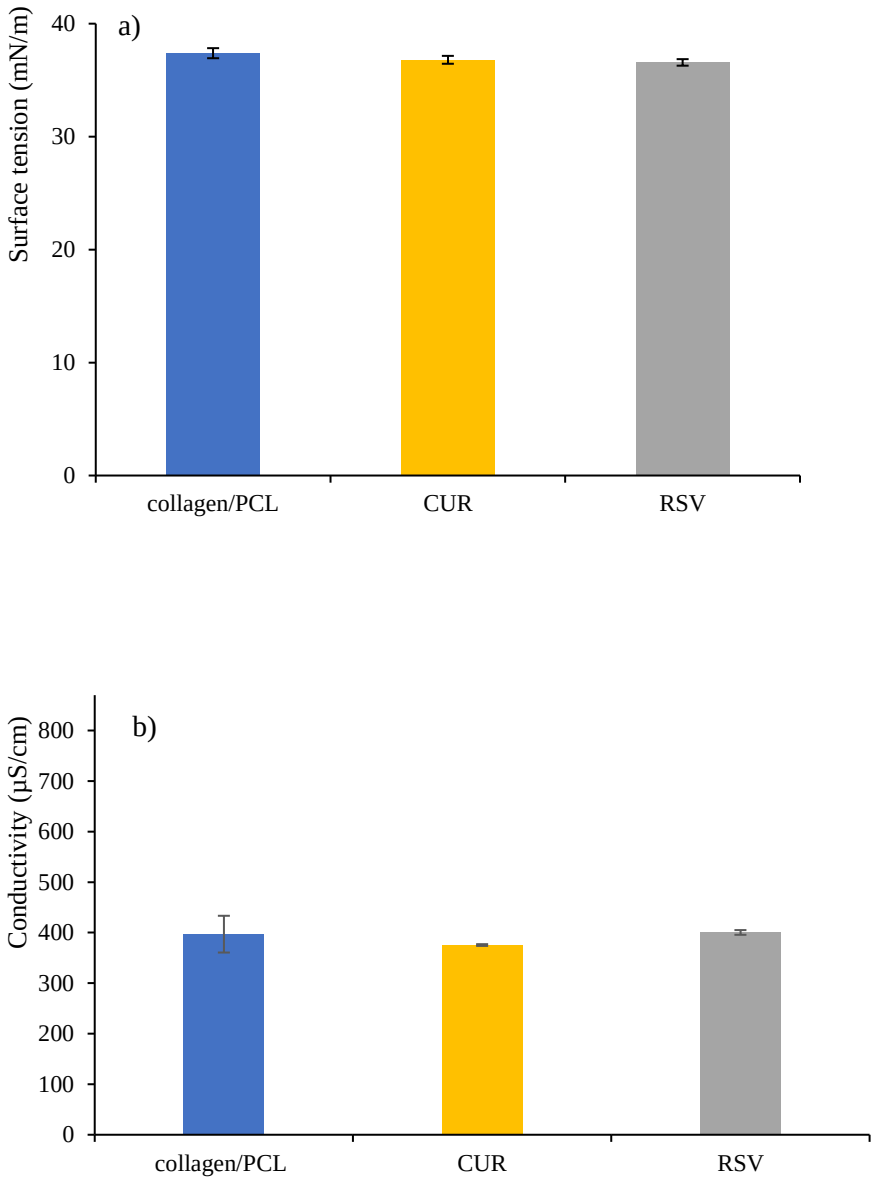

Figure 2 a) surface tension (mN/m) and b) conductivity (µS/cm) of collagen, polycaprolactone (PCL), collagen/PCL unloaded and loaded with curcumin (CUR) or resveratrol (RSV). ANOVA 1 VIA – MRT ($p < 0,05$) (mean values ± s.d.; n=5).

2.3.SEM analyses

After the preliminary physical characterization, the protein/polymer solutions unloaded and loaded with the polyphenols were electospun, nanofibrous membranes were collected and a SEM analyses were performed to assess the nanofibrous structures. The electrospun parameters employed were set on the basis of the results of a design of experiment conducted in the previous work (**Chapter III**.). SEM photomicrographs, acquired at 10 kx magnification, show uniform nanofibrous structures with no beads or relevant imperfections

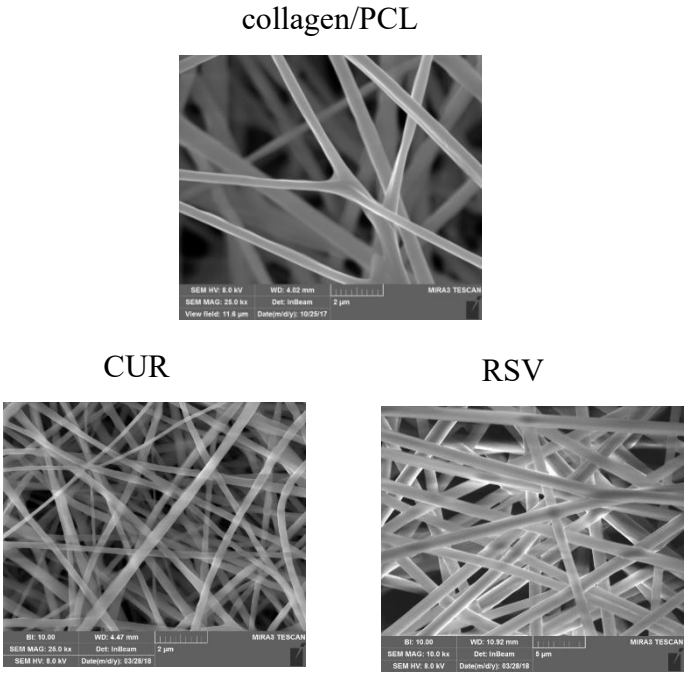

Figure 3 Photomicrographs SEM images of nanofibrous membranes collected for each formulation based on collagen, PCL and collage/PCL not loaded and loaded with curcumin (CUR) and resveratrol (RSV).

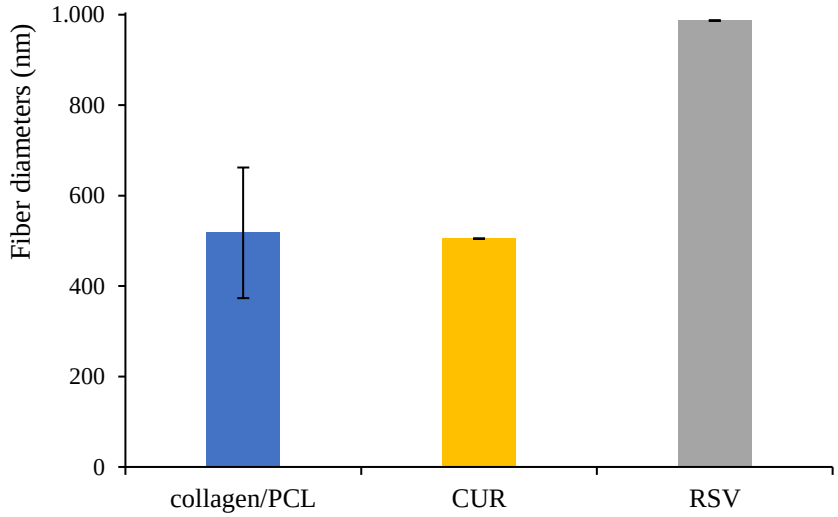

Figure 4 Size diameters of collagen, polycaprolactone e collagen/PCL without and with active ingredient: curcumin (CUR) or resveratrol (RSV) ANOVA 1 VIA – MRT ($p < 0,05$) (mean values ± s.d.; n=60) (collagen/PCL vs RSV, CUR vs RSV)

in all cases (**Figure 3**). For protein/polymer mixtures added with the active ingredient, fibers dimensions changed drastically for RSV NFs, reaching 1 µm of dimension, while in CUR NFs the mean fiber diameter was unchanged if compared with the unloaded NFs (**Figure 4**). These differences maybe could be linked to a different molecular arrangement between the compounds present in the mixture applied during the electrospinning process.

2.4.Morphological stability in hydrated state

For collagen/PCL nanofibers loaded with CUR and RSV the morphology stability in the hydrated state was evaluated. From 24 h up to 1 week of immersion in water, the architectural structure of nanofibers was preserved in both cases. A statistically significant increase of fiber diameters occurred for RSV NFs, as dimensions after 72 hours showed a statistically

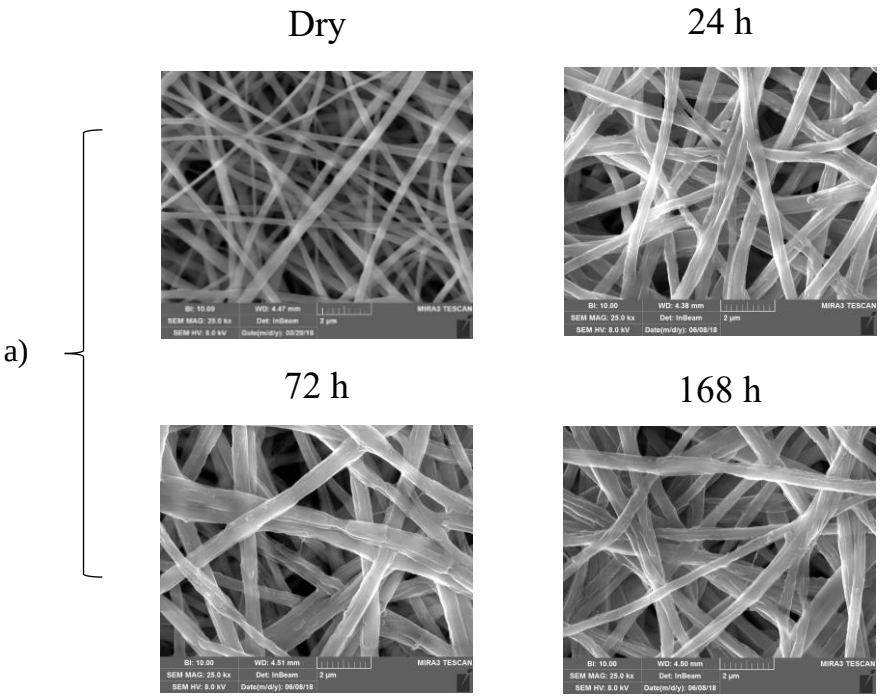

Figure 5 Photomicrographs SEM images of nanofibrous membranes based on collagen, PCL, collage/PCL 1:1: a) loaded with curcumin (CUR), b) loaded with resveratrol (RSV) after hydration in water for 24 h up to 1 week.

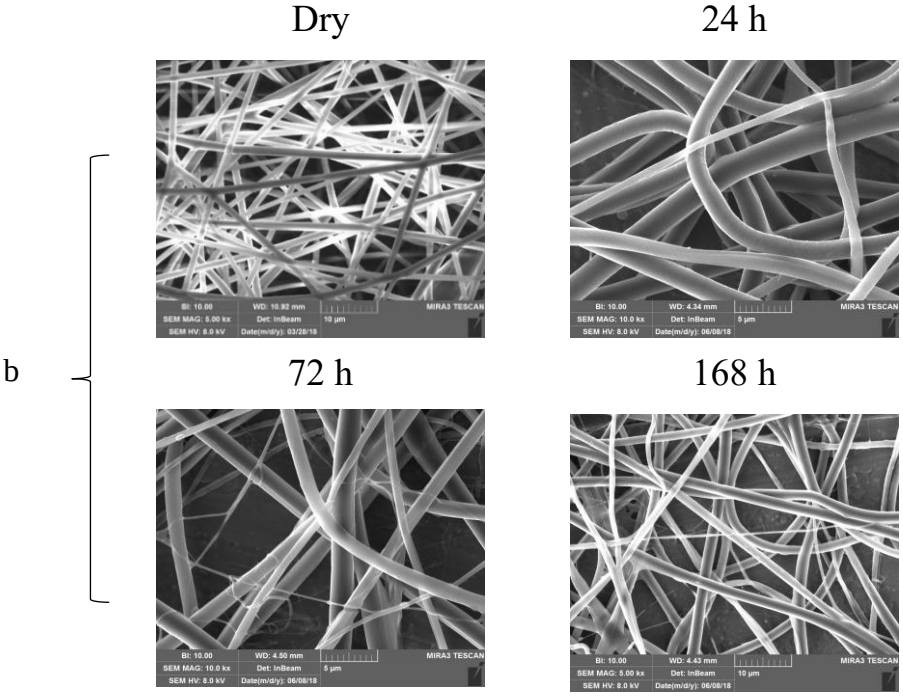

significant increase in dimensions with respect to dimensions at time zero and at 24 hours. Results are showed in SEM images (**Figure 5**) and mean fiber diameters plotted in **Figure 6**.

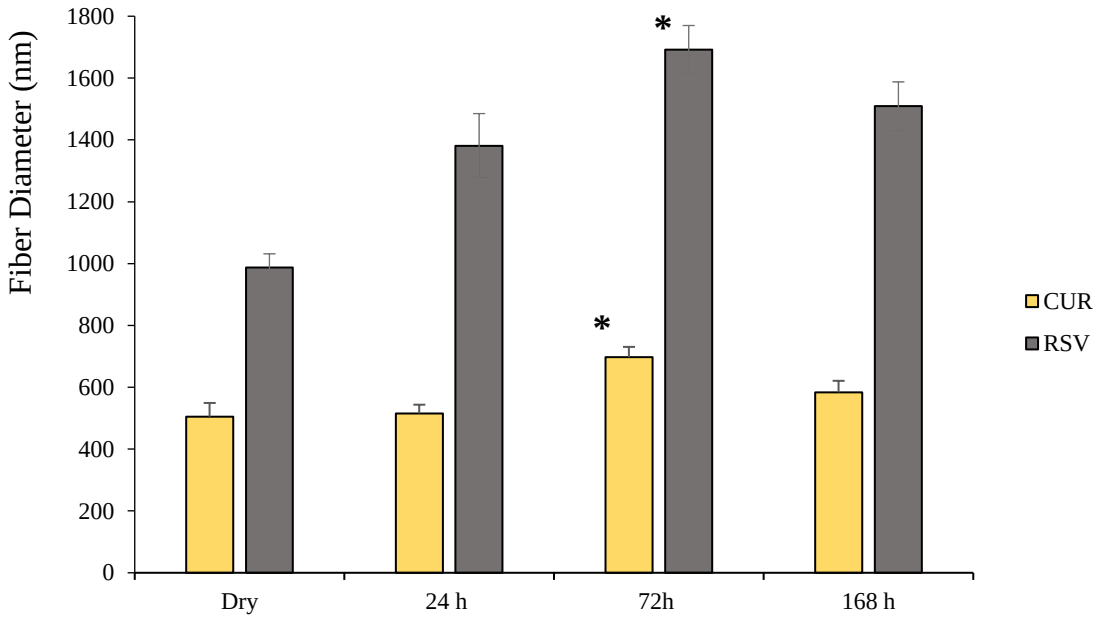

Figure 6 Size diameters comparison of collagen/PCL nanofiber loaded with CUR or RSV at different hydration time. ANOVA 1 VIA – MRT ($p < 0,05$) (mean values ± s.d., n=60).

2.5.Wettability

Results of contact angle measured for collagen / PCL membranes unloaded and loaded with CUR or RSV are reported in **Figure 7** and photographs of the analyses in **Figure 8**. Contact angle in nanofibrous membranes loaded with CUR, did not differ (in a statistically significant way) with the same unloaded nanofibers, indicating that the drug, present in low percentage, did not affect the physical parameter. On the contrary, the presence of resveratrol led to an evident halving of the contact angle values: from a mean of 90° for the collagen / PCL NFs to 45° for RSV loaded NFs. Considering these results, the variation was not related to the hydrophobic character of the molecule, but the differences seemed to be related to the structural morphology of nanofibrous mat. In particular, fiber diameters of RSV NFs (≈ 1.5 µm) were higher than unloaded or loaded CUR NFs (≈ 0.5 µm), therefore the higher degree of solid / liquid interactions given by a more extensive exposed materials with less porous mashes, led to an increase in the adhesive forces between nanofibrous membrane and the water drop.

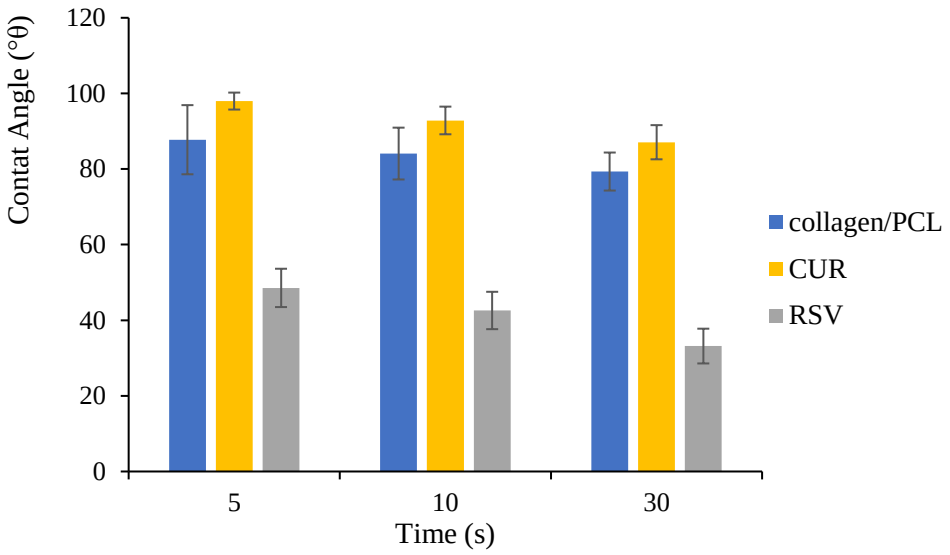

Figure 7 Comparison of contact angle values for PCL and collagen / PCL nanofibers unloaded and loaded with CUR and RSV (mean values ± s.d. n=3).

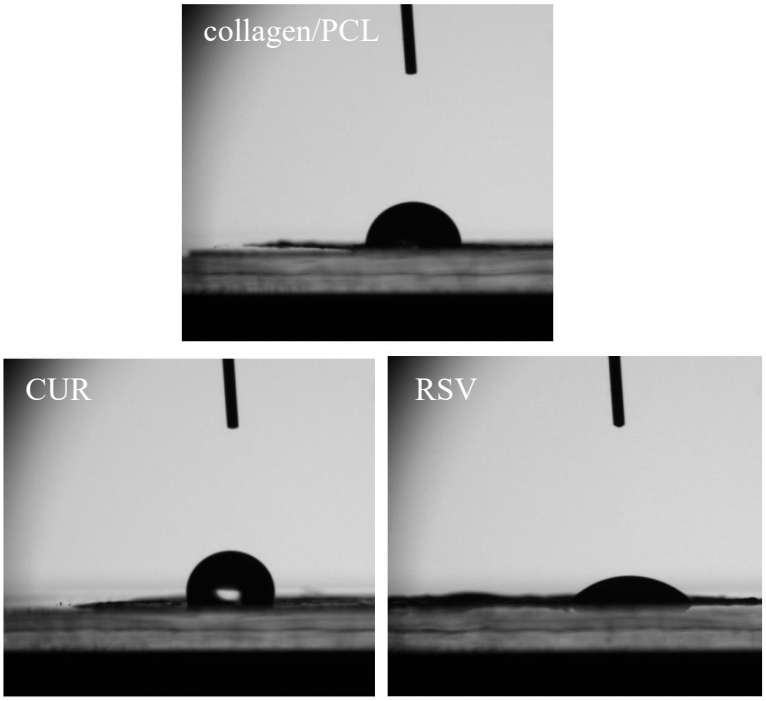

Figure 8 Photographs of PCL, collagen/PCL nanofibers unloaded and loaded with CUR or RSV kept in contact with a water droplet. The images were taken at 10 s after the first contact with the droplet.

2.6.Mechanical Properties

Maximum breaking force normalized by the thickness of the nanofibrous membranes (Stress, Pa) was plotted against elongation %. The analyzes were conducted both under dry (**Figure 9**) and under hydrated conditions (**Figure 10**), to simulate the fiber behavior in aqueous biological fluids. The tensile distances were set at 20 mm and 50 mm for dry and hydrate condition respectively. Both in the dry and wet state, the tensile strength indicated by the maximum stress (Pa) applied at the break-point appeared overlapped for all formulations (**Figure 9**), while the elongation % of the nanofibers loaded with CUR was lower than the other two formulations, indicating a lower elongation % behavior. In the hydrated condition membranes loaded with polyphenols (CUR and RSV) showed lower maximum force values than the unloaded membrane (collagen / PCL), however in all cases a higher % elongation demonstrated a better deformation of the material loaded with polyphenols (**Figure 10**). Nanofibrous membranes loaded with the polyphenols could support the regeneration of the damaged tissue, not only due to their intrinsic anti-inflammatory and anti-infective activities, but also through their ability to withstand external insults or follow the normal body movements surrounding the dressing.

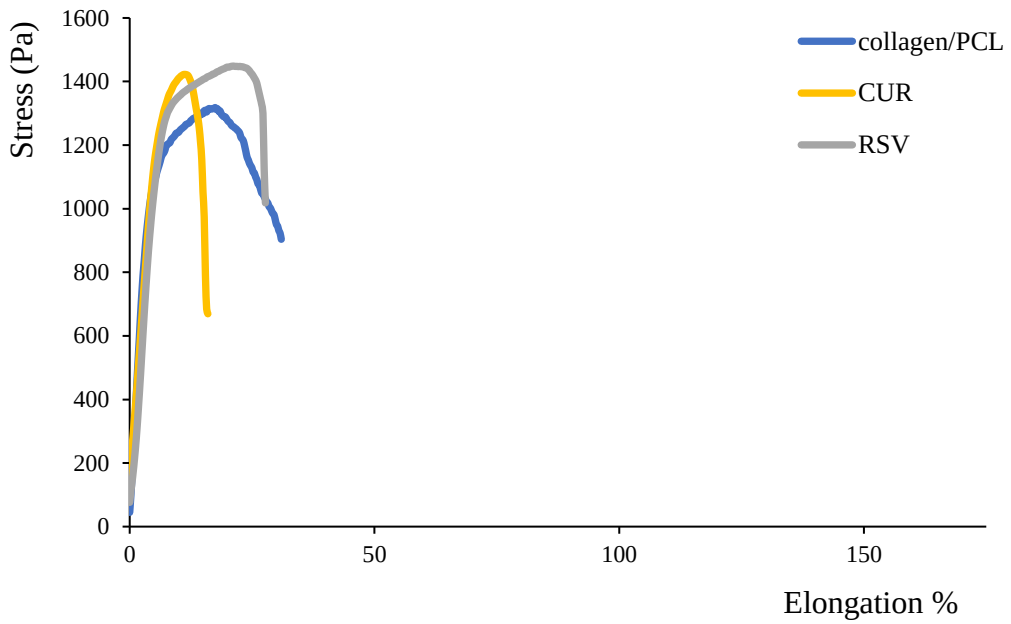

Figure 9 Stress (Pa) vs Elongation % profiles of dry collagen/PCL nanofibrous membranes unloaded and loaded with CUR or RSV (mean values ± s.d., n=6).

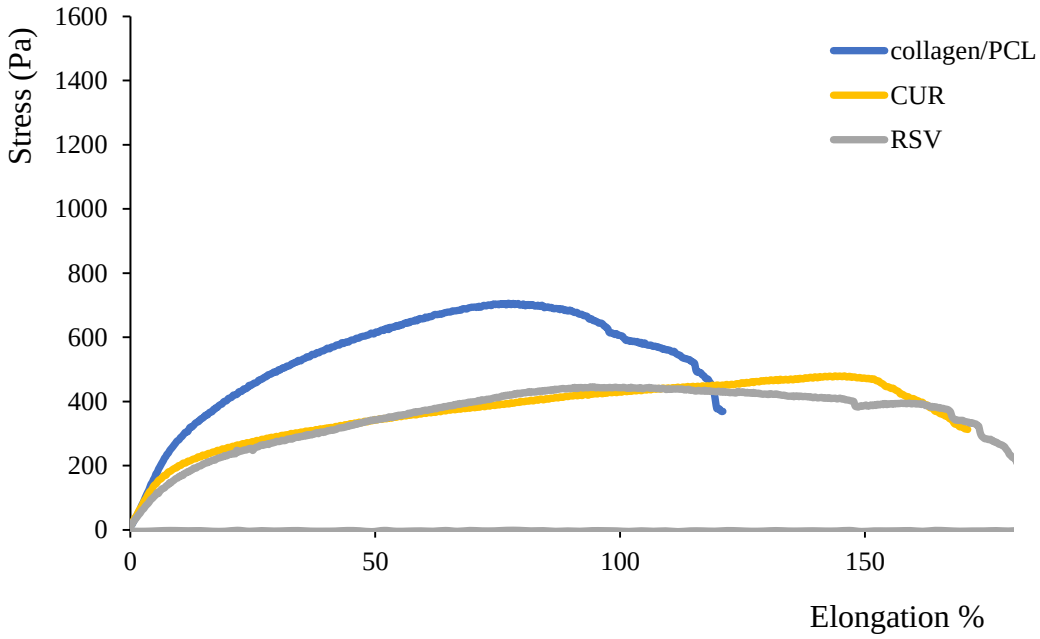

Figure 10 Stress (Pa) vs Elongation % profiles of wet collagen/PCL nanofibrous membranes unloaded and loaded with CUR or RSV (mean values ± s.d., n=6).

2.7.Chemical-physical characterization

FTIR analyses

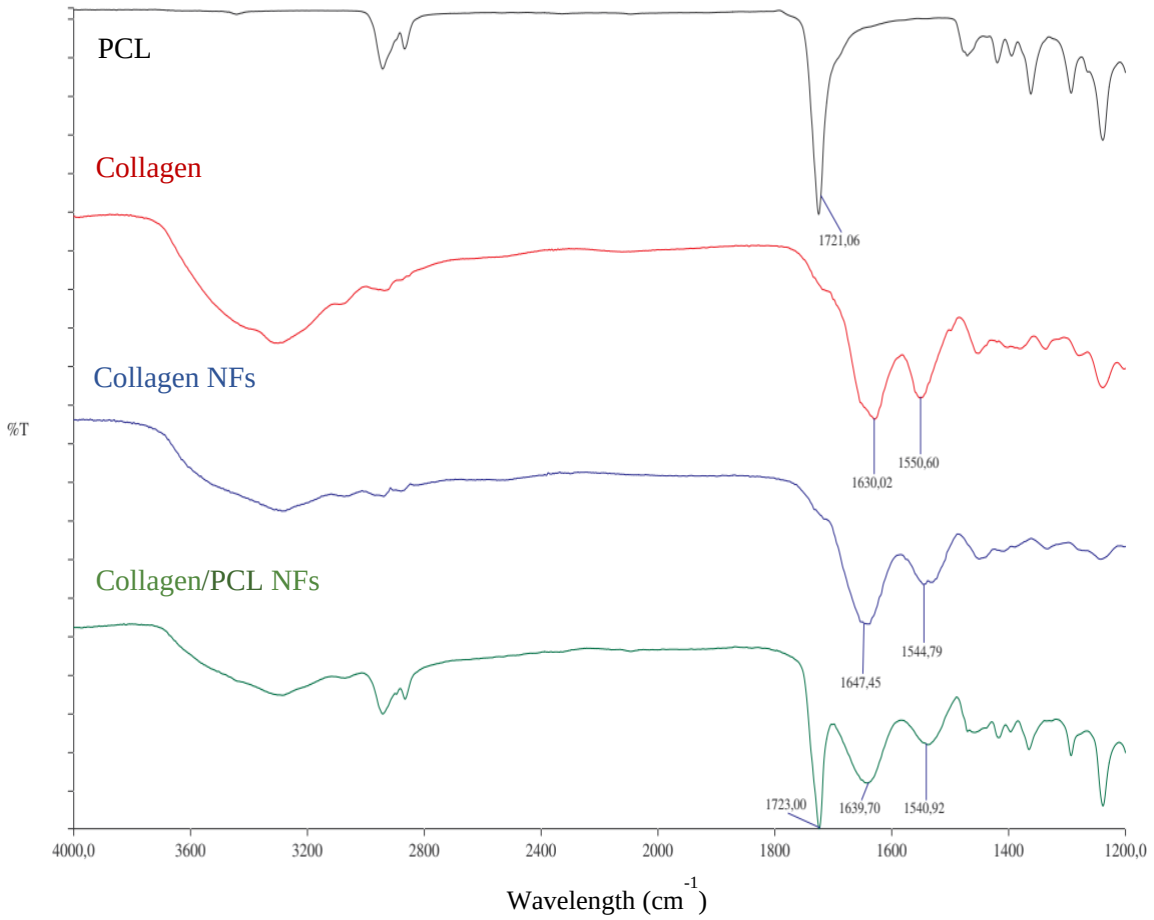

Figure 11 FTIR spectra of raw PCL, raw native collagen, and unloaded collagen/ PCL nanofibers 1:1 w/w ratio (collagen NFs and collagen/PCL NFs).

Raw materials and nanofibrous membranes unloaded and loaded with polyphenols were characterized by FT-IR and DSC to identify any possible variations in chemical-physical behaviors after electrospinning process and, at the same time, to evaluate possible interactions of the drugs into the nanofibrous membranes. In **Figure 11** FT-IR spectra of raw PCL and native collagen are compared with spectra of native collagen (20% w/w) and collagen/PCL electrospun nanofibers. The first evidence, easily detectable, was a shift in the characteristic peaks of the amidic bonds from native collagen (1630 and 1550 cm $^{-1}$) and collagen nanofibers (1647 and 1544 cm^{-1}), therefore, respect to the raw material, protein conformation was affected both by the electrospinning process and the solvent employed for its solubilization. Another shift in amide signal was recorded when PCL was added to the electrospun formulation (1639 and 1540 cm^{-1}), suggesting an effective interaction between the two components, as commonly reported in literature.[20],[21]. In FT-IR spectra of electrospun nanofibers loaded with curcumin (CUR NFs) or resveratrol (RSV NFs), no characteristic peaks of the drug and no clear differences between unloaded and loaded nanofibers were evident (**Figure 12**).

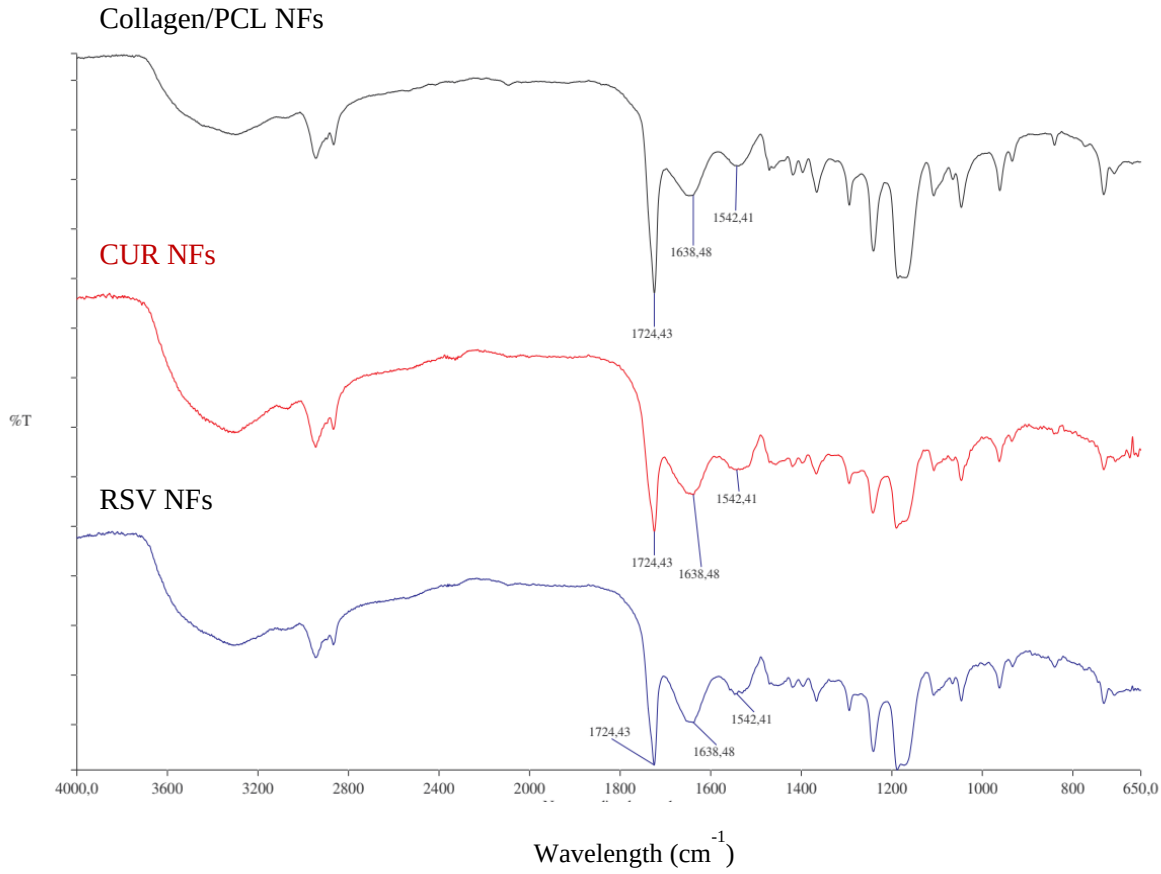

Figure 12 FTIR spectra of unloaded collagen/ PCL nanofibers, curcumin loaded nanofibers (CUR NFs) and resveratrol nanofibers (RSV NFs).

2.8.DSC analyses

Differential scanning calorimetry analyses confirmed the results obtained with the IR spectra. Regard to the spectra of PCL nanofibers the peak around 56°C corresponded to the melting point of PCL and, for collagen nanofibers peak around 125°C corresponded to the melting (denaturing) of collagen. In the blend collagen/PCL, the melting of PCL was clear, however the collagen signal was not observed. Finally, even if the PCL signal was recorded, polyphenols loaded nanofibrous membranes did not show their characteristic melting points, suggesting in both cases an amorphization of the drug (**Figure 13** and **Figure 14**).

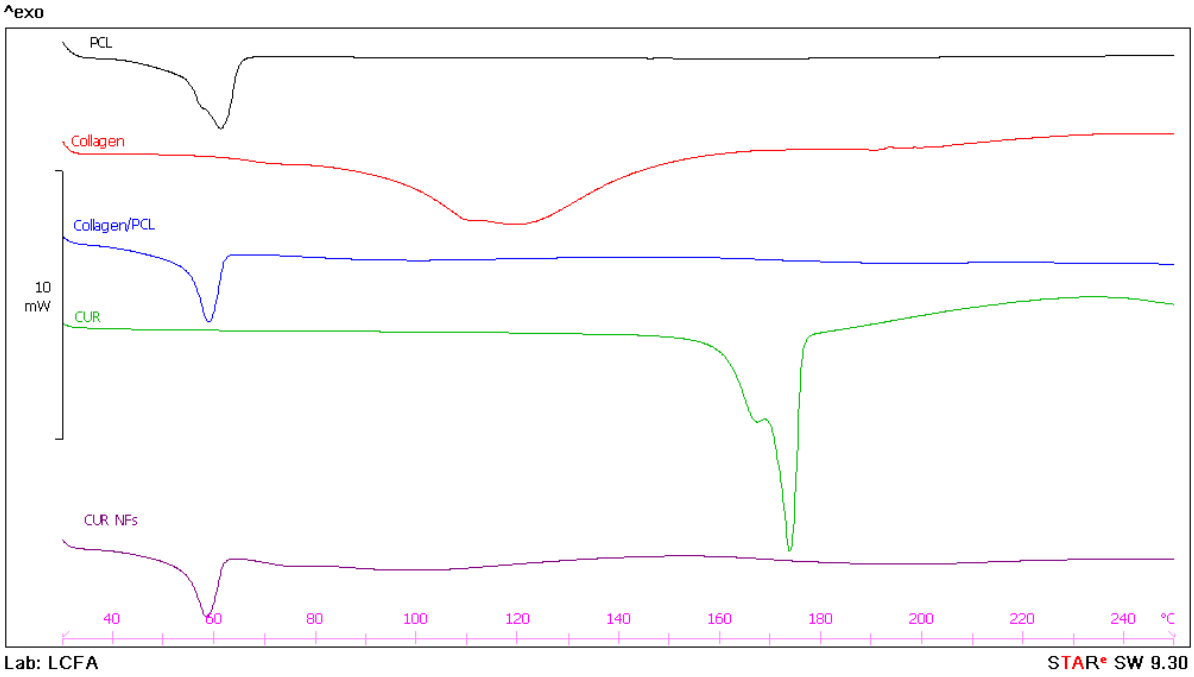

Figure 13 DSC Spectra of nanofibers based on PCL 20 % w/w, collagen 20 % w/w, collagen/PCL 1:1 w/w ratio, curcumin (CUR) and curcumin loaded nanofibers (CUR NFs).

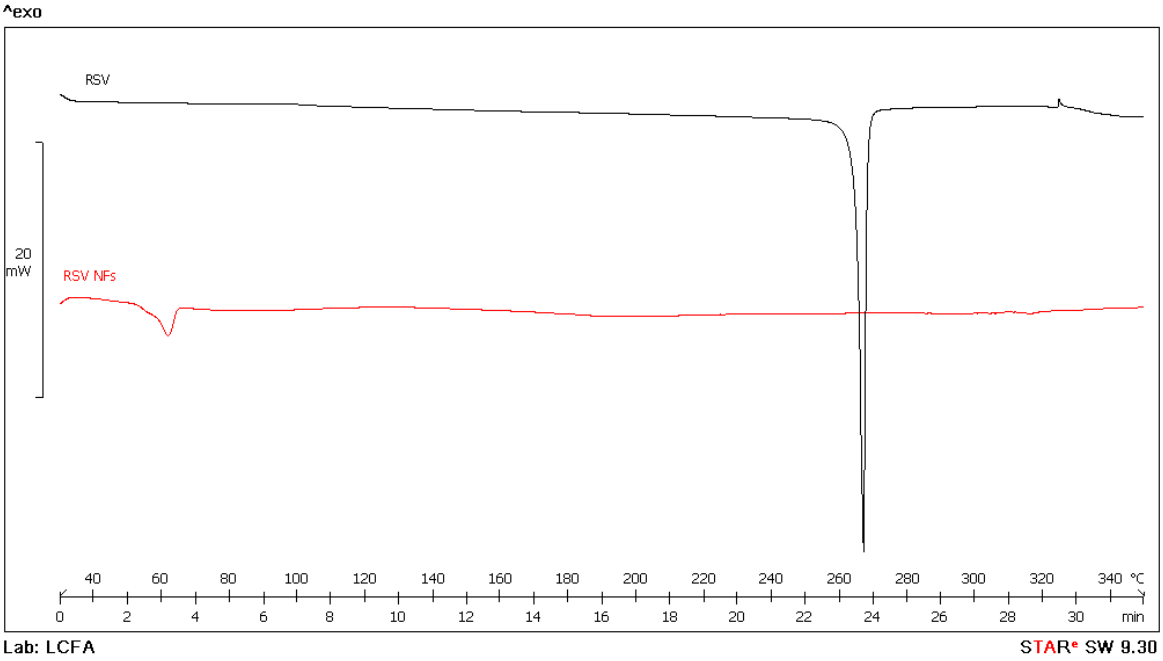

Figure 14 DSC Spectra of nanofibers based on resveratrol (RSV) and resveratrol loaded nanofibers (RSV NFs).

2.9.Drug loading efficiency

CUR and RSV loading in nanofibrous membranes was evaluated by the mean of spectrophotometric analyses after solvent extraction carried out in methanol. The % of the drug recovered after methanol extraction is indicated in **Figure 15**. A 100 % of CUR loaded in nanofibers was clearly recorded and a 90 % of RSV recovery occurred.

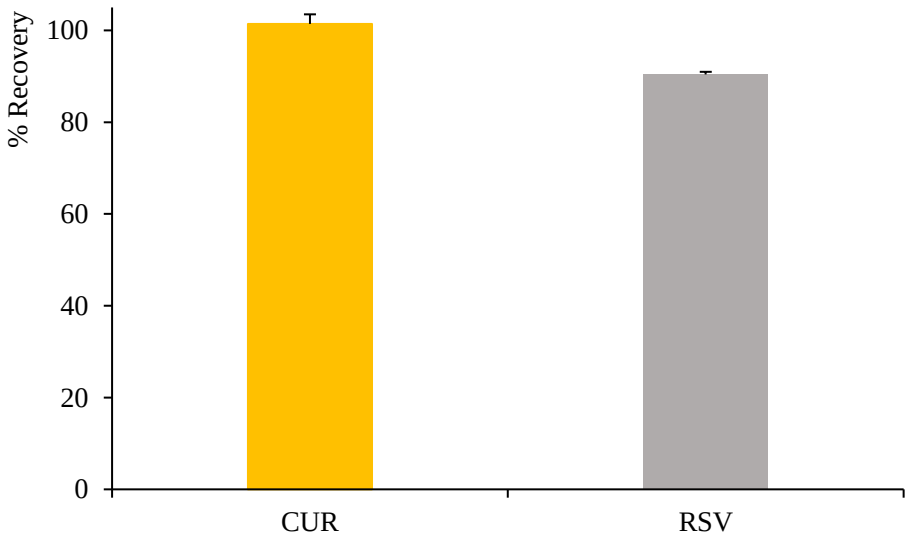

Figure 15 % Recovery of CUR and RSV after extraction in methanol (mean values ± s.d. n=4).

2.10. Release Studies

Figures 16 shows CUR and RSV release curves obtained by a release test performed on nanofibrous membranes in complete medium (DMEM + FBS 10% v / v + 1% v / v antibiotics) to simulate the *in vitro* conditions tested on fibroblast cell cultures and translate the results for *in vivo* application. The release study was conducted by refresh the media every half an hour for six hours. For both nanofibrous membranes, drugs were not totally released in 6 hours and respectively a 70 % and 60 % release of CUR or RSV were achieved. Furthermore, a plateau was not reached suggesting a reduced release rate, probably due to the involvement of a mechanism of erosion of the matrix.

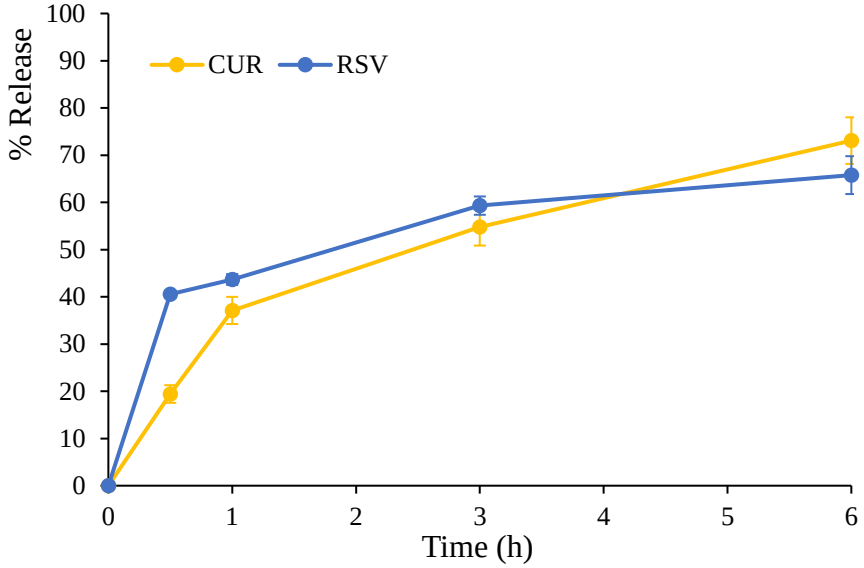

Figure 16 Drug release from collagen/PCL nanofibrous membranes loaded with CUR or RSV (mean values ± s.d., n=4).

2.11. Biocompatibility

Figure 17 shows the absorbance values (mAu) of the normal human dermal fibroblasts (NHDF) viability after seeding and culture for 3 days and 7 days on collagen / PCL nanofibrous membranes unloaded and loaded with CUR and RSV. The cells viability in complete medium (CM) was reported as a control. As can be seen from the results, electrospun nanofibers increased cell proliferation compared to control after 3 days in culture; in particular, nanofibrous membranes loaded with polyphenols, a high cellular viability was rapidly reached and maintained even after 7 days in culture. This demonstrates that this type of nanofiber is an excellent support for cell growth, migration and proliferation and can represent *in vivo* a promising tool to accelerate tissue repair and guarantee a better healing process.

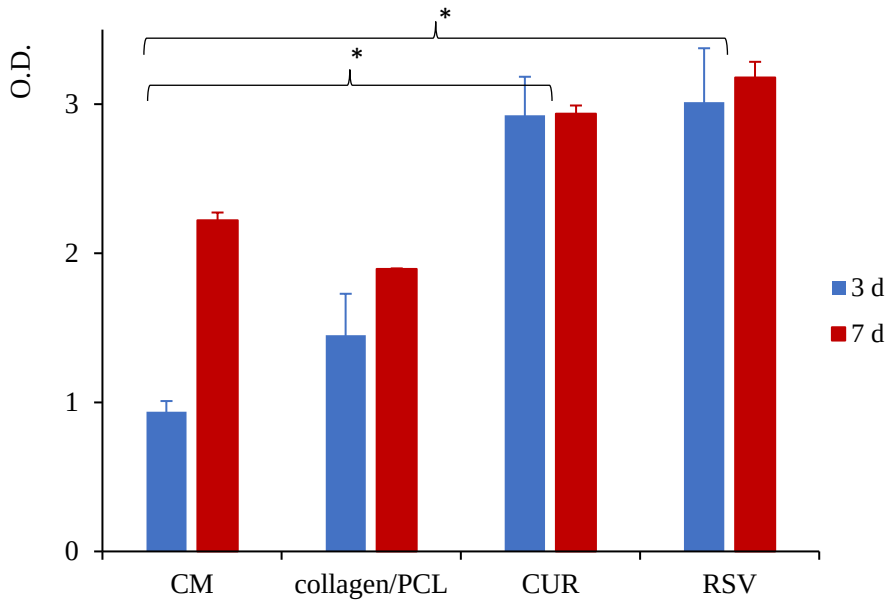

Figure 17 Cell viability absorbance (mAu) of normal human dermal fibroblasts (NHDF) after seeding on collagen/PCL nanofibrous membranes unloaded and loaded with CUR and RSV. Culture for 3 and 7 days. (ANOVA 1 via – MRT ($p<0,05$) mean values ± s.d., n=8)

2.12. Cell Adhesion

Fibroblast adhesion on collagen/PCL nanofibrous mats was assessed by electronic scanning microscopy (SEM) and confocal microscopy (CLSM). The results are shown in **Figure 18** and **19** respectively. The SEM images (**Figure 18**) show a cell spreading on the nanofibrous mat, indicating a positive interaction with the components of the nanofibers, both unloaded and loaded with the two polyphenols.

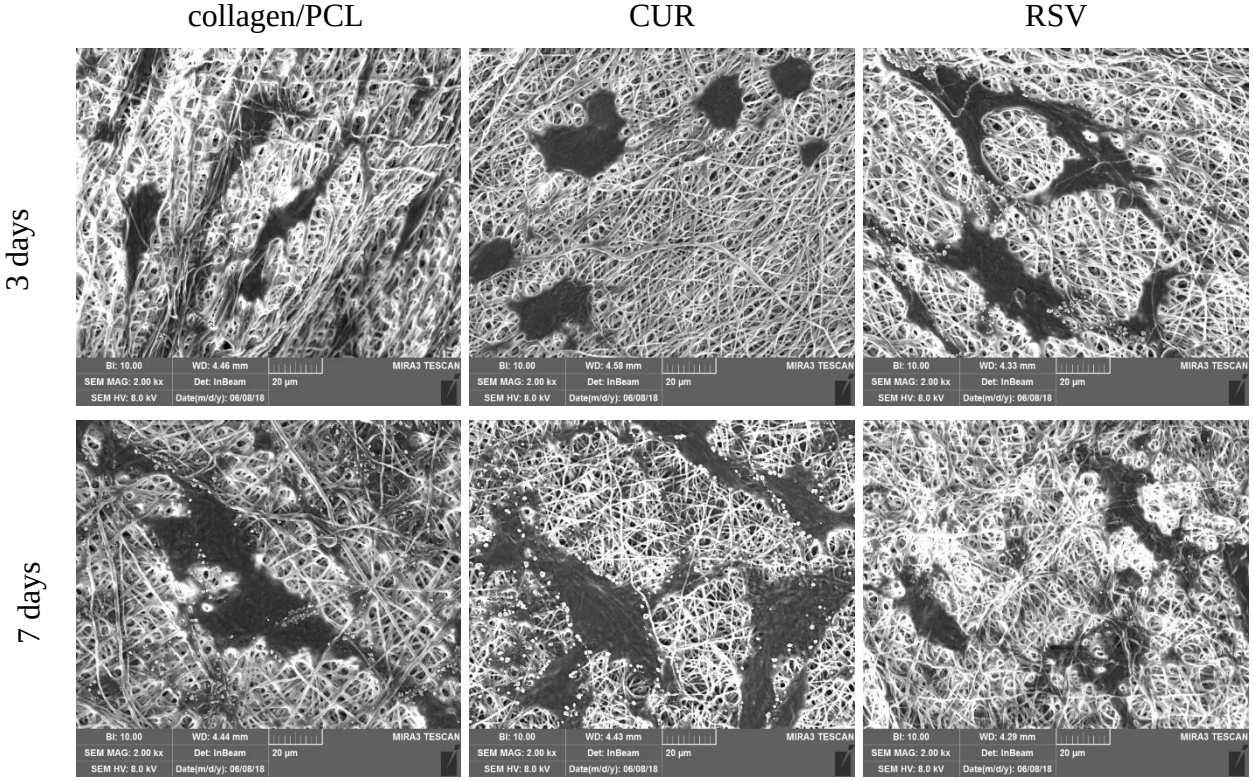

Figure 18 Photomicrographs SEM images of cell substrates grown upon nanofibrous membranes in 3- and 7-days culture – Normal Human Dermal Fibroblasts from neonatal tissue (NHDF).

Figure 19 shows the CLSM photomicrographs of cellular substrates (red-labeled nuclei with Propidium Iodide, cytoskeletons marked in green with FITC phalloidin and blue-labeled active ingredients) grown for 3 and 7 days on collagen / PCL membranes without and with CUR or RSV. Cell growth confirms the quantitative viability data obtained with the cytotoxicity test and with the cell adhesion results showed in SEM photomicrographs. In all cases fibroblasts were numerous, well adhered to the membranes and appeared as spindle elements with an elongated nucleus. In the case of membranes loaded with curcumin, the active ingredient (marked in blue) appeared to be clearly visible in the nanofibrous structure. As evident with the CLSM images for CUR nanofibers, the drug was effectively localized in the cytosolic portion, confirming that the amount released by the fibers was available for the internalization as indicated by the arrow in **Figure 20a**.

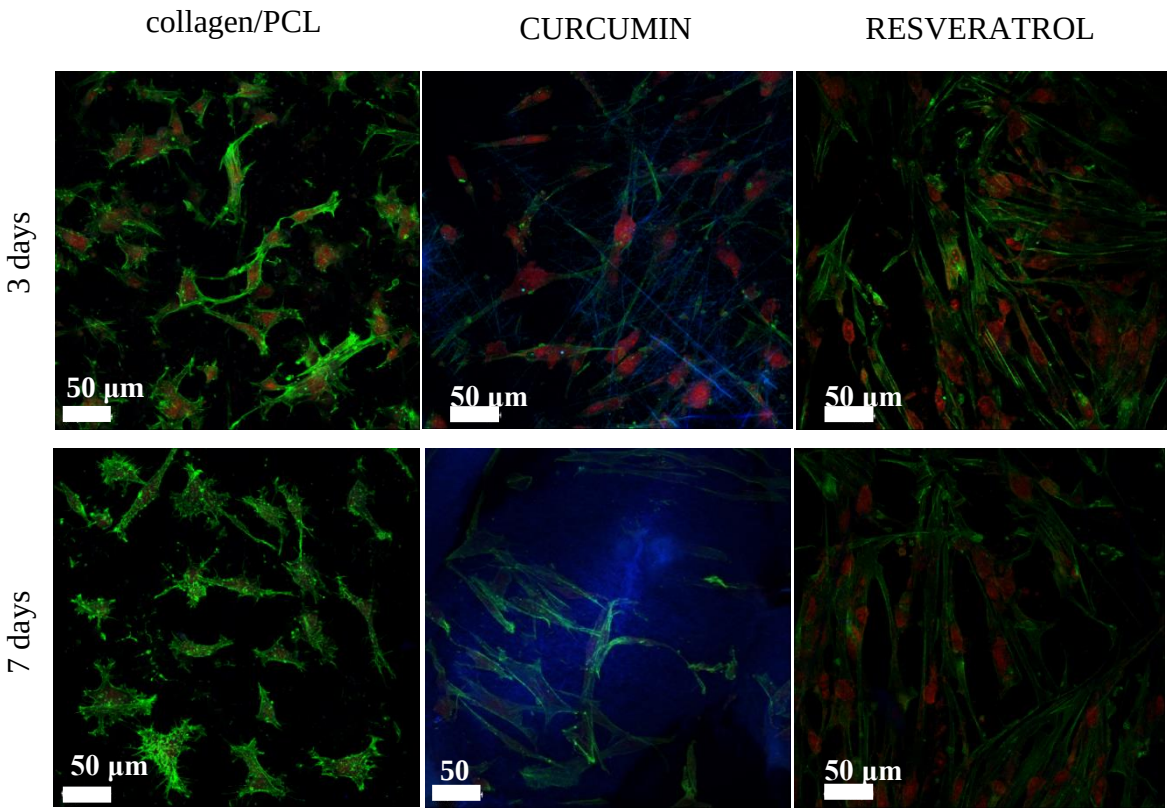

Figure 19 CLSM images of cell substrates (nucleus blue marked with Hoechst 33582) grown upon nanofibrous membranes in 3- and 7-days culture – Normal Human Dermal Fibroblasts from neonatal tissue (NHDF).

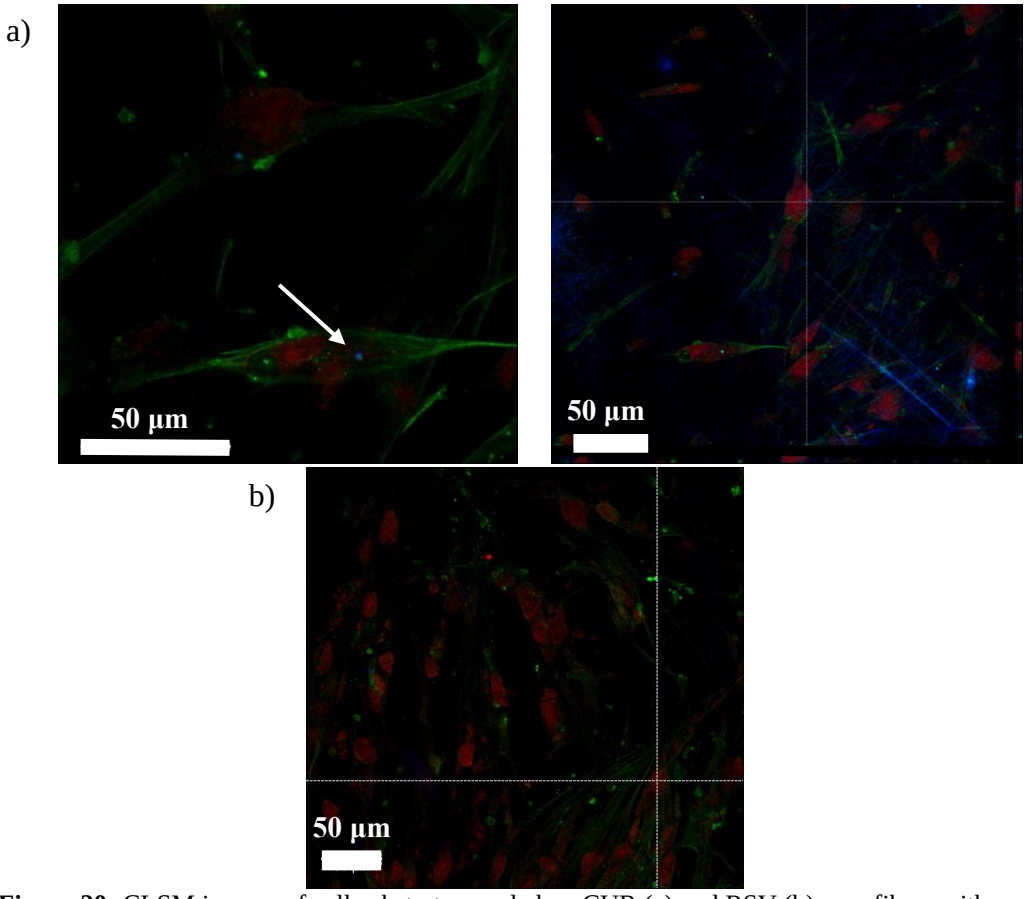

Figure 20: CLSM images of cell substrates seeded on CUR (a) and RSV (b) nanofibers with projections after three days culture.

2.13. Collagen coating

As frequently reported, electrospun nanofibrous membranes exploit great aptitudes in skin wound repair partially due to their capability of recapturing the essential attributes of native extracellular matrix (ECM) and partially to their singular structure and morphology. In skin wound repair, rapid restoration of the epithelial barrier function is essential to minimize bacterial invasion, dehydration and, therefore infections[22]. Considering this, onto the wound area a complete re-epithelialization cannot be achieved until migration of keratinocytes, on the open wound surface, occurs. Even if, as it is widely demonstrated, collagen electrospun nanofibers have a stimulatory effect on keratinocyte migration by promoting cell adhesion and spreading[23], Xiaoling Fu et al. found that PCL/ collagen nanofibrous matrices alone are no able to stimulate cell migration, while collagen gel coating could significantly increase their motility[24]. In our work as well, after biocompatibility tests performed on normal human keratinocytes, we thought useful to improve nanofibers cell versatility and adhesion by adding a gel collagen coating on electrospun membrane surface. The results of an MTT test performed on NHEK cells seeded onto collagen/PCL nanofibers unloaded and loaded with CUR and RSV and on cells treated with the active ingredient are shown in **Figure 21**. MTT test was conducted in trans-well insert by keeping the same samples on the insert and growing up the cells on the bottom of the well. In all cases viability was not extremely affected.

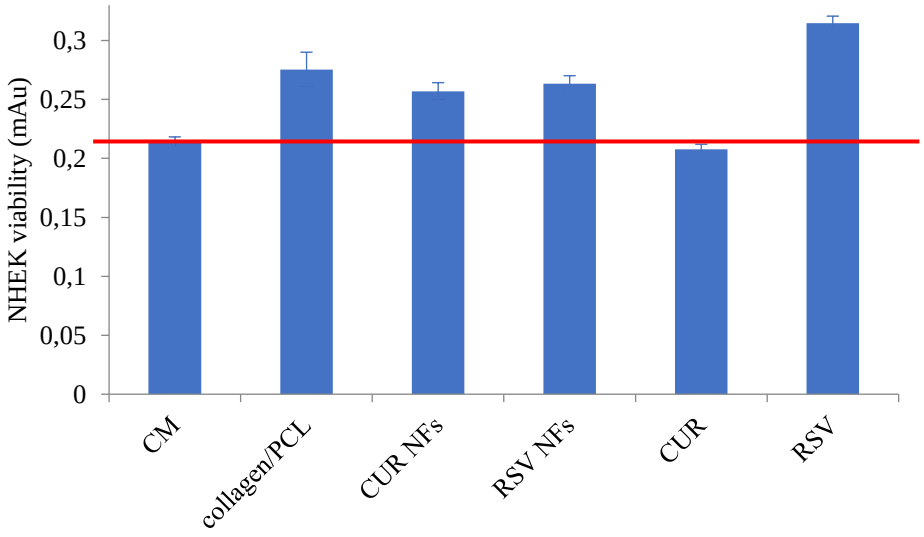

Figure 21 Cell viability absorbance (mAu) of normal human dermal fibroblasts (NHDF) after exposure to collagen/PCL nanofibrous membranes unloaded, loaded with CUR and RSV and active ingredients alone (0.5 % w/w in PBS/EtOH 90:10). Culture for 3 days.

2.13.1. SEM Analyses

Driven by these results, in a second phase of this work, nanofibrous membranes were coated using different concentration of native collagen solubilized in water (0.2, 0.5 and 1 % w/w) and different coating times were employed (15, 30 and 60 min). Comparing the coated with the uncoated nanofibers (**Figure 3**), a structural differentiation can be denoted depending on the percentage of collagen used and the coating time. Specifically, as shown from photomicrograph analyses, an irregular and wrinkled surface on nanofibrous mat was evident in all cases, on the contrary, the uncoated nanofibers showed a smooth and more uniform surface. **Figure 22** shows SEM photomicrographs of nanofibers obtained from unloaded collagen / PCL, coated with a native collagen 0.2% w/w. SEM images were acquired with 10 kx magnification. A variation in nanofibers structure seemed to be proportional to exposure coating time. A film formation on the surface of the nanofiber was already visible at 15 minutes and was particularly evident after 1h treatment, where collagen coating was completely adhered to the whole nanofibrous mat. **Figure 23** showed collagen/ PCL nanofibrous membranes coated native collagen at 0.5 % w/w. A film layer on the surface caused a morphological surface variation of the nanofibrous membrane, unlikely the lower coating collagen concentration (0.2 % w/w), the nanofiber coating was strongly evident, with a slight thickening of the film when nanofibrous membranes were exposed for 15 and 30 minutes. When collagen / PCL nanofibers were coated with the highest percentage of native collagen (1 % w/w), a film layer covered the nanofibrous mat, modifying its surface by filling and penetrating cross inter-fiber pores (**Figure 24**). **Figure 25** shows SEM photomicrographs obtained from collagen / PCL CUR loaded coated with native collagen gel at 0.2 % w/w. Differences in morphology were already visible since the first 15 min of coating respect to the same nanofibrous membranes hydrate just with water (**Figure 3**). When the same nanofibrous membranes are coated with 0.5 % w/w (**Figure 26**), no structural differences between the three coating times occurred. Furthermore, a collagen film coating can be denoted after treatment with 1 % w/w collagen even after 15 min (**Figure 27**) and an apparently a cohesive structure seemed to surround the different layers constituting the membrane. Collagen/PCL RSV loaded nanofiber and treated with 0.2 % w/w of native collagen showed no significant variation in the coating efficiency.

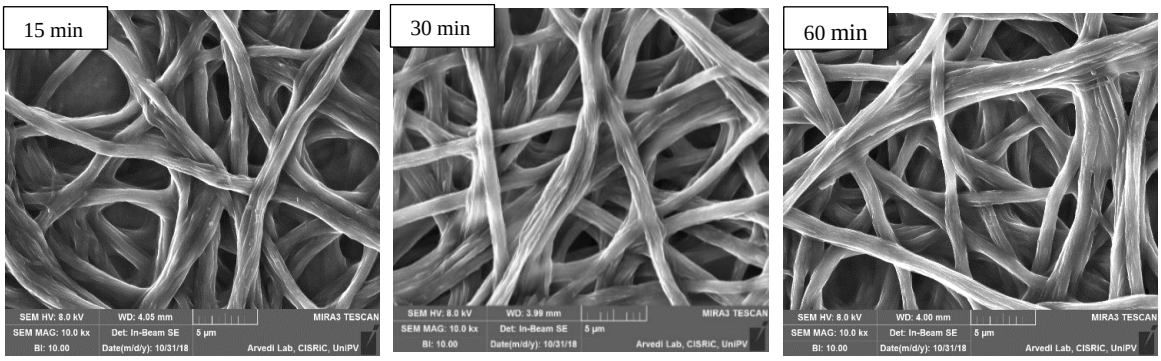

Figure 24 Collagen/PCL unloaded nanofibrous membranes coated with collagen 0.2 % w/w at three different coating times: 15, 30 and 60 min.

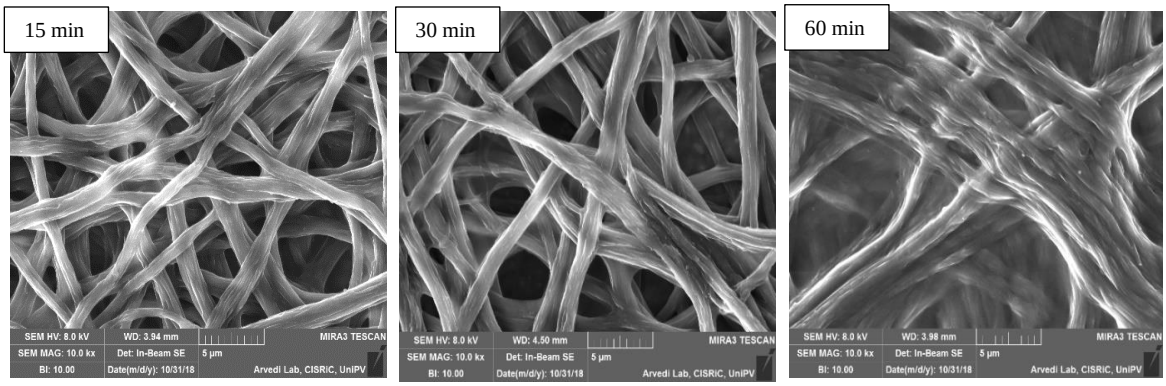

Figure 23 Collagen/PCL unloaded nanofibrous membranes coated with collagen 0.5 % w/w at three different coating times: 15, 30 and 60 min.

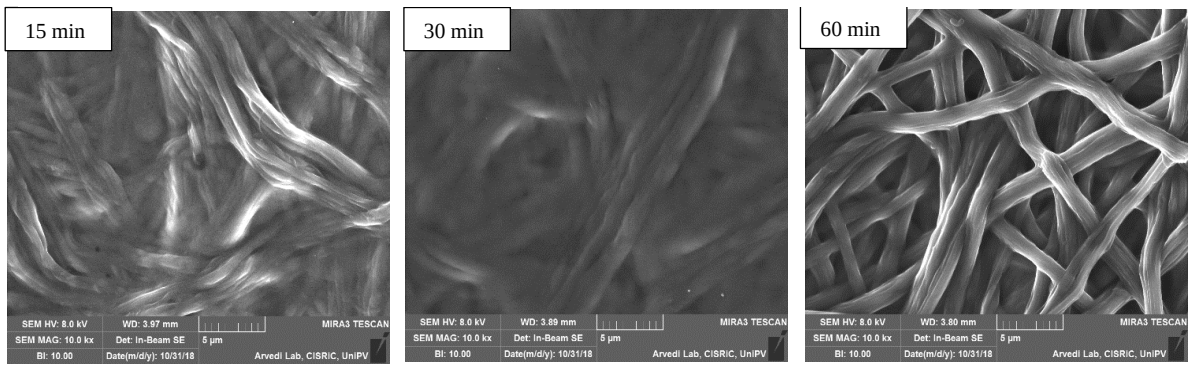

Figure 22 Collagen/PCL unloaded nanofibrous membranes coated with collagen 1 % w/w at three different coating times: 15, 30 and 60 min.

.

Comparing different coating times, in fact, no proportional correlation between surface nanofibers modification and coating time was noted (**Figure 28**). At the same time, even if collagen/PCL RSV loaded NFs were coated with native collagen 0.5 % w/w, no evident collagen film occurred, however a greater roughness in nanofibers shape was evident, after 1 h of exposure (**Figure 29**).

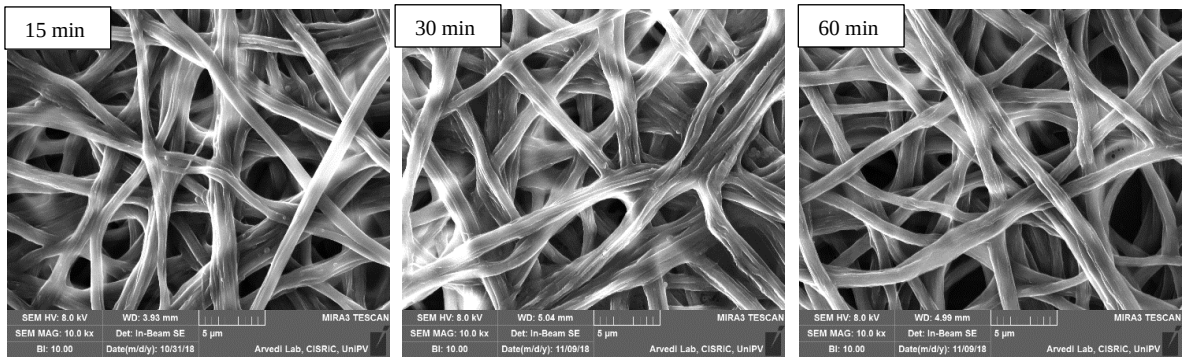

Figure 25 Collagen/PCL + CUR loaded nanofibrous membranes coated with collagen 0.2 % w/w at three different coating times: 15, 30 and 60 min.

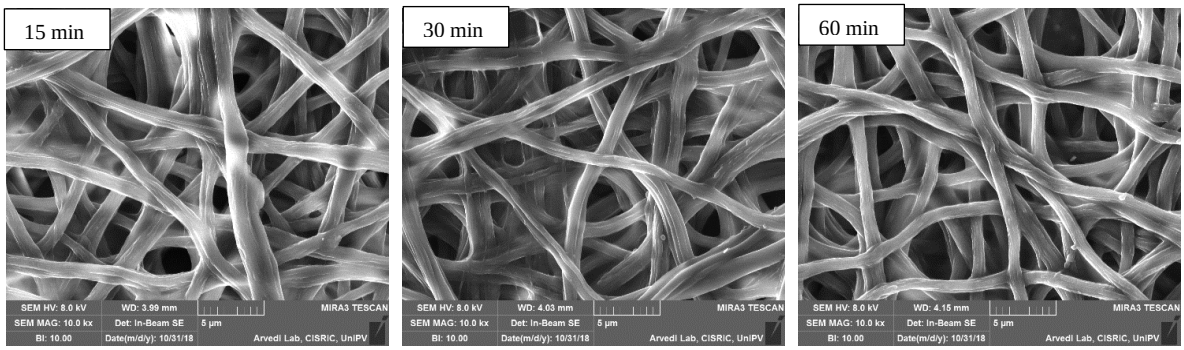

Figure 27 Collagen/PCL + RSV loaded nanofibrous membranes coated with collagen 0.5 % w/w at three different coating times: 15, 30 and 60 min.

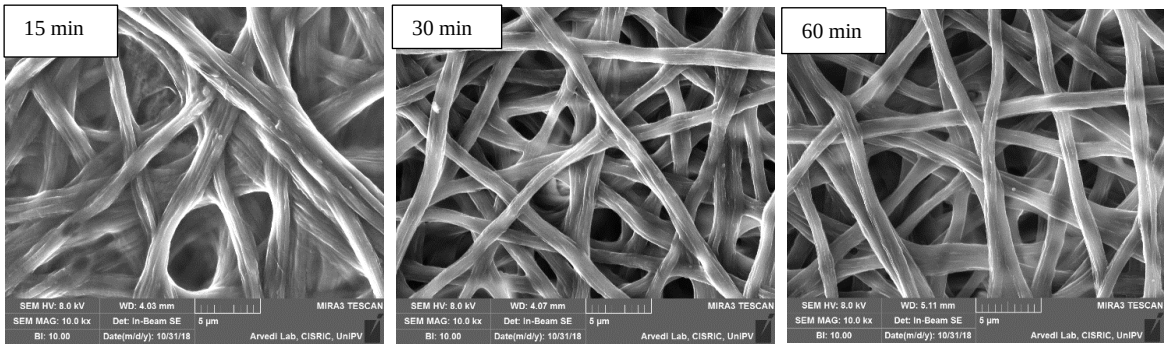

Figure 26 Collagen/PCL + CUR loaded nanofibrous membranes coated with collagen 1 % w/w at three different coating times: 15, 30 and 60 min.

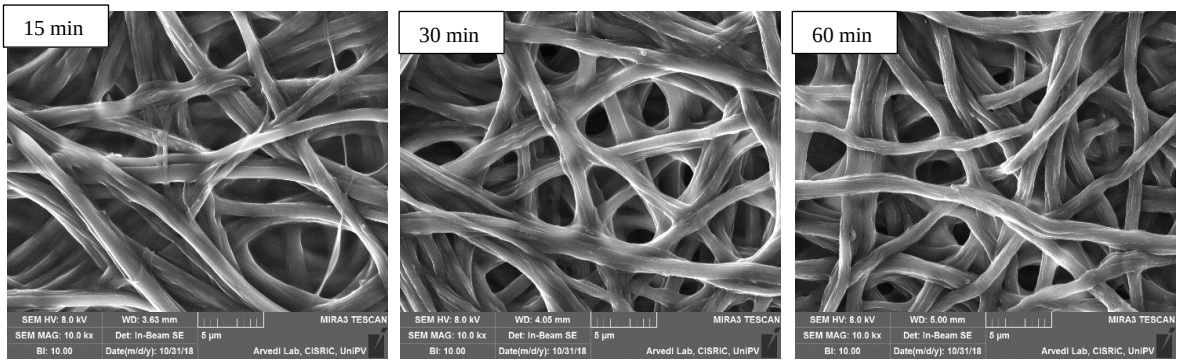

Figure 30 Collagen/PCL + RSV loaded nanofibrous membranes coated with collagen 0.2 % w/w at three different coating times: 15, 30 and 60 min.

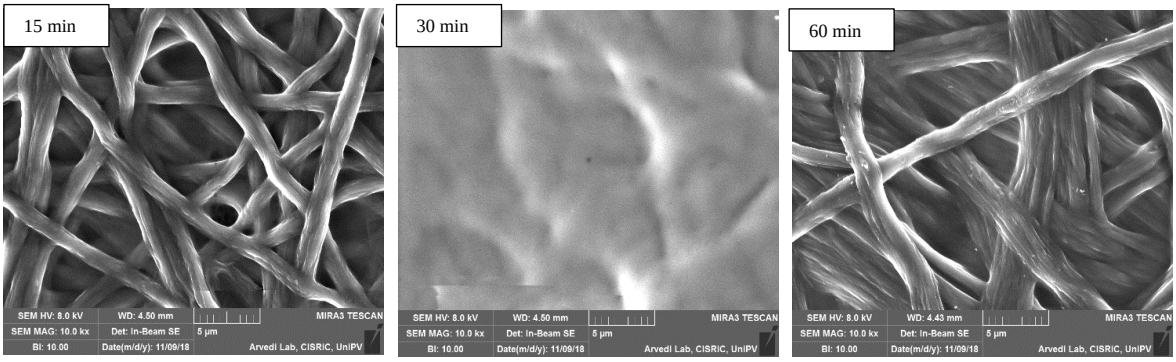

Figure 29 Collagen/PCL + CUR loaded nanofibrous membranes coated with collagen 0.5 % w/w at three different coating times: 15, 30 and 60 min.

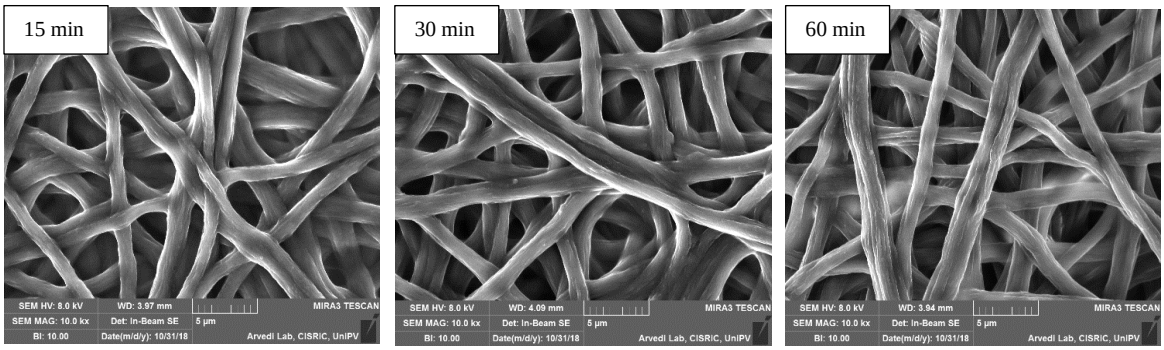

Figure 28 Collagen/PCL + RSV loaded nanofibrous membranes coated with collagen 1 % w/w at three different coating times: 15, 30 and 60 min

Photomicrograph SEM of RSV NFs coated with 1 % w/w of native collagen showed a significant differentiation in nanofibers morphology when membranes were exposed at different times.

In particular, after 30 h, native collagen clearly covered the entire nanofibrous structure, but a more defined and compact layer was evident in 1h treatment (**Figure 30**).

SEM images of all the formulations in dry and wet states are shown in **Figure 31**. Fibers structure was modified after 1 h of hydration, appearing irregular, wrinkled, unlikely the surface of the dried ones without imperfections and smooth. Furthermore, membranes loaded with polyphenols, in the hydrate in surface morphology, probably, due to the variation state seemed have minor variations in hydrophobicity related to the aqueous poorly soluble active ingredient.

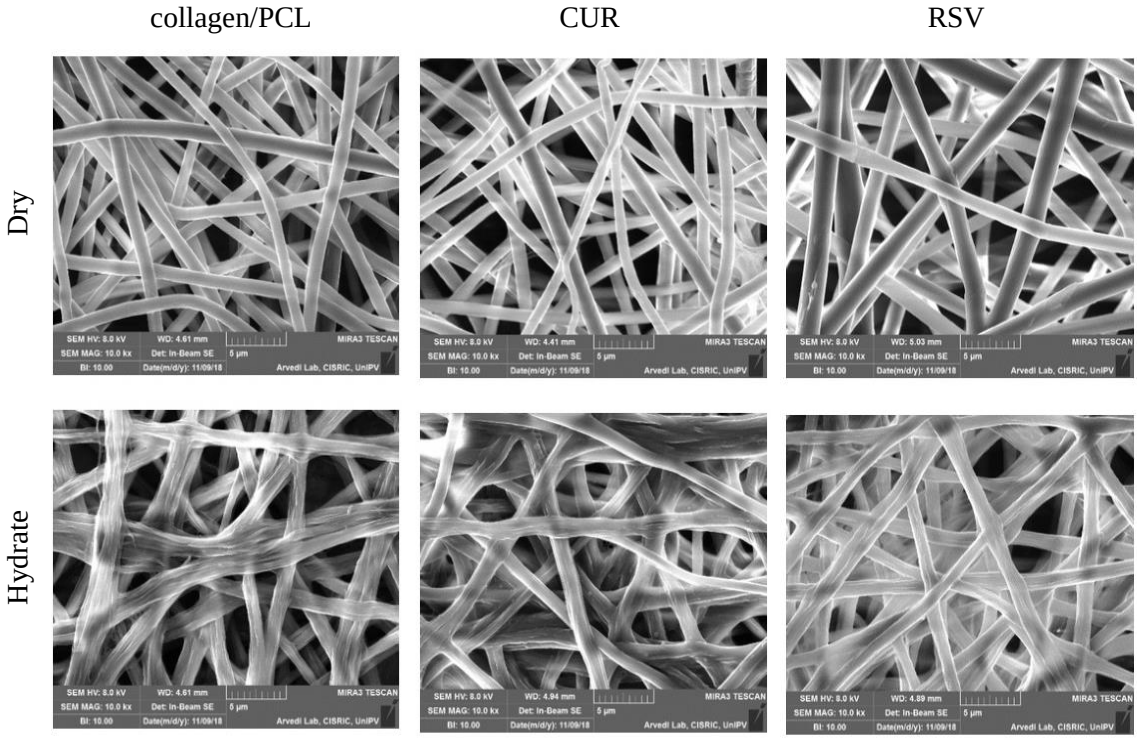

Figure 31 collagen/PCL, CUR and RSV nanofibrous membranes dried and after 1 h of hydration in water.

2.13.2. Dimensional Analyses

Plots below show the correlation between size and concentration of native collagen coating, at different coating times. Mean diameters of all analyzed nanofibers, in dry state and untreated with native collagen had dimensions within 1 µm, regardless of the presence of the active ingredient. For collagen / PCL nanofibers, as shown in **Figure 32**, size diameters slightly increased both after hydration and collagen coating reaching a maximum of 1.5 µm when treated with native collage 0.2 % w/w for 1 h. In all other concentrations and coating times, no significant variation in size occurred. A similar trend was recorded for CUR NFs, indicating no correlation between the collagen concentration and times in coating nanofibrous membranes (**Figure 33**). RSV loaded NFs coated with native collagen exhibited mean diameters overlapped to the hydrate nanofibers, however in RSV nanofibers coated with 1 % of native collagen, depending on contact time, an increase in dimensions occurred, maybe due to a large deposition of the collagenous material on the surface of the membrane (**Figure 34**).

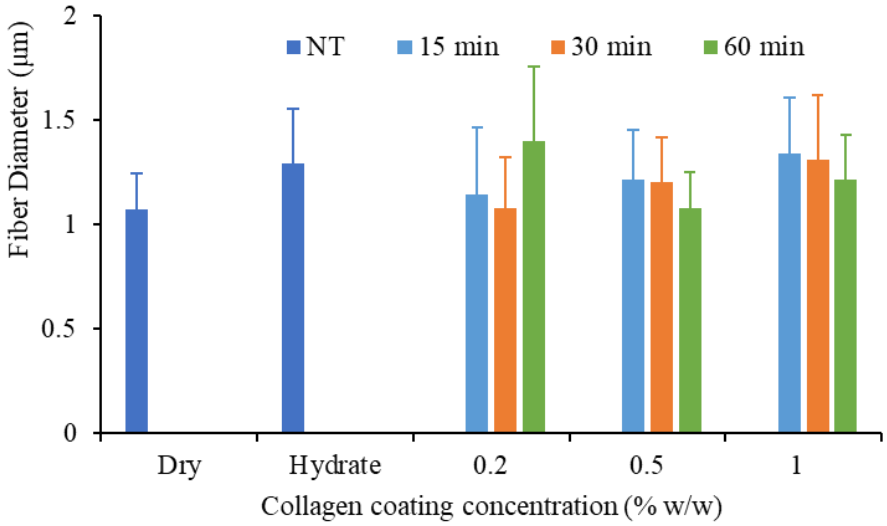

Figure 34 Size diameters comparison of collagen/PCL nanofibers uncoated in dry and hydrate state and coated with collagen at different concentrations (0.2, 0.5, 1 % w/w) for different times (15 min; 30 min; 60 min - mean values ± s.d., n=60).

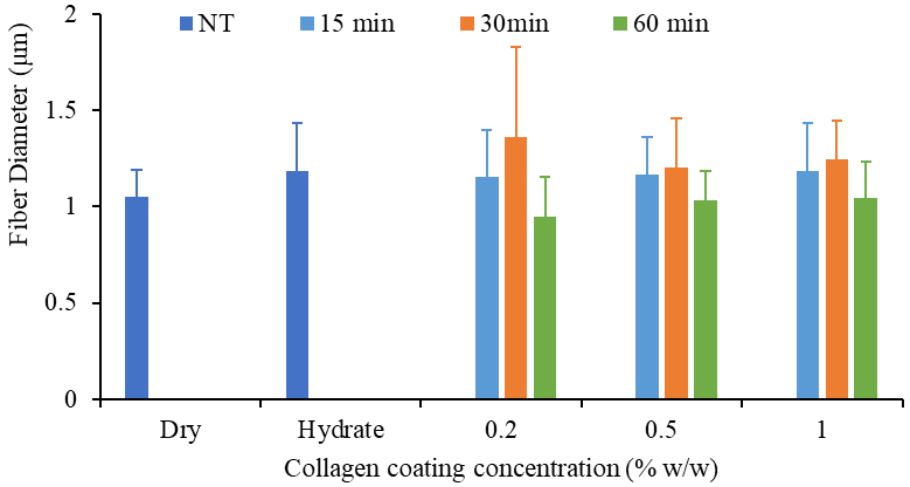

Figure 32 Size diameters comparison of CUR nanofibers uncoated in dry and hydrate state and coated with collagen at different concentrations (0.2, 0.5, 1 % w/w) for different times (15 min; 30 min; 60 min - mean values ± s.d., n=60).

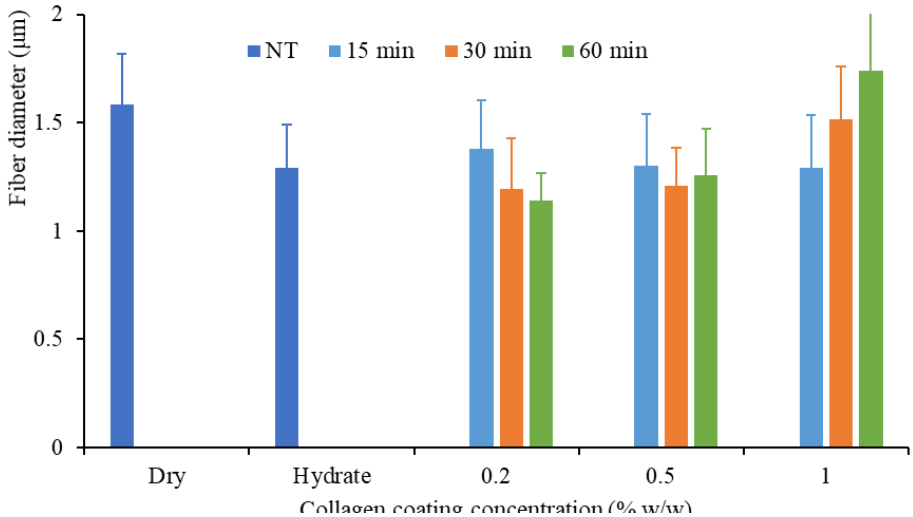

Figure 33 Size diameters comparison of collagen/PCL + RSV nanofibers uncoated in dry and hydrate state and coated with collagen at different concentrations for different times (mean values ± s.d., n=60).

2.13.3. Wettability

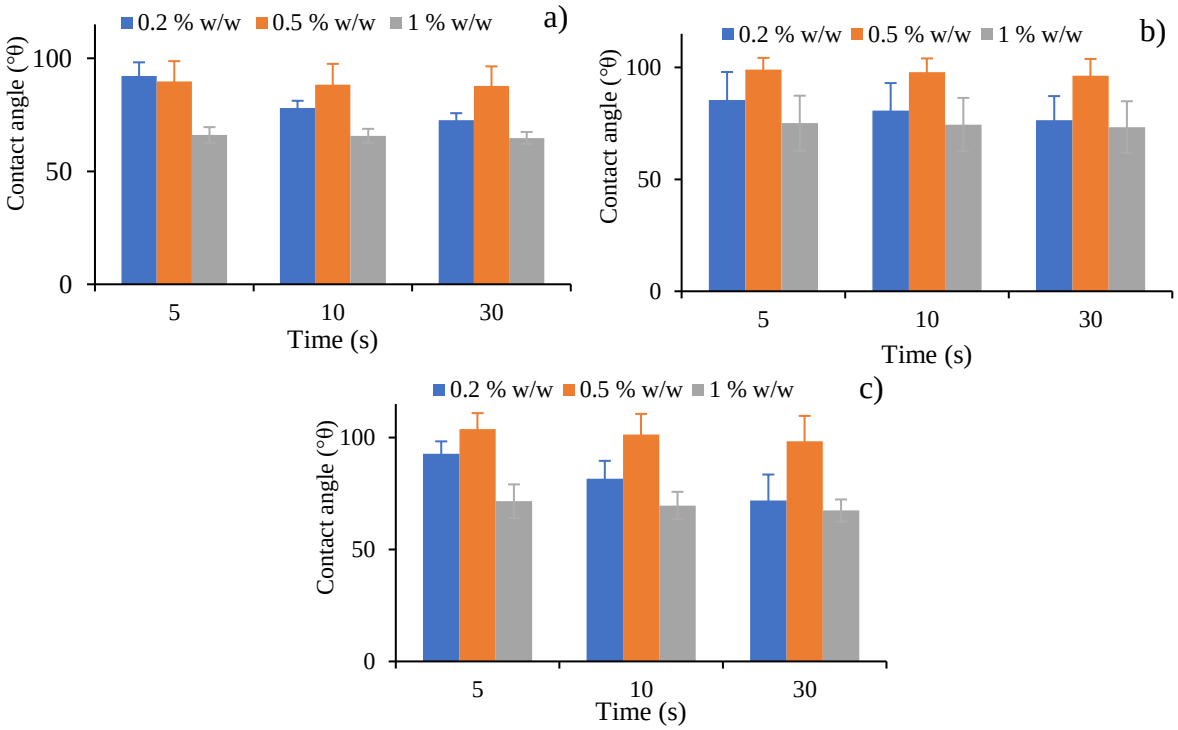

Figure 35 Comparison of contact angle values for collagen / PCL nanofibers unloaded (a) and loaded with CUR (b) or RSV (c) coated with collagen at different concentrations
(0.2, 0.5 and 1 % w/; mean values ± s.d. n=3).

Contact angle analyses were performed at 5, 10 and 30 seconds on collagen / PCL nanofibers unloaded, loaded with CUR or RSV and exposed to collagen solutions (0.2, 0.5, 1 % w/w) for one hour. In all cases, with the highest percentage of collagen coating (1% w/w) a decrease in contact angle values and, therefore, an increase in hydrophilic properties was achieved due to the addition of a high percentage of hydrophilic protein on the surface of the nanofibrous membranes (**Figure 35**). From 5s up to 30s no significant variations in wettability occurred indicating that just in 5s a balance between cohesive and adhesive forces on solid/liquid interface was reached. For CUR and RSV NFs, a slight decrease in wettability was evident when membranes were treated with native collagen at 0.5 % w/w. This phenomenon could rely on a lower and not homogeneous collagen coating on the surface of nanofibrous mat.

Comparing the results obtained from the measurement of the contact angle of the membranes coated with those of the untreated membranes, the hypothesis of the best coating with a higher collagen concentration was confirmed as it causes a significant increase in the wettability of the membrane compared to the uncoated one, unlike the other two concentrations that present a contact angle almost equal to the uncoated membrane (results in Chapter III of the thesis).

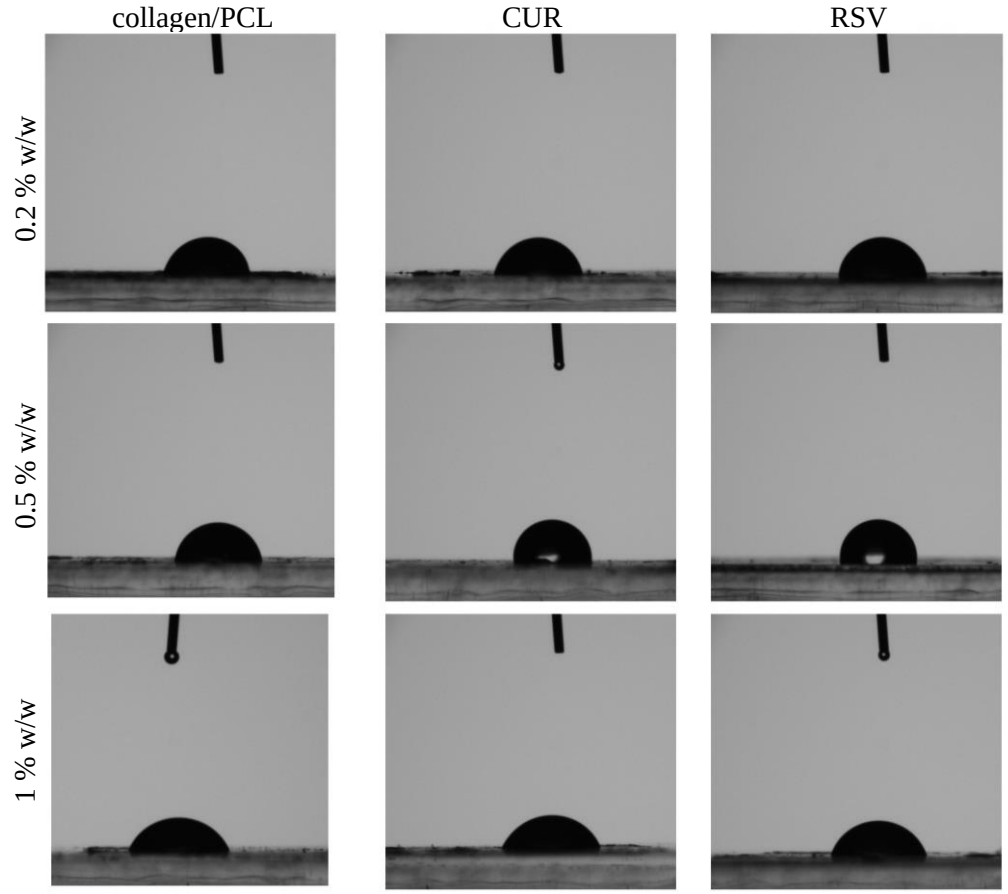

Figure 36 Photographs of collagen/PCL nanofibers unloaded and loaded with CUR or RSV coated with collagen at different concentrations and kept in contact with a water droplet. The images were taken at 10 s after the first contact with the droplet.

Figure 36 shows contact angle images of samples discussed above. Photographs were obtained at 10 seconds from the time delivery of the water drop on nanofiber surface. We can observe what has already made in evidence: in all cases the higher concentration of collagen coating led to a reduction in contact angle, therefore an increasing in wettability.

2.13.4. Mechanical Properties

Mechanical properties were evaluated on all samples coated with collagen at different concentrations (0.2, 0.5 and 1 % w/w) for one hour. The analyzes were conducted both in dry (**Figures 37a, 38a 39a**) and hydrate conditions (**Figures 37b, 38b, 39b**) applying a tensile distance of 20 mm and 80 mm respectively. Evaluation of the mechanical properties of nanofibers carried out in the hydrated state aims to determine the behavior of membranes under physiological conditions miming their contact with aqueous biological fluids. In the case of membranes not loaded with polyphenols (**Figure 37a**) analyzed at dry state, mechanical strength was significantly different between untreated and coated nanofibers with collagen at different concentrations. The collagen coating involved, at all concentrations, an increase in stress values, according to the assumption in protein deposition on the surface of the membranes. In particular, as coating collagen increases, an increase in the elasticity occurred, especially for nanofibers coated with 1 %w/w of collagen and furthermore, higher % elongation was recorded with the same coating concentration. As known, the structural unit of collagen is represented by the tropocollagen, formed by three tangled and stretch-resistant polypeptide chains; the variations recorded in the stress values were therefore, conceivably, mainly related to the different concentration of the collagenous polypeptide chains laid onto to the nanofibrous mat. For collagen coating 1% w/w, the increase in tensile strength associated to a better deformability can be justified by a random deposition of collagen fibrils on the nanofibrous surface. The balance between empty zones and areas with protein deposition, allow the material to withstand the same trigger forces, with a better degree of plastic deformation.

The increase in tensile strength also occurred in nanofibers loaded with curcumin analyzed in the dry state, observed in **Figure 38a**. Despite % elongation values are not concentration-dependent, in all cases, the coating involved a general improvement in the mechanical properties in terms of deformability if compared with nanofibers without coating. Nanofibers are less resistant, with tensile strength values almost halved compared to unloaded fibers. In the case of nanofibers loaded with resveratrol (**Figure 39a**) at the dry state, an increase in mechanical strength occurred. It seems anyway evident a different elastic behavior depending on the amount of collagen used for the coating. At 0.2 % w/w, for example, the characteristic collagen fibrils rigidity was still evident while increasing collagen concentrations (0.5 % and 1 % w/w) strength values and proportionally the % elongation increased.

The greater deposition of collagen on fibers surface is responsible of an increase either in elasticity and deformability. As already noted, possible variations in mechanical behavior can be related to a different protein arrangement on the nanofiber surface. Native collagen fibrils, randomly deposited on the nanofibrous membranes, during the mechanical deformation test, rotate, flex in different ways, modifying their own spatial geometry and transform their helical shape to a linear one, mostly in a random way[25].

Mechanical evaluation of hydrate nanofibrous membranes underlined a drastically increase in % elongation both in unloaded and loaded CUR and RSV. The remarkable deformability is mainly associated to the plasticity and flexibility of PCL highlighted in hydrate condition. Moreover, for all samples, tensile strength increased significantly compared to the same membranes not treated with native collagen, demonstrating, even in this case, protein chains were deposited on the membranes surface and dynamically act to modify the mechanical properties of the material. Hence, the triple combination collagen / PCL / native collagen was responsible, during the hydration condition, of a hybrid behavior. The final material resulted deformable and resistant, suggesting a better and promising *in vivo* performance; in physiological conditions, in fact, scaffolds can be subjected to a substantial mechanical stress given from body movements, especially close to joints and articulations.

Unloaded nanofibers with the highest amount of coating collagen (1% w/w) were more resistant, but not fragile and were able to maintain the same degree of deformability as the untreated membranes (**Figure 37b**. CUR NFs coated with collagen, in the hydrated state, acquired in all cases higher tensile strength (**Figure 38b**), however lost extremely their deformability if compared to the untreated fibers. Same conclusions can be drawn regarding nanofibers loaded with resveratrol (**Figure 39b**): clearly, in hydrate conditions, mechanical properties depend primarily on the major components of the nanofibrous mat, but also on the efficiency of the collagenous coating. Furthermore, the presence of the drug in the structure does not evidently affect mechanical behavior.

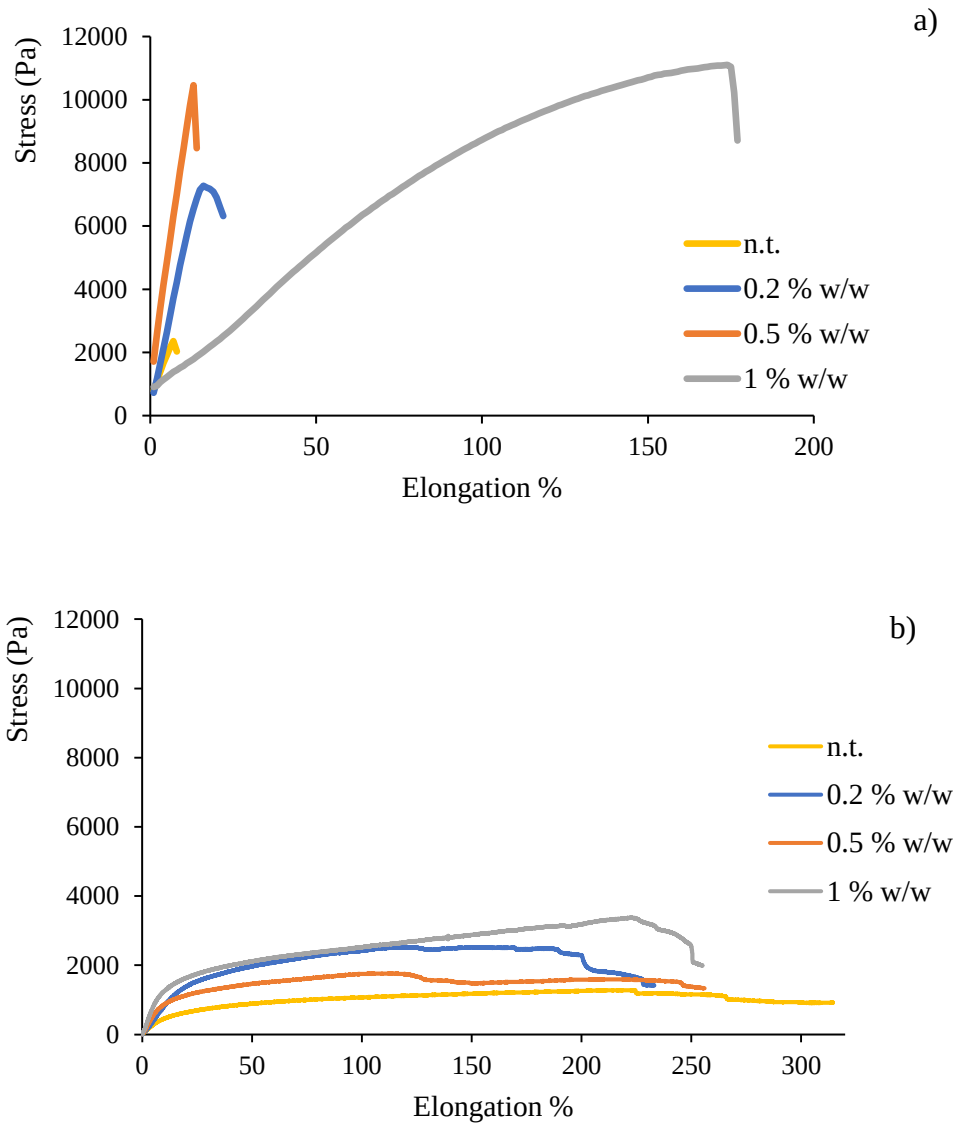

Figure 37 Stress (Pa) vs Elongation % profiles of dry (a) and hydrate (b) nanofibrous membranes based on collagen/PCL (mean values ± s.d., n=6).

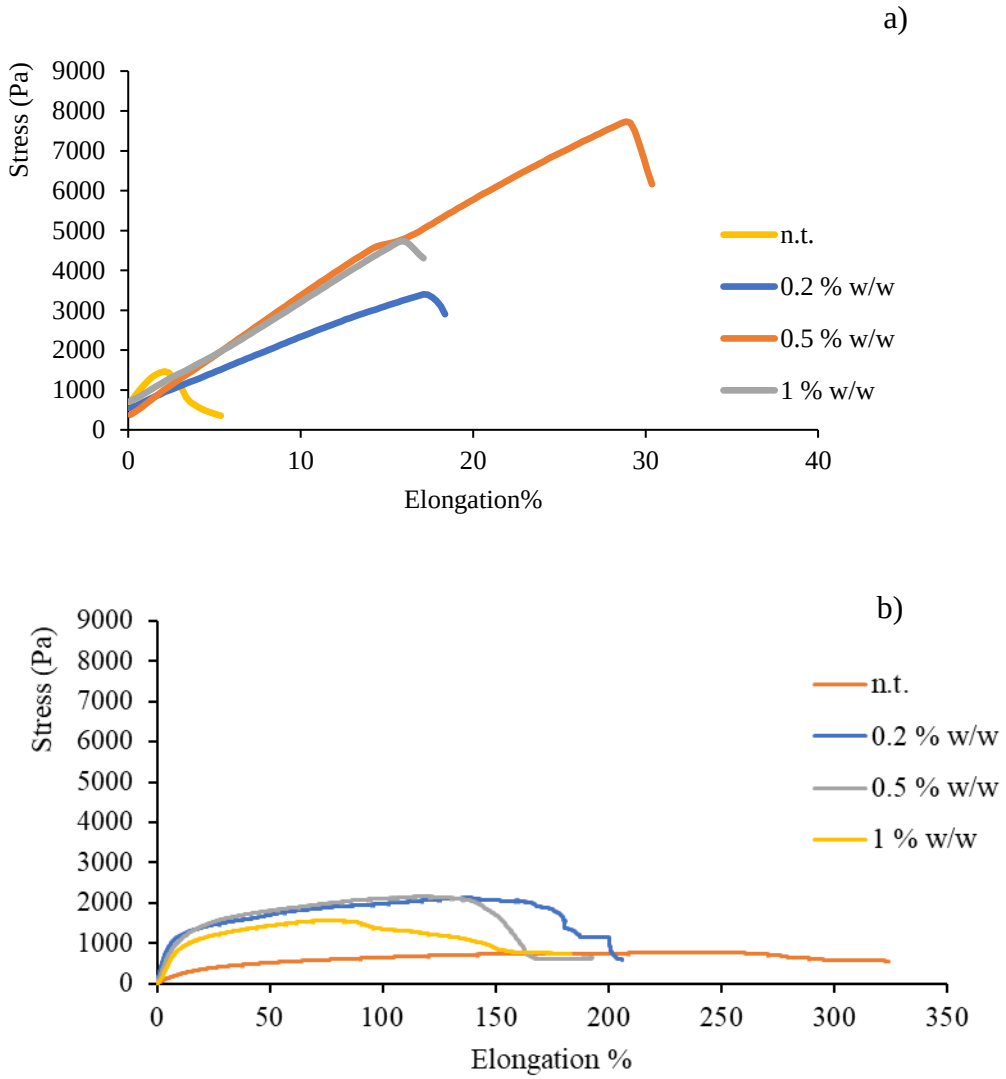

Figure 38 Stress (Pa) vs Elongation % profiles of dry (a) and hydrate (b) nanofibrous membranes based on collagen/PCL loaded with CUR and coated with different amount of collagen (mean values ± s.d., n=6).

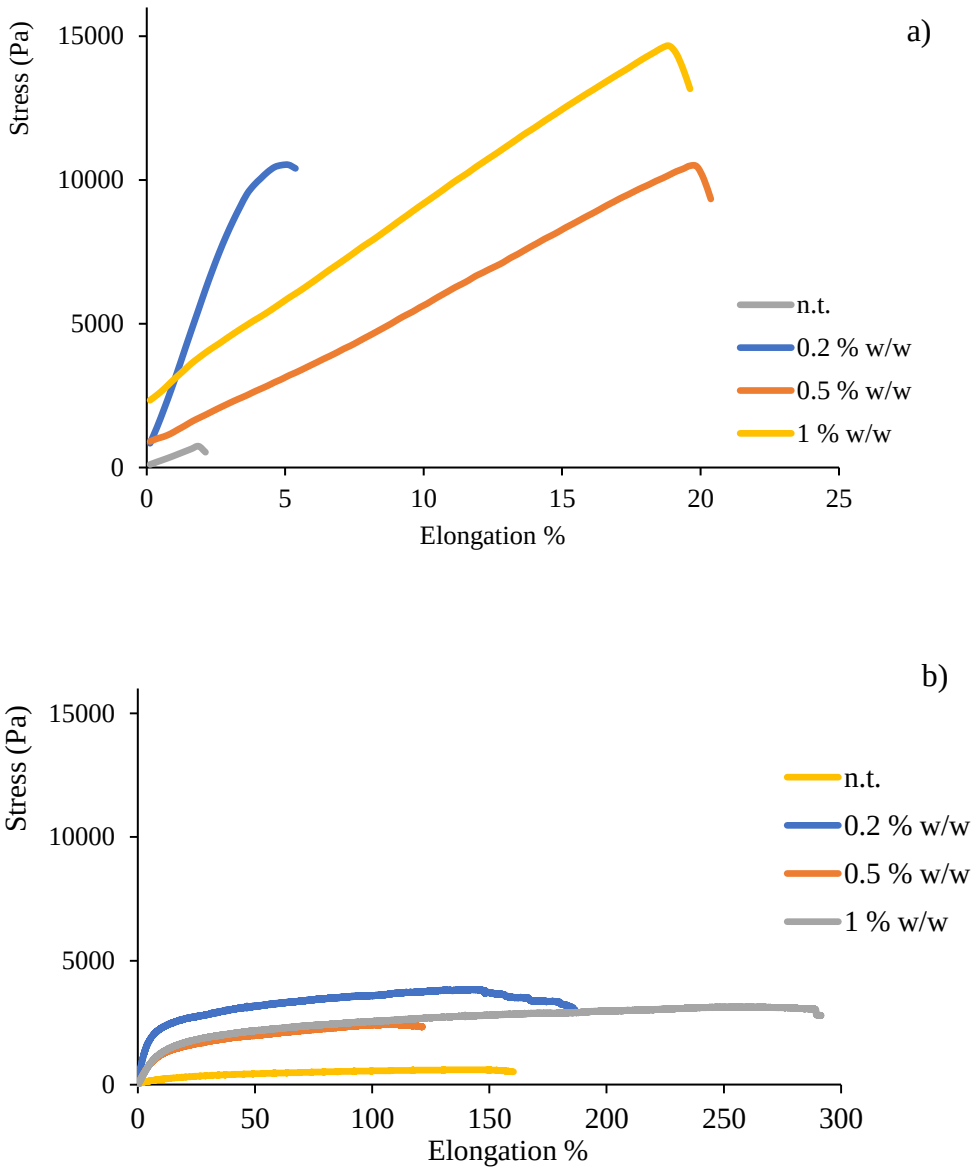

Figure 39 Stress (Pa) vs Elongation % profiles of dry (a) and hydrate (b) nanofibrous membranes based on collagen/PCL loaded with RSV and coated with different amount of collagen (mean values ± s.d., n=6).

2.13.5. Collagen dosage

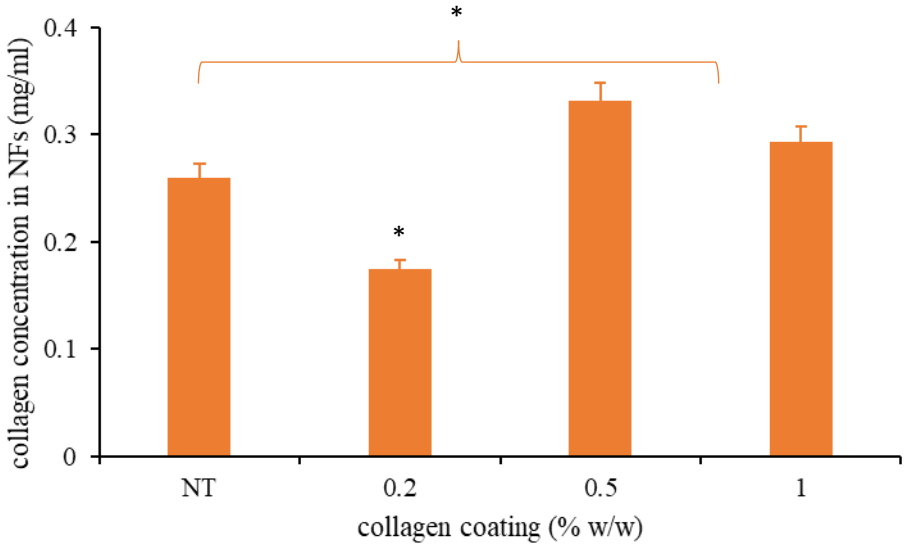

Figure 40 Collagen dosage in nanofibrous membranes coated with different collagen concentrations. ANOVA 1 way - MRT ($p < 0.05$) (mean values ± s d.; n = 3)

An hydroxyproline quantification was employed as method to quantify the amount of collagen present on the surface of the coated nanofibers (**Figure 40**). A sample of the same nanofibers, not collagen coated was also analyzed (NT) as reference. In the coated sample using 0.2 % w/w collagen, a smaller amount of protein was detected if compared to the reference. The result still require confirmation, however a partially loss of co-spun collagen in the nanofiber, not compensated by the absorption of coating protein, occurred, maybe due to the low concentration of the coating water-based solution. Samples treated with collagen 0.5 % and 1 % w/w showed an increase in quantity of collagen deposited on the nanofibers equal to 27% and 13% respectively, compared to the uncoated fibers. It seems that the method used for the coating leads to results not concentration dependent and a kind of plateau is reached. This can partially explain the lack of concentration dependence of the results obtained with mechanical properties characterization.

3. Materials and Methods

- *Materials*

Polycaprolactone (PCL - Mw 80 000), gelatin type B and Curcumin from Curcuma longa (Turmeric), powder were purchased from Sigma Aldrich (Milan, Italy). Resveratrol from Polygonum cuspidatum Sieb. & Zucc was acquired in Laboratorio Terapeutico M.R. Srl (Florence, Italy). Soluble native collagen 1% (w/v) from Kelisema S.R.L. (Como, Italy) and glacial acetic acid from Carlo Erba (Milan, Italy) was employed as solvent.

- *Methods*

3.1.Protein and Polymer Solutions

Native soluble collagen was dialyzed for 24 h in a dialysis bag (cut-off 12-14 kDa dialysis tubes, Emanuele Mires Ø = 36/32" – 28,6 mm) to remove the preservative agents; then the protein solution was freeze-dried for 48 h. Collagen/PCL solutions were prepared by solubilizing under magnetic stirring (400 rpm)10 % (w/w) of polycaprolactone in 90 % (v / v) acetic acid, in a water bath at 37 ºC for 4 h. 10 % w/w of freeze-dried collagen was added under magnetic stirring to PCL solution and a 1:1 w/w ratio blend was obtained. Protein/polymer solutions loaded with polyphenols were obtained with the same procedure and the active ingredient (curcumin, CUR or resveratrol, RSV) was added under magnetic stirring to the final protein / polymer solution at a concentration of 0.5% w / w. The solution is left under stirring, until the active principle was completely dissolved. In particular, the solution loaded with RSV was left for an hour, while CUR for four hours (**Table 1**). As comparison solutions based on PCL or collagen were prepared in acetic acid 90 % (v/v) at 20 % (w/w).

Table 1 % w / w composition of collagen, PCL and collagen / PCL solutions prepared in acetic acid at different concentrations, loaded or not loaded with curcumin (CUR) and resveratrol (RSV).

Solutions	PCL (% w/w)	Collagen (% w/w)	Curcumin (% w/w)	Resveratrol (% w/w)
PCL	20	-	-	-
Collagen	-	20	-	-
Collagen/PCL	10	10	-	-
CUR			0.5	-
RSV			-	0.5

3.2.Electrospinning of polymer, protein and polymer/protein solutions

All the solutions reported in Table 1 were subjected to electrospinning. Nanofibers were obtained by using the STKIT-40 (Linari Engineering equipment Pisa, Italy). A 10 ml glass syringe with a stainless-steel needle (OD = 0.8 mm, L = 15 mm) was filled with the proper solution and a volumetric pump (Razel R99-E) was employed for conveying. A high voltage generator (5 - 40 kV) charged the solution by applying a potential difference between the metal needle and a static collector covered with an aluminum foil. The operating spinning conditions, such as flow rate, voltage applied, and needle-collector distance were modulated according to the characteristics of the polymer solutions and to obtain continuous fibers without beads. In **Figure 41** a schematic representation of the electrospinning tecqniche is shown. Collagen and PCL solutions were electrospun follow the same process parameters employed in the previous chapter III and reported in **Table 2**. The process was carried out at atmospheric pressure, maintaining temperature and relative humidity (RH) within an optimal set interval (24-30 °C, 22-30 % RH) to allow the solvent evaporation and avoid beads formation.

Table 2 Electrospun process parameters of protein/polymer solutions.

Formulations	Distance (cm)	Voltage (kV)	Flow (ml/h)
Collagen/PCL	20	25	0.9
CUR		20	1.2
RSV			

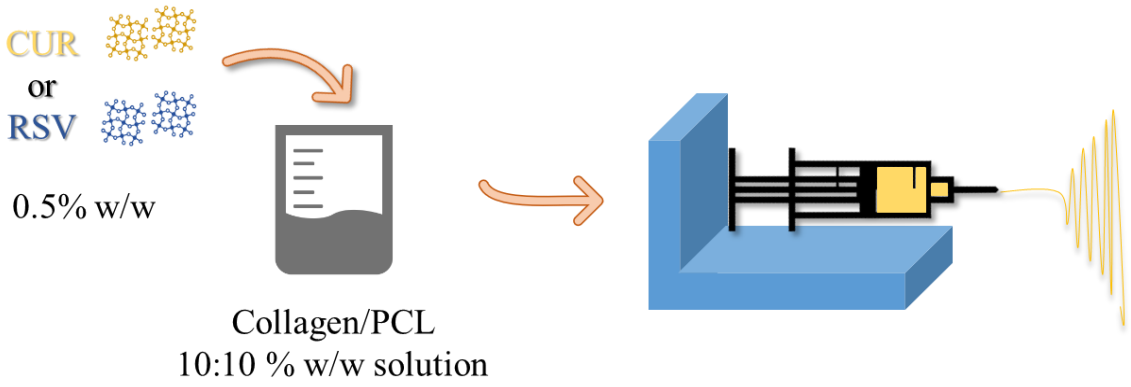

Figure 41 Schematic representation of CUR and RSV electrospun solutions.

3.3.Native collagen coating

The electrospun nanofibers based on collagen/PCL and those loaded with CUR and RSV, were immersed in an aqueous collagen solution, promoting a protein coating on their surfaces. Collagen solutions are prepared by protein freeze-dried dispersed in bi-distilled water. Collagen concentrations tested were 0.2%, 0.5% and 1% w/w. From the total amount of the electrospun nanofibrous membrane, segments of 1 cm^2 were cut and immersed in collagen solutions for different times: 15, 30, 60 minutes. Finally, the segments were dried at 25°C until complete solvent evaporation.

3.4.Characterization of polymeric and protein solutions:

Collagen/PCL mixtures prepared in acetic acid 90 % (v/v) unloaded and loaded with CUR or RSV were characterized by chemical-physical properties and compared with collagen 20 % w/w and PCL 20 % w/w solutions. Rheological analyses, conductivity and surface tension assays were performed.

3.4.1. Rheological analysis

Solutions of collagen, PCL and collagen/PCL in a 1:1 weight ratio were prepared in acetic acid 90 % (v/v) and analyzed by a rotational rheometer (Rheostress 600, Haake, Enco, Spinea, Italy). Solution viscosity (η) was measured at 25°C and at increasing shear rates in the range 10–1,000 s^{-1}. Three replicates were performed for each solution.

3.4.2. Conductivity (µS / cm)

Conductivity were performed using FiveGoTM - Mettler Toledo conductimetry. Before the analyses, the instrument was calibrated at room temperature (≈25°C) with a standard of 1413 µs/cm and three replicates were effected for each sample.

3.4.3. Surface Tension mN/m

Dynamic surface tension measurements were carried out by means of an automatic tensiometer (DyneMaster DY-300; Kyowa Interface Science Co. Ltd., Saitama, Japan) at 25°C. The analyses were performed recording a surface tension value every 3 seconds up to 300 seconds in a measurement range from 0 to 100 mN/m (ds±0,2mN/m). Three replicates were considered for each solution.

3.5.Characterization of electrospun nanofibers

3.5.1. Fiber diameter

Scanning electron microscopy (SEM) images were acquired at room temperature by using a high-resolution FE-SEM scanning electron microscope (Tescan Mira3 XMU series); a high voltage (20 kV) and a high vacuum ($6 \cdot 10^2$ Pa) were applied. Different magnifications of 10.0kx; was considered for the morphological evaluation. Fiber diameters were analyzed and processed by SEM photomicrographs using *imageJ*. Software (https://imagej.net/ImageJ). Measures were performed on at least 60 fibers of each type.

3.5.2. Solubility test

Collagen / PCL nanofibrous membranes loaded with CUR or RSV were cut in small pieces (2 cm^2) and kept at room temperature in 5 ml of deionized water from 24 h up to 7 days. After the fixed times, membranes were dried overnight and morphology and stability of nanofibers, were evaluated by SEM analysis.

3.5.3. Wettability

Wettability analysis of nanofibrous membranes based on collagen/PCL uncoated and coated with collagen, loaded or not with CUR or RSV, was carried out by the aid of a Cam tool 200 Contact Angle and Surface Tension Meter, KSV Instrument. The instrument was equipped with a telecentric camera and 55 cm focal length, monochromatic LED source, which allowed the measurement of the contact angle of a drop (volume 5µl) left lay on the scaffold and dispensed by the needle of a syringe pump. A video-camera recorded and captured an image every second for 30 seconds. Before proceeding with the measurement, PCL and collagen / PCL nanofibers (square 2 cm^2) were hydrate in water for 30s and properly adhered on a coverslip. For each sample three replicates were done.

3.5.4. Mechanical properties of nanofibrous membranes

Mechanical properties were evaluated either on nanofibrous membranes based on collagen/ PCL unloaded and loaded with CUR or RSV, and on the same nanofibers treated for 1 h coated with native collagen at different concentrations after 1 hour of coating treatment. Tensile strength was measured with a TA.XT plus Texture Analyzer (Stable MicroSystems, Godalming, UK), equipped with a 5 kg load cell. Before testing, fiber thickness was measured by a Sicutool 3955 G-50 (Sicutool, Milan, I) apparatus. The nanofibrous membranes were cut (1x3 cm) and inserted between two clamps (A/TG grips probe) to expose a surface area of 1 cm^2. The upper grip was raised at a trigger force of 1 mN under a controlled speed of 1 mm/s either 30 mm or until to the break point. Mechanical properties were evaluated in the dry and hydrated state (after 450 µL distilled water addition for 2 min). For each sample the stress % elongation profile was recorded. Five replicates for each sample were performed.

3.6.Physico-Chemical Characterization on electrospun nanofibers

3.6.1. ATR Fourier-Transform Infrared (FT-IR) Spectroscopy

On the same DSC samples IR spectra were recorded using a Fourier transform infrared spectrophotometer (Perkin Elmer SpectrumOne, Monza, Italy) with a single reflection ATR accessory (PIKE MIRacle™). Approximately 10mg of each sample were placed on ATR crystal of ZnSe and pressed down to the crystal. The spectra were collected with a resolution of 4 cm−1 within the spectral range of 650–4000cm−1.

3.6.2. Differential Scanning Calorimetry (DSC)

DSC analyses were performed on PCL, collagen and collagen/PCL electrospun nanofibers both unloaded and loaded with polyphenols. The equipment employed was a Mettler STARe system (Mettler Toledo, Novate Milanese, MI, Italy) equipped with a DSC821e Module and an Intracooler device for sub-ambient temperature analysis (Julabo FT 900) on 2–3 mg (Mettler M3 Microbalance) samples in sealed aluminum pans with pierced lid (heating rate β = 10 K min−1, nitrogen air atmosphere (flux 50 mL min−1), 30–300 ◦C temperature range)). The instrument was previously calibrated with Indium as standard reference Measurements were carried out at least in triplicate.

3.7.Drug Loading efficiency

Polyphenols loading efficiency in the nanofibrous membrane was evaluated using methanol solvent extraction. Nanofibers were immersed in 1 ml of methanol and vortexed for 5 min for a total of three extractions. Two replicates for each sample were performed. The 3 ml extracted were analyzed by the aid of two different analytical methods depending on the active ingredient loaded in the nanofibrous membrane. Curcumin extracts were diluted (1:20) and analyzed by spectrophotometer (*Lambda 25 UV / VIS Spectrometer, Perkin Elmer, Italy*) measuring the maximum absorption wavelength at 425 nm. On the other side, resveratrol extracts were analyzed by high pressure liquid chromatography (HPLC-RP, *HPLC Series 200, Perkin-Elmer, Italy*), equipped with an UV detector. The analyses were conducted using as stationary phase a *Waters C18* column *(4; 6 x 150 ηm, particle size 10 µm, 125 Angstrom)* and a mobile phase methanol:water 52:48 (v /v) with 0.05 % v/v of glacial acetic acid. The analysis was performed under isocratic conditions at a flow rate of 1 ml/min, at 25°C with detection wavelength fixed at 303 nm. Samples injection volume was 20 µl and two replicates for each sample were performed with a 5-min analysis time. A standard calibration curve was built for both drugs. Specifically, stock solutions were prepared by solubilizing drugs in methanol at a concentration of 100 µg/ml. Resveratrol stock solution was diluted to obtain a linear range of concentration from 6:25 to 75 µg/ml, while curcumin to obtain a range from 12.5 to 100 µg/ml.

3.8.Release Studies

Curcumin or resveratrol release from nanofibrous membranes was performed in DMEM w/o phenol red (Corning, USA) with 10% v / v of FBS (Fetal Bovin Serum, Biowest, USA) and 1% v / v of antibiotics (Antibiotic / Antimycotic Solution, Euroclone, I). The release medium was chosen to simulate *in vitro* physiological conditions and predict nanofibrous *in vivo* behavior. Before the test membranes were cut into 1 cm^2 segments; each segment was placed in a 2 ml vial filled with 1 ml of release medium and placed in a shaking bath at 37 ° C with a speed of 100 rpm. The test was performed in triplicate and 500 µl of the medium were withdraw and replaced with an equal volume of fresh medium at set times (30 min, 1h, 3h, 6h, 24h, 48h, 72h and 7 days). Depending on the active ingredient the release amount was assessed by two different analytical methods described in previous section.

3.9.Hydroxyproline assay

Collagen is the only protein with hydroxyproline in its amino acid structure, therefore, an hydroxyproline quantification was employed to assess the protein amount inside the nanofibrous membranes and as coating on the surface of the same scaffolds. Briefly, 1 mg of collagen/PCL nanofibers uncoated and coated with collagen at different concentrations (0.2, 0.5, 1 % w/v) were dissolved in 1 ml of acid acetic 90% (v/v), to reach 1 mg/ml concentration. 100 µl of this solution were placed in 300 µl vials and acetic acid was evaporated under nitrogen flow. At this stage, samples were subjected to acid hydrolysis in HCl 6M, at 110°C for 24h in nitrogen atmosphere. After derivatization precolumn with orthophthalaldehyde (OPA) and fluorenylmethylchloroformate (FMOC), an amino acid analysis was performed by means of a modular Jasco X-LC device equipped with a fluorescence detector (λ_{ex} / λ_{em} 340/446 for OPA-derivatization and λ_{ex} / λ_{em} 368/308 for FMOC- derivatization).

3.10. In vitro cell culture experiments

3.10.1. Biocompatibility

Normal human dermal fibroblasts (NHDFs - Promocell GmbH, Heidelberg, G) from 5^{th} to 10^{th} passage were employed and nanofibrous biocompatibility was assessed. In the first part of the work collagen/PCL nanofibers unloaded and loaded with CUR or RSV were assessed and, in a second step the same samples treated with native collagen at different concentrations for 1 hour were evaluated. All nanofibers were cut in round pieces with a punch (Ø = 4 mm) and UV irradiated for 24 h to guarantee no microbial contamination. Cells were sub-cultured in complete medium (CM) consisting of DMEM supplemented with 1% v/v antibiotic/antimycotic solution and 10% v/v inactivated fetal calf bovine serum. The pieces were placed into a 96-well plate and conditioned with 10 µl of CM. NHDFs (35.000xwell in 200 µl of CM) were seeded onto the nanofibrous membrane for 3 and 7 days. Subsequently, the eventual cytotoxic effect of nanofibrous membranes was assessed by an MTT test. First the medium was withdrawn and 50 µl per well of 7.5 µM MTT reagent

in DMEM without red phenol was added in each well; subsequently the plates were placed in incubator at 37 °C for 3h. Finally, the MTT reagent was removed and 100 µL of DMSO were added to each well to lyses the cellular membranes and to allow the complete dissolution of formazan crystals, derived from mitochondrial dehydrogenases reduction of the MTT dye. Results were expressed as % absorbance measured after contact with each sample with that measured for CM. This solution absorbance was measured by means of an iMark® Microplate reader (Bio-Rad Laboratories Inc., Hercules, CA, USA) at a wavelength of 570 and 690 nm (reference wavelength) after 60 s of mild shaking. Eight replicates were done for each sample.

3.10.2. Cell adhesion and morphology

Fibroblast adhesion and morphological shape after treatment with collagen/PCL nanofibers unloaded and loaded with CUR or RSV was assessed by means of scanning electron microscopy (SEM) and confocal laser scanning microscopy (CLSM). Briefly, nanofibers were cut in round pieces to get a surface area of 1.9 cm^2 and UV irradiated for 24 h. The pieces were laid down into a 24-well plate and conditioned with 50 µl of CM. 100,000 NHDF in 450 µl of CM were seeded in each well onto the nanofibers. After 3 and 7 days of culture, media was withdrawn, samples were washed with PBS and cells were fixed for 1 h at room temperature with 3 % v/v of a glutaraldehyde solution. Subsequently, the samples were rinsed twice with 200 µl of PBS.

For SEM analysis air dried at room temperature overnight. For CLSM analysis, according to Sigma procedure, samples were at first treated with Tryton 0.1 % v/v for 5 min to permeabilize cell membranes in order to enable cytoskeleton staining with 100 µl of Phalloidin-FTIC (concentration 50 µg/ml, Sigma, I) for 40 min, at room temperature and protected from light. Afterwards, substrates were washed twice with PBS and treated for 10 min, at room temperature and protected from light with 100 µl of Hoechst 33258 (Sigma, I) diluted in PBS 1: 10000, in order to stain the nuclei. Stained samples were then examined by CLSM and the fluorescence of Phalloidin TRITC and Hoechst 33258 (λ_{ex} = 346 nm and λ_{em} = 460 nm) were metered. The acquired images were processed using a "LAS X Life Science" software (Leika Microsystem, I).

4. Conclusion

In this research work, bioactive CUR and RSV loaded electrospun nanofibers based on collagen/PCL were obtained for the first time using acetic acid 90 % v/v, as green solvent. As expected, fiber diameters increased with the addition of polyphenols into electrospun collagen/PCL formulation, however dimensions resulted compatible with the intended applications on skin lesions. Supposedly, changing in fiber dimensions can be linked to the different polyphenol molecular weights, which affected the molecular interactions occurred during the stretching of the fluid jets subjected to a fixed high electric field. Despite this, no morphological variations, no shift from circular to flat fibers shape occurred between unloaded and loaded nanofibers, demonstrating a good stability in the electrospinnability of the materials. Fibers kept intact their architecture even after 7 days of immersion in an aqueous environment, suggesting a good ability to protect the wound for an enough time lapse, to yield the active ingredient over time and to support the growth of new tissue during healing process. The ability of these scaffolds in resisting to body movements and stress, were confirmed by mechanical strength characterization. Hydrated membranes proved to be more resistant then dried ones, showing a high deformability and simultaneously keeping a good tensile modulus. Unexpectably RSV-loaded nanofibers showed an extremely reduction in wettability behavior if compared to the unloaded and CUR-loaded fibers. The balance between pores dimension and distribution and the partition of RSV hydrophobic moieties into the nanofibrous membranes can hypothetically explain this drastic change in contact angle values. Either way, both CUR and RSV signal did not appear in FT-IR and DSC analyses, suggesting their complete amorphization, after electrospinning process. An *in vitro* release study assessed that 70 % of total drug amount loaded into the nanofibers was released in 6 hours. The ability to stimulate the repairing in damaged tissue were confirmed by *in vitro* viability assay on normal human dermal fibroblasts. Cell proliferation test indicated a promotion in cellular viability mediated by either the unloaded probably thanks to the mechanical support for cell growing, but especially by loaded fibers, indicating a positive effect of the polyphenols. This effect appears evident for three days culture, suggesting a strong acceleration in fibroblast proliferation if compared to the control. SEM and CLSM images confirmed the nanofibrous scaffolds suitability in improving cell spreading and adhesion with a healthy visible shape. When nanofibrous substrates were coated with native collagen solutions at different concentrations some drastically physical changes occurred. A topographic variation was particularly evident and collagen film in some cases was effectively denoted from SEM images as a covering layer on the surface of nanofibrous mat. Furthermore, comparing the mechanical behaviors to the uncoated nanofibers, a great improving in tensile strength and % elongation values was evident, suggesting an effective collagen deposition on the surface of the nanofibrous membranes. Protein deposition was assessed by dosing the amount of hydroxyproline residues in scaffolds both uncoated and coated. Collagen was detected in all fibers with an increase in fibers coated with 0.5 % w/v solution. Doubtless, a native collagen coating by exposing RGD-motifs that trigger binding of a5b1- and av-integrins can improve cell adhesion, spreading and motility[26]. Future steps are involved to demonstrate the effectiveness of these scaffolds as bioactive dressings for adhesion, grown, migration and proliferation either of keratinocytes, as known, the complete

re-epithelialization cannot be achieved until further migration of keratinocytes from the scaffolds and wound edge to bridge the open wound surface.

Collaborations

The studies were conducted in collaboration with Prof. Milena Sorrenti and Laura Catenacci, at Department of Drug Sciences, University of Pavia, Italy.

References

[1] Braiman-Wiksman L. et al., «Novel Insights into Wound Healing Sequence of Events», *Toxicologic Pathology* 35, 6, 2007: 767–79.

[2] Gurtner G.C. et al., «Wound Repair and Regeneration», *Nature* 453, 7193, 2008: 314–21.

[3] Wang J. et al., «Functional Electrospun Fibers for the Treatment of Human Skin Wounds», *European Journal of Pharmaceutics and Biopharmaceutics*,119, 2017: 283-299.

[4] Lakshmanan R. et al., «Evaluation of Dermal Tissue Regeneration Using Resveratrol Loaded Fibrous Matrix in a Preclinical Mouse Model of Full-Thickness Ischemic Wound», *International Journal of Pharmaceutics*, 558, 2019: 177-186.

[5] Francis A. and Baynosa R.C., «Hyperbaric Oxygen Therapy for the Compromised Graft or Flap», *Advances in Wound Care* 6,1, 2017: 23–32.

[6] Kim Y.W. and Byzova T.V., «Oxidative Stress in Angiogenesis and Vascular Disease», *Blood* 123, 5, 2014: 625–31.

[7] Marziyeh Hajialyani D.T. et al., «Natural Product-Based Nanomedicines for Wound Healing Purposes: Therapeutic Targets and Drug Delivery Systems», *International Journal of Nanomedicine* 13, 2018: 5023–5043.

[8] Mohanty C. and Sahoo S.K., «Curcumin and Its Topical Formulations for Wound Healing Applications», *Drug Discovery Today* 22, 10, 2017: 1582–92.

[9] Akbik D. et al., «Curcumin as a Wound Healing Agent», *Life Sciences* 116,1, 2014: 1–7.

[10] Panchatcharam M. et al., «Curcumin Improves Wound Healing by Modulating Collagen and Decreasing Reactive Oxygen Species», *Molecular and Cellular Biochemistry* 290, 1, 2006: 87–96.

[11] Hou J. et al., «Sustained Release of *N* -acetylcysteine by Sandwich Structured Polycaprolactone/Collagen Scaffolds for Wound Healing», *Journal of Biomedical Materials Research Part A* 107, 7, 2019: 1414–24.

[12] Zhao R. et al., «Curcumin Protects Human Keratinocytes against Inorganic Arsenite-Induced Acute Cytotoxicity through an NRF2-Dependent Mechanism», *Oxidative Medicine and Cellular Longevity* 2013.

[13] Zhao P. et al., «Anti-Aging Pharmacology in Cutaneous Wound Healing: Effects of Metformin, Resveratrol, and Rapamycin by Local Application», *Aging Cell* 16,5, 2017:1083-1093.

[14] Leonard S.S. et al., «Resveratrol Scavenges Reactive Oxygen Species and Effects Radical-Induced Cellular Responses», *Biochemical and Biophysical Research Communications*, 309, 4, 2003, 1017-1026.

[15] Lakshmanan R. et al., «Evaluation of Dermal Tissue Regeneration Using Resveratrol Loaded Fibrous Matrix in a Preclinical Mouse Model of Full-Thickness Ischemic Wound», *International Journal of Pharmaceutics* 558, 2019, 177-186.

[16] Zahedi P. et al., «A Review on Wound Dressings with an Emphasis on Electrospun Nanofibrous Polymeric Bandages», *Polymers Advanced Technology*, 21, 2010, 77-95.

[17] Lee C.H. et al., «Biomedical Applications of Collagen», *International Journal of Pharmaceutics* 221,1–2, 2001: 1–22.

[18] Georgiana M. et al., «Collagen-Based Drug Delivery Systems for Tissue Engineering», *Biomaterials Applications for Nanomedicine*, ed. Rosario Pignatello, 2011, 334-358.

[19] Rho K.S. et al., «Electrospinning of Collagen Nanofibers: Effects on the Behavior of Normal Human Keratinocytes and Early-Stage Wound Healing», *Biomaterials* 27, 8, 2006: 1452–61.

[20] Dippold D. et al., «Novel Approach towards Aligned PCL-Collagen Nanofibrous Constructs from a Benign Solvent System», *Materials Science and Engineering: C* 72, 2017: 278–83.

21 Chakrapani V.Y. et al., «Electrospinning of Type I Collagen and PCL Nanofibers Using Acetic Acid», *Journal of Applied Polymer Science* 125, 4, 2012: 3221–27.

[22] Raja et al., «Wound Re-Epithelialization: Modulating Keratinocyte Migration in Wound Healing», *Frontiers in Bioscience: A Journal and Virtual Library* 12, 2007: 2849–68.

[23] Rho K.S. et al., «Electrospinning of Collagen Nanofibers: Effects on the Behavior of Normal Human Keratinocytes and Early-Stage Wound Healing», *Biomaterials* 27, 8, 2006: 1452–1461.

[24] Fu X. et al., «Regulation of Migratory Activity of Human Keratinocytes by Topography of Multiscale Collagen-Containing Nanofibrous Matrices», *Biomaterials* 35, 5, 2014: 1496–1506.

[25] Nesbitt S. et al., «Collagen Fibrils in Skin Orient in the Direction of Applied Uniaxial Load in Proportion to Stress While Exhibiting Differential Strains around Hair Follicles» *Materials* 8, 4, 2015: 1841–57.

[26] Taubenberger A.V. et al., «The Effect of Unlocking RGD-Motifs in Collagen I on Pre-Osteoblast Adhesion and Differentiation» *Biomaterials* 31,10, 2010: 2827–35.

CHAPTER V

CHITOSAN COATED POLYMERIC NANOPARTICLES AS siRNA DELIVERY SYSTEM

ABSTRACT

Oligonucleotides therapeutics represent a novel class of molecules developed to modulate gene expression interfering with ribonucleic acids (RNA) or protein. These moieties are characterized by a strong instability and easy degradation due to exonuclease enzymes. To avoid these drawbacks and ensure an efficient delivery to target cells, viral and non- viral vectors are the two main approaches employed. Currently, viral vectors are one of the major vehicles in gene therapy; however, the potent immunogenicity and the insertional mutagenesis represent a potential problem for the patient. Non-viral vectors, such as polymeric nanocarriers, provide a safer and more efficient delivery of RNA interfering molecules. Aim of this work is to employ PLGA core nanoparticles shell-coated with chitosan oleate as carriers of siRNA. An siRNA targeted on HIV-1 and therefore directed against the viral Tat/Rev transcripts was employed as model. The idea was to obtain an ionic interaction between the oligonucleotide's moieties, negatively charged, and the positive surface charges of the chitosan shell. Non-covalent bonds can protect siRNA from nuclease degradation, guarantee a good cell internalization and a fast release of the siRNA into the cytosolic portion allowing its activation.

1. Introduction

RNA-interference (RNAi) is a natural process occurring in cells to regulate gene expression. Different organisms from protozoa to mammals preserved this event during the evolution as a mechanism of defense against viruses[1]. It consists of complex enzymatic machinery able to control post-transcriptional gene expression through the degradation of target messenger RNA (mRNA) and is initiated by double-stranded RNA (dsRNA), semi-perfectly homologous in sequence to the silenced gene [2,3]. In mammalians, the mediators of sequence specific messenger RNA degradation are 21- and 22-nucleotide small interfering RNAs (siRNAs) generated by ribonuclease III, Dicer, and cleavage from longer dsRNAs [4,5]. Once cleaved, siRNAs interact with Argonaute-2 (AGO-2), a multifunctional protein with observed catalytic activity in mammalian cells and become incorporated into RNA-induced silencing complexes (RISCs). Ago2 is the catalytic component of the RISC. For each siRNA duplex, only one strand, the guide, is assembled into the active RISC; the other strand, the passenger, is destroyed[6].The guide strand possesses the complementary sequences in target mRNAs and it is bound within the catalytic domain of AGO2 at the 5′ end that recognizes the siRNA 3′ end. The cleavage of targeted mRNA leads to a degradation of the cleaved mRNA transcript by cellular exonucleases. Because RISC can undergo multiple rounds of mRNA cleavage mediating a robust post transcriptional gene silencing (PTGS) response against the target gene, RNAi can represent a suitable tool for the therapeutic intervention of several human diseases. The key therapeutic advantage of using RNAi lies in its ability to specifically and potently knock down the expression of known sequence of disease-causing genes[7]. Several researches and clinical trials highlighted the great potential of RNA interference (RNAi)-based therapeutics either in cancer treatment, infectious diseases, and other diseases associated with specific gene disorders[8]. In particular, this approach can be useful to treat diseases with "non-druggable" targets for which conventional therapeutics, are not successful. Viral infections, ocular diseases, neurodegenerative disorders and cancer are the most common target and several preclinical and clinical studies are ongoing[9].

However, gene therapy based on exogenous oligonucleotides, as small interference RNA (siRNA), microRNA, and short hairpin RNA (shRNA), still represent a challenge due to numerous limitations in delivery. Focusing on naked siRNA, as well known, these RNAi effectors are rapidly degraded by nucleases, show non-specific and poor cellular uptake, involving low transfection efficiency. To overcome the delivery impediments, many strategies have been proposed. Oligonucleotides can be chemically modified to achieve both more stability and providing resistance to RNase by attaching different groups at ribose position (i.e. 2'-O-methylpurines and 2′-O Morfolino modifications)[10,11] Chemical modifications of siRNAs can also seek to achieve a selective systemic delivery improving specific cell-surface recognitions, lowering the dosage required at target site and reducing potential side effect to non-target tissues. Alternatively, siRNAs can be encapsulated or conjugated with natural or synthetic delivery vehicles including viral or non-viral carriers able either to enhance an active targeting, cell internalization with tissue specificity, avoiding serum degradation, macrophage phagocytosis and limiting harmful side effects[12]. Most common viral vectors employed for *in vivo* gene delivery are lentiviruses (LVs) and adeno-associated viruses (AAVs). Advantages include stable gene expression, higher transgene payloads, and, importantly, the ability to pseudo-type the vectors with a diverse heterologous viral envelope with broad or restricted cell tropism depending on the need[13],[14]. Regardless of the effectiveness of gene transfer, the use of viral vectors presents certain disadvantages. For instance, viruses are immunogenic and, when expressed in the host, may induce an immune response, thus limiting the practical application of gene perturbation in gene therapy[15]. The viral delivery itself has been considered nonspecific toward host cell types, as well as immunogenic which limits the possibility of repetitive or strengthening dosing[12]. In order to obtain a selective systemic delivery, therapeutic siRNAs have been also coupled to chemical antibodies known as aptamers. Aptamers are peptide molecules specifically designed to bind with high affinity target cells receptors and to deliver siRNA payloads[16]. They are gaining a growing interest in the field of gene therapy due to their low toxicity and immunogenicity, properties that make aptamers smart binding ligands[17]. On the other hand, due to their unique properties, such as nanoscale sizes (10–1000 nm), low toxicity, and versatility, nanoparticles have been widely investigated and applied either as drug carriers to treat diseases, and, more recently, as great promising approach to the delivery of novel gene therapeutic agents including siRNA and microRNA[15].Such delivery systems include inorganic nanoparticles (i.e. gold or silver nanoparticles)[18],[19], lipid-based systems (liposomes, lipoplex and numerous lipid lipid-like materials)[20], [21], but especially polymer-based nanostructures[22],[23],[24]. Nanoparticles based on cationic polymers, for example, can be useful as transfection agents, thanks to their ability to bind one or more large nucleic acids units, reversibly, into or onto stabilized nanoparticles protecting them against bioenvironment degradation. Cationic polymers are generally divided in synthetic and natural polymers. Synthetic polymers include polyethylenimine and poly-lysine, while natural polymers include chitosan, collagen, and cationic polypeptides[3]. Cationic polymeric nanoparticles based on chitosan, can electrostatically interact with siRNA to form stable, positively charged polyplexes, with negatively charged siRNA upon simple mixing[25]. In particular, the amino and hydroxyl groups present in the chitosan chains facilitate the chemical modification and functional properties enhancing the possibility of a better polymer-nucleic acid interaction[26]. Positive charges of chitosan rely on primary amino groups protonated at pH below 6, that make this polymer useful for applications under slightly acidic conditions, such as tumoral extracellular environments. Though, at the

physiological pH, the positive charge of chitosan is reduced, leading to a loss of both efficacy in siRNA complexation and nanoparticle stability[27]. Furthermore, many studies have been performed to identify optimal chitosan molecular properties to get an efficient nano-system able to the siRNA and exploit good gene silencing. Degree of acetylation, molecular weight, chitosan amine to siRNA phosphate ratio (N:P ratio) and preparation method to obtain siRNA-loaded nanocarrier play an important role in obtaining efficient polycomplexes[28]. Several studies investigate the suitability of siRNA-loaded chitosan nanocarriers for very different applications[27]. An interesting proposed application in the field of gene silencing involves the local delivery of siRNA. For instance, a novel approach is based on using biocompatible implants hybridized with siRNA-loaded chitosan nanocarriers to promote nerve regeneration and allow local delivery of nanotherapeutics[29], [30]. As well known, the introduction of hydrophobic modification to chitosan offers several advantages, such as easy binding to cells, enhanced nanoparticle stability in serum, better cellular uptake and protection from degradation, and easier nucleic acid dissociation from chitosan inside cells[31]. Based on all these premises the aim of our work was to employ chitosan-oleate shell coated PLGA core nanoparticles, previously synthetized[32] and characterized as poorly soluble drug delivery systems[33] to vehiculate this time siRNAs. A preliminary study was carried out in order to obtain an ionic interaction between negatively charged siRNAs phosphate groups and positively surface charged exposed by chitosan-oleate amino groups, predicting a binding strong enough to allow the delivery of siRNA to the target cells, but weak enough to release the oligonucleotide following cell internalization. An siRNA targeted on HIV-1 and therefore directed against the viral Tat/Rev transcripts was employed as model and internalization studies were performed on immortal and normal cells lines to verify the effectiveness of *in vitro* siRNAs delivery.

2. Results and discussion

1.1.Characterization of siRNA nanoparticles or chitosan siRNA nanoparticles

Chitosan oleate represents an amphiphilic biopolymer derivative obtained by electrostatic interactions with oleic acid. In recent years this hydrophobically modified derivative was employed for its ability to self-assemble in micelles structures, but especially as stabilizer in nanoemulsions. In this work nanoparticles with a PLGA hydrophobic nucleus and shell-coated with chitosan oleate (CS-OA/PLGA NPs) were obtained by solvent evaporation method. As shown in **Table 1** nanoparticles were characterized by a particle size in the nanometric range (≈ 240 nm), and a very good polydispersity index PI (≈ 0.2), indicating nanostructure with an optimal physical stability. The strongly positive zeta potential values confirmed the effective presence of protonated chitosan amino group on nanoparticles surfaces. These results are in line with results reported in previous works[32, 33].

Table 1 CS-OA/PLGA NPs mean particle size (Mean nm), polydispersity index (PI) and zeta potential (ζ mV) (mean ± s.d.; n = 3).

CS-0A/PLGA Nanoparticles	
Mean (nm)	**236.7**±4.03
PI	**0.18**±0.03
Zeta potential, ζ (mV)	**36.49**±8.55

As well known, the high degree of protonation of chitosan amino groups (NH_2) occurring at a pH below chitosan pKa (∼6.5−6.9) favors the spontaneous formation of polyelectrolyte complexes through electrostatic interactions with polyanionic molecules such as oligonucleotides[28]. On the basis of this evidence a siRNA targeted to HIV-1, directed against the viral Tat/Rev transcripts was employed as model to obtain a spontaneous ionic interaction between siRNA phosphate and CS amino groups. **Figure 1** schematizes the possible interaction between the two compounds. Colloidal NPs are synthetized in an acidic environment (pH 4.5), however siRNAs are unstable at pH below 5, to avoid any possible oligonucleotides instability during their complexation with CS-OA/PLGA NPs, the colloidal system was subjected to a buffer exchange by the aid of a dialysis bag method. After dialysis the colloidal stability was assessed by checking particle size, polydispersity index and surface charges. **Figure 2a** shows particle size and PI comparison of nanoparticles before and after buffer exchange. Results showed a significant statistical increase in particle dimensions, while polydispersity index was unaffected, therefore the colloidal system maintained its stability at pH around 6. Nanoparticles remained positively charged, however a strong drop in the zeta potential occurred (**Figure 2b**). Anionic DPBS phosphate groups, in fact, settled around the positive amino charges neutralizing them and partially reducing the positive repulsion force. This led to a minimum intraparticle distances, causing aggregation phenomena and therefore an increase in size. Nevertheless, a positive potential still allowing a good binding capacity of chitosan protonated amines to form small and stable polyplexes with the siRNA. Moreover, based on the literature data, a pH slightly lower than 7 is optimal to achieve a good balance between oligonucleotide association and dissociation[34].

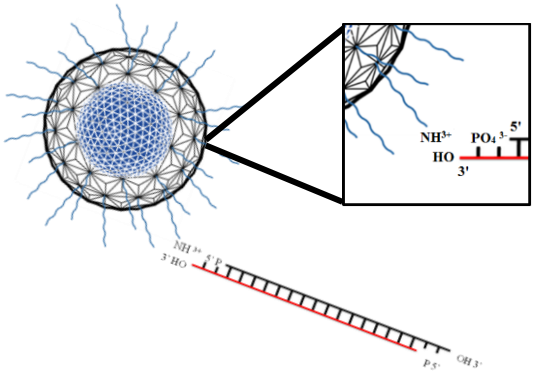

Figure 1 Schematic representation of ionic interaction between protonated CS amino groups of CS-OA/PLGA NPs and siRNAs phosphate groups.

Once assessed the stability of CS-OA/PLGA NPs in pH close to 6, a fixed volume of nanoparticles was gently mixed with different concentrations of siRNA and after 5 min of incubation at room temperature particle size and zeta potential were measured. As shown in **Figure 3a** the addiction of siRNAs did not significantly alter the size and colloidal stability, therefore these parameters seemed to not be depended from amino: phosphate ratios. On the other side a statistical increase in zeta potential values was evident reaching from ≈15 mV of naked NPs potential values of ≈28 mV with the highest concentration of siRNAs (1000nM) (**Figure 3b**). Many factors affect the formation, the structure and stability of polyplexes, including: the degree of ionization of each one of the polyelectrolytes, their charge density and charge distribution on the polymer chains, polyelectrolytes concentration, mixing ratio (Z), the nature of the ionic groups on the polymer chains, molecular weights of the polyelectrolytes, flexibility of the polymer chains, interaction time and temperature and ionic strength, as well as the pH of the medium[35]. On the basis of this evidence, the increase in zeta potential values can be likely correlated to a masking effect mediated by the siRNAs. siRNAs interposed their structures among the DPBS phosphate groups and the chitosan amino groups, causing a variation in the ionic strength and charge distribution. Furthermore, charge rearrangement seemed to be proportional to the number of siRNAs reacted, however it is so slightly that did not affect inter-particles distances, therefore no particle aggregation and increase in dimension occurred. Anyhow, the net positive charge of polyplexes are desirable to prevent particle aggregation and promote electrostatic interaction with the overall negative charge of the cell membrane[36].

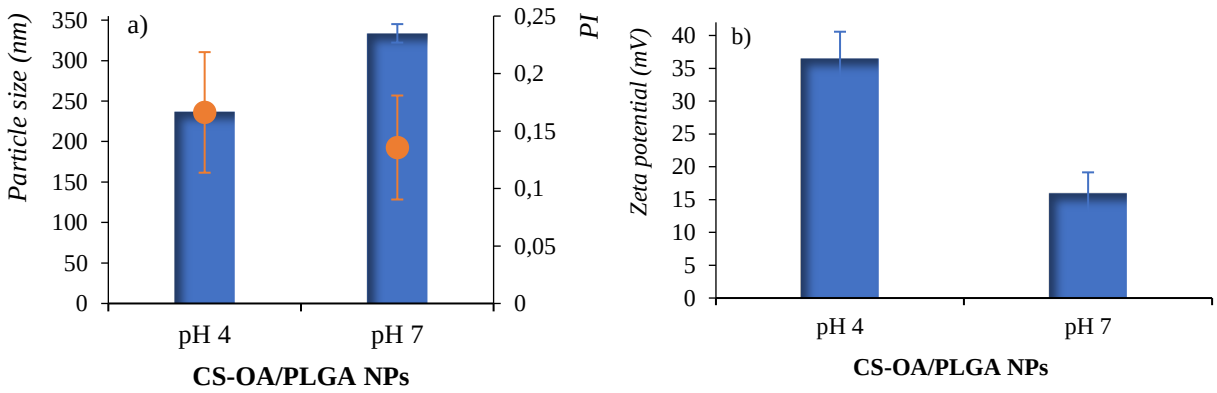

Figure 2 Average particle size (nm) CS-OA/PLGA-NPs (a) and zeta potential values (b) after buffer exchange in DPBS 1X ANOVA 1 via – MRT ($p<0,05$) mean values ± s.d., n=5.

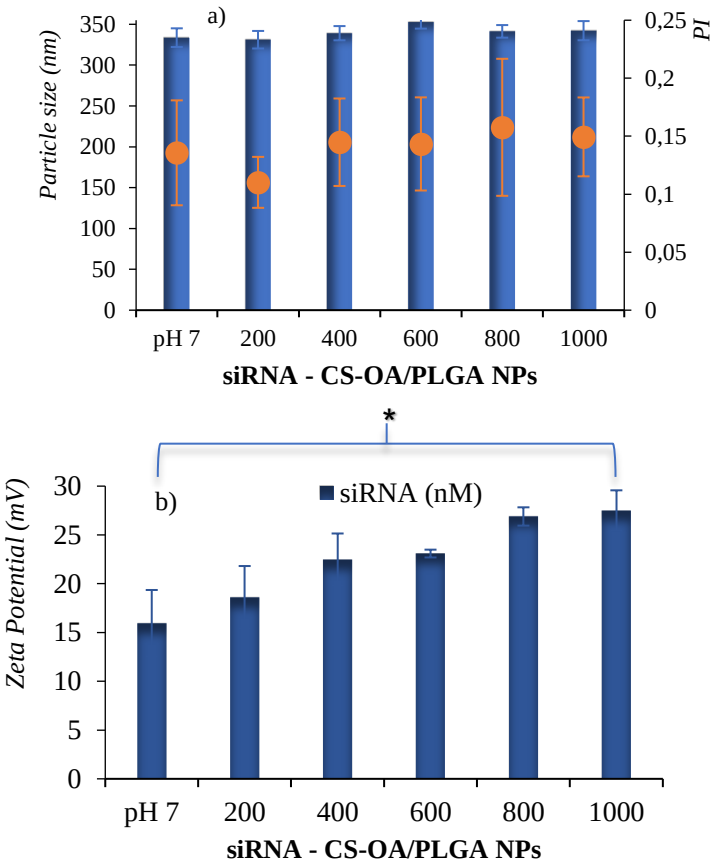

Figure 3 Average particle size (nm) siRNAs/CS NPs complexes (a) and zeta potential values (b) ANOVA 1 via – MRT ($p<0,05$) mean values ± s.d., n=5.

1.2.Qualitative determination of siRNA-NPs interaction

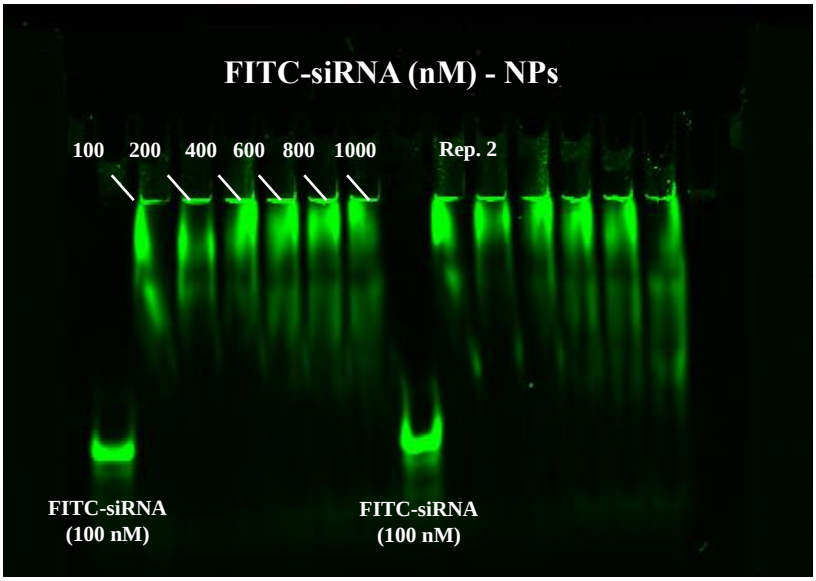

Figure 4 Binding efficiency of siRNA to CS-OA/PLGA NPs, by polyacrylamide gel electrophoresis.

, The interactions between siRNA and chitosan amino group were investigated. FITC-labeled siRNA was employed as tracking agent and a binding of siRNA with CS-OA/PLGA NPs, obtained by simple mixing, was observed (**Figure 4**). A holdback in FITC-siRNA signal occurred when the oligonucleotides were complexed with the NPs; complexes carrying net zero or positive charge is retained within the well. Moreover, no apparent differences depending on siRNA concentration employed were evident. The limitation step in the immobility of complexes in gel electrophoresis, in fact, was mainly associated to the quantity of positive surface charge, therefore on the ratio of chitosan present, which was mostly constant. However, the retardation or immobilization of the siRNA migration demonstrated the strength of interaction between siRNA-chitosan and the presence of trailing bands suggested an uncomplete binding, indicating that the interaction between chitosan and siRNA obtained by simple mixing was apparently weak. These results were in attendance with previous studies which found a more efficient binding when siRNAs were partially included in nanoparticles instead of simple complexation where siRNAs were almost placed on the surface of the cargo[38],[37]. Furthermore, as well noted, several copies of siRNAs could be complexed with chitosan instead of one molecule per cationic entity thanks to the short length of siRNAs (21 bp) and their linearity[38].

1.3.Fluorescence titration assay

The complex formation of chitosan with siRNA was confirmed by a binding titration assay. The test was performed by adding a fixed amount of siRNAs (from 50 to 400 nM) at different concentrations of NPs. The NPs concentrations were calculated in term of quantity of chitosan-oleate by progressively diluiting the colloidal system in water. **Figure 5**, shows in all cases a clear increase in FTIC-siRNA signal even with the minimum amount of NPs (CS-OA at 12.5 µg/ml). Within the lower siRNA concentrations (50 and 100 nM) no variations were recorded even if the NPs amount increased, while, with siRNA 400nM, a proportional increase in fluorecence during the modulation of NPs ratios was recorded. The increase in fluorescence could be reliable to the growing numer of primary amine group exposed on the surface of the NPs and arranged to interact with siRNAs. A saturation of binding sites seemed to be reached at 175 µg/ml of chitosan-olate, immediately followed by a reduction in fluorecence intensity with the higher concentrations, indicating a less efficience in complex formation. This proportional variation in fluorecence may indicate the formation of a different architecture of siRNA/NPs complexes and molecules arrangment, even if electrostatic interaction driving the binding entity[40].

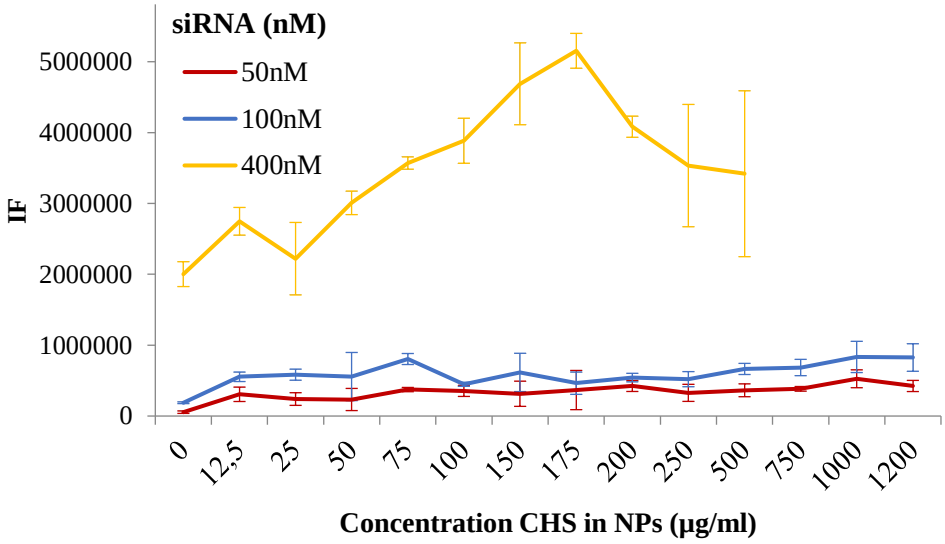

Figure 5 Fluorescence intensity of FITC-siRNA at different concentration of CS-OA/PLGA NPs (mean values ± s.d., n=8).

1.4.Internalization and Flow cytometric analyses on HepG2 and PBMCs

A fixed amount of CS-OA/NPs (60µg/ml), was complexed with increasing amount of FITC-siRNAs and the cell-internalization study were performed by FACS analysis. The entity of internalization complex was determined by detecting the amount of FITC-siRNA taken up, after 24 h of transfection. Immortalized HepG2 and normal human PBMCs were employed and in both cases the increase of the shift and the intensity of fluorescein signal in alive cells was proportional to the amount of siRNA loaded onto the nanosystem (**Figures 6** and **7**). For HepG2, even if the amount of siRNAs increased in the cells, the number of events, based on the number of cell alive, did not change and this may indicated a good cell-polycomplex interaction, without affecting cell viability. On the other side, more sensitive PBMCs, showed that the number of events decreased in function of the quantity of FITC-siRNA complexed. To investigate the dose effect of the CS-OA/PLGA NPs on PBMCs, another test was performed mantaining this time a fixed amount of FITC-siRNA. As shown from the events number (**Figure 8**) a reduction in cell viability occurred with the increase of the colloidal nanosystem concentration, demostrating a citotoxic dose- dependent effect.

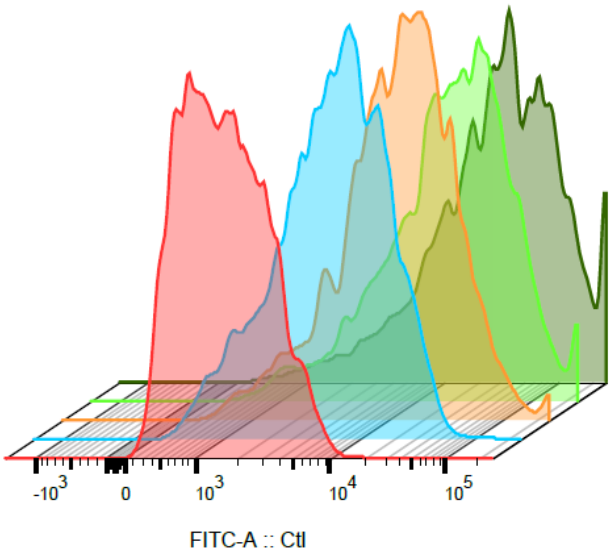

	siRNA (mM)	Cell Count
	200	3198
	400	3191
	600	3180
	800	3084
	1000	3173

Figure 6 Intracellular fluorescence intensities on HepG2 of FITC-siRNA/NPs complexes prepared at different siRNAs ratios, determined by flow cytometry.

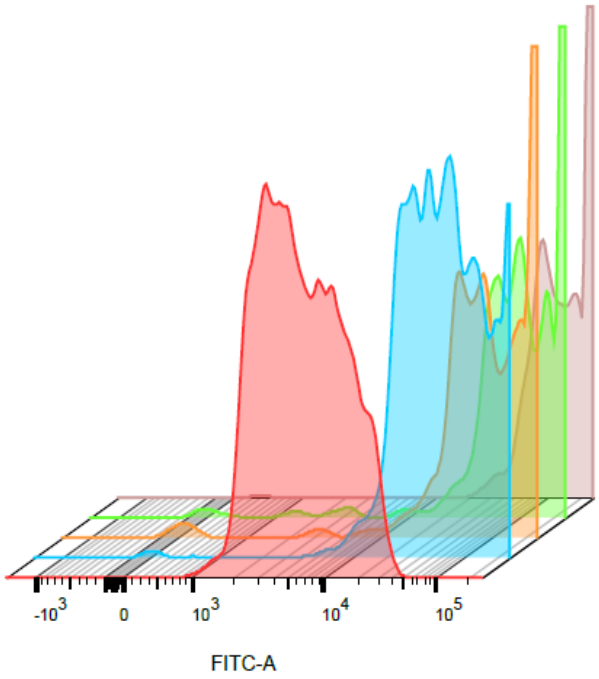

	siRNA (mM)	Cell count
	200	895
	400	1343
	600	221
	800	395
	1000	281

Figure 7 Intracellular fluorescence intensities on PBMCs of FITC-siRNA/NPs complexes prepared at different siRNAs ratios, determined by flow cytometry.

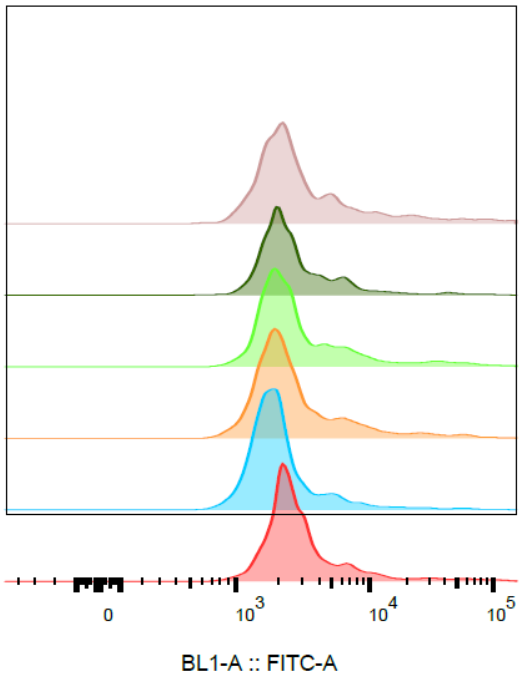

	CS-OA (µg/ml)	Cell count
	Control	1169
	0	940
	12.5	612
	25	777
	50	731
	100	547

Figure 8 Intracellular fluorescence intensities on PBMCs of FITC-siRNA/NPs complexes prepared at different NPs ratios, determined by flow cytometry.

1.5.Characterization of inflammatory response of human PBMCs on CS-OA/PLGA NPs

The inflammatory response of naked CS-OA/PLGA NPs was analyzed on PBMCs by the aid of RT-qPCR technique. The results are illustrated in **Figure 9**. The concentrations of NPs were calculated as chitosan content in the colloidal system (from 12.5 µg/ml up to 100 µg/ml) and the cytosolic production of four different cytokines (IL-6, IL-10, TNF-α and IFN-γ) was evaluated after 24h of cell exposure to NPs. Both all anti-inflammatory (IL-10) and pro-inflammatory (IL-6,TNFα,INFγ) mediators, a dose-dependent response occurred, reaching the highest level at 25 µg/ml of chitosan in the cell enviromeent. At the higher chitosan, and therefore, nanoparticle concentrations (50 and 100 µg/ml), cytokines secretion seemed to be arrested maybe due to a cytotoxic effect responsible of a decreased cell viability, as confirmed as well as by FACS analysis. As well known in literature, depending on how chitosan is processed, this polymer has distinct effects on blood coagulation and macrophage activation[39]. Water-soluble chitosan oligomers and chitosan degradation products, for example, can stimulate both macrophages differentiation and monocytes activation and can involve a dose dependent secretion of cytokines and mediators of inflammation, including interferon-γ (IFN-γ), tumor necrosis factor-α (TNF-α), interleukin-1 (IL-1), interleukin-2 (IL-2), interleukin-6 (IL-6), nitric oxide (NO)[40]. Given these premises and considering the complexity in composition of the studied NPs, the pro-inflammatory effect can be related to a nanosystem disassembling together with the release of chitosan debrids occurring after the NPs endocytosis. Is well known that cationic particles induce inflammation to a great extent than anionic and neutral ones[41].The activation of proinflammatory cytokines IL-6, IL-10, of TNF-α and INF-γ is, in fact, beared by surface chemistry and thereby the surface charge, which in turn modulates their interaction with immune cells[42]. According to these results, the chitosan coated nanoparticles under study cannot be envisaged as systemic delivery systems. However, their versatility allows to think to an opportune functionalization to get an active targeting with the aim to deliver the nano-systems directly to the target site, exploiting only there a cytotoxicity effect. Furthermore, these carriers can be loaded in specific implant or delivery system, as electrospun nanofibers, in order to explicate a topical delivery and therefore treat local diseases.

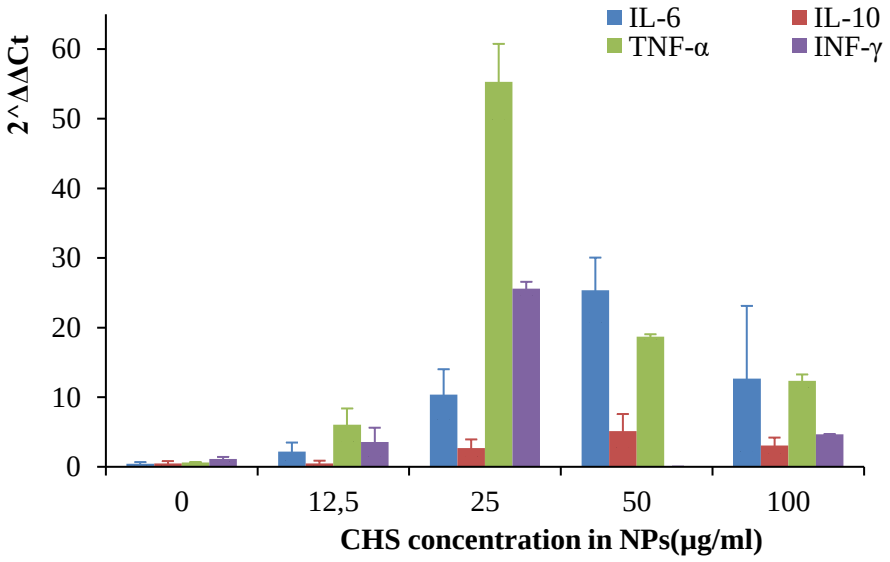

Figure 9 Cytokine induction results for CS.OA/PLGA NPs (mean values ± s.d., n=8).

3. Materials and methods

- *Materials*

Chitosan LMW (CS) (80 % Deacetylation Degree, DD), Poly-lactic-glycolic acid (PLGA) (Resomer RG 503H), ethyl acetate, acetic acid were purchased from Sigma-Aldrich (Italy and USA). Oleic acid (OA) was acquired from Fluka (Milan, Italy). All cell culture products were purchased from GIBCO (Gibco BRL/Life Technologies, a division of Invitrogen, Grand Island, NY). M-MLV Reverse transcriptase, Superscript III reverse transcriptase and Random primers were acquired from ThermoFisher. Primers and siRNAs were purchased from Integrated DNA Technologies (IDT, Coralville, IA, USA).

- *Methods*

3.1.Preparation of CS-OA/PLGA nanoparticles

Chitosan oleate (CS-OA) was obtained in situ by self-assembling[43], [44]. Briefly, chitosan was added to 100 ml of bidistilled water under magnetic stirring (300 rpm) slightly acidified (about pH 4.5) with acetic acid to obtain a 1% w/w polymer concentration. Then, 50 % of chitosan binding sites were functionalized with oleic acid, by adding dropwise a stoichiometric amount of fatty acid solubilized in acetone to the chitosan solution. Chitosan-oleate salt was obtained (CS-OA) and, after acetone evaporation, occurred under stirring overnight, CS-OA was freeze dried for 48 h. The solid residue was employed to obtain PLGA-NPs by the solvent evaporation method previously described[32,33] partially modified. Specifically, CS-OA (1.2 mg/ml) was dispersed in 3 ml of distilled water, 0.025 µl of glacial acetic acid were added to a better polymer-water dispersion and 0.25 ml of ethyl acetate solution containing 24 mg/ml of PLGA were poured during the emulsification step. This step was carried out at 70 % amplitudes by means of Q700 Ultrasonic processor (QSonica, Newtown, CT) equipped with a replaceable titanium horn (tip diameter = 12.7 mm). After 5 min, 7 ml of distilled water were added, and emulsification was carried out for further 5 min. Then, ethyl acetate was removed under stirring overnight. The day after, NPs were kept under stirring at 40 °C for about 45 min. The weight lost due to evaporation was determined and the initial volume (10 ml) was reconstituted with distilled water. Finally, NPs were sonicated for 15 min in an ice bath and centrifuged for 10 min at 3000 rpm.

3.2.Anti – Tat/Rev siRNAs

CS-OA/PLGA NPs were functionalized with a siRNA targeted to HIV-1, directed against the viral Tat/Rev transcripts and able to silence the viral expression via post-transcriptional gene silencing (PTGS). Anti-tat/rev Site I 27-mer siRNAs were chosen as model for our studies and were constituted by the antisense sequence: 5′-UGA UGA GCU CUU CGU CGC UGU CUC CGC dTdT-3′ and the sense sequence: 5′-GCG GAG ACA GCG ACG AAG AGC UCA UCA-3′. First, the extended antisense strand, end-labeled or not with FITC (MW= 13.616.2 g/mol) and the complementary extended sense strand (MW=12.508.4 g/mol) were slowly thawed in ice bath, later annealed in RNase free water and RNA buffer, at 65°C for 5 minutes, using the same molar ratio as the corresponding partner strand to form the dsRNAs. Then, annealed siRNAs were gradually cooled from 37°C to room temperature and kept in ice bath until their usage.

3.3.siRNAs – CS-OA/PLGA NPs functionalization

CS-OA/PLGA NPs are generally formulate in acidic conditions (pH= 4.5) both to ensure good colloidal stability and fully positive surface charges. However, because siRNAs are unstable at pH below 5, due to the titration nucleic bases polar groups, mainly involved in hydrogen bonding, the colloidal nano-system was subjected to a buffer exchange in phosphate buffer (DPBS 1X, pH =7.4) by the aid of a dialysis bag method **Figure 10**. Briefly, 5 ml of colloidal NPs were dialyzed in a tube (cut-off 12-14 kDa dialysis tubes, Ø = 36/32 – 28,6 mm, Sigma Aldrich) at room temperature, under magnetic stirring (300 rpm) for 1h and, suddenly, the pH (pH≈6) was checked by litmus paper. Afterwards, siRNAs end-labeled or not end-labeled with fluorescein isothiocyanate (FITC) were directly poured in 100 µl of NPs and incubated at room temperature for 5 min before further analyses.

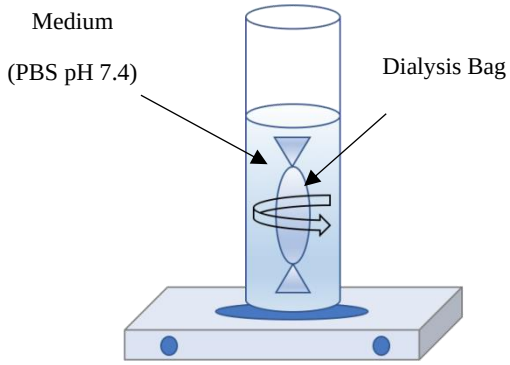

Figure 10. Schematic representation of dialysis bag method.

3.4.Characterization of siRNA nanoparticles or chitosan siRNA nanoparticles

Different molar concentrations of siRNAs (from 200 up to 1000 nM) were employed to functionalize 100 µl of NPs, maintaining a chitosan concentration of 60 µg/ml. On naked NPs and siRNA- NPs particle size and zeta potential were measured at room temperature with a Brookhaven Instruments *ZetaPALS*. Reported values are the average of five runs for nanoparticle size and of five runs with a target residual of 0.02 for zeta potential. The size measurements were performed, by diluting 100 µl of the sample in 3 ml of distilled water, while the zeta potential measurements were performed by diluting 50 µl of the sample in 1.5 ml of distilled water and setting a count rate per second (KCps) in the range of 2500–3500.

3.5.Qualitative determination of siRNA-NPs interaction

3.5.1. Gel electrophoresis

The binding between siRNAs phosphate groups and chitosan amino groups was determined by a polyacrylamide gel electrophoresis. A discontinuous gel formed from two polyacrylamide solutions, a small, low-percentage stacking gel (4% v/v), and a larger portion of gel that normally separates proteins (16 % v/v) was prepared. A master mix made on 50

% v/v glycerol solubilized in DPBS 1X and FTIC labeled siRNA – NPs containing 100 nM of FITC-labeled siRNA, was prepared. To evaluate a possible dose-dependent interaction between siRNA and CS–OA/PLGA NPs, different concentrations of unlabeled siRNA (from 200 up to 1000 nM) diluted in DPBS 1X, were added to a fixed volume of master mix for a total of 30 µl/sample. A 1:6 dilution of loading dye (Coomassie blue) was added to master mix and used as control. All samples were loaded, and electrophoresis was run at a constant voltage of 55 V for 2 h in TBE buffer (ultra purifical buffer concentrate 0.89 M Tris Borate + 20 mM sodium EDTA, pH 8.3). The siRNA bands were then visualized under a fluorescent imaging system (Gel imaging work station, Azure Biosystems – c200) fixing λ_{ex}= 490 nm and λ_{em}= 525 nm. The assay was performed in duplicate.

3.5.2. Fluorescence titration assay

A FTIC-siRNA/NPs binding titration was assessed by the mean of a spectrofluorometer (Plate reader – Spectra Max ID3, molecular Devices) reading the fluorescence intensity of FTIC labeled siRNA (λ_{ex}= 490 nm and λ_{em}= 525 nm). Fixed volumes of FTIC-siRNA (at 50, 100 and 400 nM) interacted with different CS-OA/PLGA NPs amounts calculated on the basis of CS-OA concentrations opportunely diluted in water (from 0 to 1200 µg/ml). Eight replicates for sample were effected.

3.5.3. Cell Lines and Cell Culture

3.5.3.1. HEPG2

HepG2, derived from a liver hepatocellular carcinoma of a 15 year old Caucasian male, were purchased from ATCC. HepG2 cells were grown in a polystyrene flask in complete culture medium consisting of EMEM (Eagle's minimum essential medium, 1.2 g/L sodium bicarbonate, non-essential amino acid, L-glutamine and sodium pyruvate) supplemented with 10% FBS and PenStrep (100 U/mL penicillin, and 100 µg/mL streptomycin). Cells were cultured in a humidified 5% CO_2 incubator at 37°C.

3.5.3.2. PBMCs

Peripheral blood mononuclear samples were obtained from healthy donors from the City of Hope National Medical Center. PBMCs were isolated from whole blood by centrifugation in SepMate™ tubes through a Ficoll-Hypaque solution (Histopaque-1077, Sigma), following manufactured protocol. Suspension cells were cultured in RPMI 1610 with 10% v/v FBS, PenStrep and 100 U/mL interleukin-2. Cells were cultured in a humidified 5% CO_2 incubator at 37°C.

Ethic Statement

The research involves blood specimens from anonymous human subjects with no identifiers to age, race, ethnicity, or gender. All human tissue specimens will be obtained from healthy, anonymous donors from third party sources. We use discarded peripheral blood from anonymous, healthy adult donors from the City of Hope Blood Donor Center (Duarte, CA), for isolation of peripheral blood mononuclear cells (PBMCs).

3.6.Internalization and Flow cytometric analyses on HepG2 and PBMCs

HepG2 and PBMCs were grown at 37 °C in a humidified 5% CO_2 incubator at 37°C, for 24 h in 12-well plate (CytoOne®) with seeding at 1 x 10^6 cell/well and in complete medium (EMEM and RPMI 1640 respectively). Afterward, cells were washed twice with 0.5 mL/well of prewarmed DPBS 1X. For PBMCs every wash was interspersed with centrifugation steps at 300 x G for 5 min and supernatant withdrawal. Then, cells were treated with 50 µL of FITC-siRNA/NPs diluted in 950 µL of medium without serum and antibiotics to reach siRNA final concentration from 20 up to 100 nM and CS-OA concentration about 60 µg/ml. Furthermore, PBMCs were treated with the same NPs volume at different CS-OA concentrations (from 12.5 up to 100 µg/ml) but functionalized with a fixed amount of FITC-siRNA to reach a final concentration of 40 nM. After 24 h of transfection, depending on cell line treated two procedures were done (**Figure 11**):

- HepG2 cells were washed twice with DPBS 1X, then trypsinized with 0.5 ml/well of Trypsin EDTA 1 x solution in HBSS (Irvine Scientific), collected in tubes and centrifuged at 1200 rpm for 5 minutes. Pellet were washed for another two times. Finally, cells were fixed with 0.4 ml/tube with IC fixation buffer (Invitrogen,CA,USA) diluted 1:1 in cold DPBS 1 X. Samples were stored in fridge, protect from light until FACS analysis.
- PBMCs were mechanically detached from the bottom of the well, collected in tubes, centrifuged at 300 x G for 5 minutes, the supernatant discarded, and cells were washed once in cold DPBS 1X, following by another centrifuge step. Then PBMCs were fixed using the same procedure above described.

Internalization was assessed on human cells by FACS analysis using a FACS Calibur instrument (BD Biosciences), BD Fortessa (BD Biosciences) and FlowJo software version 8.8.6. For each sample, 10,000 gated events were counted and a dot plot of forward scatter versus side scatter established a collection gat e(FSC/SSC) for cells to exclude cellular debris, dead and aggregated cells. Gating excluded events with low FSC and high SSC. Fluorescein isothiocyanate (FITC) gate was set using fluorescence minus one control, where cells were not stained and the FTIC signal intensity was recorded.

3.7.Characterization of immune responses of human PBMCs

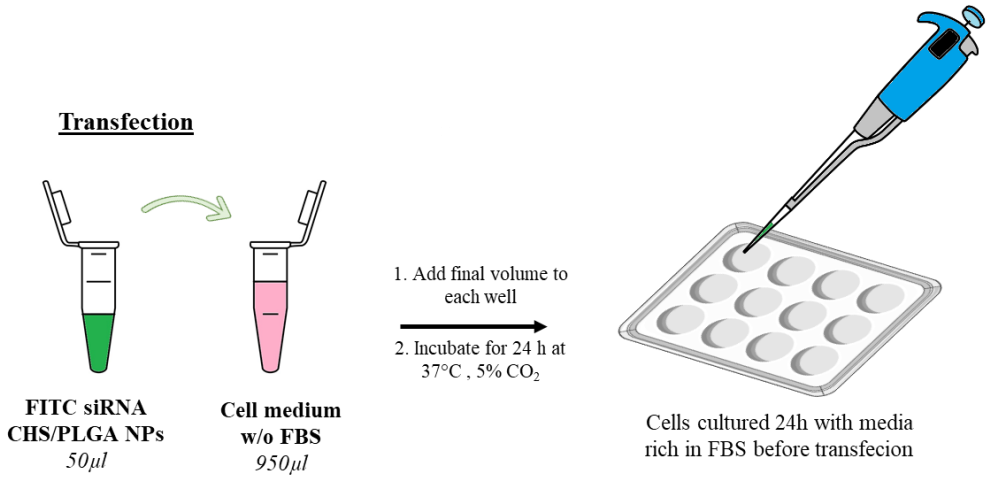

Figure 11 Schematic representation of siRNA – CS-OA/PLGA NPs cell transfection.

In order to evaluate any immune response from CO-AO/PLGA not siRNA loaded NPs on PBMCs, a qRT-PCR was performed. Four pro- and anti-inflammatory cytokines were assessed: IL-6, IL-12, TNFα and INFγ, and 1 x 10^6 cells were cultured for 24 h in a 12-well plate at 37°C in a humidified 5% CO_2 incubator. The day after, media was replaced and cells were treated with 100 µl of NPs at different CS-OA concentrations (12.5, 25, 50, 100 µg/ml) diluted in 900 µl of complete media for another 24 h. Finally, PBMCs were washed, collected and total RNAs were isolated with TriZol agent (ThermoFisher, CA, USA) according to the manufacturer's instructions. Total RNAs were quantified by using NanoDrop (ND-1000, spectrophotometer) at 230 nm. cDNA was produced using 1 µg of total RNA. Reverse transcription was carried out using iScript™ cDNA Synthesis Kit (Bio-Rad, CA, USA) according to the manufacturer's instructions procedure. Expression of the IL-6, IL-12, TNF-α and INF-γ coding RNAs were analyzed by quantitative RT-PCR using SsoAdvanced Universal SYBR Green Supermix (Bio-Rad, CA, USA) and specific primer sets at a final concentration of 400 nM, for 50 ng of cDNA. GADPH expression was used for normalization of the qPCR data. Primers were as follows:
IL-6 forward primer 5'-CCAGCTATGAACTCCTTCTC-3';
IL-6 reverse primer 5'-GCTTGTTCCTCACATCTCTC-3'.IL-12 forward primer 5'-TGTAAAACGACGGCCAGT-3; IL-12 reverse primer 5' CAGGAAACAGCTATGACC-3'; TNF-α forward primer 5'-CCG AGG CAG TCA GAT CAT CTT-3'; TNF-α reverse primer 5'AGC TGC CCC TCA GCT TGA-3'; forward primer IFN-γ TGT AGC GGA TAA TGG AAC TCT TTT; reverse primer IFN-γ AAT TTG GCT CTG CAT TAT T. GADPH forward primer 5'-CAT TGA CCT CAA CTA CAT G-3'; GAPDH reverse primer: 5'-TCT CCA TGG TGG TGA AGA C-3'. As indicated by the kit thermal cycling program was set as follow: polymerase activation was achieved in 30 seconds at 95°C; DNA denaturation at 95 °C for 15 seconds and annealing at 60 °C for 30 seconds repeating cycles 39 times. Finally melt curves were recorded.

4. Conclusion

In previous works, PLGA nanoparticles, shell coated with a hydrophobically modified chitosan (CS-OA/PLGA NPs), were characterized and studied as drug delivery systems of lipophilic drugs. The present research seemed to confirm the suitability of the same nanoparticles, as non-viral vectors, to deliver oligonucleotides, able to regulate the expression of targeted genes and act actively in fighting specific diseases. In particular, siRNA/ CS-OA/PLGA NPs polyelectrolyte complexes were obtained. They exploit electrostatic interactions among the positive surface charges of chitosan amino groups and the anionic phosphate groups of siRNAs. The poly-complexes were achieved by simple mixing. The assembly of siRNA onto CS-OA/PLGA NPs did not affect the physical stability of the colloidal system: particle size remained constant, and a slight increase in zeta potential values occurred. This increase was related to a different ionic strength established in colloidal environment, during the rearrangement in charges distributions of phosphate groups surrounding the NPs boundaries. The complex formation was demonstrated by gel retardation assay. At all siRNA/chitosan ratios, the siRNA signal was retained, indicating an effective interaction among the two components. The same results were confirmed by a fluorescence titration test. Furthermore, the cell internalization of siRNA-chitosan NPs complexes was clearly seen on two different human cell lines (immortalized, HepG2 and normal, PBMCs). In both cases the signal of the labelled-siRNA present into cells alive, was proportional to the siRNA's concentrations mixed to a fixed amount of NPs. On PBMCs a dose-dependent pro-inflammatory cytokines production was evident, in particular of TNF-α, and IFN-γ. The exposure to CS-OA/PLGA NPs induced a macrophage differentiation and activation which leads to inflammatory events responsible of the cytotoxic effects. Even if CS-OA/PLGA NPs demonstrates a good versatility as siRNA cargo, the intense immuno-stimulatory effects make them a non-ideal systemic delivery system. Nevertheless, as well known, nanoparticles based on chitosan can be applied in drug delivery in oral, local and topical routes (skin or intact mucosae)[45]. Versatile CS-OA/PLGA NPs can be therefore loaded in drug delivery systems, such as for example polymeric nanofibrous membranes envisaged as hybrid NPs-nanofiber, to obtain a modulated oligonucleotide release in proximity of the area or target of interest.

Collaboration

The project was conducted in collaboration with Ph.D. Fellow X. Xia and all research group at the laboratory of molecular and cellular biology of Prof. J.J. Rossi, at Beckman Research Center, City of Hope, 1218 Fifth ave, Monrovia, California, USA.

References

1 Obbard D.J. et al., «The Evolution of RNAi as a Defence against Viruses and Transposable Elements», *Philosophical Transactions of the Royal Society B: Biological Sciences* 364, 2009, 1513: 99–115.

2 Elbashir S. M. et al., «Duplexes of 21±nucleotide RNAs Mediate RNA Interference in Cultured Mammalian Cells», *Nature* 2001, 411, 6836, 2001: 494-8.

3 Gulino A. et al, «Nanoparticle-Based Delivery of Small Interfering RNA: Challenges for Cancer Therapy», *International Journal of Nanomedicine*, 2012, 3637-3657.

4 Castanotto D. and Rossi J.J., «The Promises and Pitfalls of RNA-Interference-Based Therapeutics», *Nature* 457, 7228, 2009: 426–33.

5 Pecot C.V. et al., «RNA Interference in the Clinic: Challenges and Future Directions», *Nature Reviews Cancer* 11, 2011: 59–67.

6 Matranga C. et al., «Passenger-Strand Cleavage Facilitates Assembly of SiRNA into Ago2-Containing RNAi Enzyme Complexes», *Cell* 123,4, 2005: 607–20.

7 Kim D.H. and Rossi J.J., «Strategies for Silencing Human Disease Using RNA Interference», *Nature Reviews Genetics* 8, 3, 2007: 173–84.

8 Bo Hu et al., «Clinical Advances of SiRNA Therapeutics», Review article, *Wiley*, 2019, 1-14.

9 Burnett J.C., Rossi J.J., et. al., «Current Progress of SiRNA/ShRNA Therapeutics in Clinical Trials», *Biotechnol. Journal*, 6, 2011: 1130-1146.

10 Koizumi M. et al., «Design of 2'-O-Methyl RNA and DNA Double-Stranded Oligonucleotides: Naturally-Occurring Nucleotide Components with Strong RNA Interference Gene Expression Inhibitory Activity», *Nucleos. Nucleot. Nucl* 2019, 1-18.

11 Kumar P. et al., «5′-Morpholino Modification of the Sense Strand of an SiRNA Makes It a More Effective Passenger», *Chemical Communications* 55,35, 2019: 5139–42.

12 Xin Xia et al., «Tissue-Specific Delivery of Oligonucleotides», Oligonucleotide-Based Therapies: Methods and Protocols, Methods in Molecular Biology; Chapter II, 2019; 17,49.

13 Hu S. et. al., «Generation of High-Titer Pseudotyped Lentiviral Vectors», *Viral Vectors for Gene Therapy* 1937, 2019: 125–34.

14 Wang D. et al., «Adeno-Associated Virus Vector as a Platform for Gene Therapy Delivery», *Nature Reviews Drug Discovery* 18, 5, 2019: 358–78.

15 Tao Y. et al., «Application of Nanoparticle-Based SiRNA and CRISPR/Cas9 Delivery Systems in Gene-Targeted Therapy», *Nanomedicine* 14, 5, 2019: 511–14.

16 Alshaer W. et. al., «Aptamer-Guided Nanomedicines for Anticancer Drug Delivery», *Advanced Drug Delivery Reviews, Aptamers in Therapeutics and Drug Delivery*, 134, 2018: 122–37.

17 Zhou J. and Rossi J.J., «Aptamers as Targeted Therapeutics: Current Potential and Challenges», *Nature Reviews Drug Discovery* 16,3, 2017: 181–202.

18 Tortiglione C. and De la Fuente J.M., «Synthesis of Gold Nanoparticles for Gene Silencing», in RNA Interference and Cancer Therapy: Methods and Protocols, ed. Lekha Dinesh Kumar, Methods in Molecular Biology, 2019, 203–14.

19 He X. et al., «AIE Featured Inorganic–Organic Core@Shell Nanoparticles for High-Efficiency SiRNA Delivery and Real-Time Monitoring», *Nano Letters* 19, 4, 2019: 2272–79.

20 Schroeder A. et al., «Lipid-Based Nanotherapeutics for SiRNA Delivery», *Journal of Internal Medicine* 267, 2010, 1: 9–21.

21 Zhi D. et al., «The Headgroup Evolution of Cationic Lipids for Gene Delivery», *Bioconjugate Chemistry* 24,4, 2013: 487–519.

22 Dong Y. et al., «Strategies, Design, and Chemistry in SiRNA Delivery Systems», *Advanced Drug Delivery Reviews*, Engineering the next wave of nanomedicine and drug delivery systems 144,2019: 133–47.

23 Davis M.E., «The First Targeted Delivery of SiRNA in Humans via a Self-Assembling, Cyclodextrin Polymer-Based Nanoparticle: From Concept to Clinic» *Molecular Pharmaceutics*.6,2009: 659–68.

24 Siegwart D.J. et al., «Combinatorial Synthesis of Chemically Diverse Core-Shell Nanoparticles for Intracellular Delivery», *Proceedings of the National Academy of Sciences* 108,32, 2011: 12996-13001.

25 Karunaratne N. et al., «Natural Carriers for SiRNA Delivery», *Current Pharmaceutical Design* 21, 31, 2015: 4529–4540.

26 Singh, B. et al., «Chemical Modification of Chitosan with PH-Sensitive Molecules and Specific Ligands for Efficient DNA Transfection and SiRNA Silencing», *Journal of Nanoscience and Nanotechnology* 14, 2014: 564–576.

27 Serrano-Sevilla I. et al., «Natural Polysaccharides for SiRNA Delivery: Nanocarriers Based on Chitosan, Hyaluronic Acid, and Their Derivatives», *Molecules* 24,14, 2019: 2570-2604.

28 Alameh M. et al., «SiRNA Delivery with Chitosan: Influence of Chitosan Molecular Weight, Degree of Deacetylation, and Amine to Phosphate Ratio on in Vitro Silencing Efficiency, Hemocompatibility, Biodistribution, and in Vivo Efficacy», *Biomacromolecules*, 19,1, 2018: 112-131.

29 Hoffmann N. et al., «Neuronal and Glial Responses to SiRNA-Coated Nerve Guide Implants in Vitro», *Neuroscience Letters* 494, 1, 2011: 14–18.

30 Mittnacht U. et al., «Chitosan/SiRNA Nanoparticles Biofunctionalize Nerve Implants and Enable Neurite Outgrowth», *Nano Letters* 10,2010:3933-3939.

31 Cao Y. et al., «Recent Advances in Chitosan-Based Carriers for Gene Delivery», *Marine Drugs* 17,6, 2019: 381-402.

32 Miele D. et al., «Chitosan Oleate Salt as an Amphiphilic Polymer for the Surface Modification of Poly-Lactic-Glycolic Acid (PLGA) Nanoparticles. Preliminary Studies of Mucoadhesion and Cell Interaction Properties», *Marine Drugs* 16, 11, 2018: 447-465.

33 Miele D. et al., «Chitosan Oleate Coated Poly Lactic-Glycolic Acid (PLGA) Nanoparticles versus Chitosan Oleate Self-Assembled Polymeric Micelles, Loaded with Resveratrol», *Marine Drugs* 17,9, 2019: 515-533.

34 Mao S. et.al., «Chitosan-Based Formulations for Delivery of DNA and SiRNA», *Advanced Drug Delivery Reviews* 62, 1,2010: 12–27.

35 Pérez Quiñones J. et.al., «Chitosan Based Self-Assembled Nanoparticles in Drug Delivery», *Polymers* 10,3,2018:235-267.

36 Katas H. et.al., «Development and Characterisation of Chitosan Nanoparticles for SiRNA Delivery», *Journal of Controlled Release*: Official Journal of the Controlled Release Society 115, 2, 2006: 216–25.

37 Techaarpornkul S. et al., «Chitosan-Mediated SiRNA Delivery In Vitro: Effect of Polymer Molecular Weight, Concentration and Salt Forms», *AAPS Pharm.Sci.Tech*.11,1, 2010: 64–72.

38 Lee D.W. et al., «Preparation and Characterization of Chitosan/Polyguluronate Nanoparticles for SiRNA Delivery» *Journal of Controlled Release* 139, 2, 2009: 146–152.

39 Hoemann C. D. et.al., «3 - Immunological Responses to Chitosan for Biomedical Applications», *Chitosan Based Biomaterials Volume 1*, ed. J. Amber Jennings and Joel D. Bumgardner, 2017: 45–79.

40 Li H. et al., «Effects of Chitosan on the Secretion of Cytokines and Expression of Inducible Nitric Oxide Synthase MRNA in Peritoneal Macrophages of Broiler Chicken», *Brazilian Archives of Biology and Technology* 57, 4, 2014: 466–71.

41 Dobrovolskaia M.A. et.al., «Immunological Properties of Engineered Nanomaterials: An Introduction», *Handbook of Immunological Properties of Engineered Nanomaterials*, 1., Frontiers in Nanobiomedical Research, 2012: 1–23.

42 Nadesh R. et al., «Hematotoxicological Analysis of Surface-Modified and -Unmodified Chitosan Nanoparticles», *Journal of Biomedical Materials Research Part A* 101, 10, 2013: 2957–2966.

43 Bonferoni M.C. et al., «A Novel Ionic Amphiphilic Chitosan Derivative as a Stabilizer of Nanoemulsions: Improvement of Antimicrobial Activity of Cymbopogon Citratus Essential Oil», *Colloids and Surfaces B*: *Biointerfaces*, 152, 2017: 385–92.

44 Bonferoni M.C. et al., «Ionic Polymeric Micelles Based on Chitosan and Fatty Acids and Intended for Wound Healing. Comparison of Linoleic and Oleic Acid», *European Journal of Pharmaceutics and Biopharmaceutics*, Theme Issue: Nanomedicine,87, 2014: 101–107.

45 Kumar A. et.al., «Why Chitosan? From Properties to Perspective of Mucosal Drug Delivery», *International Journal of Biological Macromolecules* 91, 2016: 615–22.

ACKNOWLEDGMENTS

Firstly, I would like to express my sincere gratitude to my advisor Prof. M.C. Bonferoni for the continuous support of my Ph.D study and related research, for her patience and motivation.

Besides my advisor, I would like to thank the rest of my lab group: Prof. G. Sandri, my co-advisor, Prof. F.Ferrari, my mentor, Prof. S. Rossi and Dr. B. Vigani, for their insightful comments and encouragement.

My sincere thanks also go to Prof. J.J. Rossi and Dr. X. Xia who provided me an opportunity to join their team as visiting research student, and who hosted me in the laboratory of "cellular and molecular biology" at City of Hope, Monrovia, California, USA. Without their precious support, the final part of this work would not have been possible.